MINISTÉRIO DA CIÊNCIA, TECNOLOGIA E INOVAÇÃO
INSTITUTO NACIONAL DE PESQUISAS ESPACIAIS

sid.inpe.br/mtc-m21d/2023/12.07.22.39-TDI

IMPACTS OF FRESHWATER SUPPLY ON THE COASTAL DYNAMICS OF THE ANTARCTIC PENINSULA

Luciana Shigihara Lima

Doctorate Thesis of the Graduate Course in Remote Sensing, guided by Drs. Luciano Ponzi Pezzi, and Mauricio Magalhães Mata, approved in December 06, 2023.

URL of the original document:
<http://urlib.net/8JMKD3MGP3W34T/4ABK752>

INPE
São José dos Campos
2023

PUBLISHED BY:

Instituto Nacional de Pesquisas Espaciais - INPE
Coordenação de Ensino, Pesquisa e Extensão (COEPE)
Divisão de Biblioteca (DIBIB)
CEP 12.227-010
São José dos Campos - SP - Brasil
Tel.:(012) 3208-6923/7348
E-mail: pubtc@inpe.br

MINISTÉRIO DA CIÊNCIA, TECNOLOGIA E INOVAÇÃO
INSTITUTO NACIONAL DE PESQUISAS ESPACIAIS

sid.inpe.br/mtc-m21d/2023/12.07.22.39-TDI

IMPACTS OF FRESHWATER SUPPLY ON THE COASTAL DYNAMICS OF THE ANTARCTIC PENINSULA

Luciana Shigihara Lima

Doctorate Thesis of the Graduate Course in Remote Sensing, guided by Drs. Luciano Ponzi Pezzi, and Mauricio Magalhães Mata, approved in December 06, 2023.

URL of the original document:
<http://urlib.net/8JMKD3MGP3W34T/4ABK752>

INPE
São José dos Campos
2023

Cataloging in Publication Data

Lima, Luciana Shigihara.

L628i Impacts of freshwater supply on the coastal dynamics of the antarctic peninsula / Luciana Shigihara Lima. – São José dos Campos : INPE, 2023.

xxiv + 150 p. ; (sid.inpe.br/mtc-m21d/2023/12.07.22.39-TDI)

Thesis (Doctorate in Remote Sensing) – Instituto Nacional de Pesquisas Espaciais, São José dos Campos, 2023.

Guiding : Drs. Luciano Ponzi Pezzi, and Mauricio Magalhães Mata.

1. Ice shelves. 2. Basal melting. 3. Oceanic numerical modeling. 4. Water masses. 5. Ice-ocean-atmosphere interactions. I.Title.

CDU 528.8:551.322

MINISTÉRIO DA CIÊNCIA, TECNOLOGIA E INOVAÇÃO

INSTITUTO NACIONAL DE PESQUISAS ESPACIAIS
Serviço de Pós-Graduação - SEPGR

DEFESA FINAL DE TESE DE LUCIANA SHIGIHARA LIMA
REG. 142379/2019, BANCA Nº 278/2023

No dia 06 de dezembro de 2023, de forma online, o(a) aluno(a) mencionado(a) acima defendeu seu trabalho final (apresentação oral seguida de arguição) perante uma Banca Examinadora, cujos membros estão listados abaixo. O(A) aluno(a) foi APROVADO(A) pela Banca Examinadora, por unanimidade, em cumprimento ao requisito exigido para obtenção do Título de Doutora em Sensoriamento Remoto, com a exigência de que o trabalho final a ser publicado deverá incorporar as correções sugeridas pela Banca Examinadora, com revisão pelo(s) orientador(es).

Título: IMPACTS OF FRESHWATER SUPPLY ON THE COASTAL DYNAMICS OF THE ANTARCTIC PENINSULA

Membros da banca:

Dr. João Antonio Lorenzzetti – Presidente – INPE
Dr. Luciano Ponzi Pezzi – Orientador – INPE
Dr. Mauricio Magalhães Mata – Orientador – FURG
Dr. John Michael Klinck – Membro Externo – Old Dominion University
Dra. Cristina Schultz – Membro Externo – Northeastern University

Declaração de aprovação dos Drs. John Michael Klinck e Cristina Schultz anexas ao processo.

Documento assinado eletronicamente por **MAURICIO MAGALHAES MATA (E)**, **Usuário Externo**, em 18/12/2023, às 17:36 (horário oficial de Brasília), com fundamento no § 3º do art. 4º do Decreto nº 10.543, de 13 de novembro de 2020.

Documento assinado eletronicamente por **JOAO ANTONIO LORENZZETTI (E)**, **Usuário Externo**, em 20/12/2023, às 09:15 (horário oficial de Brasília), com fundamento no § 3º do art. 4º do Decreto nº 10.543, de 13 de novembro de 2020.

Documento assinado eletronicamente por **Luciano Ponzi Pezzi**, **Pesquisador**, em 28/12/2023, às 08:57 (horário oficial de Brasília), com fundamento no § 3º do art. 4º do Decreto nº 10.543, de 13 de novembro de 2020.

A autenticidade deste documento pode ser conferida no site https://sei.mcti.gov.br/verifica.html, informando o código verificador **11551816** e o código CRC **B60E98E7**.

Referência: Processo nº 01340.009960/2023-41 SEI nº 11551816

"Panta rei.
Tudo flui.
Everything flows."

HERACLITO OF HEPESUS, 535 BC – 475 BC

A meus pais Angelica e Edegar, à meu irmao Mariano e ao meu companheiro de vida Guilherme

ACKNOWLEDGEMENTS

The *Endurance* was a three-masted sailing vessel that Sir Ernest Shackleton and 27 other crew members used to explore Antarctica. A year after its construction, it became trapped in ice and found its place at the bottom of the Weddell Sea. Nearly 107 years later, in March 2022, the ship was found with its name still legible on the stern, remarkably well-preserved.

According to the Oxford Advanced Learner's Dictionary, "Endurance" means the ability to persist in something painful or challenging for an extended period without giving up. When I came across this definition, I wondered if it was fitting to begin my thesis acknowledgments with this word. After careful consideration, I decided to maintain this analogy. The journey through a doctorate is akin to a challenging and sometimes arduous expedition. It spans a considerable amount of time and demands unwavering persistence.

Especially in the past four years, we had a period rife with difficulties for many due to the pandemic, and a challenging time for science, we have persevered and emerged stronger and more resilient. While this circumstance was unforeseen, much like the *Endurance*'s fate at the bottom of the ocean, it gave crucial lessons. Like Shackleton, who learned about ice dynamics and resilience from the ship's journey, we also acquired knowledge from our setbacks and accomplishments.

Thanks are extended to all those who made this journey lighter. To friends who navigated their own thesis voyages alongside me, offering (and receiving) shoulders to lean on (many) moments during this time. And some persons who were there just to hear me and support giving me tools to help me with my own challenges. Your presence is invaluable to me. And also my long-term friends who are always with me, also when I am a bit disappeared. I am equally thankful to those I encountered during this expedition, starting from 2019's remarkable experience at SONOAT, and to the friendships forged during my visit to the Center for Coastal Physical Oceanography (CCPO), at Old Dominion University (ODU).

My heartfelt thanks to Luciano and Mauricio for their trust in my intellectual capacity and guidance as advisors. Gratitude is also extended to all those I encountered during my Antarctic immersion.

A special acknowledgment goes to Mike Dinniman for his generous assistance, prompt responses to my inquiries, and friendship, and for hosting me at ODU for

three months. Carlos Moffat, I extend my appreciation for the insights and ideas shared during my visit to the University of Delaware (UDelaware).

Acknowledgment is due to SCAR/INSTANT and INCT da Criosfera for facilitating the scientific visit to ODU and UDelaware, and the Coordination of Superior Level Staff Improvement (CAPES) for the doctoral fellowship.

Thanks also to INPE and to the National Laboratory of Applied Science (LNCC), for the Kerana Cluster and the Santos Dumont cluster computing time provided. And to CCPO/ODU, for the computing time in the Wahab High Performance computing cluster to run the simulations, and the computer facilities and support provided by the CCPO during the three months that I spent there.

And finally, I want to thank my family who always believed in me and supported my 'crazy and passionate' pursuit of studying the ocean and the ice continent. And especially my life partner who supported me and always be available to encourage me to follow my dreams. Thank you, Gui.

ABSTRACT

This work analyzes the impact of the introduction of freshwater into the ocean resulting from the melting of ice shelves in the Antarctic Peninsula. The reduction of ice shelves not only contributes to sea level rise through increased freshwater inflow into the ocean but also has the potential to alter ocean circulation, sea ice production at the surface, and the consequent stratification, along with changes in the characteristics of water masses. In this study, we investigate the effects of basal melting (melting at the base of the ice shelves) on circulation, water, and sea ice mass production in the ocean surrounding the Antarctic Peninsula (Bellingshausen and Weddell Seas). To do this, we used the regional ocean model ROMS (Regional Ocean Model System) to simulate the dynamic and thermodynamic mechanisms in this region. Due to model limitations, the thickness and area of the ice shelves remain unchanged throughout the simulation. Two experiments were conducted: a control experiment (CTRL) and a sensitivity experiment (SENST). The CTRL experiment (with the ice shelf melting effect) was able to replicate the main oceanographic features over the simulation period (2002-2020). In the sensitivity test (SENST), the salt and heat fluxes representing the freshwater flows from melting were set to zero. An increase in sea ice production in the coastal region was observed in the CTRL experiment compared to SENST, due to the extremely cold freshwater plumes resulting from melting. There was also an increase in the production of dense bottom waters originating from mixing processes beneath the ice shelves, extremely cold ISW water from melting, with modified deep circumpolar waters (mCDW) that enter the ice shelf cavities, as well as super saline and dense waters (HSSW) resulting from sea ice production. An increase in sea ice concentration was also observed in the Weddell Gyre region in the CTRL experiment, as well as an intensification of the gyre. The increased sea ice concentration, affected by katabatic winds (strong and constant winds from the interior of the continent) and westerly winds, pushes the ice toward the center of the gyre. Also, the current intensity is affected by changes in wind stress on the ocean due to changes in sea ice thickness at the surface. Over the Bellingshausen Sea, the intensification of westerly winds increases the circulation of mCDW into the ice cavities, contributing to changes in melting and platform instability. Temporally, changes in wind patterns, sea ice formation and extent, and basal melting patterns are observed after the year 2011. While no major differences in transport were found in the studied sections between CTRL and SENST, an increase in the production of dense bottom and surface water masses, as well as the stratification process, was observed.

Keywords: Ice shelves. Basal melting. Oceanic numerical modeling. Water masses. Ice-ocean-atmosphere interactions.

IMPACTOS DO APORTE DE ÁGUA DOCE NA DINÂMICA COSTEIRA DA PENINSULA ANTARTICA

RESUMO

Este trabalho analisa o impacto da introdução de água doce no oceano decorrente do derretimento das plataformas de gelo na Península Antártica. A redução das plataformas de gelo não só contribuem para o aumento do nível do mar através do aumento nos fluxos de água doce para o oceano, como também tem potencial para alterar a circulação oceânica, a produção de gelo marinho na superfície, e a consequente estratificação, além de alterações nas características fisico-quimicas das massas de água. Aqui neste estudo verificamos os efeitos do derretimento basal (processo de derretimento na base das plataformas) na circulação, na produção de massas de água e de gelo marinho sobre o oceano que circunda a Península Antártica (mares de Bellingshausen e de Weddell). Para isso, utilizou-se o modelo regional oceânico ROMS (Regional Ocean Model System) para simular os mecanismos dinâmicos e termodinâmicos dessa região. Devido a limitações do modelo, a espessura e área das plataformas permanece inalterado durante toda a simulação. Foram realizados dois experimentos: um experimento controle (CTRL) e um experimento de sensibilidade (SENST). O experimento CTRL (com o efeito do derretimento) conseguiu reproduzir as principais feições oceanográficas ao longo do período da simulação (2002-2020). No teste de sensibilidade (SENST), os fluxos de sal e calor que representam os fluxos de água doce do derretimento, foram zerados. Foi observado o aumento na produção de gelo marinho na região costeira no experimento CTRL em relação ao SENST, devido às plumas da água doce extremamente frias resultante do derretimento sobre essas regiões. Também observou-se um aumento na produção das águas densas de fundo que se originam dos processos de mistura sob as plataformas, da água extremamente fria ISW, oriunda do derretimento, com as águas circumpolares profundas modificadas (mCDW), que adentram as cavidades das plataformas, assim como as águas super salinas e densas (HSSW) resultantes do processo de produção de gelo marinho. Observou-se também um aumento na concentração de gelo marinho no experimento CTRL, na região do giro de Weddell, assim como uma intensificação do giro. O aumento na concentração de gelo marinho, afetados pelos ventos catabáticos (ventos fortes e constantes oriundos do interior do continente) e de oeste, conduzem o gelo para o centro do giro, a intensidade da corrente é afetado pela variação no estresse do vento sobre o oceano, devido as alterações na espessura de gelo marinho na superfície. Sobre o mar de Bellingshausen, a intensificação dos ventos de oeste aumentam a circulação da mCDW para dentro das cavidades de gelo, contribuindo para as alterações no derretimento e instabilidade das plataformas. Temporalmente, nota-se uma mudança sobre os padrões de vento, de formação e extensão do gelo marinho e do derretimento basal, após o ano de 2011. Não foram encontrados grandes diferenças no transporte nas seções estudadas entre CTRL e SENST, porém, foi possível observar o aumento na produção das massas de água densas de fundo, e de superfície, assim como o processo de estratificação.

Palavras-chave: Plataformas de gelo. Derretimento basal. Modelagem numérica oceânica. Massas de água. Interações gelo-oceano-atmosfera.

LIST OF FIGURES

Page

LIST OF TABLES

Page

LIST OF ABBREVIATIONS

AABW	–	Antarctic Bottom Water
AASW	–	Antarctic Surface Water
AACC	–	Antarctic Coastal Current
ACC	–	Antarctic Circumpolar Current
AIRS	–	Atmosphere Infrared Sounder
ALOS	–	Advanced Land Observing System
AP	–	Antarctic Peninsula
APB	–	Autonomous Pinniped Bathythermographs
ASF	–	Antarctic Slope Front
ASL	–	Amundsen Sea Low
ATMOS	–	Antarctic Modeling Observation System
BM	–	Basal Melting
BMB	–	Basal mass balance
BT	–	NASA Bootstrap
CDW	–	Circumpolar Deep Water
CMIP6	–	Coupled Model Intercomparison Project Phase 6
COI	–	Cone of influence
CTRL	–	Control Experiment
DSW	–	Dense Shelf Waters
ECMWF	–	European Center for Medium-Range Weather Forecast
EVP	–	Elastic-viscous-plastic
GLORYS	–	Global Ocean Physics Reanalysis
GRACE	–	Gravity Recovery and Climate Experiment
HSSW	–	Highly Salinity Shelf Water
InSAR	–	Interferometric Synthetic Aperture Radar
INSTANT	–	INStabilities & Thresholds in ANTarctica
ISW	–	Ice Shelf Water
LCDW	–	Lower Circumpolar Deep Water
LIS	–	Larsen Ice Shelves
LTER	–	Long-Term Ecological Research
mCDW	–	Modified CDW
MOC	–	Meridional Overturning Circulation
mWDW	–	Modified Warm Deep Water
NT	–	NASA Team
OIB	–	Operation IceBridg
OSTIA	–	Operational Sea Surface Temperature and Sea Ice Analysis
PALSAR	–	Polarimetric SAR
PROANTAR	–	Brazilian Antarctic Program
REMA	–	Reference Elevation Model of Antarctica
RMSE	–	Root mean squared errors
ROMS	–	Regional Ocean Modeling System
sACC	–	Southern branch of the ACC
SAM	–	Southern Annular Mode

SCAR	–	Scientific Committee for Antarctic Research
SENST	–	Sensitivity Experiment
SH	–	Southern Hemisphere
SIC	–	Sea-ice concentration
SIE	–	Sea-ice extent
SLE	–	Sea level equivalent
SMB	–	Surface mass balance
SO	–	Southern Ocean
SSH	–	Sea surface height
SST	–	Sea surface temperature
STF	–	Subtropical Front
SW	–	Surface Water
SWOT	–	Surface Water Ocean Topography
UCDW	–	Upper Circumpolar Deep Water
WAP	–	Western Antarctic Peninsula
WDW	–	Warm Deep Water
WOD	–	World Ocean Database
WSBW	–	Weddell Sea Bottom Water
WSDW	–	Weddell Sea Deep Water
WW	–	Winter Water

LIST OF SYMBOLS

C	–	scalar quantity (i.e. temperature, salinity)
C_{pi}	–	specific heat of ice
C_{pw}	–	heat capacity of seawater at 0°C
E	–	evaporation
f	–	Coriolis parameter
g	–	acceleration of gravity
h	–	depth of sea floor below mean sea level
H_z	–	vertical grid spacing
K_C	–	vertical eddy diffusivity
K_M	–	vertical eddy viscosity
L	–	latent heat of fusion
P	–	precipitation
P	–	total pressure
S	–	salinity
S_w	–	salinity in the first layer
T	–	temperature
t	–	time
T_w	–	sea temperature in the first (uppermost) layer
u, v, w	–	are the (x, y, z) components of vector velocity $\vec{v}$
X_{obs}	–	reference data
X_{ROMS}	–	analysis data
x, y	–	horizontal coordinates
z	–	vertical coordinate
$\mathcal{D}_u, \mathcal{D}_v, \mathcal{D}_C$	–	optional horizontal diffusive terms
$\mathcal{F}_u, \mathcal{F}_v, \mathcal{F}_C$	–	forcing/source terms
ΔT	–	temperature difference between the interior and the base freezing temperature
γ^n	–	neutral density
γ_s	–	turbulent exchange coefficient for salt
γ_T	–	turbulent exchange coefficient for heat
ν	–	molecular viscosity
ν_θ	–	molecular diffusivity
ϕ	–	dynamic pressure
ρ	–	mixing layer density
ρ_i	–	average ice density
θ	–	potential temperature
ζ	–	surface elevation

CONTENTS

Page

1 INTRODUCTION

Freshwater fluxes have a significant role in the ocean structure, impacting stratification, circulation, heat, and formation of water masses, as well as contributing to sea-level rise. In recent decades, the increased enhancement of freshwater in the Southern Ocean (SO) led to complex changes in its structure and dynamics (SWART et al., 2018; BLUNDEN; BOYER, 2021). Increasing melting, precipitation, and river flow in SO, has diminished the salinity of the ocean near Antarctica, and enhanced the buoyancy of surface waters (SHI et al., 2020). In consequence, this process can lead to a stable layer of less dense water, inducing stratification. Hence, the vertical mixing of water masses and the exchange of heat and nutrients in the water column can be affected (HENLEY et al., 2020; SCHULTZ et al., 2020). The less dense water can evolve into water masses with a different characteristic than surrounding waters, affecting the ocean's overall water mass structure and composition. Also, it can inhibit sinking and disrupt deep water formation. Due to the stratification, the fresher surface water can act as an insulating layer, reducing the exchange of heat between the ocean and the atmosphere (Integorvernamental Panel on Climate Change (IPCC), 2022). Consequently, the circulation patterns in these regions can be altered, affecting large-scale ocean currents (HASKINS et al., 2020) and resulting in regional variations in sea surface temperature, which can impact global heat transport patterns.

At high latitudes, there is a complex structure of processes that contribute to the introduction of freshwater into the ocean. The export and transport of freshwater, in all states (solid, liquid, and gaseous), are driven by and affect oceanic and atmospheric circulation on a large scale, which, in turn, is strongly influenced by global climate change (RYE et al., 2020; DOUVILLE; JOHN, 2021). High latitudes are also suffering from more frequent and intense heatwaves (FERON et al., 2021). Such changes in the hydrological cycle in high-latitude areas can lead to a critical imbalance in the storage of water over the continent and the consequent increase in the introduction of freshwater into the ocean.

The freshwater flowing into the Southern Ocean originates from the melting of sea ice, the ice sheet, ice shelves and glaciers (which also contribute to iceberg introductions), and precipitation. Due to global warming, there has been an observed increase in freshwater input to the region, affecting not only the ocean but also atmospheric dynamics, influencing wind patterns, air temperature, and humidity (BOISVERT et al., 2020; HOLLAND et al., 2020; ROBINSON et al., 2020). For an understanding of

the processes in the region, the variables that need to be measured include: i) atmospheric circulation (winds, storms, evaporation, precipitation, moisture fluxes); ii) horizontal and vertical ocean circulation, including exchange between high and low latitudes and circulation beneath the sea ice through the annual cycle; iii) extent, thickness, and distribution of sea ice; and iv) the contribution of glacial ice (melting from ice shelves and iceberg production).

Changes in freshwater input due to increased precipitation in high latitudes as the atmosphere warms (MARSHALL et al., 2017) or increased glacial melting (BINTANJA et al., 2013; SILVANO et al., 2018) would also alter buoyancy and water mass formation in the Antarctic Ocean, with implications for circulation. The Southern Annular Mode (SAM) and the El Niño-Southern Oscilation (ENSO) can affect the distribution of sea ice, with the response signal depending on the timescale considered (FERREIRA et al., 2015; STAMMERJOHN et al., 2008). Also called Antarctic Oscillation (AAO), SAM is a phenomenon related to the north-south movement of the westerly winds around Antarctica. The positive and negative phases of ENSO and SAM result in different effects on the winds and consequently sea ice and weather over the AP (STAMMERJOHN et al., 2008). In positive SAM events, the belt of strong winds is contracted towards the Antarctic continent, resulting in increased wind strength near the shelf, this causes higher CDW upwelling around AP and West Antarctica. The immediate response to increased westerly winds is the intensification of northward transport of cold water by Ekman and the expansion of sea ice (PURICH et al., 2016).

Projections from the Coupled Model Intercomparison Project Phase 6 (CMIP6) indicate that the hydrologic cycle is intensifying (DOUVILLE et al., 2021). The projections show an increased global precipitation of 1-3% per Kelvin of global surface warming (SILER et al., 2019). Significant changes in the latitudinal distribution of Precipitation (P) and Evaporation (E) are expected, resulting in a difference of P-E increasing over the tropics and high latitudes and diminishing in the subtropics, which is more significant over the higher emission scenarios (DOUVILLE et al., 2021). The intensified moisture transport, the increased precipitation and evaporation over the land and global ocean, and the consequent increased runoff, partly driven by glacier melting, characterize a more intense water cycle due to global warming.

The input of freshwater and ice flows into the ocean directly impacts sea level and, in conjunction with sea ice melting, plays a crucial role in maintaining thermoha-

line circulation (MA; WU, 2011). Ice/snow/water balance changes directly affect global climate processes: alterations in radiative balance response, ocean stratification stability, thermohaline circulation, and the carbon and methane source-sink state (Integorvernamental Panel on Climate Change (IPCC), 2007; Integorvernamental Panel on Climate Change (IPCC), 2019). In summary, the processes involving the intrusion of freshwater into the Southern Ocean include the calving of large ice shelves from the continent, glacier dynamics and calving fronts, which give rise to icebergs, and the interaction between the ocean and ice shelves, contributing through basal melting. Critical atmospheric processes include katabatic and circumpolar winds, which are of high magnitude and affect the circumpolar currents, water, and air temperature. Evaporation/sublimation and precipitation processes must also be considered, as they influence the formation and ablation of ice masses. Another significant phenomenon occurring over the ocean in the Antarctic region is the formation of polynyas. Polynyas are areas of open water within the sea ice pack, on which they have a significant effect on both the ocean and atmosphere, as the enhanced exchange of energy and moisture occurs in these areas. These openings allow the nutrient exchange (productivity "windows") and significant regions of overturning (mass exchange between different depths in the water column, and connection with the atmosphere). In these regions, the atmospheric processes and heat exchange between the ocean and the atmosphere occur, affecting the water balance through evaporation and sublimation. Satellite data is crucial for understanding this phenomenon, as it mainly occurs in winter, along with data from instruments attached to marine animals and drifters (SHEPHERD et al., 2018a).

The Antarctic region has, on average, shown positive trends in sea ice extent between 1978 (the beginning of the satellite era) and 2014. However, after this period, the ice coverage exhibited unpredictable interannual variability (COMISO et al., 2017; TURNER; COMISO, 2017; PARKINSON, 2019) and is now experiencing record lows over the satellite era (RAPHAEL; HANDCOCK, 2022; PURICH; DODDRIDGE, 2023). The balance between ice loss and gain in the region is uneven: the extent has increased over the Ross and Weddell Seas, offset by the decrease in the Bellingshausen Sea. This ice accumulation and loss process along the Antarctic coast is partly explained by variations in wind, driven by stratospheric ozone depletion and increased greenhouse gas concentrations (SIGMOND; FYFE, 2010; SWART et al., 2018).

The increase in the concentration of freshwater over the ocean's surface layers, originating from the melting of Antarctic ice shelves and variations in precipitation, can

explain the increase in sea ice (HAUMANN et al., 2016). These processes reduce the water's surface density (freshwater is less dense than saltwater), reducing convection and increasing water mass stratification. Changes in stratification are indicated by various studies, showing, in particular, a decrease in surface salinity in the Ross Sea (HAUMANN et al., 2016; PAULING et al., 2016; PAULING et al., 2017). And, the circumpolar intensification of vertical salinity and temperature gradients near the surface due to the intensification of the vertical gradients due to sea ice melt (leading to fresh/warm surface areas) (STEIN et al., 2020). The transport of freshwater northward occurs as sea ice forms in relatively cold regions near the continent and releases freshwater further after transport by winds and ocean currents, resulting in significant changes in salinity distribution in the Antarctic Ocean (HAUMANN et al., 2016).

The Antarctic sea ice zone is characterized by the presence of Circumpolar Deep Waters (CDW) beneath the intermediate layer, which is warmer compared to surface waters (LECOMTE et al., 2017). Increased stability due to decreased surface salinity results in reduced vertical heat flux toward the surface layer. This ultimately favors ice production and inhibits its melting (BRONSELAER et al., 2018). The intense upward oceanic heat flux to the ice in the Antarctic Ocean is indeed a central element in sea ice development, and minor variations in its magnitude have a significant impact on ice thickness and extent, including the formation of polynyas (RINTOUL, 2018). The heat content near the surface of the Southern Ocean is critical for limiting the seasonal development of sea ice (MARTINSON, 1990), and its warming can, therefore, influence global climate by affecting Earth's albedo. Furthermore, ocean warming accelerates the melting of Antarctic ice shelves (SCHMIDTKO et al., 2014; ADUSUMILLI et al., 2020), threatening the stability of ice sheets on the continent (PAOLO et al., 2015), with global implications for sea-level rise (HELLMER et al., 2012). Although local-scale wind and wave forcings appear to be factors driving the observed sea ice trends, the relationship between changes in ice movement and breakage and sea surface temperature is not clear.

The Arctic and Antarctic regions have shown the most rapid warming rates in recent decades (about one degree Celsius per decade in the Arctic) (BANERJEE et al., 2020). There are contrasting scenarios in Antarctica, where East Antarctica mainly presented cooling trends, while West Antarctica presented warming and high loss of water to the ocean (MEREDITH et al., 2019). Eighty-seven percent of glaciers in the Antarctic Peninsula (AP) have retreated since records began in the 1950s decade (COOK, 2005), with ice loss accelerating in AP glaciers since the 2000s (WOUTERS

et al., 2015). The AP has increased its contribution of meltwater into the ocean during the last few decades (ADUSUMILLI et al., 2018). With the increasing temperature and consequent increase of meltwater being introduced into the ocean, the oceanic structure in these areas has changed in recent decades (ABERNATHEY et al., 2016).

The ice shelves are the floating part of the ice sheets. They represent the connection between the ocean and the continent. They work as a support or buttress to slow down the ice sheet movement in the sea's direction, potentially contributing to sea level rise (KONRAD et al., 2018). The increased instability of ice shelves, guided by the increased basal melting, can contribute to the consequent loss of mass of the ice sheet ((ADUSUMILLI et al., 2020; SMITH et al., 2020), Figure 1.1). West Antarctica is where the major losses are happening, dominated by ice discharge, with the rates of mass loss increasing from 37 ± 19 Gt yr^{-1} between 1992 and 1996 to 131 ± 21 Gt yr $^{-1}$ in 2012-2016, for the years 2017 to 2020 slowly slighted to 94 ± 25 Gt yr^{-1} (OTOSAKA et al., 2023). The AP presented a negative mass balance of -20 ± 15 Gt yr^{-1} in the last 25 years, with an increase of 15 Gt yr^{-1} since 2000 (SHEPHERD et al., 2018b), associated with the ice shelf collapse (COOK; VAUGHAN, 2010; ADUSUMILLI et al., 2018). However, between 2012 and 2016 the AP experienced an average reduction to 6 ± 13 Gt yr^{-1}, caused in part by the extreme snowfall in 2016 (WANG et al., 2021; CHUTER et al., 2022), with an increasing back between 2017 and 2020 to 21 ± 12 Gt yr^{-1} (OTOSAKA et al., 2023). As a consequence, the West Antarctica and AP are experiencing major changes and instabilities since the start of observations, and are the most sensitive to global warming effects.

Basal melting refers to the melting of ice that occurs beneath floating ice shelves, at the interface between the ocean and the continent. The basal melting with the horizontal motion of ice shelves (including divergence and convergence), causes variations in the thickness of the ice shelf, driven by variations in the rate of basal melting. Indirectly, the basal melting modulates the mass loss of the grounded ice sheet and contributes to the freshwater runoff, which influences climate processes in the Southern Ocean (ADUSUMILLI et al., 2020; GWYTHER et al., 2015; GWYTHER et al., 2020; SCHODLOK et al., 2016). Additionally, this process can be externally forced, for example, by climate change, interannual and multidecadal climate modes, the annual cycle, or tides. Studies have shown that a thick Deep Circumpolar Water (CDW) layer can increase the rates of basal melting of floating ice shelves (BINTANJA et al., 2013; COOK et al., 2016; WOUTERS et al., 2015; HOLLAND et

Figure 1.1 - Mass changes, basal melt, and thermal forcing around Antarctica.

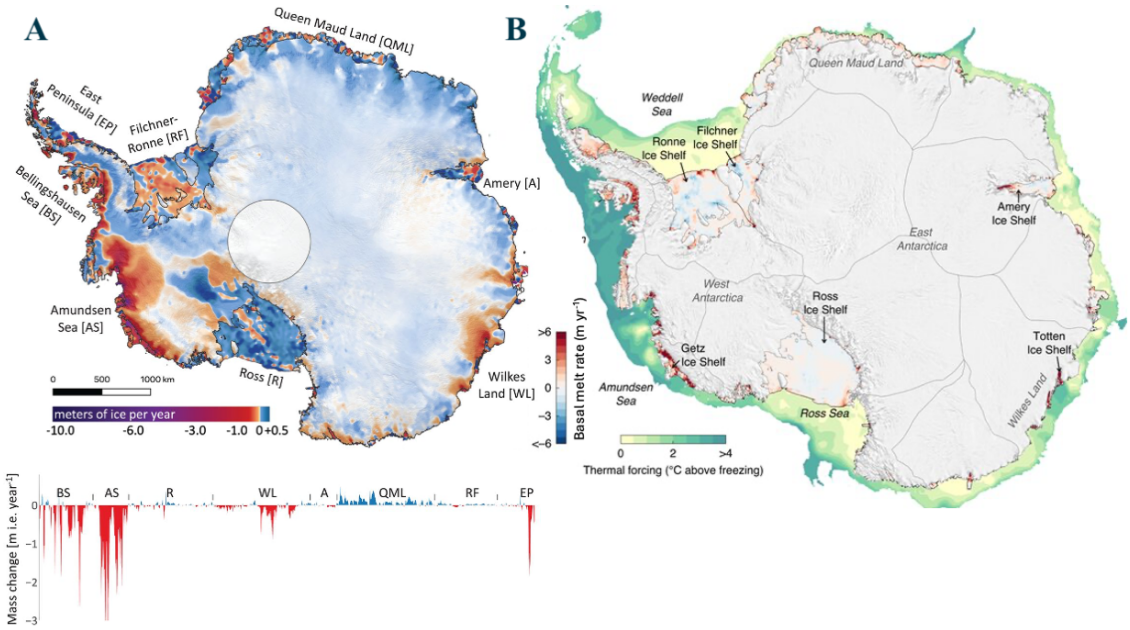

A. Mass loss from Antarctica from 2003 to 2019. The graph under the map represents the mass changes at the grounding line. B. Basal melt rates of Antarctic ice shelves averaged over 2010 - 2018. Units presented by meters of ice equivalent per year, assuming the ice density of 917 kg m^{-3}. Thermal forcing is defined as the temperature above seawater's in situ freezing point, mapped for depths shallower than 1,500 m. The seafloor thermal forcing is shown for water depths less than 200 m, and for water depths >200 m, the maximum thermal forcing between 200 m and 800 m is shown.

SOURCE: Smith et al. (2020) and Adusumilli et al. (2020).

al., 2010), demonstrating a direct link between the ocean and the cryosphere. Sea ice extent is also declining in the West region of the Antarctic Peninsula (PARKINSON; CAVALIERI, 2012; PARKINSON, 2019; SMITH et al., 2020). Although there are several theories about the causes of these changes, the result is a change in the freshwater balance of the region.

Numerical modeling is highly valuable in aiding the understanding of natural phenomena, such as the impact of climate change, particularly in high latitudes. This tool allows for the analysis of the effects of each component, whether oceanic or atmospheric. Parise et al. (2015) conducted sensitivity tests to assess the impact of variations in sea ice coverage on the Southern Ocean and its influence on regional climate, particularly the formation of cyclones in high latitudes and its effects on precipitation in South America. Through these simulations, the authors were able to evaluate the duration of sea ice persistence and the impact of maximum sea ice

coverage on the atmosphere.

The AP, situated between the Bellinghshausen Sea (to the West) and the Weddell Sea (to the East), is a prolonged (more than 1000 km) and narrow (approximately 100 km) mountain chain that composes the northern lands of Antarctica (BENTLEY, 2013). Divided by the Drake Passage to the south of South America, which connects the Pacific to the Atlantic Oceans, this area is dominated by contrasted climate regimes. The Bellingshausen Sea presents warmer waters and higher glacial and sea-ice melting rates, typically with a cold oceanic climate. At the same time, on the Weddell Sea, the semi-closed geography sustains much colder conditions, characteristically under a cold polar-continental regime. The AP is considered a climate hotspot, where we can verify more pronounced climate change effects (RIGNOT, 2004; MEREDITH; KING, 2005; KERR et al., 2018; KERR et al., 2018).

On the west side of AP, the Bellinghshausen Sea has experienced diminishing sea ice and rapid warming of the atmosphere and ocean (SHOKR; YE, 2023). Consequently, the ice shelves, in the majority, have experienced collapses and retractions of ice shelves, and accelerations and thinning of ice sheets (ANDREASEN et al., 2023). Oceanographically, the region is guided by the Antarctic Circumpolar Current (ACC) flowing from west to east. A very weak Antarctic Coastal Current (AACC) flows in the opposite direction (MOFFAT; MEREDITH, 2018). The topography along the shelf conducts the warm CDW, which flows onto the shelf, conducting a warm circulation in the shallower waters near the coast. At the bottom, signals of the Antarctic Bottom Water (AABW) can be found outside the shelf (ORSI et al., 1999). This region does not present signals of AABW production. It is widely influenced by the waters produced from the Weddell Sea (MORRISON et al., 2023).

At the east of AP, the Weddell Sea is most influenced by the continental cold and dry weather. The general circulation is characterized by the elongated cyclonic gyre, named Weddell Gyre (WG), which is limited by the AP at the West, by the Scotia Ridge at the North, extending until 20 to 30°E. Over this region, intense exchange occurs between the surface and bottom waters, mainly due to polynya processes. Over this region, the formation of the Weddell Sea Bottom Water (WSBW) and the Weddell Sea Deep Water (WSDW) occurs. These two water masses will be the basis for AABW formation, which impacts the main deep water properties, influencing thermohaline and global ocean circulation (CARMACK; FOSTER, 1975). Along the southern WG, the Filchner and Ronne ice are giant floating ice shelves where there is intense mixing and influence over water masses shelves production and

modifications. Along the East AP (West Weddell Sea), the Larsen Ice shelves also contribute to the formation of water masses through melting processes, and they are the most impacted by retreat and collapses during the last decades (SHEPHERD et al., 2003).

In recent years, the West and North AP have shown accelerated warming (SANTINI et al., 2018; SMITH et al., 2020). This region has experienced dramatic reductions in the extent (COOK; VAUGHAN, 2010; ETOURNEAU et al., 2019) and thickness (PAOLO et al., 2015) of ice shelves in recent decades. In the northeast part of AP (connection to the Weddell Sea through the Coastal Current), the collapse of the Prince Gustav and Larsen A ice shelves in 1995 was followed by the rapid collapse of most Larsen B ice shelves in 2002. On the west side of AP (Bellingshausen Sea), the Müller, Jones, and Wordie ice shelves collapsed or retreated substantially. The Wilkins ice shelf lost a significant part of its area during major breakup events in 2008 and 2009 (COOK; VAUGHAN, 2010). Most of the remaining ice shelves on the AP have experienced changes in the height of their surfaces as measured by satellite altimeters (PRITCHARD et al., 2012; PAOLO et al., 2015; ADUSUMILLI et al., 2018; ADUSUMILLI et al., 2020). The ice shelf melting and freshwater increase into the ocean can also trigger shifts in local and global circulation, water and air temperature, and consequently the climate system.

1.1 Motivation

Ice shelves and glaciers play an important role in the hydrological cycle, representing the interface and a significant contributor of freshwater to the ocean. There has been an observed increase in instability and a decrease in the area of ice shelves in the last decades. Consequently, this process provides freshwater to the ocean through basal melting or the release, and subsequent melting, of icebergs. Changes in the freshwater balance in the Southern Ocean can have profound impacts on ocean circulation, but there are still many questions surrounding the quantification of the variation in freshwater flux and content.

The Southern Ocean Observing System(SOOS) Statement 2023, developed at Hobart, Australia, at the end of the first SOOS Symposium during August 2023, highlights the importance of studies at SO, in front of the climate change impacts, which are impacting significantly the dynamics over this region. The Southern Ocean Observing System (SOOS), is a coordinated body of researchers whose main focus is to enhance and ensure data acquisition and sharing, to provide the network to develop a mainframe about the SO understanding. The establishment of a broader

view of the different processes that occur at SO can give support to policies and regulations, thereafter improving the prediction of future states. As part of the Antarctic Modeling Observation System (ATMOS) and INStabilities & Thresholds in ANTarctica (INSTANT/SCAR) projects, the aim is to contribute to the advancement of regional ocean modeling studies and contribute to the comprehension of the role of the freshwater from ice shelf melting around the AP. The ATMOS project is part of the Thematic Line "Climate Change and the Southern Ocean" - CNPq/MCTIC/CAPES FNDCT 21/2018 and is structured around *in-situ* data acquisition and collection, as well as coupled regional modeling, with the objective of studying the processes of Ocean-Wave-Atmosphere-Ice Interaction. The INStabilities & Thresholds in ANTarctica (INSTANT) Scientific Research Programme (SRP) is an initiative from the Scientific Committee for Antarctic Research (SCAR), whose main aim is to comprehend the contributions to sea level rise, encompassing different science topics related to this, such as geosciences, biology, and physical sciences.

The understanding of the rate of freshening in southern high latitudes is still developing, which gives uncertainty and deals with modeling strategies of ice-ocean interaction. Freshwater fluxes strongly contribute to the ocean dynamics and characteristics in the Antarctic marginal seas. The sea ice formation is closely related to freshwater fluxes, shaping the ocean's potential to melt ice shelves, contributing to the dense water masses production, which, in turn, conducts the deep overturning circulation. On a minor scale, the very cold fresh water from the ice shelf basal melting flowing over the surface contributes to the increase of local sea ice production. It is like a cycle where everything is interconnected.

Investigations about these dynamics, from regional numerical modeling, can potentially help to improve climate and earth system models (which still have high uncertainties in polar areas) and increase confidence in projecting potential impacts due to climate change. This work is unprecedented in focusing on ice shelf meltwater sensitivity experiments around the AP, which region presents complex and opposing dynamics on both sides: Weddell and Bellingshausen Seas.

1.2 Objective

This thesis aims to understand the impact of increased freshwater input into the oceanic system from the basal melting of floating ice shelves near the AP. This includes studying this process's temporal and spatial variations and its overall significance in the freshwater balance in the region near the Antarctic Peninsula.

1.2.1 Specific objectives

The specific objectives that guide this study are:

1) To simulate the ice shelf basal melting effects on sea ice formation over the continental shelf region.

2) To estimate the contribution of freshwater to the stratification of oceanic water masses and its influence on their formation.

3) To assess how the contribution of freshwater discharge along the AP affects the coastal currents of the Bellingshausen and Weddell Seas.

1.3 Dissertation structure

This dissertation is organized into chapters (Figure 1.2). The first chapter briefly introduces this study's topic, with the thesis's motivation and aims. The second chapter presents the theoretical background concerning the numerical model used in this thesis. The third chapter presents theoretical background related to the study area and topic, through the review article published in the Annals of Brazilian Academy of Science (LIMA et al., 2022), entitled *"Glacial meltwater input to the ocean around the Antarctic Peninsula: forcings and consequences"*. Chapter 4 presents the article entitled *"The role of ice shelf basal melting on water mass structure and ocean dynamics around the Antarctic Peninsula"* to be submitted to *The cryosphere Journal* — this chapter describes the model results and basal melting effects evaluated through sensitivity experiments. Finally, Chapter 5 discusses the overall results and conclusions of the dissertation.

Figure 1.2 - Flowchart of dissertation structure.

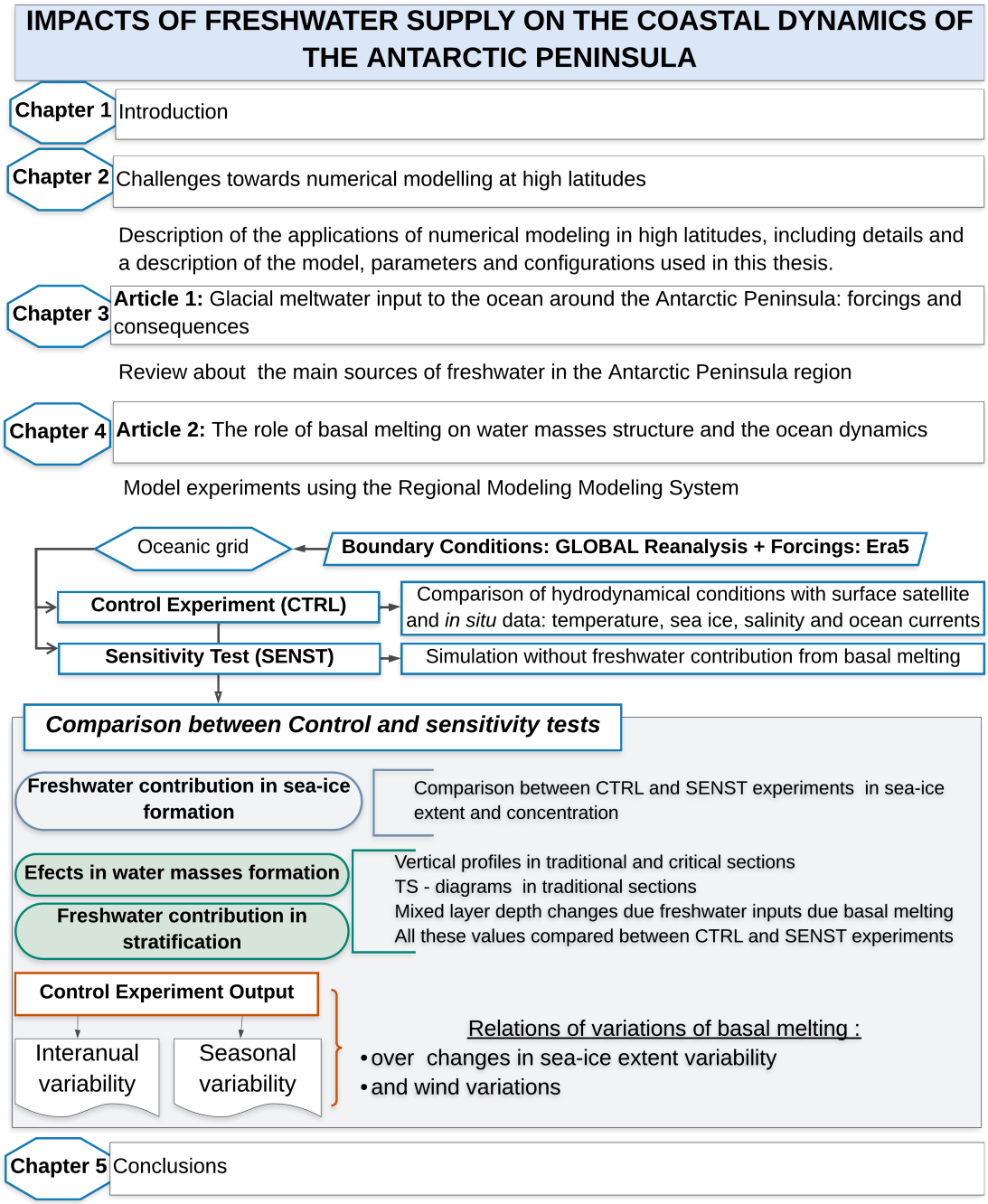

Chart of processes of the thesis structure.

SOURCE: Author.

2 CHALLENGES TOWARDS NUMERICAL MODELING AT HIGH LATITUDES

2.1 Introduction

The numerical representation of natural environmental processes is challenging due to their inherent complexity and randomness. However, searching for patterns and understanding how they occur not only aids in comprehension but also in how they are related. Numerical modeling serves to replicate and understand how natural processes occur and how they are interconnected. In addition to enabling the reproduction and deduction of natural processes based on the laws of physics, these processes are complex to observe due to the difficulty of access directly. Furthermore, they offer the possibility of generating projections (scenarios) based on specific conditions (MCGUFFIE; HENDERSON-SELLERS, 2001). This tool has a wide number of applications at high latitudes; examples of applications at SO, are the numerical replication of paleoclimatic scenarios (GASSON; KEISLING, 2020), future projections (TEWARI et al., 2022), weather predictions (POWERS, 2007), and even study cases of specific events and processes (KUSAHARA et al., 2018), and also eco/biological (HENSCHKE et al., 2023; DUVIVIER et al., 2023) and biogeochemical studies (KUSTKA et al., 2015; MACK et al., 2019), and sensitivity tests testing the impact of a specific variable over the system (DINNIMAN et al., 2012).

At high latitudes, we deal with a complex set of processes: the presence of sea ice, frequent high-speed winds, low temperatures, and a significant variation in radiation fluxes throughout the year. Consequently, these areas are also crucial concerning the ventilation of the thermohaline circulation and the formation of deep waters (CAI et al., 2023). Understanding the processes that occur in these regions plays a fundamental role in comprehending the global climate, the nutrient cycle in the oceans, and the response of the climate system to global changes. Moreover, high latitudes play an essential role in climate regulation and the Earth's balance, making them an area of great interest for scientific research and modeling studies. Accurate numerical representation of these processes is paramount since *in-situ* data collection and remote sensing are limited. Based on this premise, numerical modeling becomes an essential tool for the study and understanding of the hydrodynamic processes occurring beneath the platforms.

In regions with complex and hard access, numerical modeling can be a crucial tool to corroborate hypotheses and improve the knowledge about the complexities of the study focus. Antarctica and the surrounding ocean are vital to the Earth's cli-

mate balance. Although this region faces some challenges in acquiring *in situ* data, remote sensing techniques also have limitations in collecting precise surface and subsurface data, especially during the winter. The use of computational tools, such as numerical modeling, helps to replicate processes to enhance understanding of their potential impacts and changes. That being said, the numerical representation of climate processes and the refinement of these are extremely useful tools for identifying changes and generating forecasts. In the case presented in this dissertation, it is about verifying how the Southern Ocean has been behaving in recent decades. Consequently, evaluate the impacts of changes in the water balance caused by the input of freshwater due to the melting of the ice shelf base.

Here, we will briefly describe some challenges related to modeling at high latitudes, followed by an emphasis on the model description and configurations used in this dissertation. The oceanic simulations in this study employed the Regional Ocean Modeling System (ROMS) (HAIDVOGEL et al., 2008; SHCHEPETKIN; MCWILLIAMS, 2005). ROMS is a numerical model based on a free-surface representation, hydrostatic assumption, and terrain-following coordinate system, and is based on primitive equations of Navier-Stokes. The version used here is adapted from version 3.9, based on the Rutgers/UCLA Regional Ocean Model System, with sea-ice (BUDGELL, 2005) and ice shelf (DINNIMAN et al., 2007) code implemented. The code is available in github.

2.2 Southern Ocean modeling efforts

Freshwater fluxes around the Antarctic marginal seas are closely linked to sea ice formation, exerting a strong influence on ocean conditions, leading to the melting of ice shelves, and consequently, affecting the dense water masses that contribute to the deep overturning circulation. Reproducing these processes through modeling is a challenge, due to the complex processes and dynamics related to them.

When we model high-latitude regions, the stereographic projection is the best choice to avoid the distortions related to the transformation of the three-dimensional surface into a bi-dimensional plane surface (HAZIOT; MARYNETS, 2018). The stereographic minimizes distortions, preserves angles, and maintains consistent cell sizes, which are essential for accurately representing ice shelves and sea ice formation near the South Pole. Projections like Mercator are more suitable for equatorial regions and large areas, while Lambert projections are suitable for mid-latitude regions and smaller areas. Besides, this cartographic projection is widely used to reproduce the main processes in the Southern Ocean.

The vertical and horizontal resolution guides the precision in representing properly the processes that occur under shelves, but also the oceanographic conditions in the open ocean. Since the fact that the low stratification in coastal areas, and the higher Coriolis parameter, the Rossby deformation (which characterizes the spatial scale of eddies) around many ice shelves is small, compared with global patterns. These circulation patterns formed by eddies with smaller scales (4 to 8 km) influence the warmer mCDW flows under the ice shelves (ST-LAURENT et al., 2013; GILLE et al., 2016; DINNIMAN et al., 2016). The heat transport at the Antarctic continental shelf break is strongly influenced by eddies. In models where the eddies are well represented ("eddy-resolving"), the results present lower biases concerning the ocean temperature and stratification, mainly along the Bellingshausen ice shelves (warm mode (mode 2) ice shelf cavities) (MACK et al., 2019; BILGEN; KIRTMAN, 2020). However, increased high resolution requires more computational space and time processing.

There are many models that simulate the ice shelf/ocean interaction based on a three-dimensional primitive equation. Idealized and realistic models have been developed in recent years focused on improvements in the representation of ice-shelf dynamics. Efforts like the ISOMIP (Ice Shelf - Ocean Model Intercomparison Project), which is a Climate and Cryosphere (CliC) target activity of the World Climate Research Programme (WCRP), helped to improve the sub-ice shelf cavities dynamics. The comparison between different models with their particularities, idealized and realistic simulations, under the ISOMIP objective, such as the grid configurations and numerical components, gives us an overview and a comprehensive evaluation and validation of current sub-ice shelf cavity ocean models. Some of the models considered in ISOMIP, and ISOMIP+ (2nd Ice Shelf–Ocean Model Intercomparison Project), are the MITgcm (LOSCH, 2008), NEMO (Nucleus for European Modelling of the Ocean, (MATHIOT et al., 2017)), FVCOM - Finite Volume Community Ocean Model(ZHOU; HATTERMANN, 2020), COCO - CCSR Ocean Component Model,(KUSAHARA; HASUMI, 2013), MOM6 - Modular Ocean Model 6 (STERN et al., 2019), BRIOS - Bremerhaven Regional Ice Ocean Simulations (HELLMER, 2004), FESOM - Finite Element Sea-ice Ocean Model (TIMMERMANN et al., 2012), MetROMS (NAUGHTEN et al., 2018), ROMS (DINNIMAN et al., 2007).

The Whole Antarctic Ocean Model - WAOM (RICHTER et al., 2022), based on ROMS, is a high-resolution (approximately 2 km) circumpolar model that includes an ice shelf configuration and tidal effects but does not incorporate a sea-ice model. MetROMS (NAUGHTEN et al., 2018), based on ROMS version 3.6, features ice-

shelf thermodynamics and is coupled with the sea-ice model CICE version 5.1.2 (Community Ice CodE) using MCT 2.9 (LIPSCOMB et al., 2010). ROMS offers two sea-ice configurations: a simpler and more robust one (BUDGELL, 2005) integrated into the ROMS code and a more complex and detailed model, which is coupled with CICE under the COAWST framework. ROMS-Budgell is specifically designed for regional ocean simulations, focusing on ocean-ice interactions, and employs an EVP rheology for sea ice dynamics based on the thermodynamics model by Mellor e Kantha (1989), featuring a single ice and snow layer. In contrast, ROMS-CICE combines the ROMS model with the CICE sea-ice model and exchanges information between them through the MCT coupling. CICE employs dynamic-thermodynamic modeling with multiple ice thickness layers and energy-conserving thermodynamics.

2.3 Hydrodynamical ocean model structure

The Regional Ocean Model System (ROMS) is a tridimensional numerical model of high resolution, written in F90/F95. Several coupled models use it for biogeochemical, air-sea interactions, sediment, and sea ice applications. Composed by a set of several physical and numerical algorithms that integrate the primitive Reynolds equations, discretized by finite difference methods, solving the Navier-Stokes equations. This model assumes Boussinesq approximations (constant pressure), except in the contribution to the buoyant force in the motion and hydrostatic equation, where it assumes the vertical pressure gradient equals the buoyant force (SHCHEPETKIN; MCWILLIAMS, 2005; HAIDVOGEL et al., 2008). Vertical coordinates are expressed in sigma coordinates (Figure 2.1) and horizontal coordinates are expressed in Cartesian coordinates in an Arakawa-C type grid. This brings great computational ease when it is used to model areas with uneven reliefs.

The barotropic and baroclinic modes are solved separately (split-explicit time-step scheme), preserving the volume conservation and consistency necessary for the tracers (SHCHEPETKIN; MCWILLIAMS, 2005). The dynamical equations, in the form of flux in horizontal Cartesian coordinates and as a function of sigma coordinates, are given by Equation 2.1 for the zonal component, Equation 2.2 for the meridional component, and Equation 2.3 for the vertical component. The continuity equation is given by Equation 2.4, and scalar transport is described by Equation 2.5.

$$\frac{\partial u}{\partial t} + \vec{v} \cdot \nabla u - fv = -\frac{\partial \phi}{\partial x} - \frac{\partial}{\partial z}\left(\overline{u'w'} - \nu \frac{\partial u}{\partial z}\right) + \mathcal{F}_u + \mathcal{D}_u \tag{2.1}$$

$$\frac{\partial v}{\partial t} + \vec{v} \cdot \nabla v + fu = -\frac{\partial \phi}{\partial y} - \frac{\partial}{\partial z}\left(\overline{v'w'} - \nu \frac{\partial v}{\partial z}\right) + \mathcal{F}_v + \mathcal{D}_v \tag{2.2}$$

$$\frac{\partial \phi}{\partial z} = \frac{-\rho g}{\rho_o} \tag{2.3}$$

$$\frac{\partial u}{\partial x} + \frac{\partial v}{\partial y} + \frac{\partial w}{\partial z} = 0. \tag{2.4}$$

$$\frac{\partial C}{\partial t} + \vec{v} \cdot \nabla C = -\frac{\partial}{\partial z}\left(\overline{C'w'} - \nu_\theta \frac{\partial C}{\partial z}\right) + \mathcal{F}_C + \mathcal{D}_C. \tag{2.5}$$

An equation of state is also required:

$$\rho = \rho(T, S, P) \tag{2.6}$$

Where: $C(x, y, z, t)$ is the scalar quantity(i.e. temperature, salinity), $\mathcal{D}_u, \mathcal{D}_v, \mathcal{D}_C$ are optional horizontal diffusive terms, $\mathcal{F}_u, \mathcal{F}_v, \mathcal{F}_C$ are forcing/source terms, $f(x, y)$ is the Coriolis parameter, g is the acceleration of gravity, $h(x, y)$ represents the depth of sea floor below mean sea level, $H_z(x, y, z)$ is the vertical grid spacing, ν, ν_θ is the molecular viscosity and diffusivity, K_M and K_C are the vertical eddy viscosity and diffusivity, P represents the total pressure ($P \approx -\rho_o g z$), $\phi(x, y, z, t)$ is the dynamic pressure ($\phi = (P/\rho_o)$), $\rho_o + \rho(x, y, z, t)$ is total *in situ* density, salinity and temperature are represented by $T(x, y, z, t)$ and $S(x, y, z, t)$, time is t, u, v, w are the (x, y, z) components of vector velocity $\vec{v}$, x and y are the horizontal coordinates, z is the vertical coordinate, and $\zeta(x, y, t)$ is the surface elevation.

The overbar represents the time average, and the prime represents the mean fluctuation. These equations are closed by parameterizing the Reynolds stresses and turbulent tracer fluxes as:

$$\overline{u'w'} = -K_M \frac{\partial u}{\partial z}; \qquad \overline{v'w'} = -K_M \frac{\partial v}{\partial z}; \qquad \overline{C'w'} = -K_C \frac{\partial C}{\partial z}. \tag{2.7}$$

The vertical and horizontal boundary conditions structure and the detailed description of the grid computation can be found in the Technical Manual, by Hedström (2018). This manual also describes all the functions and options of numerical schemes available on ROMS.

Figure 2.1 - Sigma configuration with ice shelves.

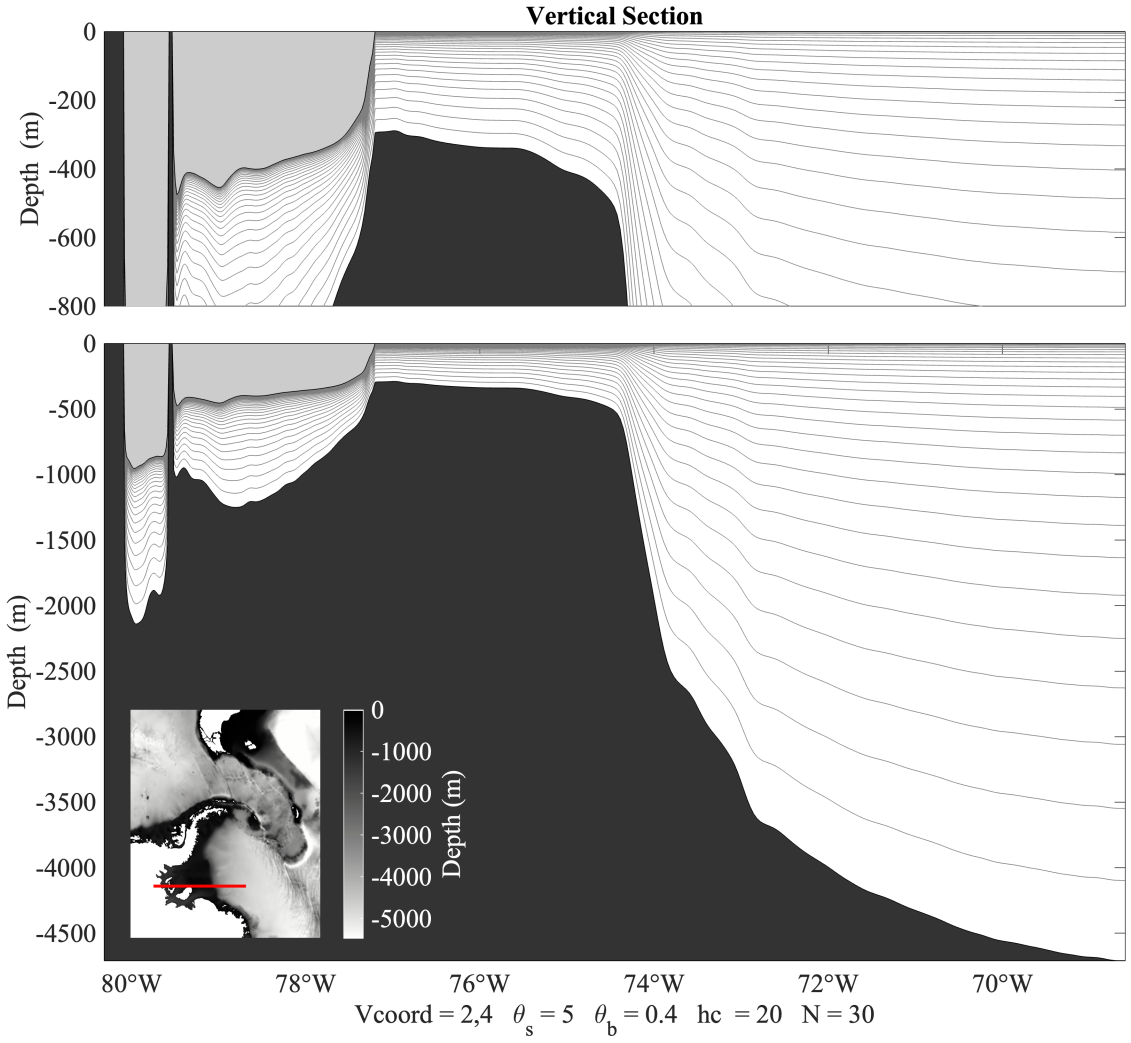

Vertical section with sigma representation. Light gray area represents the ice shelf structure, dark gray area represents the bottom of sea floor. Lines represent the sigma layers, and red line on the mapzoom with bathymetry is the section represented in the figure.

SOURCE: Author.

2.4 Representation of sea-ice

The sea-ice model used in this study is the ROMS-Budgell version (BUDGELL, 2005), which combines the elastic-viscous-plastic (EVP) rheology (HUNKE; DUKOWICZ, 1997; HUNKE, 2001) with one layer of snow and ice thermodynamics and a molecular sub-layer beneath the ice (Figure 2.2) (MELLOR; KANTHA,

1989). The EVP approach governs the rheological behavior of sea ice through three key processes: elasticity, allowing for reversible deformation after the application of force; viscosity, handling irreversible deformation responsible for sea ice deformation and movement, leading to changes in its structure; and the plastic module, managing permanent deformation when the applied stress exceeds a certain limit, resulting in a non-reversible deformation. This combination of components enables the EVP model to represent sea ice's response to various conditions, including its ability to answer accordingly under different forcing magnitudes: deform elastically under light loads, flow viscously under moderate loads, and experience plastic deformation under heavy loads(KIMMRITZ et al., 2015).

The EVP approach is great for simulating sea-ice behavior facilitating the modeling of processes such as ice deformation, fracture formation, and ice movement in response to external forces. The thermodynamic layers conduct the melting and freezing processes associated with the sea ice formation. This model can reproduce the effects of ice drift, melting and freezing of sea ice, interacting with the ocean fields. Also, this configuration shares the same time and grid steps as the ROMS model, sharing the same parallel encoding structure. The EVP model is based on an elastic mechanism, reproducing the variations of sea-ice dynamics of deformation and rigid breaking. The ice thermodynamics is reproduced in two layers of ice and one of snow, solving the heat conduction equation. It calculates the sea ice melting (growing) in the surface, bottom, and sides of the ice floes, as well as the frazil ice[1] formation.

[1]Frazil ice formation: the process of ice formation due to the cooled seawater by the atmosphere becomes supercooled and freezes. This process also can contribute to the *brine* effect, a phenomenon which consists of the main ejection of salt during the freezing process(SCHAEFER, 1950).

Figure 2.2 - Ice thermodynamics variables diagram: different locations where ice melting and freezing can occur.

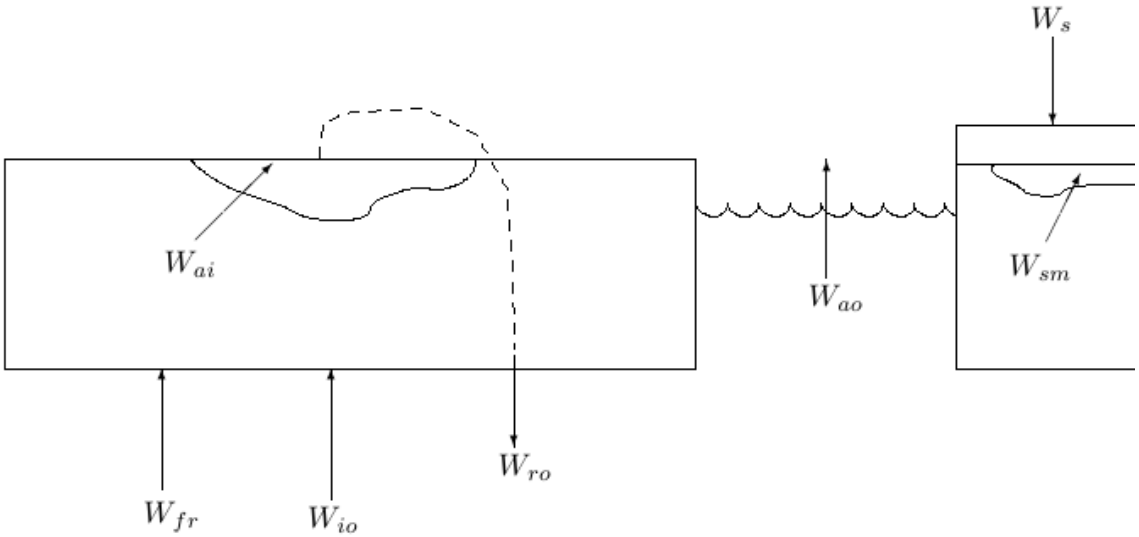

Sea-ice thermodynamics scheme reproduced by the sea-ice module (BUDGELL, 2005). Where: W_{fr} - frazil ice formation, W_{io} - freeze rate at the ice/water interface, W_{ai} - melt rate on the upper ice/snow surface, W_{ro} - rate of runoff of surface melt water, W_{ao} - freeze rate at the air/water interface, W_{sm} - snow melt rate, W_s - snowfall rate.

SOURCE: Hedström (2018).

2.5 Ice shelf computation

ROMS has a module that simulates the processes that occur under the cavities of the ice shelves (DINNIMAN et al., 2007), which are constant in thickness and extension over time, but contribute thermodynamically, through changes in the salinity and temperature of the water that circulates under these areas. Below the shelves, the most superficial layers do not follow the sea level, but instead conform to the base of the ice shelves (Figure 2.1). Also, the pressure under these areas takes into account the thickness of the ice. The atmosphere effects in momentum and buoyancy flux are set to zero. The friction between the ice and water is computed as a quadratic stress coefficient in the three first surface layers. The conservation of heat and salt and the freezing point computations are represented by a parametrization with a viscous sublayer model. Three equations are employed to represent the conservation of heat (Equation 2.8), salt (Equation 2.9), and the freezing point of seawater (Equation 2.10) as a function of salinity and pressure. These equations account for the transport

and exchange of heat and salt between the water and the ice shelf, as well as the effect of pressure on the freezing point of seawater.

$$\rho_i \left(L - C_{pi}\Delta T\right) \frac{\partial h}{\partial t} = \rho C_{pw} \gamma_T \left(T_b - T_w\right) \tag{2.8}$$

where ρ_i is the average ice density, L is the latent heat of fusion, C_{pi} is the specific heat of ice, ΔT is the temperature difference between the interior and the base freezing temperature at the ice shelf, ρ is the mixing layer density, C_{pw} is the heat capacity of seawater at 0°C, γ_T is the turbulent exchange coefficient for heat,T_b is the temperature at the ice shelf base, and T_w is the sea temperature in the first (uppermost) layer.

$$\rho_i S_b \frac{\partial h}{\partial t} = \rho \gamma_s \left(S_b - S_w\right) \tag{2.9}$$

where γ_s is the turbulent exchange coefficient for salt,S_b is the salinity at the ice shelf base, S_w is the salinity in the first layer, and ρ_i is the average ice density.

$$T_b = 0.0939 - 0.057 S_b + 7.641 * 10^{-4} h \tag{2.10}$$

where h is the depth below the mean sea level.

2.6 Conclusions and perspectives

Numerical modeling is a powerful technique to help us understand the complex interactions in high-latitude regions and the challenges presented by extreme conditions, and environmental changes due to climate change. The representation of sea ice dynamics, coupled with the integration of high-resolution regional models and Earth System Models, are crucial to enhancing our understanding of polar climates. And, they could play an important role in the sustainable management and conservation of these ecologically significant and remote regions.

The utilization of models like ROMS, adapted to simulate the effects of basal melting and freshwater inputs to the ocean, provides a powerful tool for addressing specific questions related to these processes. ROMS can offer valuable insights into the dynamics of ice-ocean interactions and their consequences, aiding in the understanding of the impacts of changing environmental conditions. Here, we focus specifically on increased freshwater inputs resulting from ice shelf melting and their effects on polar oceans.

3 GLACIAL MELTWATER INPUT TO THE OCEAN AROUND THE ANTARCTIC PENINSULA: FORCINGS AND CONSEQUENCES[1]

3.1 Introduction

The Southern Ocean (SO) has an important role in Earth's global climate. It is a significant sink for heat and CO2 and is the world's most biologically productive ocean (LIU; CURRY, 2010). In the last decades, studies indicate that the SO is changing rapidly, with significant warming of the Antarctic Circumpolar Current (ACC) (GILLE, 2002; GILLE, 2008; AUGER et al., 2021), freshening (ANTONOV et al., 2002; BOYER et al., 2005; DURACK; WIJFFELS, 2010; SWART et al., 2018), decreasing in oxygen (SHEPHERD et al., 2017), and acidification (MCNEIL; MATEAR, 2008; HENLEY et al., 2020; FIGUEROLA et al., 2021).

The Antarctic Peninsula (AP) is the northernmost region of Antarctica and is located at the west side of the Antarctic Continent (Figure 3.1). The AP has increased its contribution of meltwater into the ocean during the last few decades (ADUSUMILLI et al., 2018). Some of the most significant changes have been detected in that area, with the retreating of nearly 87% of the glaciers, not counting the countless collapses of ice shelves (COOK et al., 2016). Part of the increased melting is related to the warmer atmosphere associated with the intensification of the Southern Annular Mode (SAM) positive phase (DICKENS et al., 2019). This climate mode influences the strengthening of warmer westerly winds and consequent surface melting on the AP's eastern side (WACHTER et al., 2020).

The declining height and extension of AP ice shelves stem from a complex set of processes on the atmosphere, ocean, glaciers, and sea-ice. Changes in the freshwater balance resulting from variations in precipitation rate, sea-ice and the ocean-ice interactions can affect regional and thermohaline circulation strength (LAGO; ENGLAND, 2019; PARK; LATIF, 2019). Decreases in the extension of sea-ice further drive warming through the ice-albedo relationship due to the significant albedo reduction as the ice masses break and melt (VIZCAíNO et al., 2010). The increasing high-latitude precipitation as the atmosphere warms (DURACK, 2015) or increasing glacial melt (BINTANJA et al., 2015; PELLICHERO et al., 2018) can also modify buoyancy forcing and water masses formation in the SO, with implications for the

[1]This chapter is an adapted version of the paper:
LIMA, L. S.; PEZZI, L. P.; MATA, M. M.; SANTINI, M. F.; CARVALHO, J. T.; SUTIL, U. A.; CABRERA, M. J.; ROSA, E. B.; RODRIGUES, C. C.; VEGA, X. A. Glacial meltwater input to the ocean around the antarctic peninsula: forcings and consequences. **Anais da Academia Brasileira de Ciencias**, Academia Brasileira de Ciencias, v. 94, 2022. ISSN 16782690

Figure 3.1 - Map of the Antarctic Peninsula.

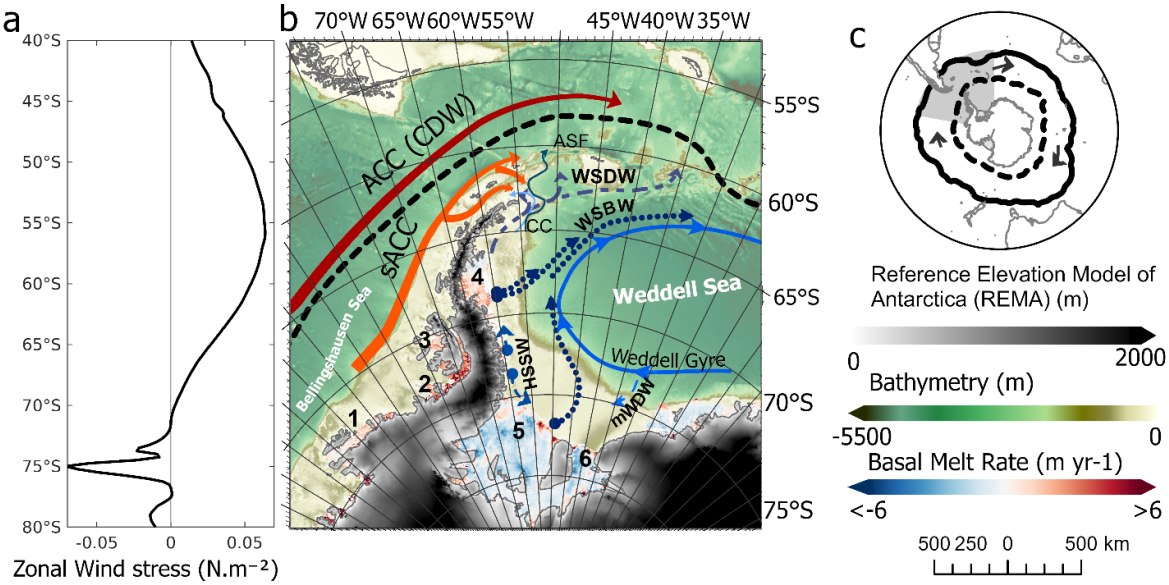

Map of the Antarctic Peninsula (and model domain) with schematically ocean currents and water masses of the region. Antarctic Circumpolar Current (ACC); southern branch of the ACC (sACC); Coastal Current (CC), Antarctic Slope Front (ASF), Circumpolar Deep Water (CDW); Weddell Sea Bottom Water (WSBW); Weddell Sea Deep Water (WSDW); High Salinity Shelf Water (HSSW); modified Warm Deep Water (mWDW). Ice-shelves: 1. Abbott; 2. George VI; 3. Wilkins; 4. Larsen-C; 5. Ronne; 6. Filchner. (a) Mean zonal wind stress from ERA5 dataset (1998-2017). (b) The red tones (blue tones) continuous lines represent Bellingshausen Sea (Weddell Sea) currents. The dashed lines represent the water masses. Black dashed line (continuous) represents the position of the Subtropical Front (STF) in the positive phase (negative phase) of SAM. The black arrows in (c) indicate the westerly winds and STF migrations in the SAM phases. The bathymetry data is from ETOPO1 (AMANTE; EAKINS, 2009), for elevation in the Antarctica continent Reference Elevation Model of Antarctica (REMA) (HOWAT et al., 2019), and basal melt rates from (ADUSUMILLI et al., 2020).

SOURCE: Lima et al. (2022).

overturning circulation. The glacial freshwater fluxes primarily come from melting icebergs and ice shelves. The increase of glacial meltwater into the SO alters the freshwater cycle and contributes to increased sea-ice cover (ZHANG, 2007; BINTANJA et al., 2013).

The input of glacial meltwater into the ocean adds to multiple SO trends perceived in observations (particularly in sea temperature, salinity, sea-ice extent (SIE), and sea

surface height (SSH)). Here, we review the freshwater input into the ocean around the AP. This region has contrasts between each side, on the Bellingshausen Sea (west) and the Weddell Sea (east) and is considered a climate hotspot (where climate change are more pronounced and well documented) (RIGNOT, 2004; MEREDITH; KING, 2005; KERR et al., 2018). This study shows the relevance of each process in freshwater contribution to the ocean and discusses the perspective about freshwater processes and their changes over high latitudes, focusing on the AP. Moreover, this study presents a general overview of techniques to quantify the hydrological cycle in the AP (Figure 3.2).

The contribution of this review summarizing each climate process related to freshwater dynamics in the AP is timely as it presents a contrasting climate states and ocean dynamics of each coast side. For instance, the Bellingshausen Sea presents high melt rates consistent with a warmer ocean on the western side. In contrast, the Weddell Sea presents massive ice shelves collapse associated with surface melting and intensified atmospheric changes on the eastern side. In this sense, this review aims to contrast the principal processes that occur in each side of the AP, related to glacial freshwater and how it contributes to each climate component and its effects, regionally and globally.

3.2 The antarctic ice sheet mass balance (context)

Ice sheet mass balance results from variations of mass of ice over a stated time (ROBIN, 1972; HANNA et al., 2013). It is expressed through the negative (loss or ablation) and positive (gain or accumulation) signals (COGLEY et al., 2011). When the accumulation and ablation are in balance over a long time, we have the balanced or "steady state" situation (ROBIN, 1972). It is determined by the surface mass fluxes (surface mass balance, SMB) and the ice flux across the grounding line (ice discharge, D). Also, the basal mass balance (BMB) is determined by the balance between accretion and ablation at the ice shelf base (DEPOORTER et al., 2013). During condensation, precipitation, and deposition, mass accumulates at the surface. The mass is lost when meltwater is not retained in the firn by freezing and capillary forces, leaving the ice sheet as runoff. Also, the wind can act by redistributing the snow, causing erosion and deposition, and sublimation, either from the surface or from drifting snow particles (10, 11, 13, in Figure 3.2). Once accumulated, snow crystals are slowly deformed into ice, changing their structure and densifying. The firn layer can be between 0 and more than 100 m thickness, depending on the local climate (LIGTENBERG et al., 2011). The glacier ice movement, from the interior

Figure 3.2 - Water cycle over ice-shelves.

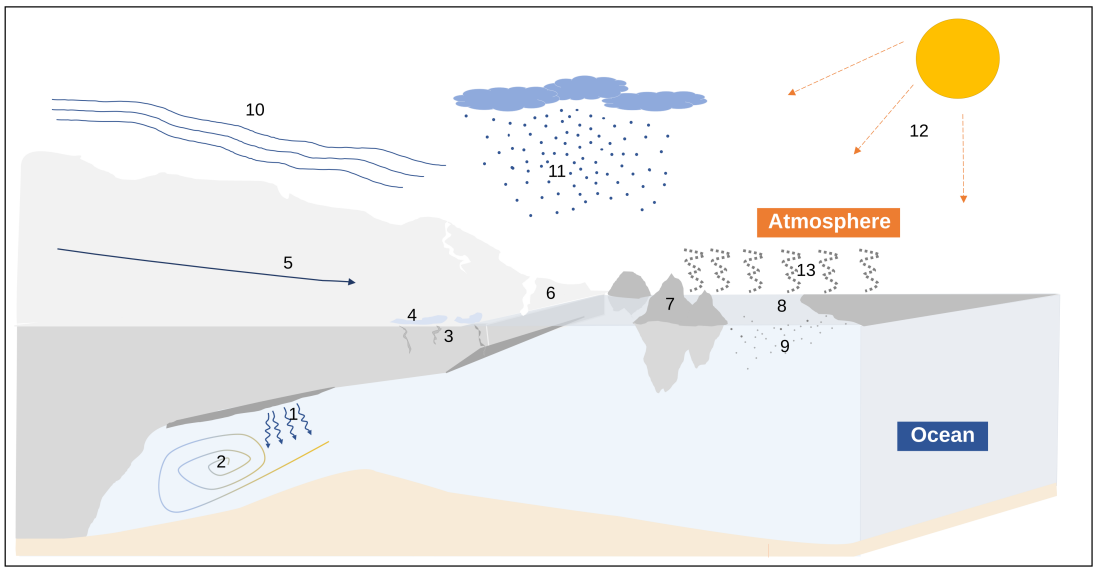

Water cycle over ice-shelves. 1. Basal melting – melting under ice shelf; 2. Water that upwells close to Antarctica is converted to denser bottom water by cooling and brine released during sea-ice formation; 3. Ice shelf crevasses – points of instability in ice-shelves where potentially can collapse; 4. Melting ponds – surface melting above ice-shelves; 5. Ice-velocity – ice movement from the continent into the ocean through ice-shelves; 6. Ice-shelves disintegration – formation of icebergs; 7. Icebergs – ice portions floating in the ocean; 8. Sea-ice – ice formatted by the cooling of the ocean as heat lost into the atmosphere, it causes brine rejection, increasing salinity in the ocean near these regions; 9. Salt rejection from sea-ice formation due brine rejection;10. Westerly and katabatic winds – contributing in the evaporation and heat transfer from continent, ocean and atmosphere; 11. Snow and precipitation; 12. Solar radiation; 13. Evaporation and sublimation.

SOURCE: Lima et al. (2022).

ice sheet to the margins, can also influence the ablation, driven by basal sliding and internal deformation, followed by solid ice discharge when the ice crosses the grounding line and starts to float on the ocean.

The mass budget concerns physical processes that control the ice mass loss, i.e., the SMB, representing the difference between accumulation, runoff, and other forms of ablation, and glacier dynamics (the ice mass fluxes into the ocean). Moreover, the surface meltwater in ice sheets and the adjacent floating ice shelves can significantly

impact ice-sheet mass balance due to albedo changes and instability crevasses over the ice.

Given the difficulty of access and the high cost of expeditions to the Antarctic continent and the surrounding areas, remote sensing has proved to be fundamental for investigating these processes. Among the Antarctic region's balance, we have the accumulation of snow and ice process (input) and the loss of water by runoff (liquid form or ice movement) or evaporation (output) (LOEWE, 1967). Runoff is due to melting, which can occur on the ice sheet surface, ice shelves, and glaciers. Water distribution can be measured by observing ice and snow dynamics (RIGNOT, 2004; RIGNOT et al., 2008; RIGNOT et al., 2019; MOUGINOT et al., 2012). The new generation of satellites, such as Surface Water Ocean Topography (SWOT) (DURAND et al., 2010), promise synoptic observations of water balance aspects, including snow and ice thickness, which cannot be measured on a large spatial and temporal scale using conventional methods. Also, there are CryoSat-2, Jason-3, and Sentinel-4 acquisitions, as well as Jason-CS/Sentinel-6, and ICESat-2 data collection.

3.3 Atmospheric interactions

The last five decades have shown a rapid increase in air temperatures over the AP (Figure 3.3a), accompanied by increased precipitation (Figure 3.3c), and regionally opposing trends in sea-ice cover, with a decrease in Bellingshausen side, and increase in Weddell side (KUMAR et al., 2021). The SO has presented a small but significant increase in sea-ice cover associated with near-surface cooling (ARMOUR et al., 2016). The ocean surrounding AP has presented significant freshening and less dense trends, with impacts on the water volume (AZANEU et al., 2013; HELLMER et al., 2011; SCHMIDTKO et al., 2014; BARLETT et al., 2018; DOTTO et al., 2021). Freshwater input into the ocean from the continent influences SSH, and affects the formation of water masses and, consequently, global circulation. The melting of ice shelves and glaciers contributes to a positive signal in freshening along the AP coast. Due to the nonlinearity in the equation of state for seawater, at cold temperatures (high latitudes), salinity changes are more efficient at altering the density of the seawater than changes in temperature (SATHIYAMOORTHY; MOORE, 2002).

The most significant warming trends have been in the western and northern parts of the AP (Figure 3.3a and Figure 3.4a). Air surface temperature trends show a significant increase across the AP and, to a lesser extent, to most of the western portion of the Antarctic continent since the early 1950s. Moreover, only slight changes have been observed across the rest of the continent (TURNER et al., 2005; CARRASCO,

Figure 3.3 - Yearly trends over Antarctic Peninsula through results of ERA5 Reanalysis.

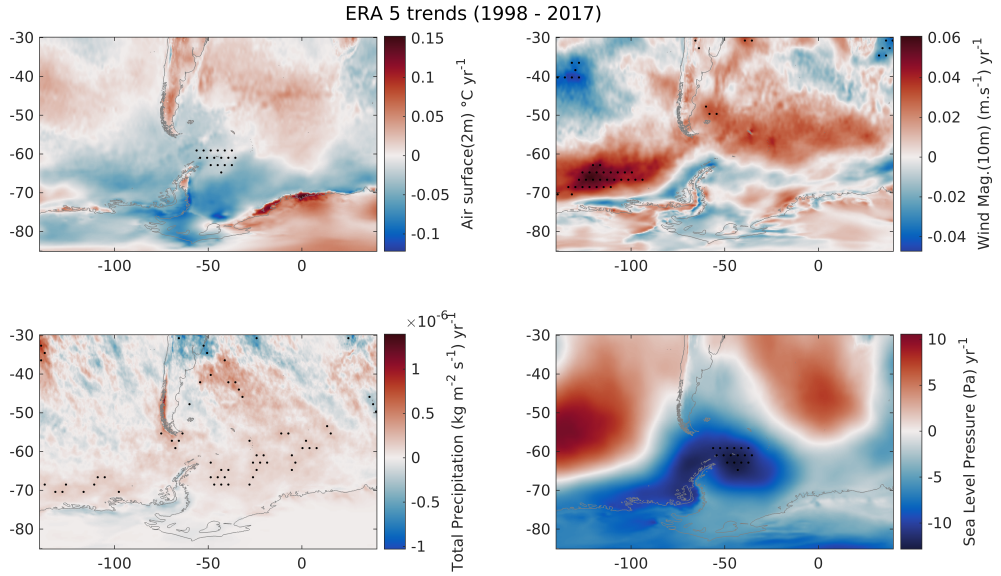

Yearly trends over Antarctic Peninsula through results of ERA5 Reanalysis data between 1998 and 2017), variables: (a) Air temperature at 2m (°C); (b) Wind Magnitude at 10m (m s-1); (c) Total Precipitation (kg m2 s-1); (d) Sea level pressure (Pa). Black dots represent the areas with significance of 0.05. Created with Climate Data Toolbox for Matlab (GREENE et al., 2019).

SOURCE: Lima et al. (2022).

2013). The western Antarctic Peninsula (WAP) has shown the highest average in air temperatures over the past five decades, pronounced during winter (KING et al., 2003; VAUGHAN et al., 2003; CARRASCO, 2013). The ocean water, in surface and bottom over large parts of the WAP, has warmed and has suffered salinity changes (Figure 3.4c, freshening the water masses due to increasing melting (MARTINSON et al., 2008; MEREDITH et al., 2018) and has declined in sea-ice extent and thickness (PARKINSON, 2019)(Figure 3.4d).

The westerly winds that overlie the SO have intensified over recent decades (Figure 3.3b). This is associated with enhanced warm advection due to changes in SO atmospheric circulation, resulting in increased air temperature over the AP and influencing its climate. More frequent positive phases of the SAM and the deepening of the Amundsen Sea Low (ASL) influence the regional meridional wind field, which

Figure 3.4 - Yearly trends over Antarctic Peninsula through results of GLORYS Reanalysis.

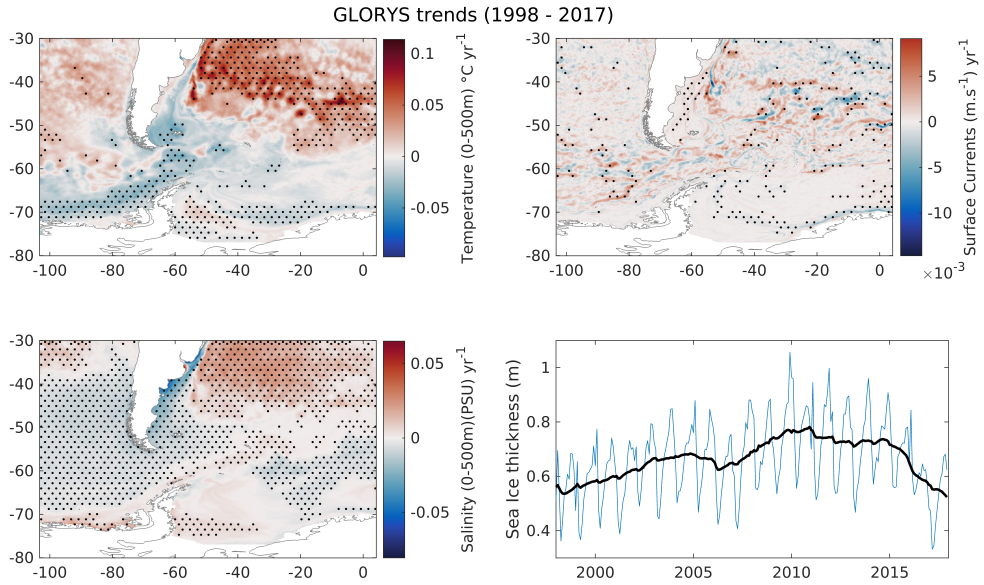

Yearly trends over Antarctic Peninsula through results of GLORYS Reanalysis data between 1998 and 2017, variables: (a) mean water temperature in °C for the first 500 meters; (b) Currents magnitude at the surface (m s-1); (c) mean water salinity for the first 500 meters; (d) Mean sea-ice thickness (m), blue line is monthly mean, and dark line represents the yearly mean. Black dots represent the areas with a significance of 0.05. Created with Climate Data Toolbox for Matlab (GREENE et al., 2019).

SOURCE: Lima et al. (2022).

controls the moisture advection and heat into the continent. The main impacts on AP due to the location and intensity of ASL, are the potential impacts in air temperature, wind, and pressure over the region, which can often lead to anomalies of opposite signs in sea temperature, sea ice, and precipitation on the coast and shelf region (RAPHAEL et al., 2016). SAM is characterized by westerly circumpolar circulation variability related to the strong meridional pressure gradient between the high and mid-latitudes of the Southern Hemisphere (SH), which significantly influences synoptic-scale activity over the SO (sea level pressure trends presented Figure 3.3d). The positive SAM causes poleward displacement of the cyclone tracks and reinforces the ASL, promoting surface warming over the AP (MARSHALL, 2003; PARISE et al., 2015). The SAM can also affect the distribution of sea-ice as a sign

of the response, depending on the time scale considered (FERREIRA et al., 2015).

The instantaneous response to increasing westerly winds is the intensification of Ekman's cold-water transport to the north and the sea-ice expansion. Although the SAM expands the ice to the north, it reduces its average thickness (LEFEBVRE; GOOSSE, 2005). The wind intensification can increase the inflow of warmer waters into the WAP continental shelf but not necessarily cause the increase of ice shelf basal melting (except for the shallower ice shelves) (DOTTO et al., 2021). SAM can also interfere over wind-driven Weddell Sea Gyre on the eastern AP, influencing inter-annual variations in bottom-water properties (DICKENS et al., 2019).

The estimative of evaporation over the ocean requires the derivation of three surface variables obtained by satellites: air temperature, wind, and specific humidity (SCHLÜSSEL, 1996). The sea ice and snow cover modulate the interaction between the ocean surface and the atmosphere just above. These structures strongly reflect solar radiation, resulting in efficient insulators, and prohibiting the exchange of heat and humidity. Boisvert et al. (2020) proposed a specific algorithm (turbulent flux algorithm) to estimate evaporation, combining derived data from satellite and numerical model reanalysis. They used air temperature and surface humidity data from Atmosphere Infrared Sounder (AIRS) onboard NASA's Aqua satellite and wind at 10 meters from NASA's MERRA-2 reanalysis and sea-ice concentration from SMMI. They estimated the daily evaporation between 2003 and 2016 and contributed to increased detail and reduced evaporation estimation errors over SO, an important variable in the water cycle and energy budget.

3.4 Glacier dynamics

Glaciers are large amounts of ice that slowly move downslope under the pull of gravity. The surplus ice mass forces the ice movement from years of accumulation in the higher altitudes (accumulation area) needs to be compensated by the outflow of ice in the ablation areas, where the ice is lost through melting and calving (e.g., (SHARP; TRANTER, 2017)). These formations appear static, but they slowly move like rivers of ice. The force of ice movement carries rocks, sediments, and debris from the surface. They also influence local and regional climate, driving cold and conserving low air temperatures and katabatic drainage winds, including nutrient delivery dynamics and influence of ecosystem structure over multiple trophic levels in coastal and fjord environments (DEBEER et al., 2020).

Nearly 80% of the world's freshwater is locked up in glaciers and ice sheets

(VAUGHAN et al., 2013). The Antarctic and Greenland ice sheets have approximately 33 million km^3 of ice, holding the capacity to raise global sea level by 70 m (sea level equivalent, SLE) (RIGNOT; THOMAS, 2002). It is estimated that the Antarctic Ice Sheet has more than 55 SLE m (MORLIGHEM et al., 2017; SUN et al., 2020), and Greenland Ice Sheet, 7.42 SLE m (MORLIGHEM et al., 2017). Glacier melting also has a significant role in sea-level rise contribution, Farinotti et al. (2019) estimates of 0.32 $\pm$ 0.08 SLE m from global glacier volume. The quantification of glacier mass loss at regional and global scales is a challenge due to the sparsity of direct measurements and the limitations of remote sensing data (relatively short time and coarse resolution of gravity-based measurements, e.g. NASA Gravity Recovery and Climate Experiment - GRACE), and other problems in deriving digital elevation models from optical and altimetric data (HUGONNET et al., 2021).

Basal melting contributes to decreasing glacier mass. The meltwater from the glacier bed supplies the slow and gradual ablation of the glaciers. This process also contributes to ice sliding and increasing the ice velocity. Also, the subglacial conduits caused by melt form instability regions where glaciers stay more fragile (HOW et al., 2017). In the land/ocean interface, the cold fresh water from basal melt enters the ocean above warm salty water, driving diffusive convection that influences the ocean's vertical structure (ROSEVEAR et al., 2021). Consequently, with the basal melting increase, we can expect effects over sea-ice and ocean mixed layer depth in the near ice-shelves areas (PARISE et al., 2015).

3.5 The role of ice shelves and icebergs

Ice-shelves are in the interface between the ocean and the continent (1 to 6 in Figure 3.2). They represent the floating extensions of grounded ice sheets and modulate the release of grounded ice and water discharge to the ocean. They are responsible for the stability and play an important role in the mass balance of ice sheets (STARK et al., 2019). The gain of mass is due to snow accumulation and freezing of marine ice undersides the shelves and loss through iceberg calving and basal melting (RIGNOT et al., 2013). Icebergs and ice-shelves introduce freshwater in different depths in the water column. Hence, it is a potential cause of vertical instability. The major collapse events coincide with southward migration of the mean-annual -9^{o}C and -5^{o}C isotherms driven by regional atmospheric warming in the last years (MORRIS; VAUGHAN, 2003). These isotherms are the proxy of summer surface melting that can lead to hydrofracturing (6 in Figure 3.2), which is instability points over ice shelves where they can collapse (SCAMBOS, 2004; SCAMBOS et al., 2013).

The disintegration of ice shelves is the source of icebergs (7 in Figure 3.2). They can float away from their calving region and provide heat and freshwater fluxes further away from their origin (MERINO et al., 2016). They concentrate mainly on offshore flowing branches of Antarctic subpolar gyres, with a large fraction found in the South Atlantic section of the SO. Melting icebergs can increase sea-ice concentration and thickness over most SO due to the convective overturning reduction capacity, limiting the heat supply from the deep ocean to the surface. However, in the Bellingshausen Sea, the iceberg melt results in thinner sea-ice due to the warmer waters advection flowing along with the ACC (PAOLO et al., 2015; MERINO et al., 2016).

Studies concerning atmospheric changes, including anthropogenic and stratospheric ozone influence over Antarctica and its effects, are still recent (TURNER et al., 2016). The atmosphere can influence ice shelves SMB and near ocean height due to air pressure (MUNNEKE et al., 2017). Air temperature and winds are highly correlated, which has a consequent influence on surface waters (TURNER et al., 2019). The wind has an important role in the ocean-atmosphere energy exchange. Both winds and meltwater imply changes over ocean ventilation south of the ACC, where surface and bottom waters interact through deep convection. Poleward intensifying winds increase mixing, causing the strengthening of deep water ventilation and mode water formation, while meltwater reduces the vertical mixing increasing the stratification, freshening the surface (ABERNATHEY et al., 2011; BRONSELAER et al., 2020). Also, the wind influences coastal polynyas formation and its consequent deep-water production, which can further influence the ocean heat flux under ice shelves. The energy exchange from the water phase affects directly over atmospheric heating, mainly through precipitation (P) and evaporation (E) (GUTENSTEIN et al., 2021). The difference between E and P rates (E-P) is the freshwater flux across the surface to the atmosphere, which is positive (negative) where E (P) dominates (11 to 13 in Figure 3.2).

Icebergs have complex characteristics, with high variability in shapes, sizes, and high disintegration dynamics. These aspects result in difficulties faced by numerical modeling of these processes (RACKOW et al., 2017). Therefore, the use of remote sensing is fundamental for detecting icebergs. The high spatial and temporal resolution makes it possible to estimate a variety of parameters and measurements such as drift speed and tracking of icebergs and meltwater injected into the ocean. Furthermore, iceberg tracking is also a powerful tool to detect ocean circulation patterns in remote areas with sparse data (COLLARES et al., 2018; BARBAT et al., 2019; BARBAT et al., 2021). Iceberg monitoring is essential not only for their contribution

to the entry of freshwater into the ocean but also for the safe navigation of vessels. Synthetic Aperture Radars Interferometry (InSAR) and SAR technology sensors are the most used to detect icebergs in the ocean (TOURNADRE et al., 2016; BARBAT et al., 2019). The use of artificial intelligence to identify and monitor the space-time evolution of these ice features and their variation in size and distribution can contribute to understanding the role and impact of melting icebergs and the formulation of more accurate numerical models.

3.6 The role of the ocean

The SO has, on average, warmed (GILLE, 2002; AUGER et al., 2021) and freshened (DURACK et al., 2012) over the past several decades. At mid-depths and within the latitudes of the ACC, the warming has proceeded at nearly twice the rate of global upper ocean warming (GILLE, 2002). The ACC northern branch has presented a significant reduction of 0.01 in salinity per decade since the 1980s (BÖNING et al., 2008; GIGLIO; JOHNSON, 2016). These changes can impact the deep ventilation and global thermohaline circulation. Another effect observed is the westerlies intensification due to increased greenhouse gas forcing. These results in enhanced cyclonic wind forcing, inducing westward flow closer to the Antarctic Continent, displaces the ACC southerly, affecting the Weddell Gyre and its strength (VERNET et al., 2019).

The Antarctic Bottom Water (AABW) exported from the Weddell Sea is freshening at decadal time scales (JULLION et al., 2013; PURKEY; JOHNSON, 2013; HOLLAND et al., 2015; KERR et al., 2018). The AABW is formed through surface buoyancy losses via cooling and brine rejection from winter sea-ice formation on the Antarctic continental shelf (High Salinity Shelf Water – HSSW). The shelf water interacts and mixes with the Circumpolar Deep Water (CDW) that flows onto the shelf, characteristically warmer and saltier, and mixes too with the cold meltwater from the base of marine shelves, called Ice Shelf Water (ISW) (JACOBS et al., 1992; SNOW et al., 2016).

Larsen ice shelves collapse at Weddell Sea, and accelerated glacier flow is most responsible for the shelf waters freshening of the AP's eastern side (HELLMER et al., 2012). The collapse of Larsen A and B ice shelves and glacial runoff acceleration (mainly Larsen C) is associated with the summertime intensification of the circumpolar westerly winds over SO, which are attributed in part to anthropogenic processes (SCAMBOS et al., 2013; JULLION et al., 2013), including ozone depletion (SWART et al., 2018).

The declining extent and height of ice shelves from AP are attributed to a complex set of processes and interactions of the ocean, atmosphere, and sea-ice dynamics (PRITCHARD et al., 2012; PAOLO et al., 2018; ADUSUMILLI et al., 2018). The major collapse events were associated with the southward migration of mean-annual -9°C isotherm of surface air temperature (MORRIS; VAUGHAN, 2003). Changes in atmospheric conditions are highly correlated with the sea ice concentration and thickness, which causes changes in wind stress effects over ocean circulation (KIM et al., 2017). It also affects the ocean-atmosphere heat exchange and ocean mixing (DINNIMAN et al., 2012). The deep-water production in coastal polynyas, impacting overheat fluxes under ice shelves, affects the basal melt rates and freshwater exportation (ADUSUMILLI et al., 2018; HOLLAND et al., 2020).

3.7 The role of sea-ice

The increase of meltwater input into the ocean can have a significant influence on sea-ice formation. Fresher waters present a higher freezing point, and consequently, less energy is required to produce sea ice (DIERSSEN et al., 2002). Also, the stratification in the upper water column caused by the cold and less dense freshwater input can influence the heating and cooling rates of the sea surface, influencing the onset of sea-ice formation. The sea-ice-ocean interactions occur more intensely sea ice limits (mainly through sea-ice lateral melting) and converge to reduce the oceanic vertical mixing caused by the enhanced buoyancy (PARISE et al., 2015).

The sea-ice melt contributes to the cold and freshwater entrance into the ocean mixed layer, principally on the edge, through the sea-ice lateral melting. These waters stored in the upper ocean layers have a climate memory of approximately eight years, which can affect heat loss for the atmosphere (PARISE et al., 2015). The surface freshening due to melting water input can also explain besides the sea-ice expansion, the Sea Surface Temperature (SST) cooling, and its influence over the mixed layer (SCHULTZ et al., 2020).

The seasonal sea-ice cover has the potential to duplicate along the year (Figure 3.4d), with a slow autumn advance (March to early September) and a rapid spring retreat (November to early February) (GORDON, 1981). This variation has a potential effect on the climate system, affecting and interplaying with the planetary albedo, atmospheric circulation, ocean productivity, and thermohaline circulation (EAYRS et al., 2019).

3.8 Eastern (cold) vs Western (warm) Antarctic Penninsula

The AP is one of the most rapidly warming regions of the world registered in the twentieth century, where approximately 75% of the ice shelves have already reduced and retreated over the past decades (RIGNOT et al., 2013). This reduction of ice shelves affects the glaciers stability and the ice sheet mass balance, contributing to increased sea-level rise due to increased freshwater input into the ocean (RIGNOT et al., 2019). The AP presents different ocean dynamics on each side. The Bellingshausen Sea on the western side presents warmer waters and higher glacial and sea-ice melting rates, typically with a cold oceanic climate. On the eastern side of AP, the semi-closed geography of the Weddell Sea sustains much colder conditions, characteristically under a cold polar-continental regime.

The AP glaciers dynamics are changing and mainly becoming wet-based, influenced mainly due to climate factors, which contribute to high erosion and melting (GOLLEDGE, 2014). The glacial thermal regime determines the subglacial processes based on the ice temperature and pressure. The wet-based glaciers have meltwater at the glacier's base, increasing the basal sliding and inducing rapid ice velocities (KLEMAN; GLASSER, 2007). On the surface, meanwhile, the melt ponds are the primary source of meltwater and critically affect the ice shelves stability, implying hydro fractures and later collapses (SIEGERT et al., 2019).

The cumulative mass loss is dominated by the WAP (PRITCHARD et al., 2012), from George VI, West Graham Land, Wordie, Stange, and Bach (RIGNOT et al., 2019). Also, Wilkins Ice Shelf presented break-up events in 2008 and 2009 (COOK; VAUGHAN, 2010). Muller, Wordie, and Jones ice shelves have collapsed or retreated, increasing the freshening on the Bellingshausen Sea (ADUSUMILLI et al., 2020). Stange ice shelf, situated to the west of George VI Ice Shelf, displays relative stability in an area that may be subject to atmospheric and oceanic forcing. Bach Ice Shelf, located between Wilkins Ice Shelf and George VI Ice Shelf southern ice front, has increased glaciological changes in the last years. It has presented significant areas of passive ice that have already or will be removed, resulting in enhanced recession within the next decade (HOLT; GLASSER, 2021).

On the eastern side of AP, the changes in water masses sourced in the Weddell Sea continental shelf may have directed the freshening signal (CASPEL et al., 2015; CASPEL et al., 2018). Besides, the significant break-up of ice shelves collapse occurred since 1995, e.g., Larsen-A followed by Larsen-B in 2002, has been through abrupt contributions of great amounts of freshwater into the Weddell Sea. The col-

lapse of Larsen-B caused the loss of approximately 3250 km^2 by calving huge icebergs to the ocean (COOK; VAUGHAN, 2010). Before Larsen-A and Larsen-B collapse, the most northerly eastern ice shelf, the Prince Gustav ice shelf, collapsed in 1995. There is evidence to suggest that this ice shelf became separated from the Larsen Ice Shelf in the late 1940s (COOPER, 1997), retreating to Cape Longing. Since then, there has been a rapid retreat from 1957 to 1961, followed by a steadier retreat until the collapse in 1995 (COOK; VAUGHAN, 2010).

The Larsen-C is the largest ice shelf of the AP. Situated on the northern part of the peninsula, it has retreated in the last years. In 2017, a large section collapsed, leading to the calving off A68 iceberg (LAROUR et al., 2021), which represents a 10% from the Larsen-C size (HOGG; GUDMUNDSSON, 2017). The warm ocean waters are pointed as the main responsible for driving melting at the ice-shelf base and leading to ice-shelf instability.

3.9 Natural variability

In contrast to Arctic sea-ice decreasing due to increased surface air temperature, observations show an expansion of SO sea-ice extent during the satellite era (1979-nowadays) (PAULING et al., 2017; MERINO et al., 2018; PARKINSON, 2019). It is correlated to the observed SO cooling trend. Although, the sea surface temperature (SST) and sea-ice concentration (SIC) trends are not homogeneous in space (SIMPKINS et al., 2013; SWART et al., 2018), with opposing signs in the Amundsen-Bellingshausen seas versus the Ross and Weddell seas (STAMMERJOHN et al., 2008). Several explanations were proposed to explain these trends, including an increase in poleward-intensified westerly wind stress changes. The intensified winds are correlated by the positive trend of SAM, in reply to stratospheric ozone depletion, and a deepened ASL driven by tropical Pacific or North Atlantic SST anomalies (ZHANG et al., 2019).

The SAM is the principal mode of climate variability over the extratropical Southern Hemisphere (SH) (MARSHALL, 2003). It corresponds to the main answer of Antarctic climate to southern mid-latitudes climate and tropical variability (FOGT; MARSHALL, 2020). The SAM positive trend in the last decades can cause the weakening of the SO carbon sink (KEPPLER; LANDSCHüTZER, 2019). Additionally, modeling studies indicate that the stronger zonal winds caused by the positive SAM can decrease sea-ice extent due to warm circumpolar deep water upwelling close to the Antarctic coast through enhanced surface easterly flow. The increased warming of coastal Antarctic waters through changes in the upwelling of CDW has been linked

to the melting of outlet glaciers, with influence over global sea-level rise (PURKEY; JOHNSON, 2013).

3.10 Climate change and future

Surface waters in the northern part of SO have warmed, freshened, and cooled in the southern part since the 1980s. The AABW has become less voluminous in SO and globally, and the eddy field has intensified since the early 1990s (Integorvernamental Panel on Climate Change (IPCC), 2019). Projections of future trends in the SO indicate the potential of continued strengthening westerly winds (CHEON; KUG, 2020) and the warming and increasing of freshwater input from both increased net precipitation (FYKE et al., 2017) and changes in sea-ice and meltwater export (BRONSELAER et al., 2018; BRONSELAER et al., 2020).

The westerly winds increasing trend will continue intensifying the eddy field (MUNDAY et al., 2013), with potential effect over upper-ocean overturning circulation, including heat, carbon-oxygen and nutrients (SWART et al., 2019). Another effect of westerly wind intensification is the sea-ice increase in extension and decrease in thickness due to sea-ice movement caused by the strong winds (HOLLAND; KWOK, 2012).

Models have shown that meltwater from Antarctic ice sheets and shelves can affect the slowing increase of global temperatures and warming subsurface ocean temperatures especially near Antarctica and permit positive feedback more further ice melt and sea-level rise (BRONSELAER et al., 2018).

3.11 Conclusions

The freshwater dynamics over AP has changed drastically over the past decades. AP is a critical region that is under climate change influences, but its effects are still poorly understood. The increase in ozone depletion caused by anthropogenic gases is associated with the cause of Antarctica's westerly wind intensification. This intensification can result in changes in water balance, increasing evaporation and hence precipitation. The wind changes also directly interfere with the currents magnitude (Figure 3.4b), modifying sea water transport below ice shelves. The introduction of warmer water under ice shelves can contribute to the basal melting increasing. The surface melt can also weaken these ice masses' stability, contributing to their instability and high potential for collapse.

Regarding the effects on a global scale due to Antarctica changes, it is essential to

consider and forecast the possible situations and their climate impacts. The positive and high entrance of meltwater on the ocean trend will affect the freshwater balance critically on a regional scale, principally near the AP, where occurs essential seawater masses formation, carrying on global consequences due to thermohaline circulation. Even, the freshwater from sea-ice melting has a potential effect over the ocean mixed layer, as described by Parise et al. (2015) and Schultz et al. (2020).

In this context, it is necessary to discretize freshwater contributions to ocean dynamics near AP. Here, we highlighted the main tools to quantify and describe the known water processes. However, the knowledge of the variability and acceleration of the hydrological cycle and its consequences on regional and pursues global climate are still incipient. Therefore, it is necessary to improve and carry out specific studies on each variable of this complex climate region. The role of melting from different sources and the process that affects the increase or decrease of freshwater ocean input is still misunderstood. Studies leading each process separately, and sensitivity studies leading the direct effect of each freshwater source, can also bring an explanation and the relevance of each contribution. This review brings together a description of likely processes that contribute to variations of freshwater inputs into the ocean, as well as the contrasts that we have on each side of the Antarctic Peninsula.

This study is a part of the activities and planning developed by the Antarctic Modelling Observation System (ATMOS) project, which is a response to the Brazilian Antarctic Program (PROANTAR). This project aims to improve our understanding of sea-ice–ocean-atmosphere–waves interactions and turbulent fluxes exchanges in their interface, at micro and mesoscales in the Atlantic sector of the Southern Ocean.

4 THE ROLE OF ICE SHELF BASAL MELTING ON WATER MASS STRUCTURE AND OCEAN DYNAMICS AROUND THE ANTARCTIC PENINSULA [1]

4.1 Introduction

The Southern Ocean (SO) is responsible for transporting large amounts of salt, heat, and nutrients across the global ocean basins. Therefore, any change in the ocean and climate over this region directly influences the global climate (RINTOUL, 2018). Any variation in freshwater balance, whether resulting from changes in precipitation, sea ice, or ocean-ice interaction can affect the strength of regional and thermohaline circulation (LAGO; ENGLAND, 2019; PARK; LATIF, 2019; MEREDITH et al., 2018). The ice shelves around Antarctica connect the grounded ice sheet to the Southern Ocean and are influenced by changes in the ocean, the atmosphere, and the dynamics of the ice sheets. The confined ice shelves exert return stresses on the ice in the ground, a process called "buttressing" (DUPONT; ALLEY, 2006). They act as barriers, preventing the acceleration of ice flows coming from the continent. When this reinforcement is reduced through ice shelf collapse, substantial thinning, or mechanical weakening, ice flows and glaciers flowing into the ocean accelerate, contributing to sea level rise (PRITCHARD et al., 2012; SCAMBOS, 2004; SHEPHERD et al., 2004).

Basal melt is the melting of ice that occurs under floating ice shelves. As a result of this process, variations in ice shelf thickness can occur, driven by varying basal melt rates, and ice movement. This modulates the mass loss of the grounded ice sheet and consequently contributes to sea level rise, in addition to contributing to freshwater melt flows, which influence climatic processes in the Southern Ocean (ADUSUMILLI et al., 2020; GWYTHER et al., 2015; GWYTHER et al., 2020; SCHODLOK et al., 2016; GUDMUNDSSON et al., 2019; BRONSELAER et al., 2018). The increase in sea level results not directly due to the ice shelf melting, but from the consequent rise due to the acceleration of glacier flow into the ocean due to the collapse of the shelves.

Approximately half of the mass loss of the Antarctic ice sheet is due to basal melting (1454 $\pm$ 174 Gt/year) (DEPOORTER et al., 2013). The melting under the ice shelves has a profound impact on the ocean structure. The high ocean tempera-

[1] This chapter is an adapted version of the paper that will be submitted:
LIMA, L. S.; PEZZI, L. P.; MATA, M. M.; DINNIMAN, M. The role of basal melting on water masses structure and the ocean dynamics. To be submitted: **The cryosphere**

ture (compared to the freezing point) leads to melting at the base of the ice shelf (PRITCHARD et al., 2012; DAWSON et al., 2022). Several different mechanisms can increase the supply of warmer water to the ice shelf cavities, including changes in wind patterns (DINNIMAN et al., 2012), changes in polynya formation, and interactions with sea ice (GWYTHER et al., 2015; HOLLAND et al., 2010; MASSOM; STAMMERJOHN, 2010; SILVANO et al., 2018), variations in the depth of the thermocline and mixing layer (HATTERMANN; LEVERMANN, 2010; HATTERMANN et al., 2014; SCHULTZ et al., 2020), and the redirection of coastal currents (HELLMER et al., 2012; JACOBS et al., 2011). Furthermore, this process can be forced externally by climate change, inter and multi-decadal climate modes, annual cycles, and tides. The Antarctic Peninsula presents the highest values in the retreating of ice shelves in Antarctica with the loss of 6693 km^2 between 2009 and 2019 (ANDREASEN et al., 2023). This results in changes in the surrounding ocean due to the increasing of meltwater into the ocean.

The ice shelf melting is categorized into three modes due to the oceanographic processes that modulate the melting (JACOBS et al., 1992; TAMSITT et al., 2021). The first mode is characterized by the melting in the deep grounding lines of the "cold-water" ice shelves ("dense shelf mode") driven by inflows of the dense and high-salinity water (HSSW), produced by the formation of sea ice in the continental self (HOOKE, 2019). This water is characterized by high salinity and very low temperatures. It is often at the freezing point at the surface but can still melt deep ice due to the pressure-dependent freezing point of seawater. This water flows inside the shelf cavity, melts the deeper ice and leads to rising plumes of melted water, and generates Ice Shelf Water (ISW). This potentially supercooled water can lead to water refreezing once it flows to a shallower depth along a sloping ice shelf, creating a layer of sea ice at the base of the ice shelf (GWYTHER et al., 2015). The second mode ("warm mode") occurs in "warm-water" ice shelves, such as the west AP ice shelves, where the subsurface warm Circumpolar Deep Water, also called modified CDW (mCDW), is transported into the ice shelf cavity. The third mode, also called "fresh mode", occurs near the ice front, where the seasonal warmed Antarctic Surface Water (AASW) is transported into the cavities of the shallow ice by the ocean variability and tides, and possibly other mechanisms such as sea ice dynamics (MALYARENKO et al., 2019). These three modes are highly variable in the melt contribution around Antarctica, and various external processes influence each mode, including regional oceanic and atmospheric conditions, including the transport and production of sea ice (ADUSUMILLI et al., 2020).

The meltwater fluxes into the ocean have a significant role in the ocean structure, impacting stratification, circulation, heat, and formation of water masses (HENLEY et al., 2020). The structure and dynamics of the ocean are impacted due to the enhancement of freshwater, affecting the sea-ice concentration and extent, and water masses production (SWART et al., 2018). The sea-ice modulates the interaction between the atmosphere and ocean, it works as a barrier and influences the exchange of heat and mass (SCHLOSSER et al., 2018). It can interfere with the climate over the Southern Hemisphere, affecting the meridional displacement of storm track and jet stream (KIDSTON et al., 2011; PARISE et al., 2015), and also affect the carbon cycle due to the exchange factors between ocean, ice, and atmosphere (FOGWILL et al., 2020). The enhanced freshwater in the ocean can lead to a stable layer of less dense water, inducing stratification, mainly over the continental shelf. Also, it can inhibit the sinking and disrupt deep water formation. Consequently, the circulation patterns in these regions can be altered, affecting large-scale ocean currents (HASKINS et al., 2020). Due to the stratification, the fresher surface water can act as an insulating layer, reducing the exchange of heat between the ocean and the atmosphere (Integorvernamental Panel on Climate Change (IPCC), 2022). This can result in regional variations in sea surface temperature, impacting global heat transport patterns.

Here, we focus on the meltwater influence from basal melting around the AP, identifying the major contributions and contrasts between both sides. The Bellingshausen Sea presents warmer waters and higher glacial and sea-ice melting rates, typically with a cold oceanic climate. At the same time, on the Weddell Sea, the semi-closed geography sustains much colder conditions, characteristically under a cold polar-continental regime. However, both sides of the AP have been presenting high melting rates on ice shelves (ADUSUMILLI et al., 2020), and in some cases, their rapid retreat and collapse. The AP is considered a climate hotspot, where we can verify more pronounced climate change effects (KERR et al., 2018; KERR et al., 2018; MEREDITH; KING, 2005; RIGNOT, 2004). This region has experienced dramatic reductions in the extent (COOK; VAUGHAN, 2010; ETOURNEAU et al., 2019) and thickness (PAOLO et al., 2015) of ice shelves in recent decades. Most of the remaining ice shelves on the AP have experienced changes in the height of their surfaces as measured by satellite altimeters (ADUSUMILLI et al., 2018; ADUSUMILLI et al., 2020; COOK et al., 2016; PAOLO et al., 2015; PRITCHARD et al., 2012). The ice shelf melting and freshwater increase into the ocean can also trigger shifts in local and global circulation, water and air temperature, and consequently, the climate system.

The goal of this study is to evaluate the role of basal melting in ocean structure near the Antarctic Peninsula: assess how the contribution of freshwater discharge of basal melting along the AP affects the formation and stratification of water masses of the Bellingshausen and Weddell Seas. A further goal is to evaluate, as a consequence of fresh and cold water into the ocean, the ice shelf basal melting effects on sea ice formation over the continental shelf region. To achieve these objectives, we ran two experiments using a regional oceanic thermodynamical numerical model. The first experiment simulated the basal melting introduction into the ocean column, called the Control Experiment (CTRL), and the second one (the Sensitivity Experiment: SENST), where this meltwater introduction was deactivated.

4.2 Hydrographic background: water masses structure

The Southern Ocean has an important role in the water masses formation. Over this region, important water masses are formed by complex processes and interactions between the ocean, meltwater, sea ice, and atmosphere. These processes directly affect the northward flow of the Meridional Overturning Circulation (MOC) and, consequently, the Earth's Climate (PARDO et al., 2012; RINTOUL; GARABATO,). The water masses are distinguished by water bodies with similar properties and common formation history (LIU; TANHUA, 2021). There are many ways to distinguish the water masses, such as ranges of temperature, salinity, density, depth, oxygen, nutrients, isotopes, mixing, and current regimes. Here, we will use a range of potential temperatures, salinities, and neutral density as physical properties and their origin to classify the different water masses studied. The Table 4.1 presents these values for each region evaluated in the study.

Along the Antarctic slope is formed the densest water that fills the global ocean: the Antarctic Bottom Water (AABW) (ORSI et al., 1999). AABW results from a mixture of different water masses originated in the coastal and deep ocean. Its properties are deeply affected by the complex processes that occur in the atmosphere-ocean-cryosphere. Its formation and transformation are highly dependent on sea ice growth, brine rejection, opening coastal polynyas, melting glacier processes (mainly deep basal melting) deep convection, and entrainment of overlying surrounding water masses (FOLDVIK et al., 2004; NICHOLLS et al., 2004; ABRAHAMSEN et al., 2019). The AABW is produced in the Weddell and Ross seas and several places along East Antarctica, through a mixture of shelf water near the freezing point (High Salinity Shelf Water - HSSW, and Ice Shelf Water - ISW, also known as Dense Shelf Waters -DSW), with relative salty and warm intermediate waters (Warm Deep

Water - WDW, modified Warm Deep Water - mWDW, Circumpolar Deep Water - CDW and modified Circumpolar Deep Water - mCDW). The WSDW formed near the Larsen Ice Shelves (LIS), is relatively lighter and fresher than the AABW formed near RFIS (GORDON et al., 2001; JULLION et al., 2013). Here, we maintain the same water mass limits for both regions (RFIS and LIS).

During the winter, the Antarctic Surface Waters (AASW) loses buoyancy due to the salinification due to sea-ice formation. The coastal polynyas in the Weddell Sea, in front of the Ronne Ice Shelf, forced by cold and strong katabatic winds from the continent, sustain the constant sea-ice production. This process, linked with the coastal and ice shelf geometry, allows the continuous production and accumulation of HSSW, formed from winter cooling and salinification due to brine rejection during sea-ice formation (WANG et al., 2021). Part of this water flows northward and flows down the continental slope over the Weddell continental shelf and mixes with the mWDW, before descending to the abyss of Weddell Sea. The other part goes southwards, flowing underneath Ronne Ice Shelf, undergoing a change, due to interaction with the Filchner-Ronne Ice Shelf, being cooled and freshened, and producing the ISW. ISW is a supercooled water mass with a temperature below the surface freezing point (approximately -1.9 C for these salinities) (ZHOU et al., 2023; SCHODLOK et al., 2016; JANOUT et al., 2021). The ISW has an important role in the Dense Shelf Water formation. The mixture of the ISW with HSSW feeds the deep ocean, contributing to the formation of the Weddell Sea Deep Water and the Weddell Sea Bottom Water (WSDW and WSBW), both of which will compose the AABW (ORSI et al., 1999).

In recent decades, the AABW around Antarctica has undergone a freshening and warming process, with a consequent volume reduction (BINDOFF; HOBBS, 2013; PURKEY; JOHNSON, 2013; ABRAHAMSEN et al., 2019). This "freshening" process is highly related to the circulation and mixing of less dense and warmed water masses, changes in ice melt, and freshwater input. Hence, the AABW has been deeply influenced by the increased warming around Antarctica, wind, sea ice, and freshwater introduction into the ocean (ZHOU et al., 2023). The freshening process of AABW is attributed to changes in the freshwater budget around Antarctica (JULLION et al., 2013), and one of the causes cited is the increased glacial loss, due to collapses of ice shelves, and subsequent acceleration of glacier buttressing and retreat. An increasing introduction of warmer waters beneath the platforms not only accelerates the melting and instability processes but also compels the introduction of freshwater into the ocean.

The Bellinghshausen Sea has been experiencing a highly increased warming (SCHMIDTKO et al., 2014), with a consequent reduction of sea ice production and increased melting of ice shelves (CHRETIEN et al., 2021; MEREDITH; KING, 2005). The western part of the AP contains a relatively deep continental shelf (200-500 m). The region is mainly influenced by the ACC flowing northwesterly close to the shelf break, and southward coastal current (KLINCK et al., 2004). The water structure over the shelf is mainly formed by Surface Water (SW), Winter Water (WW), and Circumpolar Deep Water (CDW). This region does not present the dense, cold, and salty waters found in the Weddell and Ross Seas. Outside the continental shelf, the CDW is subdivided into Upper Circumpolar Deep Water (UCDW) with relatively high temperatures (1 to 1.4 °C), occupying a range of 300-600 m depth, transported mainly across the shelf break. The Lower Circumpolar Deep Water (LCDW) is found between 700 to 1000 m depth, and barely transported across the shelf.

To evaluate the basal melting effect over the water masses formation cross-slope sections based on the work of Kerr et al. (2012) were chosen, to investigate the water masses flow along the coast, highlighted in blue in Figure 4.1. To investigate the exportation of the water masses that are leaving the continental shelf, two along-shelf-break hydrographic sections around the 1000m isobath, highlighted in orange (I and II in Figure 4.1), were defined. For these transects, the total transport flows perpendicular to the section, were examined as well as the spatial analysis due to the visualization of the vertical profiles.

Table 4.1 - Definitions of water masses in terms of neutral density (γ^n), salinity, and potential temperature (θ) intervals used in this study.

Water Masses			Definition			Reference
			$\gamma^n(kg/m^3)$	S	$T(\theta°C)$	
Bellinghshausen Sea	(1 – 3)	AASW	<28			1,2
		SW	<27.55	33 to 34.5	<1	
		WW	27.55 to 28 (27.7)	34	-1.7	
		UCDW	27.7 to 28	34.6	1 to 1.4	3,4
		LCDW	28 to 28.27	34.6	1.25 to 1.75	4,5
		AABW	>28.27			
SR4 E DR	(A – B)	AASW	<28	-	-	
		SW	<27.55	34 to 34.5	-1.6 to 1	2
		WW	27.55 to 28	34 to 34.5	-1.9 to -1.6	
		CDW/WDW	28 to 28.27	34.65 to 34.75	>0	2,6,7
		AABW				
		WSDW	28.27 to 28.4	34.64 to 34.7	-0.7 to 0	2,7,8,9,10,11,12,13,14,15
		WSBW	>28.4	>34.55	< -0.7	
Weddell Sea	(4 – 7)	AASW	<28	-	-	
		SW	<27.55	34 to 34.5	-1.6 to 1	16,17,18
		WW	27.55 to 28	34 to 34.5	-1.9 to -1.6	
		WDW	28 to 28.1	34.65 to 34.75	0 to 1	16, 17, 19, 20
		mWDW	28.1 to 28.27	34.4 to 34.6	-1.6 to -0.6	18
		DSW -> AABW				
		ISW	-	34.55 to 34.60	<-1.9	21,22
		HSSW	>28.27	34.6 to 34.85	-1.9 to -1.6	
		AABW	>28.26	34.64 to 34.7	-0.7 to 0	
		WSDW	28.26 to 28.31	>34.55	-1.5 to -0.7	8, 21,23
		WSBW	>28.31			
	(I – II)	AASW	<28	-	-	
		SW	<27.55	34 to 34.5	-1.6 to 1	16,17,18
		WW	27.55 to 28	34 to 34.5	-1.9 to -1.6	
		CDW/WDW	28 to 28.27	34.6 to 34.75	0 to 0.6	21
		AABW	>28.26			
		WSDW	28.26 to 28.31	34.64 to 34.7	-0.7 to 0	8, 21,23
		WSBW	>28.31	>34.55	-1.5 to -0.7	

References related with each water mass characteristic: 1.Jenkins e Jacobs (2008); 2.Brown et al. (2015); 3.Klinck et al. (2004); 4.Abernathey et al. (2016); 5.Santini et al. (2018); 6.Kerr et al. (2012); 7.Orsi et al. (2002); 8.Abrahamsen et al. (2019); 9.Fahrbach et al. (2001); 10.Llanillo et al. (2023); 11.Foster e Carmack (1976); 12.Fahrbach et al. (1996); 13.Foldvik et al. (2004); 14.Garabato et al. (2002); 15.Gordon et al. (2001); 16.Nicholls et al. (2004); 17.Hutchinson et al. (2020); 18.Akhoudas et al. (2021); 19.Darelius et al. (2014); 20.Franco et al. (2007); 21.Schodlok et al. (2016); 22.Janout et al. (2021).

SOURCE: Author.

4.3 Model and experimental design

The Antarctic Peninsula circulation model is based on the Rutgers/UCLA Regional Ocean Model System (SHCHEPETKIN; MCWILLIAMS, 2005) (adapted version of v3.9). The configuration used here includes a dynamical sea ice model (BUDGELL,

2005), and the mechanical and thermodynamical effects of static ice shelves, with basal melting contributions (DINNIMAN et al., 2007; HOLLAND; JENKINS, 1999). Even though tides can have an impact on sea-ice and ice-shelf dynamics (RICHTER et al., 2022; HUOT et al., 2021), tidal forcing was not activated here. The grid defined for the simulation comprises between the coordinates 84°S – 50°S and 100°W – 0°. This area encompasses the Bellingshausen and West Weddell Seas, with the Antarctic Peninsula and the Drake Passage at the center (Figure 4.1). The grid has a stereographic projection, resulting in a 5km horizontal resolution. This resolution is not eddy-resolving over the continental shelves but is eddy-resolving over the open ocean. The vertical discretization is given by sigma coordinates, which follow the topography with 30 sigma levels. The bathymetry and ice shelf morphology are from RTopo2 (SCHAFFER et al., 2016).

Figure 4.1 - Bottom topography and ice-shelf morphology in the model.

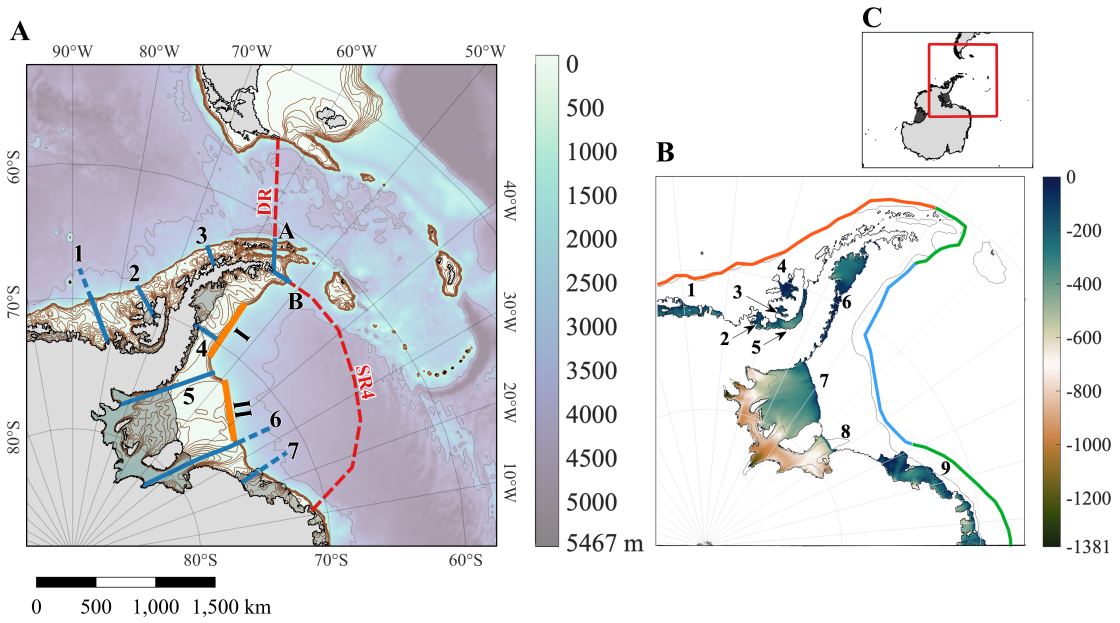

Bottom topography and ice-shelf morphology in the model domain. (A) Bottom topography based on RTopo2. The light brown lines represent the 200 m isobaths from 0 to 1000 m, and the gray line represents the 4000 m isobaths. Blue lines (1-7) represent the cross-slope sections represented in the study, and A and B indicate the sub-sections (limited by 1000 m isobath) from the common transects of Drake Passage (DR) and WOCE SR-4 (SR4) used to calculate the volume and water masses transport described in section 4.5.5. Orange lines (I and II) represent the along-shelf-break sections used in this study. B. Ice shelves morphology based on RTopo2: 1. Abbott; 2. Stange; 3. Bach; 4. Wilkins; 5. George VI; 6.Larsen Ice Shelves (LIS); 7. Ronne; 8. Filchner; 9. Burnt – Stancomble Wills – Riiser Larsen. The colored line delimits the regions with each mode regime, based on (THOMPSON et al., 2018): Red: Warm (Mode 2), Blue: Dense (Mode 1), and Green: Fresh (Mode 3); (C) Model domain.

SOURCE: Author.

The atmospheric database used is the ERA5 reanalysis, produced by the European Center for Medium-Range Weather Forecast (ECMWF) (HERSBACH et al., 2020). The horizontal resolution is 31 km and features hourly and monthly temporal resolution. Here, we used a 6-hourly temporal resolution. The initial and oceanic open boundary conditions are based on the Global Ocean Physics Reanalysis (GLORYS12V1) (JEAN-MICHEL et al., 2021). Table 4.2 presents the bathymetry morphology and oceanic and atmospheric forcing used in the model.

Table 4.2 - Model forcing variables. Atmospheric forcing is from ERA5 by ECMWF, and Oceanic forcing is from Global Ocean Physics Reanalysis (GLORYS12V1) product by the CMEMS. The bathymetry and the bottom of the ice shelves represented are from RTopo2.

Grid	**Atmospheric forcing**	**Oceanic forcing**
Bathymetry and	Zonal Wind (10m)	Sea Surface Height
Bottom of ice shelves	Meridional Wind (10m)	Zonal current velocity
from RTopo2	Air temperature (2m)	Meridional current velocity
	Surface Air Pressure	Water temperature
	Specific Humidity (2m)	Salinity
	Net short wave radiation flux	Sea ice concentration
	Long wave radiation flux	
	Total precipitation	

SOURCE: Author.

4.3.1 Experiments performed

The ocean model was spun up from August 1993 to December 2002. The large time of spin-up is due to the large areas that were pre-defined with constant values(T(-1.9°C), S(34), U, and V (0 m/s)), due to the absence of data, mainly under the ice shelves. The results used here in the analysis are after 10 years of integration when the solution has reached the statistically quasi-steady state. Figure 4.2 presents the time evolution for the volume-averaged kinetic energy computed for both simulations (control and sensitivity experiments). In this case, it is possible to visualize that both simulations adjust to their steady state within ten years.

Surrounding the Southern Ocean, we have the world's most intense and energetic ocean current, called the Antarctic Circumpolar Current (ACC). Due to the fact that the model grid represents a quarter of Antarctica, we had to address this current at the model's edges. We implemented a flow relaxation scheme based on Martinsen e Engedahl (1987), which involved relaxing temperature and salinity at the borders with the GLORYS data climatology for the first twenty cells nearest to the lateral open boundary. This was done to mitigate numerical instabilities that could introduce errors in the ocean properties across the domain.

Figure 4.2 - Kinetic Energy time-series.

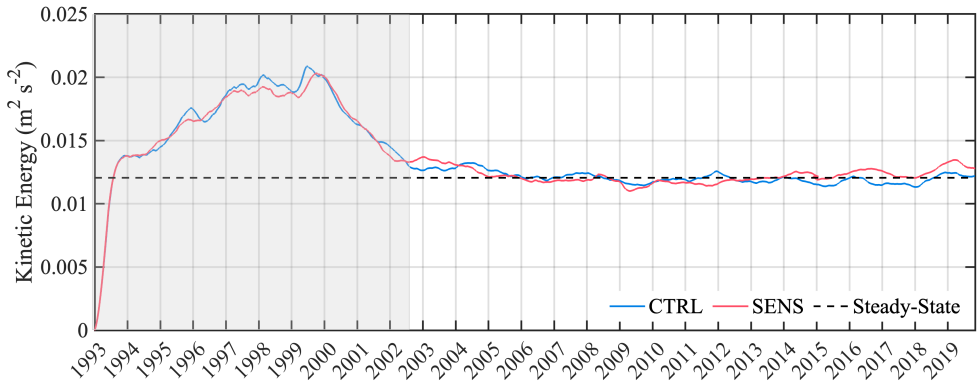

Plot of volume-average kinetic energy for the Control and Sensitivity (CTRL and SENST, respectively) runs from 1993 to 2020. Dashed line represents the steady-state line. And the shaded light gray period represents the spin-up time, discarded for the analyses.

SOURCE: Author.

For this study, two experiments were run: one which was defined as a control experiment (CTRL), where we have the effects of the basal melting into the ocean, modulated by the ice shelf melting configuration described by Dinniman et al. (2007), and the second experiment where there was no ice shelf basal melt, the sensitivity test (SENST). The process of melting from ice shelves is parameterized by a three equations scheme, based on the pressure-depending freezing point and conservation equations of heat and salinity (HOLLAND; JENKINS, 1999). These equations calculate the heat and freshwater (salinity) fluxes into the ocean, thereby simulating the basal melting processes.

In the sensitivity test, the salt and temperature fluxes are set to zero, eliminating the effects of melting in the simulation. The grid domain and forcing conditions remain the same, but the results of meltwater rates do not affect the oceanic structure at any point in time. In other words, the sensitivity test allows for isolating and assessing the impact of ice shelf melting on the ocean by eliminating the effects of this melting. This helps to understand how significant ice shelf melting is as an isolated factor, separated from other oceanic processes.

The ice shelves represented are Abbott, Stange, Bach, Wilkins, George VI in the western AP, surrounded by the Bellinghshausen Sea; and Larsen-C, the minor

Larsen-D, E, and F, Ronne, and Filchner, and the Brunt-Riiser-Larsen-Stacomble ice shelves in the eastern side of AP, in the Weddell Sea (highlighted in the Figure 4.1). Due to the limitations of the ice shelf module, the ice shelves have a constant extent and thickness during all the time of simulation. Therefore, the major collapses of ice shelves weren't represented by any changes in the ice-shelves area coverage. Over the period of simulation, major iceberg calving events and collapses were registered in Wilkins (2008-2009) (SCAMBOS et al., 2009), and Larsen-B (2002) (SCAMBOS, 2004), and the Larsen-C calving event, with a reduction of $\approx 10\%$ of it area (HOGG; GUDMUNDSSON, 2017).

In the CTRL experiment, passive tracers were released from each ice shelf proportional to the melt rate at each model grid cell, which marked the meltwater concentration originated by the basal melting process. These tracers started to be released at the same time at the ice shelf base and were transported passively by the ocean flow. The objective here is to verify the behavior of basal meltwater over time, verify the areas with more influence of the meltwater, and quantify and classify each ice shelf contribution in each point of the model domain.

4.4 Model assessment

In order to evaluate the model, we compared the CTRL experiment output with satellite products and observed hydrographic data. Rye et al. (2020) indicates that the reproduction of meltwater from melting in models results in better representation when compared with observations. Based on this premise, it is expected that the CTRL simulation will yield values closer to the observation than the results of the SENST experiment. It is also for this reason that the experiment simulating the introduction of melted water from the ice shelves is being treated as the CTRL experiment.

The bias and root mean squared errors (RMSE) were calculated for the sea ice, and the surface temperature and salinity. To assess the vertical structure, two regions were chosen due to the availability of a well-established series of observational data and a comprehensive body of literature regarding the oceanographic processes taking place there. Data obtained from the PAL-LTER project and the transect known as SR4 from the WOCE (red line SR4 in 4.1) were compared with the model's results at the same coordinates. For these locations, TS diagrams, vertical profiles of temperature and salinity, as well as probability histograms and correlation plots, were generated for the first 300 meters of depth. Biases are calculated as in Equation 4.1, where X_{ROMS} is the analysis data and X_{obs} is the reference data, and n is referred

to the number of data values. The RMSE is calculated as Equation 4.2.

$$bias = \frac{\sum_i^n (X_{ROMS,i} - X_{obs,i})}{n} \tag{4.1}$$

$$RMSE = \sqrt{\frac{\sum_i^n (X_{ROMS,i} - X_{obs,i})^2}{n}} \tag{4.2}$$

The sea ice outputs were compared with the product from the National Snow and Ice Data Center, NOAA, called Climate Data Record of Passive Microwave Sea Ice Concentration, Version 4. It is a dataset of sea ice concentration measured by passive microwave data. It uses an algorithm that combines two well-established algorithms: the NASA Team (NT) algorithm (CAVALIERI et al., 1984) and the NASA Bootstrap (BT) algorithm (COMISO; SULLIVAN, 1986). This dataset has a 25 km spatial coverage and temporal resolution of 1 day. Here, we resampled to the same spatial and temporal resolution as the CTRL Experiment.

We must consider that our data acquisition is irregular throughout the year. Additionally, during the winter months, we face solar limitations, which hinder optical remote sensing measurements, and encounter challenges with *in-situ* campaigns due to the harsh conditions of overwintering. During this period, *passive* microwave sensors, *active* remote sensing systems (TEDESCO, 2015; BAUMHOER et al., 2018), the autonomous Argo Floats (WONG et al., 2020; WILSON et al., 2019) and marine mammals sensors (TREASURE et al., 2017) have an essential role in gathering information (MEREDITH et al., 2013). The *active* sensor systems, e.g., laser altimeters and radars, are the major tools to estimate the ice sheet and ice shelf dynamics (e.g., ICESat, ERS-1, ERS-2, Envisat, and Cryosat, among others) (TEDESCO, 2015; RIGNOT; THOMAS, 2002; BAUMHOER et al., 2018; ADUSUMILLI et al., 2020).

The NOAA Optimum Interpolation (OI) Sea Surface Temperature (SST) V2 was used to compare with the CTRL SST. This dataset has 1/4° High-Resolution daily data; it is an SST analysis spatially gridded and provides global fields that are based on a combination of observations from satellite (AVHRR, AMSR) and *in situ* platforms (i.e., ships and buoys) (REYNOLDS et al., 2002). Since it presents an irregular distribution, a statistical method (optimal interpolation, OI) is applied to fill where there are missing values. This methodology corrects possible bias from satellite data to *in situ* data prior to interpolation. The version used here (OI.V2,(REYNOLDS

et al., 2007; BANZON et al., 2016)) has an improvement in the estimation of SST from sea-ice concentrations. To estimate the SST from the model, the surface sigma layer was resampled to represent the first 0.5m depth, regridded to 1/4° horizontal resolution.

For over 30 years, data has been collected and analyzed, and the dynamics have been modeled of the ocean west of the Antarctic Peninsula by the Palmer Long-Term Ecological Research (LTER) (SMITH et al., 1995). We used the hydrographic measurements dataset from this project to evaluate the vertical oceanic features of the model at the west continental shelf of the Antarctic Peninsula. To evaluate the east side of AP, at the Weddell Sea, and the Weddell Gyre structure, we used hydrographic measurements from Autonomous Pinniped Bathythermographs (APB) data collection, available at the World Ocean Database (WOD).

The World Ocean Atlas (WOA) is a set of climatological fields of *in situ* temperature, salinity, oxygen parameters, silicates, phosphates, and nitrate, objectively analyzed with 1° and 1/4° resolution (BOYER et al., 2018). The salinity climatology fields from the 2005-2017 period were used here to compare with the salinity surface climatology fields of the CTRL experiment for the same time period.

To evaluate the basal melting rates from the model, we compared the model results with satellite-derived estimations formulated by Rignot et al. (2013) and Paolo et al. (2023). Both authors estimated, by different approaches, rates of basal melting from remote sensing products. Rignot et al. (2013) presents an accurate estimation for each ice shelf around Antarctica, for the period of 2003-2008. They estimated parameters such as ice thickness (H), ice velocity (v), surface mass balance (SMB), the rate of thickening ($\delta H/\delta t$), the net basal melting (B) and divergence in the volume flux (Hv). To achieve this, they used the Regional Atmospheric and Climate Model RACMO2, forced by global reanalysis from the ECMRWF, ice shelf thickness from Operation IceBridge (OIB) (MACGREGOR et al., 2021) and BEDMAP-2, which estimates from altimetry the ice shelf surface elevation. Interferometric Synthetic Aperture Radar (InSAR) estimated the ice fluxes and grounding lines. Ice fronts were defined from a 150-m spacing mosaic of Advanced Land Observing System (ALOS) Polarimetric SAR (PALSAR) data for 2007 and 2008. All these variables characterize the ice shelf structure and dynamics.

Through another approach, Paolo et al. (2023) employed data from four satellite radar altimeters (ERS-1 (1991–1996), ERS-2 (1995–2003), Envisat (2002–2010), and CryoSat-2 (2010 – 2017) to create a time series of ice shelf thickness and basal melt

rates with very high resolution (3 km, with three-month intervals) spanning from 1992 to 2017. For this study, we extracted the relevant time frame from this database, covering the period from 2002 to 2017 (post-spin-up period), in order to assess the performance of the CTRL simulation in simulating the basal melting process.

4.5 Results and discussion

The results and discussion are organized as follows: first, the results of the model analysis are presented, where the CTRL simulation is compared with observational data to assess whether the key oceanographic fields are well represented. Then, we will discuss the effects and differences in sea ice formation between the CTRL and SENST simulations, considering the impact of basal meltwater and the main differences in sea ice distribution, concentration, and extent between the two simulations. Subsequently, we will analyze the relationships over time between sea ice formation and basal melting, as well as the influence of westerly winds on these processes. To conclude the analysis, we will assess the production of water masses in specific transects, as well as calculate the transport in these sections. Thus, we will locally assess the effects of meltwater on the production and export of water masses throughout the domain.

4.5.1 Mean state analysis

A detailed assessment of the CTRL simulation, considering the representation of processes that occur around the AP, will be discussed in this section. A comparison between the CTRL simulation output and available hydrographic observations and remote sensing products showed that the main modeled processes are in agreement with observations. Because much of the comparison data are already included in the Global Ocean Physics Reanalysis (GLORYS) used as the boundary and initial conditions for the model, these comparisons cannot be considered as a fully independent test of the model skill.

The sea-ice concentration (SIC) and extent (SIE) are well represented in seasonality, with an overestimation during austral summer (DJF), as can be seen in Figure 4.3. SIC represents the percentage of areal coverage of ice within the grid cell, while the SIE is the integral sum of the areas of all grid cells with at least 15% of ice concentration. The sea-ice models coupled in ROMS, tend to perform better in simulating sea ice concentration during winter than during summer (KUMAR et al., 2021). Besides this misrepresentation during summer, the main pattern of sea-ice formation and extent were well represented, with a good agreement in SIC ($r =$

$0.68, p < 0.05$) and in SIE with the observation along the year ($r = 0.969, p < 0.05$), the main concentration errors are overestimated during summer over Weddell Gyre and the continental shelf in Western Antarctic Peninsula (spatial mean in SIC RMSE over the domain: 23.54% (DJF), 14.54 % (MAM), 11.81 % (JJA), 13.83 % (SON)). The model represents very well the interannual differences in the maximum ice (Figure 4.3.C).

Figure 4.3 - Sea-ice evaluation.

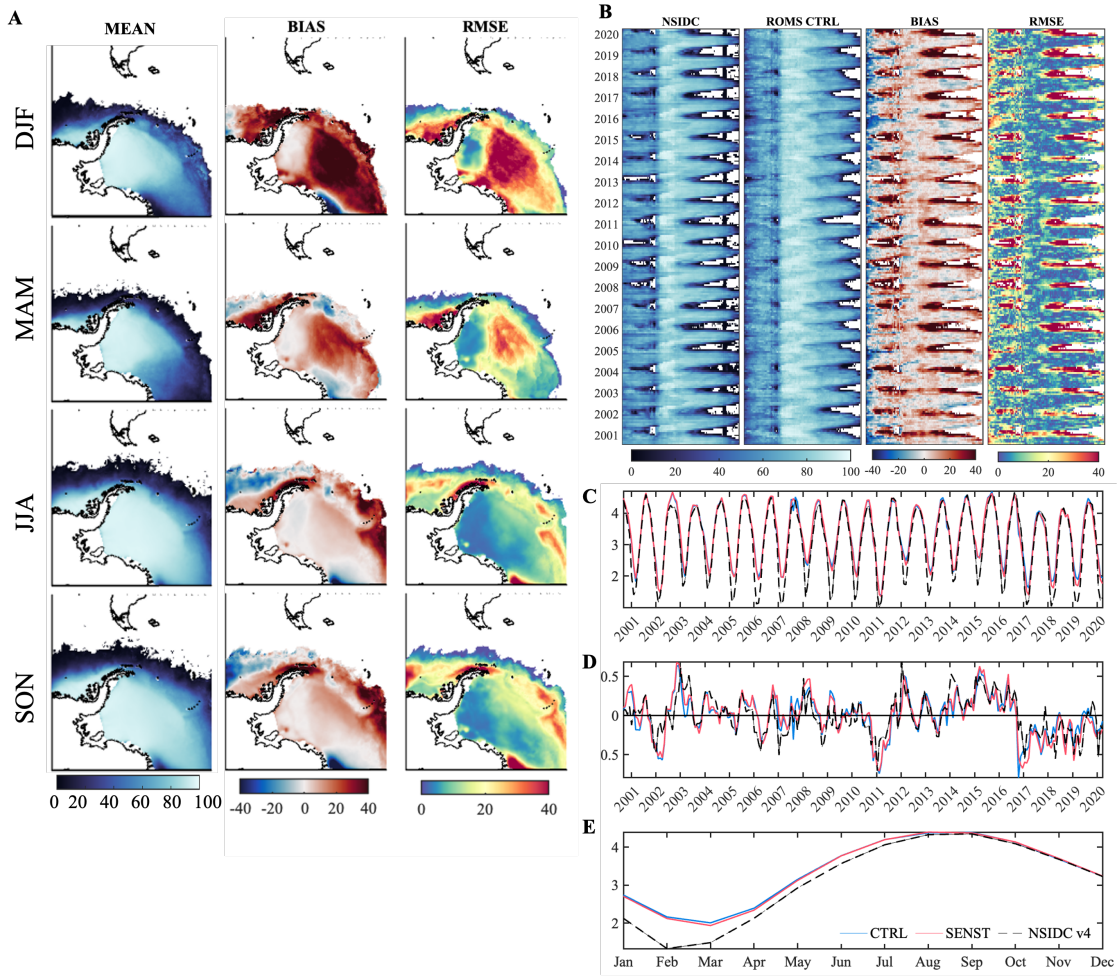

Comparison of observed and modeled Sea-ice concentration and extent along the domain. (A) Spatially bias, and RMSE for Sea-ice concentration(%) along the experiment, comparison between CTRL and NSIDC CDR. (B) Hovmoler longitudinal diagrams for mean NSIDC CDR, CTRL Experiment, bias, and RMSE. The x-axis represents the longitudinal coordinates; (C) Monthly mean sea ice extent ($10^6 km^2$) CTRL, and SENST experiments along the simulations experiments compared with NSIDC CDR. (D) Monthly anomalies along the simulations experiments compared with the NSIDC CDR ($10^6 km^2$); (E) Climatology cycle of SIE ($10^6 km^2$).

SOURCE: Author.

The SST was compared with the products from remote sensing of (OI) SST V2. It is well represented in seasonality, with an underestimation along the year, as shown in Figure 4.4.D. The main errors are concentrated along the ACC (Figure 4.4. A), which makes sense since it is a very energetic area. Also, there is a large temperature

gradient across the ACC, so if the model ACC is shifted in the location from observations, that will show up as a larger error. The seasonality is well represented, but it presents a mean bias in temperature of ≈ 1.17°C colder than observation throughout the year, in which both SENST and CTRL results are colder on the surface when compared with observation. Major discrepancies occur in summer and autumn with mean RMSE of 0.62°C (DJF), and 0.43°C (MAM) respectively, winter and spring present mean RMSE of 0.31°C (JJA) and 0.29°C (SON). Meanwhile, the anomalies follow the observation, with differences in specific years. In 2003 the minimum anomaly month presents a displacement, the year 2010 presents a negative anomaly which is not presented in (OI) SST V2, and in the following years, the anomalies are higher than the observation. However, the results are considered acceptable and reproduce properly the main features along the simulation. The mean negative bias in temperature can explain the increased concentration of sea ice and its difficulty in melting properly during summer.

Figure 4.4 - Temperature evaluation.

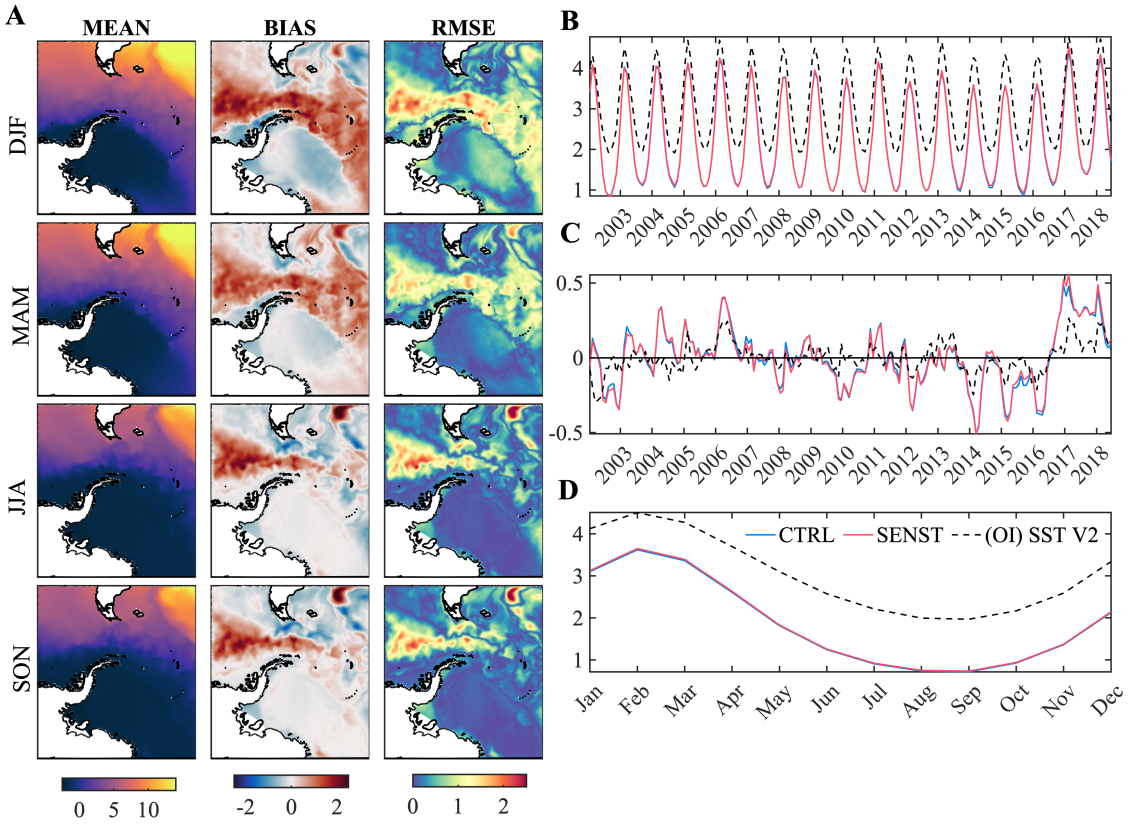

Comparison of observed and modeled sea surface temperature along the domain. (A) Spatially mean, bias, and RMSE for SST (°C) along the experiment, comparison between CTRL and (OI) SST V2. (B) Monthly mean temperature (°C); (D) Monthly anomalies along the simulations experiments compared with the (OI) SST V2 (°C). (E) Climatology cycle of SST (°C).

SOURCE: Author.

The salinity was compared with the climatology from WOA at the surface level (0-5m, Figure 4.5). The main errors occur at the limits of sea ice extent. The mean RMSE for each season is 0.26 (DJF), 0.27 (MAM), 0.24 (JJA), and 0.23 (SON). To analyze vertically, we selected two regions where we obtained *in situ* data, by the PAL LTER research cruises dataset, and by Autonomous Pinnipeds (APB), from the World Ocean Database (WOD). The region in the west of AP was compared with the PAL-LTER database, for the months of January from 2002 to 2017. Along the WOCE SR4 transect the APB dataset from WOD, from 2001 to 2020 was used.

The comparison with the PAL-LTER dataset (Figure A.1) reveals that the modeled

temperature is colder $\approx$ 1°C than the observations in the upper 50 m, with the mean thermocline shifted from the mean of $\approx$ 80 m to $\approx$ 50 m depth. From 80 to 150 m, the model was warmer than observed, and below 150 m it presented a mean bias of $\approx$ 0.5 °C. The simulated mean salinity presented the same behavior in overestimate near the surface, and below 150 m, with a difference of around 0.1. Besides, both temperature and salinity mean profiles are significantly correlated with the PAL-LTER January (2002-2017) observations, with $r = 0.64, p < 0.01$, and $r = 0.82, p < 0.01$, respectively.

Along the WOCE SR4 transect, the histograms (A.2. E and F) indicate that the temperature and salinity from the model agree well with observation, but underestimate the temperatures above than $\approx$ 0°C and below ≈ -1.5°C, and salinities above $\approx$ 34.6. The mean temperature from the model is warmer than observation until 200 m, with the highest differences around the thermocline, with $\approx$ 0.5 °C. The salinity profile indicates that the model follows the mean salinity until $\approx$ 150 m, below this depth the model tends to underestimate in $\approx$ 0.05. The temperature and salinity are very correlated, with $r = 0.65$ and 0.79 ($p < 0.01$), respectively.

Figure 4.5 - Salinity evaluation.

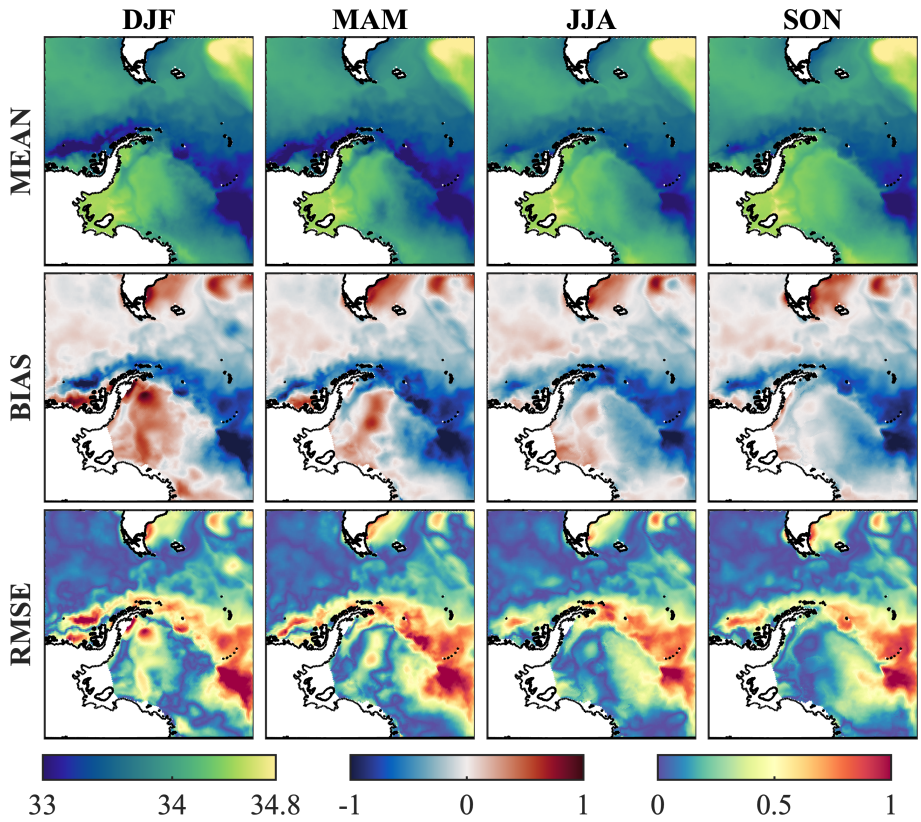

Comparison of observed and modeled sea surface salinity (SSS). Spatially Bia (second line) and RMSE (third line) for SSS along the experiment, comparison between CTRL and WOA.

SOURCE: Author.

4.5.2 Basal melting

During the eighteen years of simulation, a mean of 268.8 Gigatons of meltwater, originating from the basal melting process, is released from the ice shelves annually. To assess the total melting originating from each ice shelf, comparisons were made with data obtained from Paolo et al. (2023) and Rignot et al. (2013). Table 4.3 compares the CTRL experiment results with the results found in the two cited articles. It is possible to verify the area of each ice shelf and it differs possibly due to the limits considered for each one (in Rignot et al. (2013) case), and the database of ice shelf morphology. This study and Paolo et al. (2023) were calculated considering the same limits and resolution scale. Although in the study by Paolo et al. (2023), the ice shelf area changes through the years, we considered the average area for all

the time studied.

The results found are consistent, but the model generates less basal melt in all ice shelves. Abbott Ice Shelf presented the highest difference between studies, underestimating the basal melting approximately 40 Gt/yr and 30 Gt/yr, when comparing with Paolo et al. (2023) and Rignot et al. (2013) respectively. Wilkins presents an underestimation of 18.22 Gt/yr and 8.57 Gt/yr. In the Weddell Sea, the Ronne Ice Shelf has a melting rate of 54.38 ± 3.9, whereas the aforementioned studies report averages of 139.98 ± 138.08 and 113.5 ± 35, respectively. The circulation under this and the Filchner ice shelf cavity is driven mainly by tides and density currents associated with the High Salinity Shelf Water (HSSW) (VERNET et al., 2019). We are not considering tides in our simulation, which can be considered a limitation of the model in representing the melting under these shelves.

In our analysis, we considered the Abbott, Venable, and Ferrigno ice shelves together due to their proximity and size. We also grouped the Larsen ice shelves (Larsen-B, Larsen-C, Larsen-D, Larsen-E, Larsen-F, Larsen-G) as the "Larsen group", and the Brunt-Stancomble and Riiser-Larsen ice shelves as the "BSRL group." Due to this grouping, the rates and areas from Rignot et al. (2013) were grouped, and new rates were estimated. The deviations were omitted due to the fact that they could not be estimated by the limitations of the data available.

The total values computed in Table 4.3 are referent to the sum of the basal melt rates for each ice shelf and group (LIS and Abb/Ven/Ferr) detailed in the table. However, minor ice shelves are present in the model domain, and contributes in minor level to the total freshwater introduced into the ocean. The total meltwater produced on this study is 293.2 Gt/yr in a area of 686.550 km². Wordie and other minor ice shelves were omitted here for the analysis. Wordie ice shelf is a special case, because it collapsed in the early 90s, but it still remains some glacial tongues and it contributes with a rate of 6.5 ± 3 Gt/yr (RIGNOT et al., 2013) and our study estimates 1.72 ± 0.42 Gt/yr for the same period (2003 - 2008).

The year 2008 is important due to the Wilkins break-up event and also noticed an increase of basal melting from Wordie glaciers (FRIEDL et al., 2018; RIGNOT et al., 2013; DEPOORTER et al., 2013). The major break-up events and increased rates of basal melting have been associated with the enhanced westerly winds due to the positive phase of the Southern Annular Mode (SAM), which results in increased CDW flowing through the continental shelf, carrying more heat and influencing the increased basal melting, especially the shelves in the Bellinghshausen Sea sector

(VERFAILLIE et al., 2022). The ice shelf morphology remained unchanged throughout the simulation, and the use of RTopo-2 as the source for bathymetry and ice shelf morphology has some limitations in defining the grounding line (SCHAFFER et al., 2016). Consequently, the simulation did not reproduce events like the Wilkins break-up and the Larsen-C calving event in 2017, which led to the formation of the A-68 iceberg.

Table 4.3 - Area and basal melting rates for the ice shelves.

Ice Shelf	Area (km²)			Basal Melt Rate Gt/yr (m/yr) 2002 - 2017		Basal Melt Rate Gt/yr (m/yr) 2003 - 2008	
	This study	Rignot et al. (2013)	Paolo et al. (2023)	This study	Paolo et al. (2023)	This study	Rignot et al. (2013)
Abb/Ven/Fer	32,300	32,999	22,745	24.34± 3.44 (0.63 ± 0.11)	67.15±16.86 (3.21 ± 0.8)	21.61±3.18 (0.73±0.1)	76.3 (2.52) *
Bach	4,000	4,579	4,331	4.99± 2.37 (1.36 ± 0.64)	4.94± 2.83 (1.24 ± 0.71)	6.88±2.12 (1.87 ± 0.58)	10.4 ± 1 (2.3±0.3)
Wilkins	14,400	12,866	12,994	8.38 ± 2.79 (0.63 ± 0.21)	26.6 ± 23.93 (2.23 ± 2.00)	9.83±2.66 (0.74 ± 0.20)	18.4 ± 17 (1.5 ± 1)
George VI	23,575	23,434	29,907	68.61 ± 13.71 (3.17 ± 0.63)	99.35 ± 20.75 (3.62 ± 0.75)	81.53 ± 6.65 (3.77 ±0.26)	89.0 ± 17 (3.8 ± 0.7)
Stange	7,325	8,027	7,458	6.71 ± 3.17 (0.99 ± 0.47)	32.99 ± 6.82 (4.83 ± 0.99)	9.78 ± 2.27 (1.45 ±0.33)	28 ± 6 (3.49 ± 0.7)
LIS	70,325	78,192	72,511	10.93 ± 2.08 (0.16 ± 0.03)	59.65 ± 38.29 (0.89 ± 0.57)	10.73 ± 1.53 (0.16 ±0.02)	38 (0.52) **
Ronne	303,250	338,887	304,404	54.38 ± 3.9 (0.19 ± 0.01)	139.98 ± 138.08 (0.50 ± 0.49)	55.05±3.29 (0.20 ± 0.01)	113.5±35 (0.3±0.1)
Filchner	111,175	104,253	116,272	35.18 ± 1.56 (0.34 ± 0.01)	46.92 ±35.21 (0.44 ± 0.33)	35.33 ±0.95 (0.35 ± 0.009)	41.9 ± 10 (0.4±0.1)
BSRL	115,300	80,344	137,923	55.26 ± 10.20 (0.52 ± 0.09)	52.64 40.19 (0.41 ± 0.31)	49.74 ± 7.70 (0.47 ± 0.07)	9.7 (0.13) ***
Total	**681,050**	**683,581**	**708,545**	**268.8 ± 27.35 (0.43 ± 0.04)**	**530.22 ± 213.59 (0.82 ± 0.33)**	**280.48 ± 24.44 (0.44 ± 0.04)**	**425.2 (0.59)**

Area and basal melting rates from each ice shelf discussed in this study. Comparison between the results from this study, the results from Rignot et al. (2013), and Paolo et al. (2023). *We considered Abbott, Venable, and Ferrigno ice-shelves contributions together, **LIS as all Larsen ice shelves (Larsen-B, Larsen-C, Larsen-D, Larsen-E, Larsen-F, Larsen-G), So, it summed the volume per year from each one to assess the total Larsen Gt/yr in Rignot et al. (2013). ***The same occurs in BSRL, on which we considered that together the Brunt-Stancomble and Riiser-Larsen ice shelves.

SOURCE: Author.

Figure 4.6 presents the seasonal time series of data obtained by Paolo et al. (2023) with their corresponding error bars and the CTRL time series obtained in this study. The error bars are relatively large, which results in our results being representative in most cases. In the George VI ice shelf, the CTRL experiment closely follows the trend observed in Paolo et al. (2023)'s series. The uncertainty surrounding the methods used to estimate basal melting remains significantly high. This is primarily attributed to challenges in data acquisition, a wide spectrum of missing information

due to limited access, and the uncertainties associated with the chosen techniques for estimating basal melt rates (HOLLAND, 2013).

Figure 4.6 - Ice shelf basal melting seasonal time-series.

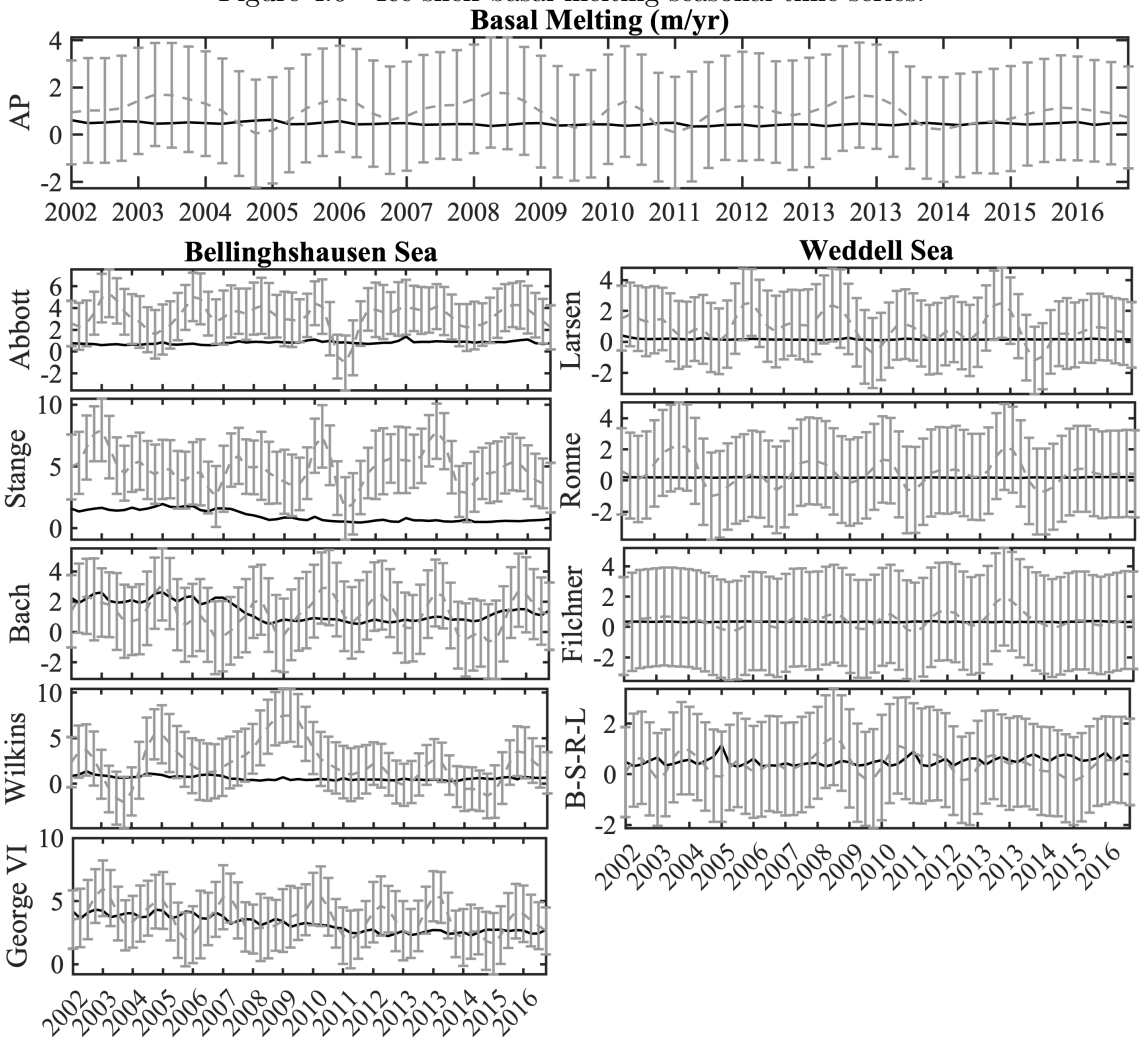

Time series with error bars of basal melt rate (in meters of ice equivalent per year) for all the area of each ice shelf. The solid dark line represents the model mean output, and the gray dashed line with error bars represents Paolo et al. (2023) outputs.

SOURCE: Author.

The virtual tracers marking the basal meltwater from each ice shelf along the water column were released for ten years (2006 - 2016). The quantity of virtual tracers gradually grows over time. Figure 4.7 shows a time frame of meltwater concentration along the water column at the end of the fifth year (2011, July), after this period the

concentration of dyes starts to be saturated and it becomes difficult to differentiate the concentrations. The meltwater from the Weddell Ice shelves remains mainly over the continental shelf and it is guided mainly by the Antarctic coastal current to the west side of the AP. Meanwhile, the meltwater from the Bellinghshausen is advected by the ACC flowing outside of the continental shelf, but the highest concentrations remain over the shelf.

The Antarctic Slope Current plays an important role in encompassing the meltwater into the continental shelf (THOMPSON et al., 2018). The coastal regions concentrate the major accumulation of tracers, with 92.44 % (except Abb/Ven/Fer) of all volumes of basal meltwater (for July 2011). When considering Abb/Ven/Fer, the meltwater decreases to 51.51 % over the shelf. When comparing the mean dispersion pattern with other studies ((DINNIMAN et al., 2016; KUSAHARA; HASUMI, 2014)), the mean advection pattern of the meltwater is well represented, except Abb/Ven/Fer. The Abbot/Venable/Ferrigno ice shelves are the main ones responsible for the advection of tracers outside of the continental shelf (Figure A.3). It is possible that the proximity to the boundary limits could be the main cause of this dispersion, due to the influence of the unstable conditions along the boundary limits of the model.

Figure 4.7 - Horizontal distribution of the basal meltwater tracers averaged vertically over the entire water column.

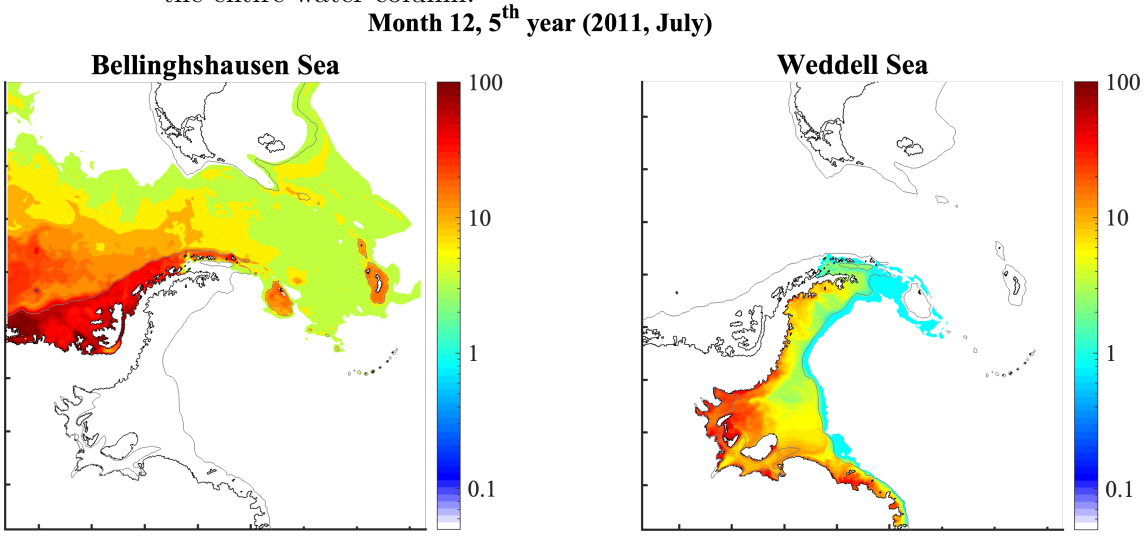

Horizontal distribution of the basal meltwater tracers along the water column. The one dye unit of the dye concentration represents the freshwater concentration of 10^{-4}. Here is the concentration five years from the start of the initial dye spread.

SOURCE: Author.

When we look vertically at the meltwater distribution, we can see three main different modes of distribution, which all are found in our domain: the Warm Mode, also known as Mode 2, found mainly over the western part of the domain, along the WAP, the Dense Mode (Mode 1), found along the Weddell side of the AP, and the Fresh mode (Mode 3), typically from the BSRL region (examples of the three modes can be found in Figure 4.8). These three vertical transects are respectively the cross-slope sections 1, 6, and 7, represented until the end of dashed lines (until isobath of 4000m) in Figure 4.1.A. In Figure 4.1.B, the colored line indicates the corresponding zones where each mode is found, based on Thompson et al. (2018).

Figure 4.8 - Three modes of ice-shelf basal melting.

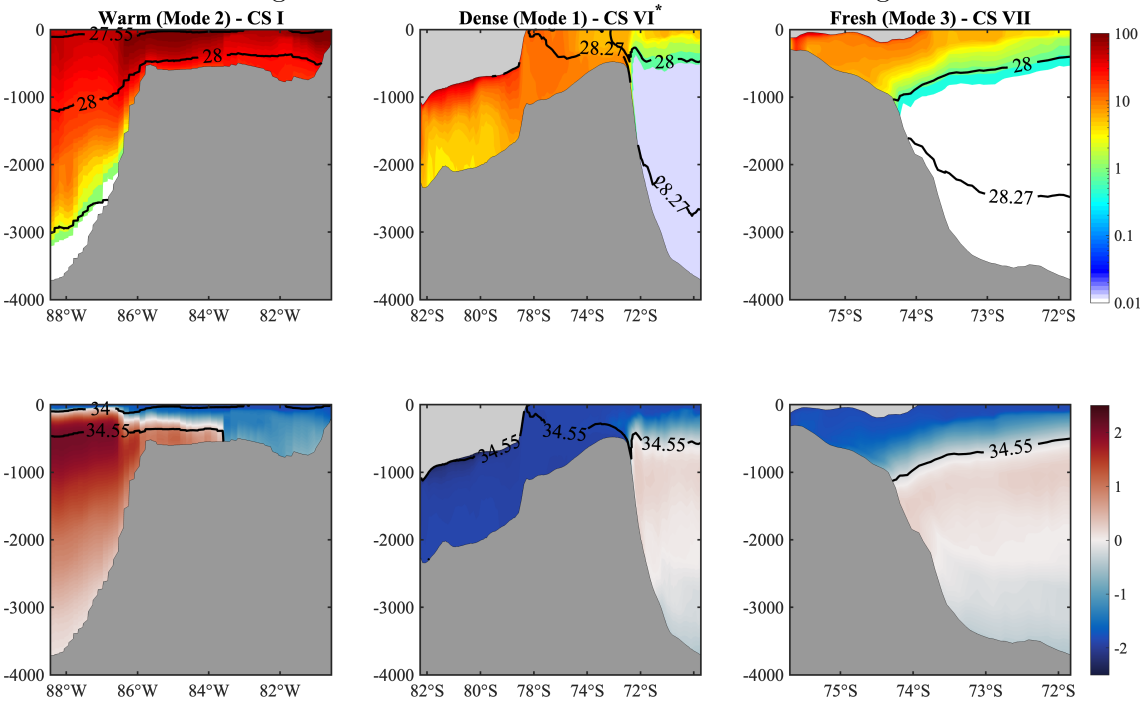

Vertically distribution of the basal meltwater tracers, neutral density (γ^n), temperature and salinity distribution along the water column, for the same time-frame (July 2011) of the Figure 4.7. Upper lines: Meltwater concentration, lines represent neutral density. The one dye unit of the dye concentration represents the freshwater concentration of 10^{-4}. Here is presented the concentration five years from the start of the initial dye spread. Cross-section 1 is a typically warm ice shelf mode (Type II), cross-section 6 (*here extended until isobath of 4000 m) is a typical Dense Ice shelf mode (Type I), and cross-section 7 is related to a typical fresh mode (Type III). Lower lines: potential temperature (θ °C) in colors. Lines represent the potential salinity.

SOURCE: Author.

We can see that the spread of the meltwater between the three modes is very different along the water column, mainly due to the currents that influence the advection, but also the bathymetry and main depth of the water inflows inside the cavities.

4.5.3 Freshwater contribution in sea-ice formation

The sea ice is formed by the cooling of the ocean's surface. Through this process, brine rejection occurs (which is the separation of the salt from the freezing water), making the surrounding water saltier and consequently denser. The sea ice production primarily happens during March - September (autumn and winter), and the melt process during late September - February (spring and summer), affects the distribution of salt and freshwater along the year (PELLICHERO et al., 2018).

The cold and fresh water from the melting of ice shelves has a strong impact on the sea ice (HELLMER, 2004; KUSAHARA, 2021; KUSAHARA et al., 2023). With other variables, such as atmosphere parameters (e.g., air temperature, surface winds, precipitation), the introduction of very cold and fresh waters from melting ice shelves contributes to the increase of sea ice production, especially over the region near the ice shelves. In contrast, the sea ice production also affects the basal melting. The sea ice modulates the intensity of the atmosphere-ocean interaction. When sea ice decreases or creates polynyas near the ice shelves, the heat exchange between the ocean and ice shelf is modified due to changes in the water masses properties and distribution (KHAZENDAR et al., 2016).

The CTRL and SENST experiments do not show a significant difference in the sea ice extent but differences are present in concentration (Figure 4.9). The differences along the coast are in the order of 2% of SIC along the WAP and very near the shelves, with the main parts showing larger concentration in the CTRL experiment (Figure 4.9. C), and it reaches 10 $cm\ s^{-1}$ of difference along the East AP (Figure 4.10). The very cold waters from the basal melting process contribute to the increased sea ice concentration, mainly in the shelf-ocean interface regions. Over the Weddell Gyre, we have the highest differences, mainly during the summer/autumn. The strong katabatic winds from the continent and the westerly winds along the latitudes lower than 60°S, and the topography, including continental boundaries and seabed structures, guide the sea ice to the middle of the Weddell Gyre, increasing its thickness. The increasing sea ice layer at the surface, in consequence, works as a barrier between the ocean and atmosphere, reducing the movement of heat and wind stress over the water column. As a consequence, the currents under the sea ice are reduced, and it increases along the borders where the exchange occurs more

easily.

Figure 4.9 - Differences in sea ice concentration between CTRL and SENST experiments.

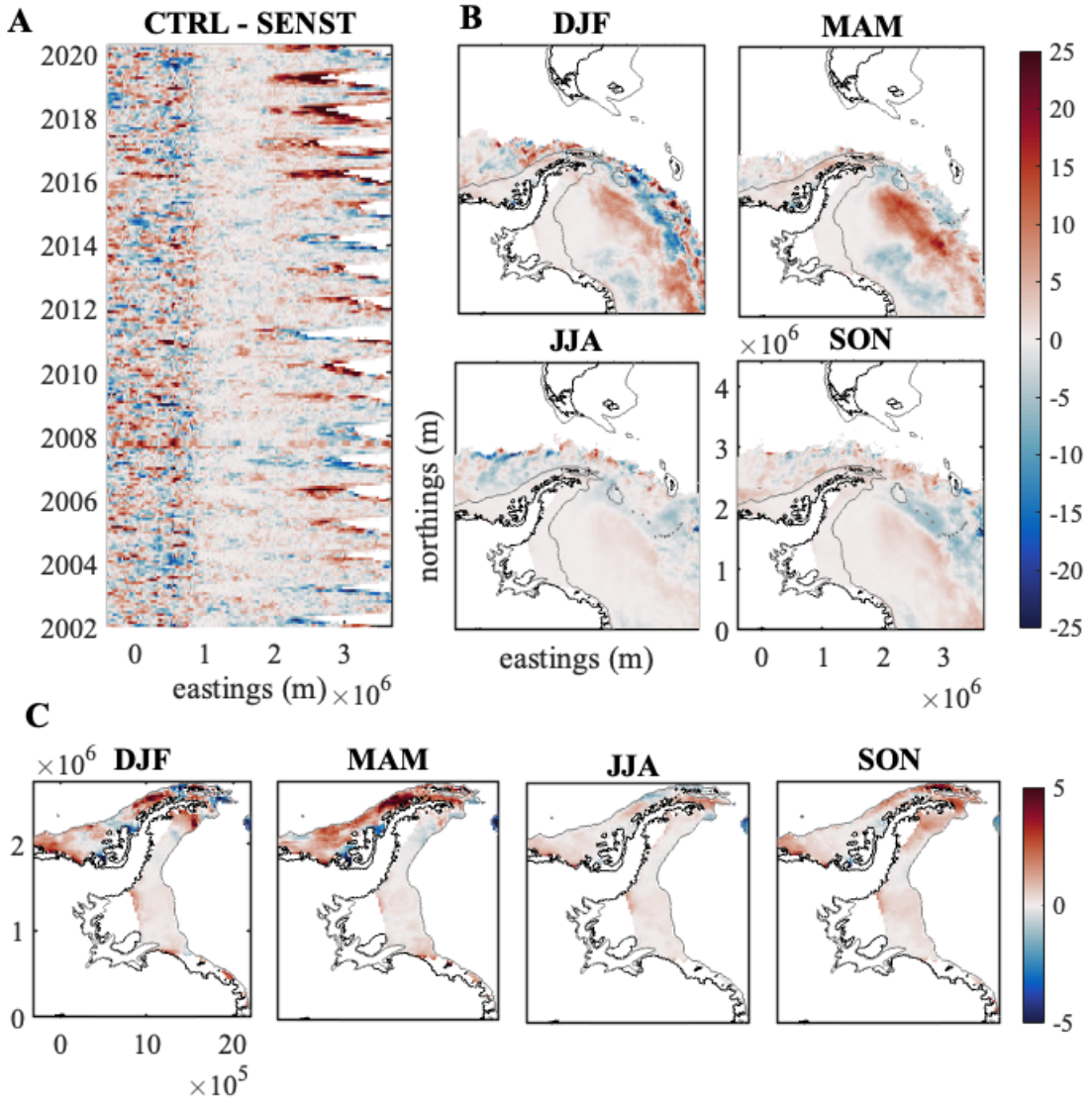

Differences between CTRL and SENST sea ice concentration. Red tones indicate that CTRL has higher values, and blue tones indicate that SENST presents higher values. A. Hovmoler longitudinal diagram. B. Austral Summer (DJF), Autumn (MAM), Winter (JJA), and Spring (SON) mean spatial differences in sea ice. C. Zoom in the continental shelf region.

SOURCE: Author.

Figure 4.10 - Differences in currents velocity magnitude and sea ice thickness between CTRL and SENST experiments.

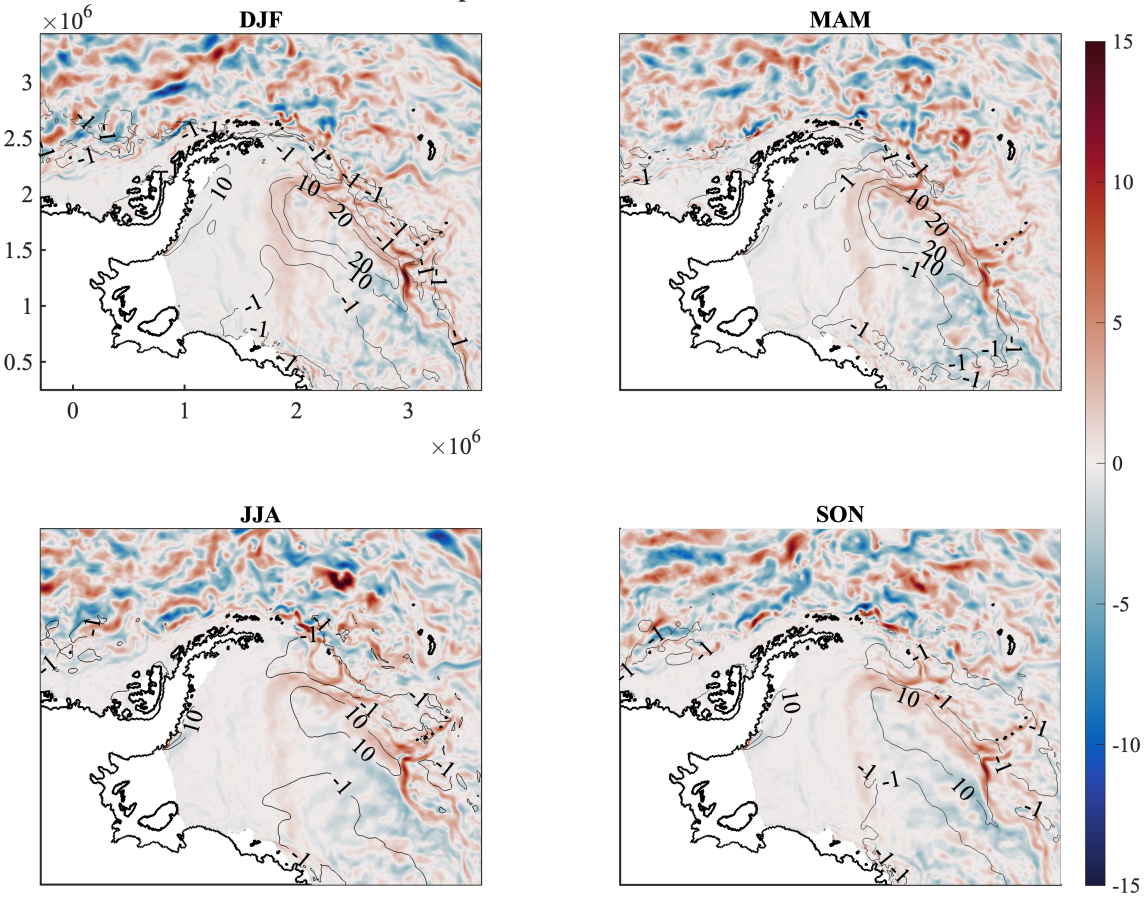

Differences between CTRL and SENST experiments. Currents magnitude (cm s^{-1}), red tones indicate current strengthening in the CTRL experiment, and blue tones indicate current weakening. The contour lines indicate the difference between CTRL and SENST ice thickness in cm.

SOURCE: Author.

The effect of the stratification of the water column, due to the introduction of the very cold waters from the basal melting process, the strong katabatic winds from the continent, and the westerly winds along the latitudes below 60°S, enclosures into the middle of the clockwise direction of the Weddell Gyre conducts the cold waters from the Weddell Sea over the northern part of the Gyre and contributing to the deepening of the mixed layer depth there. This increased stratification, and enhanced fresh and cold surface waters contribute to the increased concentration in the CTRL results.

Since the beginning of 2016, the CTRL experiment presented an increased sea ice concentration in the Weddell Sea, concurrent with the negative Antarctic and AP anomaly in the extension of the sea ice (PURICH; DODDRIDGE, 2023). This increased concentration in CTRL explains and corroborates the intrinsic correlation between sea ice and basal melting. With less coverage of sea ice, the surface waters warm in contact with the atmosphere, causing the increasing melting of the shelves (AOKI et al., 2022).

The increase in the concentration of freshwater over the surface layers of the ocean, originating from the melting of Antarctic ice shelves and variations in precipitation, can explain the increase in sea ice (HAUMANN et al., 2016). These processes lead to a decrease in water density at the surface (freshwater is less dense than saltwater), reducing convection and increasing water mass stratification. Changes in stratification are indicated by various studies, particularly demonstrating a decrease in surface salinity in the Ross Sea (HAUMANN et al., 2016; PAULING et al., 2016; PAULING et al., 2017) and a circum-polar intensification of vertical salinity gradients near the surface and temperature gradients due to the brine effect (STEIN et al., 2020). The transport of freshwater to the north occurs as sea ice forms in relatively cold regions near the continent and releases freshwater further along after being transported by winds and ocean currents, resulting in significant changes in salinity distribution in the Southern Ocean (HAUMANN et al., 2016).

In summary, the processes of sea ice formation, melting ice shelves, and the resulting surface stratification, and their impact on the formation of water masses, are intrinsically linked. Atmospheric factors that affect the water surface and ice formation modulate the dynamics at the surface and in the subsurface, subsequently affecting the entire water column structure in different scales. However, further studies are still needed to understand these processes completely.

4.5.4 Basal melting, sea ice, and winds

Basal melting rates, sea ice dynamics, and winds are highly related. It has been shown that the Southern Annular Mode (SAM) contributes to the wind westerlies intensity, which, in turn, contributes to the ocean and sea ice dynamics (VERFAILLIE et al., 2022; FOGT; MARSHALL, 2020; DICKENS et al., 2019; KEPPLER; LANDSCHüTZER, 2019). The SAM index is calculated as the sea level pressure difference between 40°S and 65°S (HO et al., 2012). The positive signals of this index indicate an intensification and poleward shift of the westerly winds, affecting the air temperature and precipitation. This process, in turn, induces subsurface warming

along the Antarctic shelf, shoaling the coastal thermocline and enhancing the flow of warming currents to the inside of ice shelf cavities, contributing to the increase of basal melting.

Along the Antarctic Peninsula, different dynamics induce the increased melting. Due to the positive SAM, the stronger westerly winds increase the wind stress curl over the Weddell Sea, inducing an increased WSBW export by depressing the depth of the pycnocline over the continental slope (GORDON et al., 2010). In longer periods, strong westerly winds give rise to greater injection of warm CDW into WG, which contributes to adding salt to the shelf, increasing deep water production. However, the low-pressure anomaly at the east AP region reduces the formation of the HSSW (ACKLEY et al., 2001) due to the weakening of winds, freshening the surface layer. On the WAP, the enhanced winds induce the warm CDW inflow to the shelf, enhancing the melting of the shelves (WALKER; GARDNER, 2017). Figure 4.11.A shows the time series of the sea ice extent, basal melting and zonal winds monthly anomalies, and the Southern Annular mode monthly index. The light orange shaded areas are positive SAM moving 12-month average periods (Figure 4.11. A). The variables here analyzed are the CTRL outputs, and the zonal wind used to force the model (ERA-5).

The ice shelf basal melting shows higher values in summer and minimum values in winter, almost the opposite of sea-ice extent (Figure 4.11. B). Throughout the year, we have a lag between the minimum and maximum of Basal Melting and sea ice extent. The higher melting from shelves occurs between February and March when the sea ice is close to its minimum extent. Meanwhile, the maximum sea ice extent occurs in August - September, and the minimum volumes from basal melting occur in June. Figure 4.11. C indicates the correlations between the two climatologies (SIE x BM), where we can see a negative correlation during the first semester and positive correlations during the second semester. Significant negative correlation coefficients exist during March and April ($r<-0.5$, $p<0.05$).

The model reproduces the seasonal and interannual sea ice variability, and also the anomalies (Figure 4.3). While seasonal variability is not evident in basal melting (Figure 4.6), the anomalies are accurately represented, aligning with the findings in Kusahara (2021). The author of the study has linked the strong negative anomaly in sea-ice extent in 2016 with a subsequent increase in basal melting six months later. This suggests that the extent of sea ice, particularly where it approaches the coast during summer, can serve as a proxy for the coastal water masses and, in turn,

influence ice shelf basal melting.

Figure 4.11 - Sea Ice Extent and Basal Melting relations.

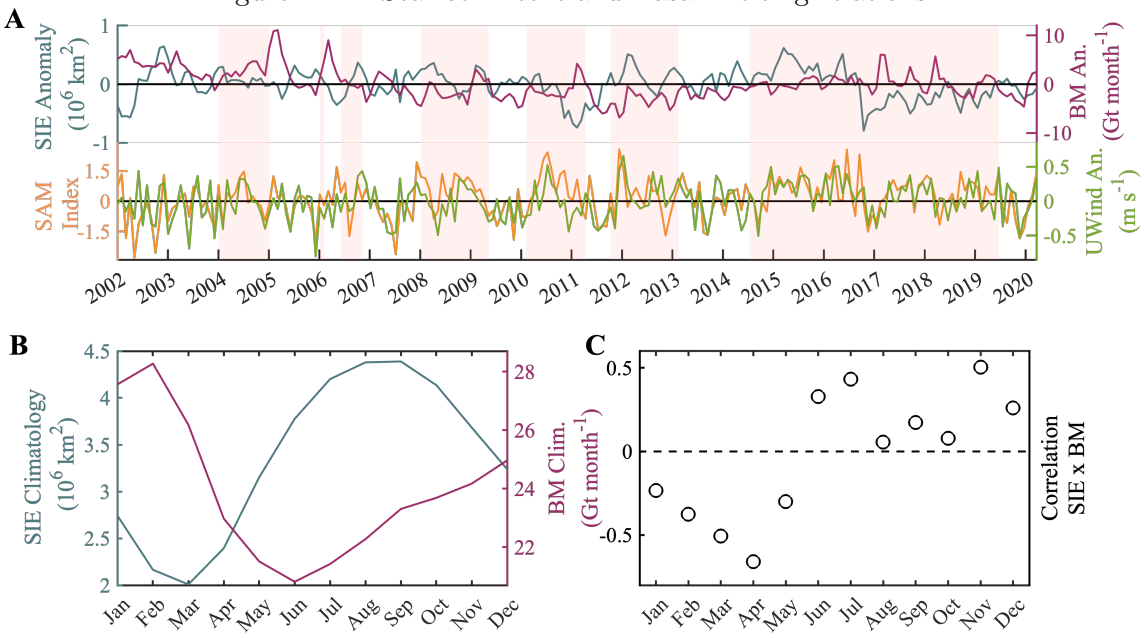

Sea Ice Extent (SIE), Basal Melting (BM), SAM index and zonal wind relations. A. Time series of monthly sea ice extent anomalies (in 10^6 km), Ice Shelf Basal Melting Anomalies (Gt/month), and SAM Index, the shaded areas on the graph are the periods of positive SAM; B. Climatology of sea-ice extent and ice shelf basal melting; C. The monthly correlation coefficients between BM and SIE climatologies.

SOURCE: Author.

To evaluate the relations between these variables and signals over time, the wavelet transform analysis was applied and after, to verify the relations in between them the wavelet coherence was applied. The wavelet transform (WT) can be used to analyze time series and detect, within a signal, components of different frequencies and the time variation of these frequencies. In other words, it permits the capture of high and low frequency components. The wavelet mother chosen here was the Morlet wavelet, it is a non-orthogonal and complex wavelet, very often used in climatological analysis, because it is better suited to capture oscillatory behavior and expected variations in wavelet amplitude (TORRENCE; COMPO, 1998). Here the WT is presented by 4 graphs: the first represents the time series (a); the second one is the wavelet power spectrum (b), where the x axis represents the wavelet location in time, y axis represents the wavelet period in years, and colors indicates

the relative power ($(value)^2$), at certain scale and a certain time, the wavelet power decreases according to the following order: yellow, orange, green, blue and white, the heavy black contours represent the 5% significance level against red noise (with a lag-1 coefficient of 0.72), and the gray contour and white shadow, represents the cone of influence. The white shaded areas have no statistical significance; letter (c) indicates the power spectrum for each period, the red line indicates the 95% confidence level; and (d) The scale-average wavelet power time series is an average of the variance in a certain band, here chosen 6 - 24 months interval. The dashed line is the 95% confidence.

Wavelet analysis (Morlet wavelet) (TORRENCE; COMPO, 1998) decomposes the basal melting anomaly time series into time and frequency space which shows significant periodicity at different frequency bands ranging from 6 months and 2 years (Figure 4.12). The scale-average wavelet power indicates significant power variance in the years 2005-2006 corresponding to the positive anomaly in BM. We have another peak in the year 2011 corresponding also to a positive anomaly, but here the variance is not significant. We have another significant peak in 2017 at a 0.5-month period.

Figure 4.12 - Basal Melting relations wavelet transform analysis.

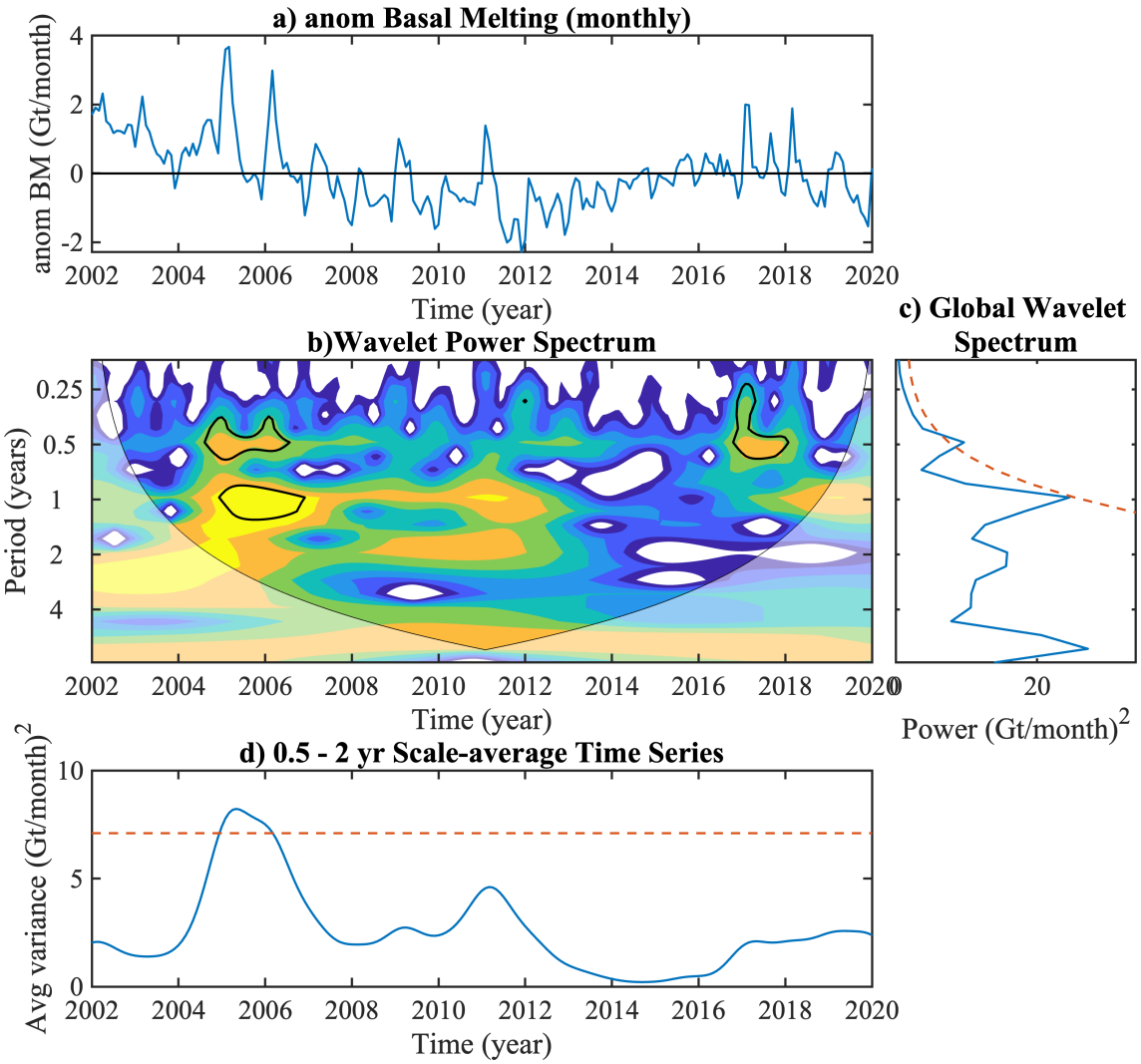

(a) Monthly anomaly in Basal melting rate (Gt/month); (b) The wavelet power spectrum using Morlet mother wavelet; (c) The global wavelet power spectrum. The dashed line is the 5% significance level for the global wavelet spectrum; and (d) Scale-average wavelet power over the 6 - 24 months' band. The dashed line is the 95% confidence.

SOURCE: Author.

When analyzing the sea ice extent it is noticed one signal in 2002-2003 is above the 95% confidence dashed line. Although, we have power near the significance line, around the one-year period. And since 2010 we have a high magnitude spectrum around 2-4 year periods. The variance spectrum for 6 months-2 years scales, has no significant values, only in 2002-2003.

Figure 4.13 - Sea Ice Extent wavelet transform analysis.

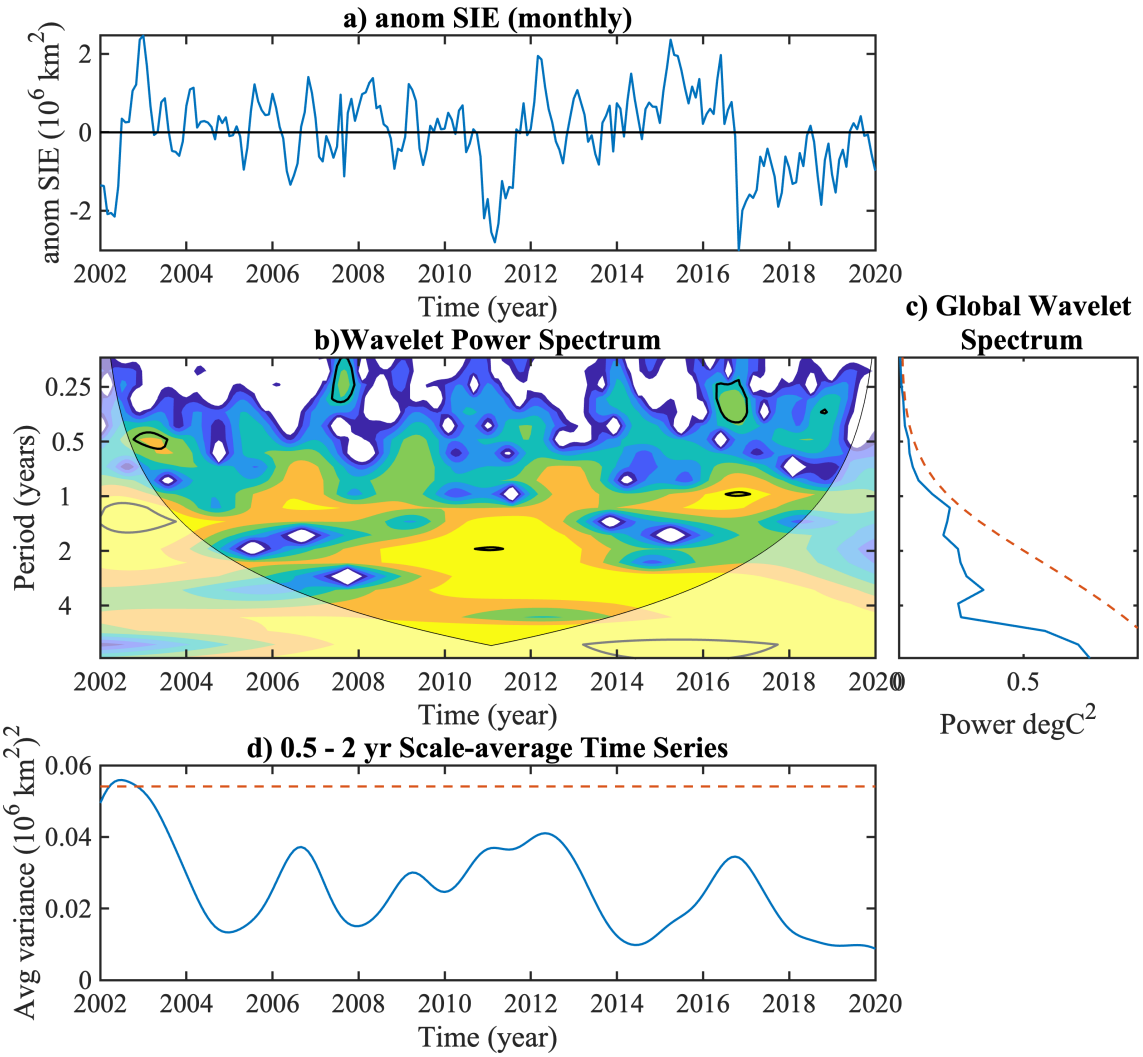

(a) Monthly anomaly in Sea Ice extent ($10^6 km^2$); (b) The wavelet power spectrum using Morlet mother wavelet; (c) The global wavelet power spectrum. The dashed line is the 5% significance level for the global wavelet spectrum; and (d) Scale-average wavelet power over the 6 - 24 months' band. The dashed line is the 95% confidence.

SOURCE: Author.

The wind WT indicates a significant high-frequency signal of less than 6 months period during most of the time series. For the periods 2007-2009, a 1-year signal was noticed, and in 2012, another signal of 10 months.

Figure 4.14 - zonal wind wavelet transform analysis.

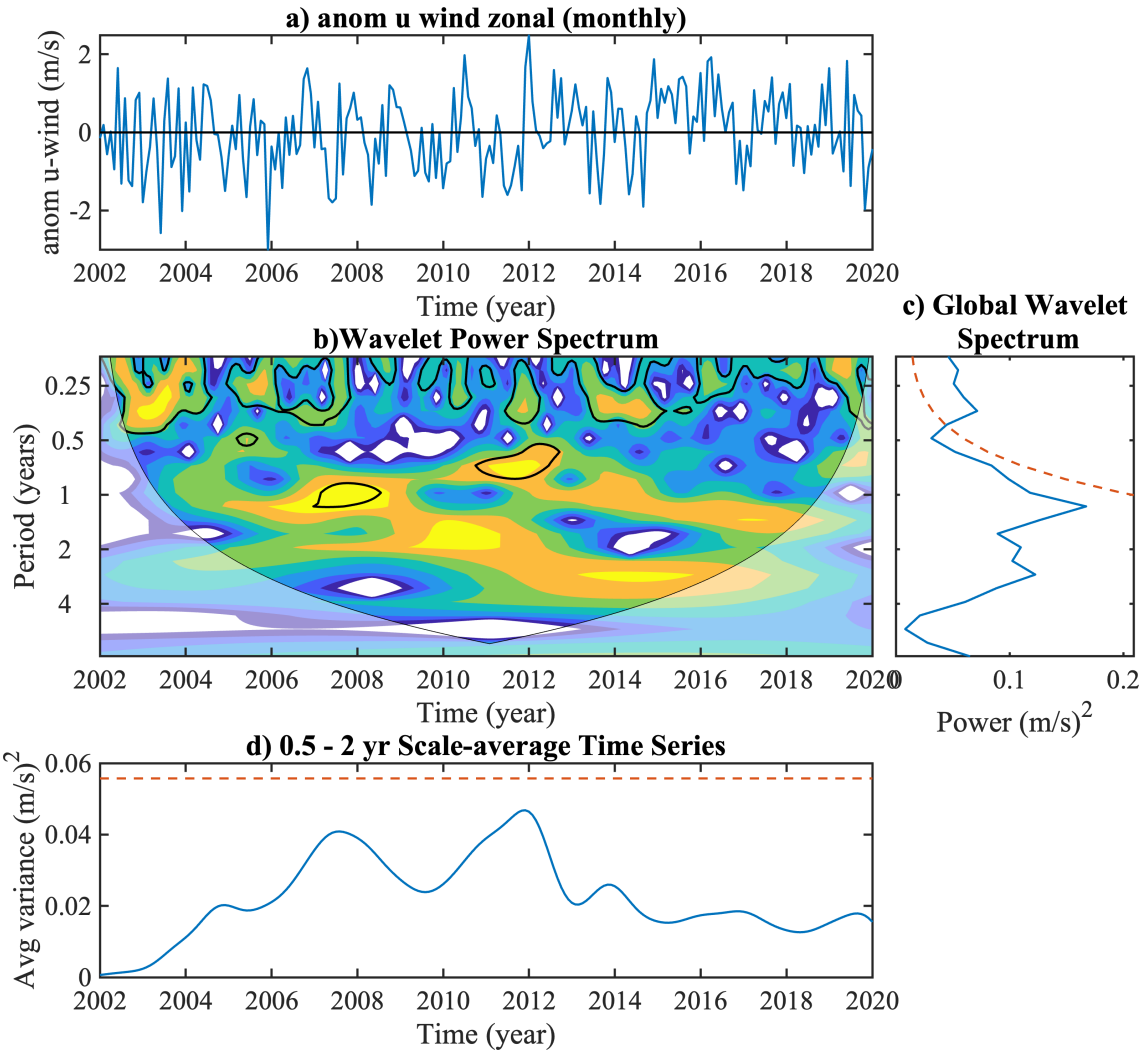

(a) Monthly anomaly in zonal wind (m/s); (b) The wavelet power spectrum using Morlet mother wavelet; (c) The global wavelet power spectrum. The dashed line is the 5% significance level for the global wavelet spectrum; and (d) Scale-average wavelet power over the 6 - 12 months' band. The dashed line is the 95% confidence.

SOURCE: Author.

To verify the relationship between the basal melting anomalies and the sea ice extent, and the influence of SAM over these processes, were applied a Wavelet Coherence analysis (GRINSTED et al., 2004). This analysis determines the most significant correlations between variables, their timing (x-axis), frequency (y-axis), and lags (arrows). Basically, this analysis allows us to identify patterns, relations, and periodicity between two time series. The direction and position of the arrow indicate the

lag timing of the second variable in relation to the first one. In areas where there are no arrows or very short arrows, it suggests a weak or no relationship between the two signals at that time and frequency scale. In the case here, we are using a monthly time series but analyzed yearly, so, to exemplify, when the arrow is horizontal and pointing to the left (0°), it will indicate a phase relationship where the first variable is delayed by half of the wavelet's oscillation period. In the context of yearly data, this would correspond to a lag of approximately six months (half a year). In the case of the arrow pointing $\sim 45°$ downward, it will correspond to a lag of approximately 0.25, or three months. The white shadows in Figures 4.12,4.13,4.14, 4.15 indicate the cone of influence (COI), where edge effects might distort the analysis. Outside of this cone, the results do not have significance. The black contours enclose regions where the 5% significance level against red noise (related to stochastic signals).

We compared the Basal Melting Anomaly (BM) with the Sea Ice Extent Anomaly (SIE), and each one with the Zonal Wind Anomaly (UWIND). Notice the strong signal in the three relations in the seasonal and year time scales. There is also a signal of 2-4-year time scales in the relations BM x SIE and SIE x UWIND. These periods align with the observed oscillation patterns changes described by Venegas e Drinkwater (2001), and AABW export reported by Kerr et al. (2012). We observed a substantial coherence between the Basal Melting and sea ice extent (Figure 4.15. A) within the 1 to 2-year, with the slanted arrow indicating an approximate 1/2 cycle phase difference between the two time series. The sea ice extent demonstrated significant coherence between 2009 and 2014 concerning basal melt. This alignment is coherent, considering that there is a six-month disparity between the respective maxima of both variables. Also, there is a slight signal of a year lag for the sea ice in response to the basal melting.

When we compared the BM with the zonal wind along the years 2007 - 2013, they were in phase, for the same two years. And for the sea ice x zonal wind for the same 2-year period, along the years 2008 - 2013, we have a lag of 3 months in relation to the wind. On this last relation, we can also see another signal over the four years period from 2009 until 2019, with a phase relationship where SIE is leading the wind by one full oscillation cycle (lead of one year).

In the years between 2007 and 2012, we had the highest peaks of the SAM index and the highest anomalies of the zonal winds. Also, in 2016 and 2017, however, the wind anomalies for this last period didn't follow the SAM peak. These findings agree with the findings from other authors (VERFAILLIE et al., 2022; LEFEBVRE; GOOSSE,

2005; HALL; VISBECK, 2002), which indicates a lack of coherence between the SAM and the ice shelf melting and sea ice extent, and between sea ice extent and basal melting.

The high values of coherence between the variables indicates that they present correlation signals varying in timing. It indicates that they are related and show a delay indicated by the arrow direction. BM and SIE (Figure 4.15.A) are related in the fact when we have less sea ice coverage, we have more interaction between the atmosphere and the ocean. The increased wind (Figure 4.11.A) and temperatures (not evaluated here), acting over the ocean with less sea ice, will increase the temperature of the ocean on the upper levels. This warmed waters flowing into the ice shelf cavities increases the basal melt rates.

Sea ice extent and basal melting are intrinsically linked, aligning with findings from other studies (HELLMER, 2004; BINTANJA et al., 2013; BINTANJA et al., 2015; MERINO et al., 2018) that suggest a significant impact of basal melting on sea ice production. Our observations indicates that a strong relation between sea ice and BM in the annual (1 year) and biennial scale (2 years). Even so, smaller scales (6 months and less than 3 months). Mainly over these signals have a lag (except the 6 months signals in 2008-2009 and 2014-2015) where the sea-ice signal result be after than BM.

Zonal winds have a strong influence over CDW variability that flows onto the continental shelf, affecting coastal upwelling and the consequent circulation under the ice shelves (STEIG et al., 2012; DUTRIEUX et al., 2014). This process influences the BM production and consequently freshwater influx into the ocean. A strong phase coherence between BM and westerly winds was evident during the two-year period from 2007 to 2013, with less significant coherence present before 2007. Between 2000 and 2014, Antarctica presented increased sea ice extent, reaching the maximum in 2014, with the high annual mean SIE of 12.8 million km² (PARKINSON, 2019).The intensified (weakened) winds can induce an increased (decreased) movement of sea ice inducing to the advance (retreat) in extension (EAYRS et al., 2021).

Further analysis is necessary to confirm these relationships. The sectorized analysis (divided into BS and WS) may yield additional insights into the behavior and relationships among basal melting, sea ice extent (and concentration), sea and air temperatures, and winds. Taking into account the influence of the Southern Annular Mode (SAM) and other indices that affect Antarctic climate, can potentially provide further clues regarding the connections between sea ice and basal melting. Neverthe-

less, the observed aspects here indicate the existence of relationships between these variables.

Figure 4.15 - Sea Ice Extent, Basal Melting and Zonal Wind wavelet coherence graphs.

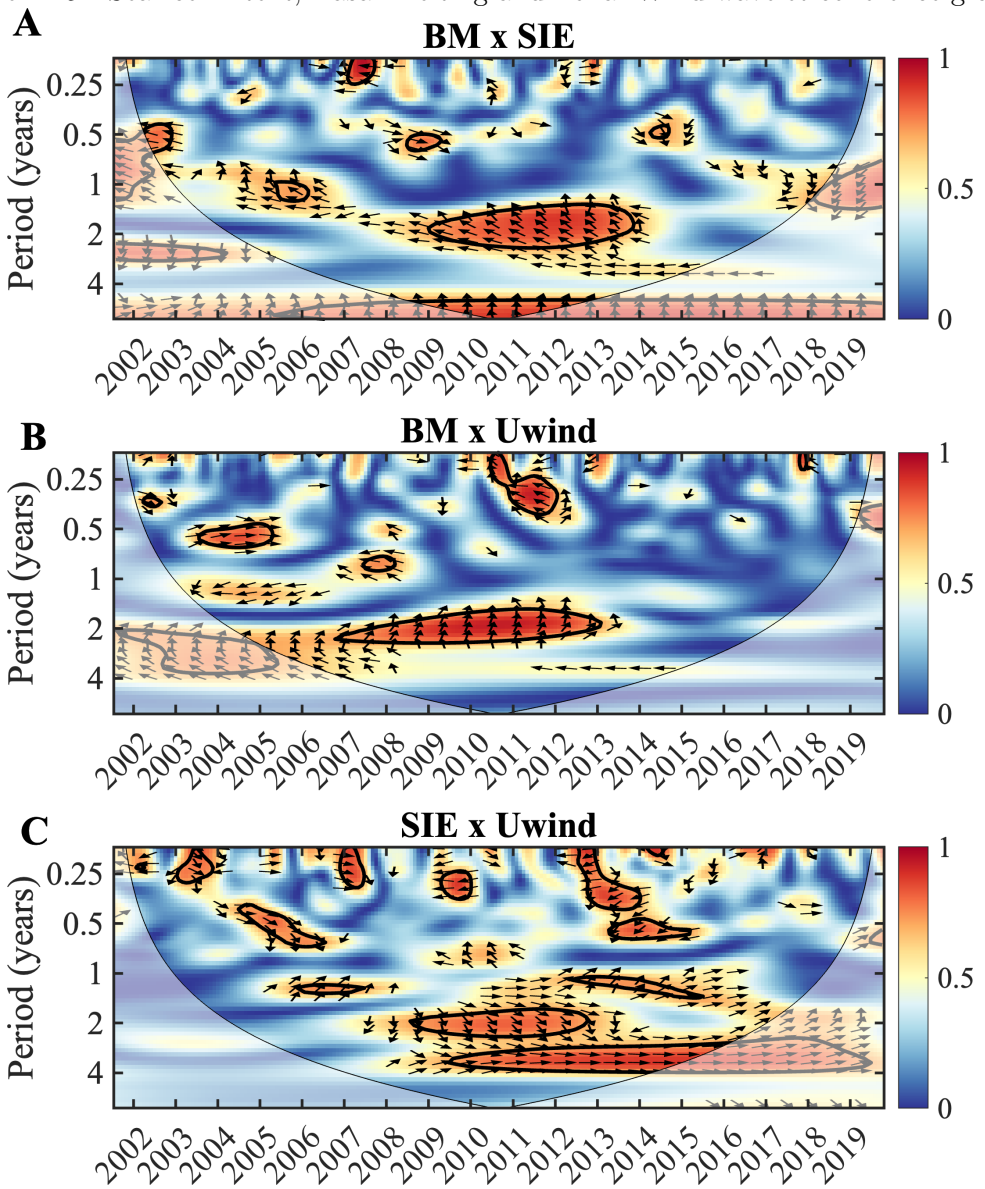

A. BM x SIE, B. BM x zonal wind, and C. SIE x zonal wind Wavelet Coherence graphs.

SOURCE: Author.

4.5.5 Basal melting and water masses relations

The basal melting process plays an essential part in shaping and transforming water masses. On the other hand, water masses circulating beneath the ice shelves also influence the melting rates. The circulation of warm ocean water inside the ice shelf cavities guides the processes of meltwater fluxes. It involves different temporal and spatial scales (DINNIMAN et al., 2016; TAMSITT et al., 2021; THOMPSON et al., 2018).

Here, we aim to understand better the seasonal and interannual variability of the water masses and the impact of the basal melt process on the production and transformation, as well as the impact of this process over the vertical structure and impacts on the oceanic stratification. We chose nine cross slope transects: three over the Bellinghshausen Sea, four in the Weddell Sea, and two based on the known transects in the Drake Passage and the WOCE SR4 (Figure 4.1). Since our focus here is to determine the water masses structure over the continental shelf, the transects were defined until the 1000 m isobath to determine the transport and water masses analysis. And the Along shelf transects follow the 1000 m isobath, to visualize the shelf break structure.

Figure 4.16 shows the differences between CTRL and SENST in the $\theta - S_A$ relationship at the cross-slope transects defined in Figure 4.1. The main difference is the formation of the dense and saline waters HSSW ($\gamma^n > 28.26, S = 34.6$ to $34.85, \theta = -1.9$ to -1.6) and ISW ($S = 34.55$ to $34.6, \theta < -1.9$) on the Weddell transects, originating from the melting processes by ice shelves. These water masses contribute significantly to the dense water formation.

Compared with observation and other studies (ZHOU et al., 2023), the CTRL experiment resulted in a better reproduction of the water column. The main difference results in more volume of dense water, as we can see in Figure 4.17 the detailed relation between CTRL and SENST along the WOCE SR4-transect. The CTRL experiment presents higher-density water in deep levels, the cold and fresh waters from basal melting in deep levels (around 2000-3000 meters depth) can be noticed in the difference temperature figure (letter (E) in Figure 4.17. The increased salinity at the bottom levels in CTRL is due to the time accumulation of WSBW along the simulation. The high salinity at the first 50 m depth around the gyre location ($\approx$ 50°W - 40°W, letter H in Figure 4.17) is due to the brine rejection during sea ice formation.

Figure 4.16 - TS-diagrams over the transects along the domain.

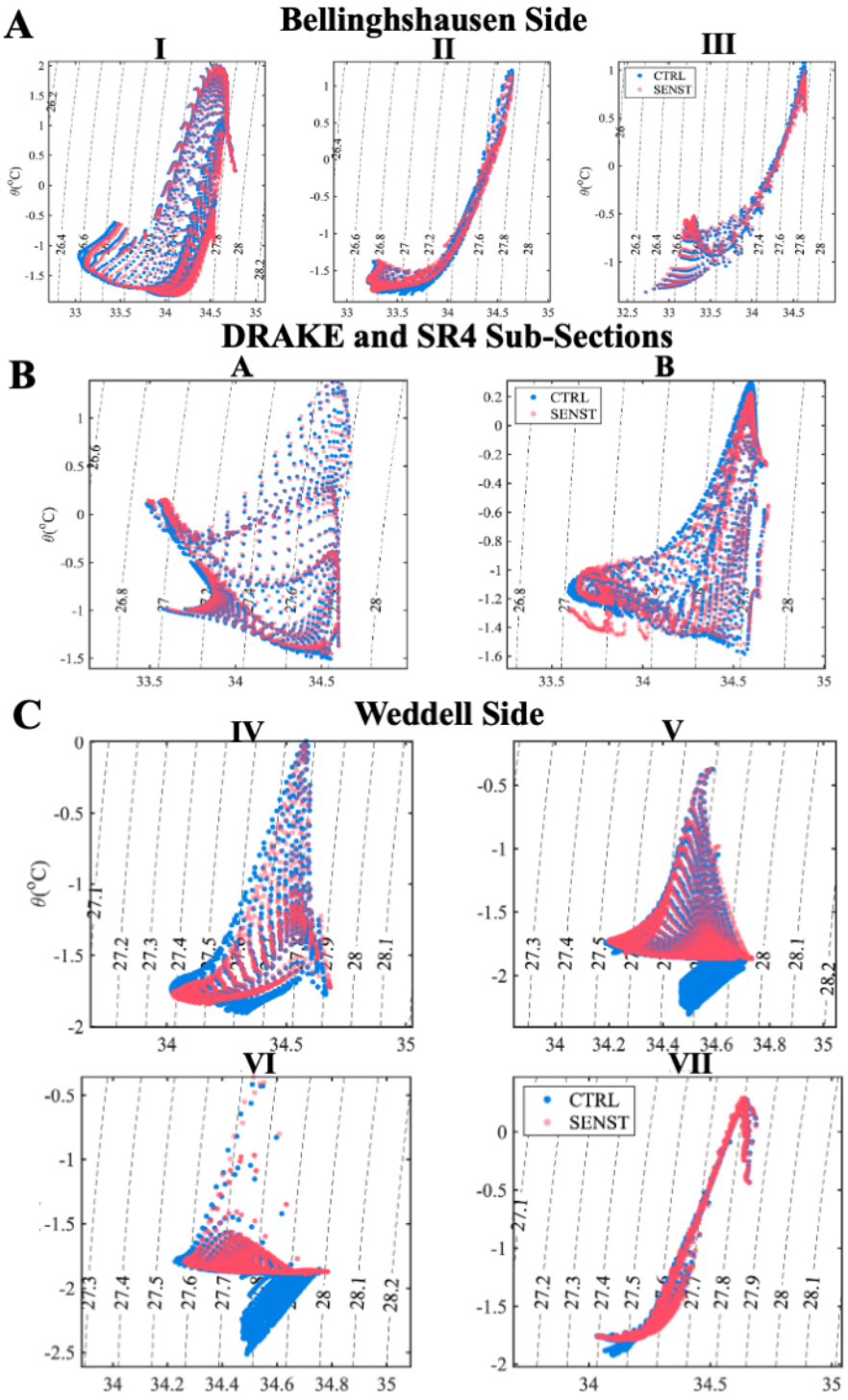

Temperature–Salinity (TS) diagrams showing the mean values recorded from August 2002 to March 2020 at the Cross-slope Sections. Black dashed lines are the water density $\sigma(kg.m^{-3}) - 1000$. A.Bellingshausen side transects. B. Drake and SR4 sub-sections; and C. Weddell Side transects.

SOURCE: Author.

Figure 4.17 - Temperature, salinity and neutral density profiles at WOCE - SR4 section.

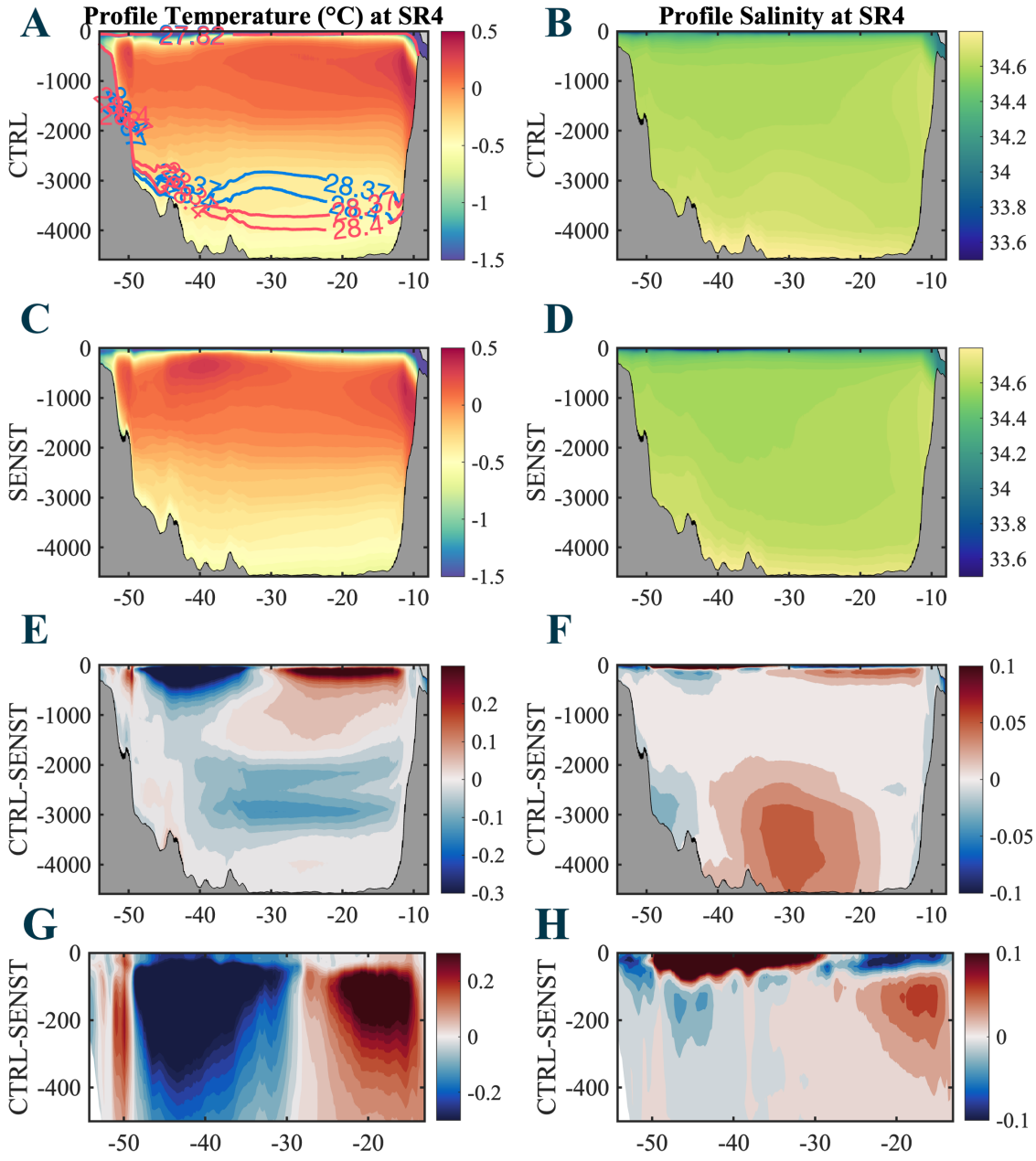

Temperature, salinity, and neutral density profiles showing the mean values recorded from August 2002 to March 2020. E, F, G, and H represent the difference between CTRL and SENST. Red colors indicate higher values in CTRL. The last two lines (G and H) are a zoom for the first 500 m depth. The x-axis represents the longitude (°W). The transect SR4 is represented in the Figure 4.1.

SOURCE: Author.

In the CS-I, CS-II, and CS-III, in BS, we found relatively warm and salty waters,

predominantly dominated by variations of CDW (Figures A.4, A.5, and A.6), in the continental shelf. The fresh and cold water derived by melting, flows near the surface and along the shelf. It is also noted that, at Bellingshausen Sea transects, we have the predominance of UCDW at CTRL, when compared with SENST, indicating lower density waters along the transects (A.15, A.16, and A.17). We do not expect the AABW formation along the WAP, so, it is expected that we do not notice the presence of AABW on these profiles.

At the Weddell Sea, the cross-section 4 (Figure A.7), near the Larsen ice shelves, shows that the cold and salty HSSW, formed by melting and mixing under the shelf, flows near the bottom. The deeper Filchner-Ronne Ice shelves (Figures A.8 and A.9), present along almost all water columns colder and fresher waters when compared with SENST, indicating the meltwater effect, with the main differences near the bottom when it flows outside the shelf. The section CS 7, near Brunt-Stacomble-Riiser-Larsen ice shelves, in the southern branch of the Weddell Sea, has a temperature under the shelf that is warmer than SENST, and only very near the ice shelf base is colder. The salinity pattern indicates a fresher pattern in the CTRL experiment near the surface and under the ice shelf. Sections A and B (Figures A.11 and A.12), respectively the subsections of Drake and SR-4, indicate a stratification pattern, with a thick fresh layer over the surface, followed by salty and cold water under it. In section B, warmer waters are flowing outside the Weddell, with a thick fresh layer at the surface.

The along-shelf break sections ASI (Figure A.13) near the LIS region and ASII (Figure A.14) near Ronne Filchner region, have signals of exportation of colder and fresher waters near the bottom in the CTRL case. At ASI there is also a signal of fresher waters near the surface, and at ASII, we have warmer waters near the surface and fresher waters at the first 500 meters.

The volume transport between simulations CTRL and SENST do not show significant differences (Table 4.4). However, there are differences when comparing the percentages of water masses found in each section. The freshwater contribution to stratification and effect on the water masses volume production is mainly observed with the ISW production in Weddell Sea transects (A.19 and A.20).

Table 4.4 - Volume Transport (Sv).

Volume Transport (Sv)		
Cross-slope	CTRL	SENST
BS-1 - (lat)	-2.42 ± 5.84	-3.58 ± 6.4
BS-2 - (lon)	0.0027 ± 0.31	-0.0093 ± 0.31
BS-3 - (lon)	0.45 ± 0.46	0.38 ± 0.46
WS-4 - (lon)	3.05 ± 1.04	3.01 ± 0.98
WS-5 - (lat)	0.25 ± 2.78	0.8 ± 2.36
WS-6 - (lat)	-3.53 ± 3.55	-3.41 ± 2.70
WS-7 - (lat)	-2.16 ± 6.4	-1.73 ± 7.11
A-DR - (lat)	1.4 ± 1.35	1.19 ± 1.26
B-SR4 - (lon)	4.73 ± 10.15	7.58 ± 8.99
Along-Shore		
AS-I - (lat)	3.04 ± 5.67	3.05 ± 6.72
AS-II - (lon)	25.82 ± 8.46	26.67 ± 8.15
Sections		
Drake - (lat)	145.62 ± 5.47	145.26 ± 5.46
WOCE-SR4 - (lon)	39.72 ± 21.54	25.2 ± 28.473

Volume transport in CTRL and SENST experiments, for each section defined. Positive (negative) values indicate the predominant direction South-North (North-South) in "lon" transects, and East-West (West-East), in "lat" transects.

SOURCE: Author.

The AABW formed in the southern Weddell Sea takes approximately two years to reach the main export region along South Scotia Ridge (near the North AP) (KERR et al., 2012), and near the limits of SIE. Along the path, the water is subjected to transformation through mixing with other water masses, and consequently, the changes in thermohaline properties may eventually change the water characteristics exported from the Weddell Sea.

The pattern of water mass proportions changed after 2011, in both simulations, along all transects, but was more pronounced at Weddell Sea transects. Note that there is an increase of WSBW and mWDW at CS5 just after the negative anomalies of SIE at the domain, and following increase of BM. However, for a better analysis, the sea ice production should be evaluated locally to verify the possible influence of sea ice over the water masses dynamics.

At Drake and SR4 sub-sections we can notice a decreased presence of dense waters since 2011, which indicates a decreased export from Weddell of dense waters. Here,

the classification of the water masses is based on the neutral density (except ISW, which was defined by temperature and salinity). These results can indicate the freshening and warming process that is happening with the AABW since the density has changed. However, more studies need to be done, such as heat transport analysis, to corroborate the decreased AABW and changes in water mass characteristics.

4.6 Summary and conclusions

In this study, we have shown the basal meltwater impacts in the water column, near the AP, at the Bellingshausen Sea and Weddell Sea. To reach this, two experiments were run, where the only difference between them was the deactivation of the influence of the basal meltwater from the ice shelf cavities. The deactivation occurred by equalizing to zero the parameterized equations of heat and salt flux from shelves.

The model reproduced properly the ocean dynamics around the AP, seasonally and interannually. Besides the grid boundaries resulting in a strong and very energetic oceanic current (ACC), the mean features were well represented, concentrating the main errors near the ACC, which is expected, probably due to the large property gradients across the ACC. The sea-ice extent and concentration presented a positive bias, mainly during summer, which also had a negative bias on the sea surface temperature and salinity.

The main differences observed between the CTRL and SENST simulations are in the sea-ice concentration and thickness at the continental shelf, with a consequent effect of the wind over the ocean currents, due to the sea ice coverage. The freshwater, extremely cold water at the surface impacts sea ice formation, increasing its concentration. The increase in sea ice contributes to the increase in the formation of HSSW, which, in turn, contributes to the formation of WSDW and WSBW.

The heat content near the surface of the SO is critical for limiting the seasonal development of sea ice, and the warming of the upper levels of the seawater can lead to the acceleration of melting of ice shelves, which in turn, compromises the stability of the ice sheets in the continent, contributing to sea level rise. The efforts to understand the relations between sea-ice-ocean-atmosphere help with the prognosis, and fortunately climate projections, in climate change scenarios.

Basal melting plays a primary role in the formation of ISW, which plays a significant role in the formation and structuring of water masses. Subsequently, the ISW affects the water column structure, increasing the dense shelf water volume. BM process also

causes freshening, changing the buoyancy and convection along the water column.

At the Bellinghshausen Sea, fresher waters increase the buoyancy along the shelf, enhancing the stratification in this area. The consequent effect is the increasing melting rates of the ice shelves. The Weddell gyre presents significant differences between both simulations. Driven by Ekman transport, the center of the gyre accumulates through time, the lighter, fresher, and colder waters. These colder surface waters lead to more sea ice formation, resulting in saltier surface waters. The northern branch of the gyre is intensified (a result of both winds and melting water), due to the thicker sea ice at the boundaries of the gyre. The deepening of the MLD in the Weddell Gyre results in increased stratification. This deepening is mainly caused by the increasing salinity process at the surface from brine rejection.

This work provides an initial view of the BM effect over the oceanic structure around AP. Further studies need to be continued, to fully understand the basal meltwater impacts around Antarctica. Considering the limitations of this model, due to the ACC and sea ice summer bias, the results presented here indicate important effects over the water masses structure from BM input. We also corroborate the findings from Kerr et al. (2012), and (VENEGAS; DRINKWATER, 2001), indicating the strong relation between the westerly winds and sea ice production, and Kusahara (2021), indicating the strong relation between the BM process with sea ice, and coastal water masses. Further studies considering tidal, and more complex sea ice structures will supplement our findings.

5 CONCLUSIONS

In this study, we aimed to assess the primary factors contributing to basal melting dynamics and the influence of the meltwater from ice shelves on ocean dynamics in Bellinghshausen and Weddell Sea. To achieve this, the research was conducted based on a numerical approach simulating the oceanic conditions with and without the basal melting process impacting the ocean. The experiment through the simulation of a regional ocean model ROMS, with a thermodynamically active sea ice and ice shelf parametrization, and subsequent sensitivity experiment, without ice shelf contributions of heat and salt which reproduces the meltwater introduction, permitted the evaluation of the effects of basal melting by the differences in both simulations.

This work provides a comprehensive compilation of the role of meltwater from ice shelves in the oceanic structure around the Antarctic Peninsula. The first chapters are dedicated to compiling knowledge related to the efforts and challenges of numerically reproducing oceanic processes at high latitudes, followed by a review of glacial meltwater dynamics and the mechanisms that transport freshwater from the melting ice to the ocean around the AP. The next chapter presents the numerical results of a sensitivity experiment conducted to answer the main questions raised in the thesis.

The numerical experiments conducted here reproduced the main oceanic features of the ocean surrounding the AP. We demonstrated that the ice shelves play an important role in the formation of the shelf water masses, and carry out the improvement of water masses production since the dense shelf waters are intrinsically related to the basal melting process and exchanges that occur in the ice shelf cavities (see summary in Figure 5.1). Inclusive the consequent effect over the bottom water properties cascading down the slope feeding the deep sea waters. The freshwater discharge along the AP shelf indirectly affects the coastal currents, by changes in the sea ice production, and variations in thermohaline structure. Variations in sea ice thickness will directly impact the interaction of the atmosphere with the surface layers of the ocean. More ice in certain areas and less ice in others lead to changes in the intensity of currents due to the effect of winds on these thinner regions. The lightening and freshening by stratification inclusive diminishes the exchange along the water column, affecting the water properties and consequent effects in the thermohaline circulation.

As expected, the sea ice concentration over the continental shelves in the CTRL

simulation is higher than in the SENST simulation, primarily due to the very cold freshwater export process associated with the ice shelf. Both the CTRL and SENST experiments successfully replicated the primary water masses within the domain. However, the CTRL experiment was particularly effective in reproducing the deep water masses, including the signal of the Ice Shelf Water (ISW), generated by the basal melting process.

Regarding the temporal analysis, the seasonal variability of BM was not well represented, mainly over the Weddell Sea ice shelves. However, the interannual variability was consistent with the observed data, even though the structure of the ice shelves remains static over time. During the simulation period, it happened significant break-up events in both sides of AP. At Bellingshausen Sea, the Wilkins ice shelf presented a break-up event at the end of 2008. At the Weddell Sea, the Larsen-B presented significant retraction in 2002. The Larsen-C calving event that generated the A-68 iceberg in 2017, wasn't reproduced here, since the ice shelf limits didn't change over time. That is a limitation of the model, however, the general pattern of basal melting over these shelves was satisfactory.

When assessing anomalies in basal melting, sea ice, and zonal wind time series, it induces that there is a relationship among them. As more intense westward winds occur, coupled with the effects of katabatic winds, they impact sea ice movement. This, in turn, affects the heat exchange between the ocean and the atmosphere, either isolating or allowing their interaction as sea ice thickness changes. Moreover, the production of High-Salinity Shelf Water (HSSW) resulting from sea ice formation is influenced when less sea ice is being formed. Consequently, the rates of dense waters are affected. With the reduction of sea ice and the subsequent freshening, the basal melting process increases (or decreases) as warmer deep waters circulate within ice cavities. When this process intensifies, greater quantities of freshwater and cold water are introduced into the ocean, contributing to increased water column stratification.

When evaluating the production of water masses over time, a pattern of change in the production of dense waters has been observed since 2011. This is strongly related to the aforementioned relationships. Therefore, a more in-depth analysis of these relationships is necessary, as well as an understanding of how these processes are interdependent. Hence, further investigation into this topic is required to explore these relationships. Additionally, how the warmer climate, with a consequently warmer ocean, affects the heat exchange between ice shelf cavities and the

open ocean structure, as well as the subsequent freshwater enrichment process due to increased freshwater input, impacts water column stratification and the potential influence on water mass formation, particularly in the deep layers.

The present study significantly contributes to the assessment of the role of the basal melting process on oceanic structure. Obtaining observational data within ice shelf cavities remains challenging due to limited access. Numerical modeling has enabled a better understanding of the thermodynamic processes occurring in these regions. This work was conducted within the scope of the SCAR INSTANT project, aimed at evaluating the Antarctic ice sheet's contribution to sea level rise and its consequent effects on global climate. It also falls under the ATMOS project, which seeks to study the primary interactions between atmospheric, oceanic, and cryospheric dynamics and thermodynamics in the Atlantic sector of the Southern Ocean, along with their relations to South American climate.

Figure 5.1 - Final Remarks: Summary of main findings of the thesis.

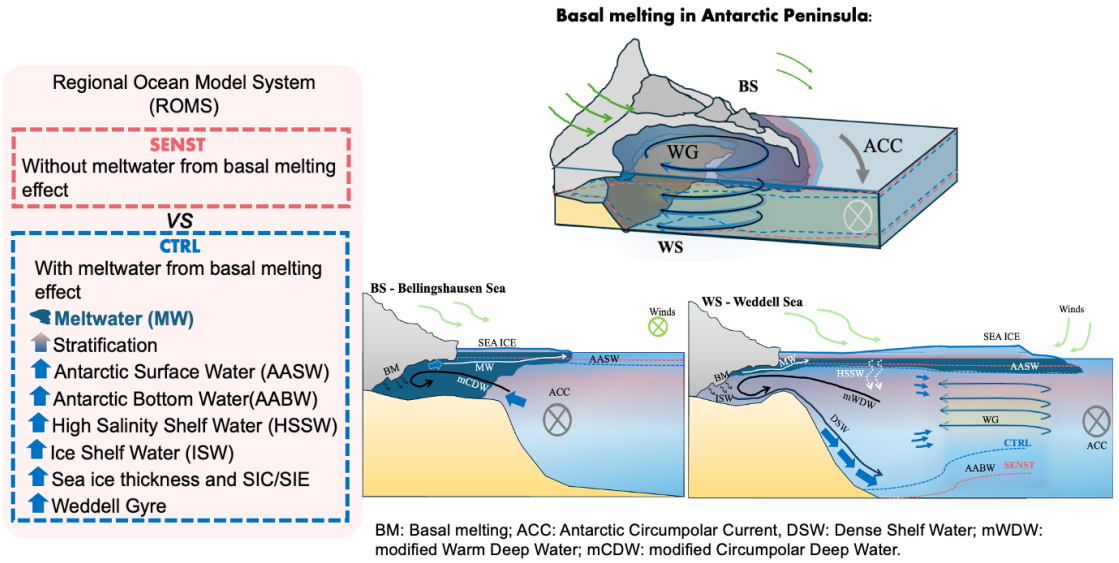

Summary of the main effects of basal melting around the Antarctic Peninsula. Results of the simulations with and without the basal melting effect. The winds are represented by the green arrows. The meltwater are represented by the dark blue plume. The differences between water densities are represented by the blue and pink dashed lines. On the CONTROL experiment we have the strengthening of the Weddell gyre, and the increased effect of meltwater and the dense waters production. In detail we see also the main processes that occurs in Bellingshausen and Weddell seas. And differences between the sea ice production on each simulation presented by the blue and pink stains.

SOURCE: Author.

REFERENCES

ABERNATHEY, R.; MARSHALL, J.; FERREIRA, D. The dependence of southern ocean meridional overturning on wind stress. **Journal of Physical Oceanography**, v. 41, p. 2261–2278, 2011. ISSN 00223670. 32

ABERNATHEY, R. P.; CEROVECKI, I.; HOLLAND, P. R.; NEWSOM, E.; MAZLOFF, M.; TALLEY, L. D. Water-mass transformation by sea ice in the upper branch of the southern ocean overturning. **Nature Geoscience**, v. 9, p. 596–601, 8 2016. ISSN 17520908. 5, 45

ABRAHAMSEN, E. P.; MEIJERS, A. J.; POLZIN, K. L.; GARABATO, A. C. N.; KING, B. A.; FIRING, Y. L.; SALLéE, J. B.; SHEEN, K. L.; GORDON, A. L.; HUBER, B. A.; MEREDITH, M. P. Stabilization of dense antarctic water supply to the atlantic ocean overturning circulation. **Nature Climate Change**, v. 9, p. 742–746, 10 2019. ISSN 17586798. 42, 43, 45

ACKLEY, S. F.; GEIGER, C. A.; KING, J. C.; HUNKE, E. C.; COMISO, J. The ronne polynya of 1997/98: observations of air-ice-ocean interaction. **Annals of Glaciology**, v. 33, p. 425–429, 9 2001. ISSN 0260-3055. Disponível em: <<https://www.cambridge.org/core/product/identifier/S0260305500264483/type/journal_article>>. 69

ADUSUMILLI, S.; FRICKER, H. A.; MEDLEY, B.; PADMAN, L.; SIEGFRIED, M. R. Interannual variations in meltwater input to the southern ocean from antarctic ice shelves. **Nature Geoscience**, v. 13, p. 616–620, 9 2020. ISSN 17520908. 4, 5, 6, 8, 24, 35, 39, 40, 41, 51

ADUSUMILLI, S.; FRICKER, H. A.; SIEGFRIED, M. R.; PADMAN, L.; PAOLO, F. S.; LIGTENBERG, S. R. M. Variable basal melt rates of antarctic peninsula ice shelves, 1994-2016. **Geophysical Research Letters**, v. 45, p. 4086–4095, 5 2018. ISSN 00948276. Disponível em: <<http://doi.wiley.com/10.1002/2017GL076652>>. 5, 8, 23, 34, 41

AKHOUDAS, C. H.; SALLéE, J. B.; HAUMANN, F. A.; MEREDITH, M. P.; GARABATO, A. N.; REVERDIN, G.; JULLION, L.; ALOISI, G.; BENETTI, M.; LENG, M. J.; ARROWSMITH, C. Ventilation of the abyss in the atlantic sector of the southern ocean. **Scientific Reports**, v. 11, 12 2021. ISSN 20452322. 45

AMANTE, C.; EAKINS, B. Etopo1 1 arc-minute global relief model: Procedures, data sources and analysis. **NOAA Technical Memorandum NESDIS NGDC-24**, p. 19, 2009. 24

ANDREASEN, J. R.; HOGG, A. E.; SELLEY, H. L. Change in antarctic ice shelf area from 2009 to 2019. **The Cryosphere**, v. 17, p. 2059–2072, 5 2023. ISSN 1994-0424. Disponível em: <<https://tc.copernicus.org/articles/17/2059/2023/>>. 7, 40

ANTONOV, J. I.; LEVITUS, S.; BOYER, T. P. Steric sea level variations during 1957-1994: importance of salinity. **Journal of Geophysical Research: Oceans**, v. 107, p. 1–8, 2002. ISSN 21699291. 23

AOKI, S.; TAKAHASHI, T.; YAMAZAKI, K.; HIRANO, D.; ONO, K.; KUSAHARA, K.; TAMURA, T.; WILLIAMS, G. D. Warm surface waters increase antarctic ice shelf melt and delay dense water formation. **Communications Earth and Environment**, v. 3, 12 2022. ISSN 26624435. 68

ARMOUR, K. C.; MARSHALL, J.; SCOTT, J. R.; DONOHOE, A.; NEWSOM, E. R. Southern ocean warming delayed by circumpolar upwelling and equatorward transport. **Nature Geoscience**, v. 9, p. 549–554, 2016. ISSN 17520908. 27

AUGER, M.; MORROW, R.; KESTENARE, E.; SALLéE, J. B.; COWLEY, R. Southern ocean in-situ temperature trends over 25 years emerge from interannual variability. **Nature Communications**, v. 12, p. 1–9, 2021. ISSN 20411723. Disponível em: <<http://dx.doi.org/10.1038/s41467-020-20781-1>>. 23, 33

AZANEU, M.; KERR, R.; MATA, M. M.; GARCIA, C. A. Trends in the deep southern ocean (1958-2010): Implications for antarctic bottom water properties and volume export. **Journal of Geophysical Research: Oceans**, v. 118, p. 4213–4227, 2013. ISSN 21699291. 27

BANERJEE, A.; FYFE, J. C.; POLVANI, L. M.; WAUGH, D.; CHANG, K.-L. Chapter 15: polar regions (arctic and antarctic). **Nature**, v. 579, p. 544–548, 3 2020. Disponível em: <<http://www.nature.com/articles/s41586-020-2120-4>>. 4

BANZON, V.; SMITH, T. M.; CHIN, T. M.; LIU, C.; HANKINS, W. A long-term record of blended satellite and in situ sea-surface temperature for climate monitoring, modeling and environmental studies. **Earth System Science Data**, v. 8, p. 165–176, 4 2016. ISSN 1866-3516. Disponível em: <<https://essd.copernicus.org/articles/8/165/2016/>>. 52

BARBAT, M. M.; RACKOW, T.; HELLMER, H. H.; WESCHE, C.; MATA, M. M. Three years of near-coastal antarctic iceberg distribution from a machine learning approach applied to sar imagery. **Journal of Geophysical Research: Oceans**, v. 124, p. 6658–6672, 9 2019. ISSN 2169-9275. Disponível em: <<https://onlinelibrary.wiley.com/doi/abs/10.1029/2019JC015205>>. 32, 33

BARBAT, M. M.; RACKOW, T.; WESCHE, C.; HELLMER, H. H.; MATA, M. M. Automated iceberg tracking with a machine learning approach applied to sar imagery: a weddell sea case study. **ISPRS Journal of Photogrammetry and Remote Sensing**, v. 172, p. 189–206, 2 2021. ISSN 09242716. Disponível em: <<https://doi.org/10.1016/j.isprsjprs.2020.12.006https://linkinghub.elsevier.com/retrieve/pii/S0924271620303440>>. 32

BARLETT, E. M. R.; TOSONOTTO, G. V.; PIOLA, A. R.; SIERRA, M. E.; MATA, M. M. On the temporal variability of intermediate and deep waters in the western basin of the bransfield strait. **Deep-Sea Research Part II: Topical Studies in Oceanography**, v. 149, p. 31–46, 2018. ISSN 09670645. 27

BAUMHOER, C.; DIETZ, A.; DECH, S.; KUENZER, C. Remote sensing of antarctic glacier and ice-shelf front dynamics—a review. **Remote Sensing**, v. 10, p. 1445, 9 2018. ISSN 2072-4292. Disponível em: <<http://www.mdpi.com/2072-4292/10/9/1445>>. 51

BENTLEY, C. R. Glacial and subglacial geography of antarctica. In: _____. [s.n.], 2013. p. 11–25. Disponível em: <<http://doi.wiley.com/10.1029/GM007p0011>>. 7

BILGEN, S. I.; KIRTMAN, B. P. Impact of ocean model resolution on understanding the delayed warming of the southern ocean. **Environmental Research Letters**, v. 15, p. 114012, 11 2020. ISSN 1748-9326. Disponível em: <<https://iopscience.iop.org/article/10.1088/1748-9326/abbc3e>>. 15

BINDOFF, N. L.; HOBBS, W. R. Oceanography: Deep ocean freshening. **Nature Climate Change**, v. 3, p. 864–865, 10 2013. ISSN 1758678X. 43

BINTANJA, R.; OLDENBORGH, G. J. van; DRIJFHOUT, S. S.; WOUTERS, B.; KATSMAN, C. A. Important role for ocean warming and increased ice-shelf melt in antarctic sea-ice expansion. **Nature Geoscience**, v. 6, p. 376–379, 5 2013. ISSN 1752-0894. Disponível em: <<http://www.nature.com/articles/s41586-020-2120-4http://www.nature.com/articles/ngeo1767>>. 2, 5, 6, 24, 76

BINTANJA, R.; OLDENBORGH, G. van; KATSMAN, C. The effect of increased fresh water from antarctic ice shelves on future trends in antarctic sea ice. **Annals of Glaciology**, v. 56, p. 120–126, 7 2015. ISSN 0260-3055. Disponível em: <<https://www.cambridge.org/core/product/identifier/S0260305500261314/type/journal_article>>. 23, 76

BLUNDEN, J.; BOYER, T. State of the climate in 2020. **Bulletin of the American Meteorological Society**, v. 102, p. S1–S475, 8 2021. ISSN 0003-0007. Disponível em: <<https://journals.ametsoc.org/view/journals/bams/102/8/2021BAMSStateoftheClimate.1.xml>>. 1

BOISVERT, L.; VIHMA, T.; SHIE, C. L. Evaporation from the southern ocean estimated on the basis of airs satellite data. **Journal of Geophysical Research: Atmospheres**, v. 125, p. 1–26, 2020. ISSN 21698996. 1, 30

BÖNING, C. W.; DISPERT, A.; VISBECK, M.; RINTOUL, S. R.; SCHWARZKOPF, F. U. The response of the antarctic circumpolar current to recent climate change. **Nature Geoscience**, v. 1, p. 864–869, 12 2008. ISSN 1752-0894. Disponível em: <<http://www.nature.com/articles/s41586-020-2120-4http://www.nature.com/articles/ngeo362>>. 33

BOYER, T. P.; GARCíA, H. E.; LOCARNINI, R. A.; ZWENG, M. M.; MISHONOV, A. V.; REAGAN, J. R.; WEATHERS, K. A.; PAVER, B. O. K.; R.;, C.; SEIDOV, D.; SMOLYAR, I. V. **World Ocean Atlas 2018**. [S.l.: s.n.], 2018. 52

BOYER, T. P.; LEVITUS, S.; ANTONOV, J. I.; LOCARNINI, R. A.; GARCIA, H. E. Linear trends in salinity for the world ocean, 1955-1998. **Geophysical Research Letters**, v. 32, p. 1–4, 2005. ISSN 00948276. 23

BRONSELAER, B.; RUSSELL, J. L.; WINTON, M.; WILLIAMS, N. L.; KEY, R. M.; DUNNE, J. P.; FEELY, R. A.; JOHNSON, K. S.; SARMIENTO, J. L. Importance of wind and meltwater for observed chemical and physical changes in the southern ocean. **Nature Geoscience**, v. 13, p. 35–42, 2020. ISSN 17520908. Disponível em: <<http://dx.doi.org/10.1038/s41561-019-0502-8>>. 32, 37

BRONSELAER, B.; WINTON, M.; GRIFFIES, S. M.; HURLIN, W. J.; RODGERS, K. B.; SERGIENKO, O. V.; STOUFFER, R. J.; RUSSELL, J. L. Change in future climate due to antarctic meltwater. **Nature**, v. 564, p. 53–58, 2018. ISSN 14764687. 4, 37, 39

BROWN, P. J.; JULLION, L.; LANDSCHüTZER, P.; BAKKER, D. C. E.; GARABATO, A. C. N.; MEREDITH, M. P.; TORRES-VALDéS, S.; WATSON, A. J.; HOPPEMA, M.; LOOSE, B.; GARA-BATO, A. C. N.; JONES, E. M.; TELSZEWSKI, M.; JONES, S. D.; WANNINKHOF, R. Carbon dynamics of the weddell gyre, southern ocean. **Global Biogeochemical Cycles**, v. 29, 2015. Disponível em: <<https://hal.science/hal-01254978>>. 45

BUDGELL, W. P. Numerical simulation of ice-ocean variability in the barents sea region. **Ocean Dynamics**, v. 55, p. 370–387, 12 2005. ISSN 1616-7341. 14, 16, 18, 20, 46

CAI, W.; GAO, L.; LUO, Y.; LI, X.; ZHENG, X.; ZHANG, X.; CHENG, X.; JIA, F.; PURICH, A.; SANTOSO, A.; DU, Y.; HOLLAND, D. M.; SHI, J.-R.; XIANG, B.; XIE, S.-P. Southern ocean warming and its climatic impacts. **Science Bulletin**, v. 68, p. 946–960, 5 2023. ISSN 20959273. Disponível em: <<https://linkinghub.elsevier.com/retrieve/pii/S2095927323002268>>. 13

CARMACK, E. C.; FOSTER, T. D. On the flow of water out of the weddell sea. **Deep Sea Research and Oceanographic Abstracts**, v. 22, p. 711–724, 11 1975. ISSN 00117471. Disponível em: <<https://linkinghub.elsevier.com/retrieve/pii/0011747175900777>>. 7

CARRASCO, J. F. Decadal changes in the near-surface air temperature in the western side of the antarctic peninsula. **Atmospheric and Climate Sciences**, v. 03, p. 275–281, 2013. ISSN 2160-0414. Disponível em: <<http://www.scirp.org/journal/doi.aspx?DOI=10.4236/acs.2013.33029>>. 27, 28

CASPEL, M. van; HELLMER, H. H.; MATA, M. M. On the ventilation of bransfield strait deep basins. **Deep Sea Research Part II: Topical Studies in Oceanography**, v. 149, p. 25–30, 3 2018. ISSN 09670645. Disponível em: <<https://linkinghub.elsevier.com/retrieve/pii/S0967064517301984>>. 35

CASPEL, M. van; SCHRöDER, M.; HUHN, O.; HELLMER, H. Precursors of antarctic bottom water formed on the continental shelf off larsen ice shelf. **Deep Sea Research Part I: Oceanographic Research Papers**, v. 99, p. 1–9, 5 2015. ISSN 09670637. Disponível em: <<http://dx.doi.org/10.1016/j.dsr.2015.01.004https://linkinghub.elsevier.com/retrieve/pii/S0967063715000199>>. 35

CAVALIERI, D. J.; GLOERSEN, P.; CAMPBELL, W. J. Determination of sea ice parameters with the nimbus 7 smmr. **Journal of Geophysical Research**, v. 89, p. 5355–5369, 1984. 51

CHEON, W. G.; KUG, J.-S. The role of oscillating southern hemisphere westerly winds: Global ocean circulation. **Journal of Climate**, v. 33, p. 2111–2130, 3 2020. ISSN 0894-8755. Disponível em: <<http://journals.ametsoc.org/doi/10.1175/JCLI-D-19-0364.1>>. 37

CHRETIEN, L. M. S.; THOMPSON, A. F.; FLEXAS, M. M.; SPEER, K.; SWAIM, N.; OELERICH, R.; RUAN, X.; SCHUBERT, R.; LOBUGLIO, C. The shelf circulation of the bellingshausen sea. **Journal of Geophysical Research: Oceans**, v. 126, 5 2021. ISSN 2169-9275. Disponível em: <<https://agupubs.onlinelibrary.wiley.com/doi/10.1029/2020JC016871>>. 44

CHUTER, S. J.; ZAMMIT-MANGION, A.; ROUGIER, J.; DAWSON, G.; BAMBER, J. L. Mass evolution of the antarctic peninsula over the last 2 decades from a joint bayesian inversion. **The Cryosphere**, v. 16, p. 1349–1367, 4 2022. ISSN 1994-0424. Disponível em: <<https://tc.copernicus.org/articles/16/1349/2022/>>. 5

COGLEY, J. G.; HOCK, R.; RASMUSSEN, L. A.; ARENDT, A. A.; BAUDER, A.; BRAITHWAITE, R. J.; JANSSON, P.; KASER, G.; MöLLER, M.; NICHOLSON, L.; ZEMP, M. **Glossary of glacier mass balance and related terms**. 2011. 114 p. Disponível em: <<https://doi.org/10.5167/uzh-53475>>. 25

COLLARES, L. L.; MATA, M. M.; KERR, R.; ARIGONY-NETO, J.; BARBAT, M. M. Iceberg drift and ocean circulation in the northwestern weddell sea, antarctica. **Deep-Sea Research Part II: Topical Studies in Oceanography**, v. 149, p. 10–24, 2018. ISSN 09670645. Disponível em: <<https://doi.org/10.1016/j.dsr2.2018.02.014>>. 32

COMISO, J. C.; MEIER, W. N.; GERSTEN, R. Variability and trends in the arctic sea ice cover: Results from different techniques. **Journal of Geophysical Research: Oceans**, v. 122, p. 6883–6900, 2017. ISSN 21699291. 3

COMISO, J. C.; SULLIVAN, C. W. Satellite microwave and in situ observations of the weddell sea ice cover and its marginal ice zone. **Journal of Geophysical Research**, v. 91, p. 9663, 1986. ISSN 0148-0227. Disponível em: <<http://doi.wiley.com/10.1029/JC091iC08p09663>>. 51

COOK, A. J. Retreating glacier fronts on the antarctic peninsula over the past half-century. **Science**, v. 308, p. 541–544, 4 2005. ISSN 0036-8075. Disponível em: <<https://www.sciencemag.org/lookup/doi/10.1126/science.1104235>>. 4

COOK, A. J.; HOLLAND, P. R.; MEREDITH, M. P.; MURRAY, T.; LUCKMAN, A.; VAUGHAN, D. G. Ocean forcing of glacier retreat in the western antarctic peninsula. **Science**, v. 353, p. 283–286, 7 2016. ISSN 0036-8075. Disponível em: <<https://www.sciencemag.org/lookup/doi/10.1126/science.aae0017>>. 5, 6, 23, 41

COOK, A. J.; VAUGHAN, D. G. Overview of areal changes of the ice shelves on the antarctic peninsula over the past 50 years. **The Cryosphere**, v. 4, p. 77–98, 2 2010. ISSN 1994-0424. Disponível em: <<https://tc.copernicus.org/articles/4/77/2010/>>. 5, 8, 35, 36, 41

COOPER, A. P. Historical observations of prince gustav ice shelf. **Polar Record**, v. 33, p. 285–294, 1997. ISSN 00322474. 36

DARELIUS, E.; MAKINSON, K.; DAAE, K.; FER, I.; HOLLAND, P. R.; NICHOLLS, K. W. Hydrography and circulation in the filchner depression, weddell sea, antarctica. **Journal of Geophysical Research: Oceans**, v. 119, p. 5797–5814, 9 2014. ISSN 21699291. 45

DAWSON, E. J.; SCHROEDER, D. M.; CHU, W.; MANTELLI, E.; SEROUSSI, H. Ice mass loss sensitivity to the antarctic ice sheet basal thermal state. **Nature Communications**, v. 13, 12 2022. ISSN 20411723. 40

DEBEER, C. M.; SHARP, M.; SCHUSTER-WALLACE, C. **Glaciers and Ice Sheets**. [s.n.], 2020. 182-194 p. ISBN 9780124095489. Disponível em: <<http://dx.doi.org/10.1016/B978-0-12-409548-9.12441-8https://linkinghub.elsevier.com/retrieve/pii/B9780124095489124418>>. 30

DEPOORTER, M. A.; BAMBER, J. L.; GRIGGS, J. A.; LENAERTS, J. T. M.; LIGTENBERG, S. R. M.; BROEKE, M. R. van den; MOHOLDT, G. Calving fluxes and basal melt rates of antarctic ice shelves. **Nature**, v. 502, p. 89–92, 10 2013. ISSN 0028-0836. Disponível em: <<http://www.nature.com/articles/nature12567>>. 25, 39, 60

DICKENS, W. A.; KUHN, G.; LENG, M. J.; GRAHAM, A. G.; DOWDESWELL, J. A.; MEREDITH, M. P.; HILLENBRAND, C. D.; HODGSON, D. A.; ROBERTS, S. J.; SLOANE, H.; SMITH, J. A. Enhanced glacial discharge from the eastern antarctic peninsula since the 1700s associated with a positive southern annular mode. **Scientific Reports**, v. 9, 12 2019. ISSN 20452322. 23, 30, 68

DIERSSEN, H. M.; SMITH, R. C.; VERNET, M. Glacial meltwater dynamics in coastal waters west of the antarctic peninsula. **Proceedings of the National Academy of Sciences of the United States of America**, v. 99, p. 1790–1795, 2002. ISSN 00278424. 34

DINNIMAN, M.; ASAY-DAVIS, X.; GALTON-FENZI, B.; HOLLAND, P.; JENKINS, A.; TIMMERMANN, R. Modeling ice shelf/ocean interaction in antarctica: a review. **Oceanography**, v. 29, p. 144–153, 12 2016. ISSN 10428275. Disponível em: <<https://tos.org/oceanography/article/modeling-ice-shelf-ocean-interaction-in-antarctica-a-review>>. 15, 63, 78

DINNIMAN, M. S.; KLINCK, J. M.; HOFMANN, E. E. Sensitivity of circumpolar deep water transport and ice shelf basal melt along the west antarctic peninsula to changes in the winds. **Journal of Climate**, v. 25, p. 4799–4816, 7 2012. ISSN 0894-8755. Disponível em: <<http://journals.ametsoc.org/doi/10.1175/JCLI-D-11-00307.1>>. 13, 34, 40

DINNIMAN, M. S.; KLINCK, J. M.; SMITH, W. O. Influence of sea ice cover and icebergs on circulation and water mass formation in a numerical circulation model of the ross sea, antarctica. **Journal of Geophysical Research: Oceans**, v. 112, 2007. ISSN 21699291. 14, 15, 20, 46, 49

DOTTO, T. S.; MATA, M. M.; KERR, R.; GARCIA, C. A. E. A novel hydrographic gridded data set for the northern antarctic peninsula. **Earth System Science Data**, v. 13, p. 671–696, 2 2021. ISSN 1866-3516. Disponível em: <<https://essd.copernicus.org/articles/13/671/2021/>>. 27, 30

DOUVILLE, H.; JOHN, A. Fast adjustment versus slow sst-mediated response of daily precipitation statistics to abrupt 4xco2. **Climate Dynamics**, v. 56, p. 1083–1104, 2 2021. ISSN 14320894. 1

DOUVILLE, H. K.; RAGHAVAN, J.; RENWICK, J.; ALLAN, R.; ARIAS, P.; BARLOW, R.; CEREZO-MOTA, A.; CHERCHI, T.; GAN, J.; GERGIS, J.; JIAN, D.; KHAN, A.; POKAM, W.; ROSENFELD, D.; TIERNEY, J.; ZOLINA, O. **Water Cycle Changes**. 2021. 1055-1210 p. 2

DUPONT, T. K.; ALLEY, R. B. Role of small ice shelves in sea-level rise. **Geophysical Research Letters**, v. 33, p. L09503, 2006. ISSN 0094-8276. Disponível em: <<http://doi.wiley.com/10.1029/2005GL025665>>. 39

DURACK, P. Ocean salinity and the global water cycle. **Oceanography**, v. 28, p. 20–31, 3 2015. ISSN 10428275. Disponível em: <<https://tos.org/oceanography/article/ocean-salinity-and-the-global-water-cycle>>. 23

DURACK, P. J.; WIJFFELS, S. E. Fifty-year trends in global ocean salinities and their relationship to broad-scale warming. **Journal of Climate**, v. 23, p. 4342–4362, 2010. ISSN 08948755. 23

DURACK, P. J.; WIJFFELS, S. E.; MATEAR, R. J. Ocean salinities reveal strong global water cycle intensification during 1950 to 2000. **Science**, v. 336, p. 455–458, 4 2012. ISSN 0036-8075. Disponível em: <<https://www.sciencemag.org/lookup/doi/10.1126/science.1212222>>. 33

DURAND, M.; FU, L. L.; LETTENMAIER, D. P.; ALSDORF, D. E.; RODRIGUEZ, E.; ESTEBAN-FERNANDEZ, D. The surface water and ocean topography mission: Observing terrestrial surface water and oceanic submesoscale eddies. **Proceedings of the IEEE**, v. 98, p. 766–779, 2010. ISSN 00189219. 27

DUTRIEUX, P.; RYDT, J. D.; JENKINS, A.; HOLLAND, P. R.; HA, H. K.; LEE, S. H.; STEIG, E. J.; DING, Q.; ABRAHAMSEN, E. P.; SCHRöDER, M. Strong sensitivity of pine island ice-shelf melting to climatic variability. **Science**, v. 343, p. 174–178, 1 2014. ISSN 0036-8075. Disponível em: <<https://www.science.org/doi/10.1126/science.1244341>>. 76

DUVIVIER, A. K.; MOLINA, M. J.; DEPPENMEIER, A. L.; HOLLAND, M. M.; LANDRUM, L.; KRUMHARDT, K.; JENOUVRIER, S. Projections of winter polynyas and their biophysical impacts in the ross sea antarctica. **Climate Dynamics**, 2023. ISSN 14320894. 13

EAYRS, C.; HOLLAND, D.; FRANCIS, D.; WAGNER, T.; KUMAR, R.; LI, X. Understanding the seasonal cycle of antarctic sea ice extent in the context of longer-term variability. **Reviews of Geophysics**, v. 57, p. 1037–1064, 2019. ISSN 19449208. 34

EAYRS, C.; LI, X.; RAPHAEL, M. N.; HOLLAND, D. M. Rapid decline in antarctic sea ice in recent years hints at future change. **Nature Geoscience**, v. 14, p. 460–464, 7 2021. ISSN 1752-0894. Disponível em: <<https://www.nature.com/articles/s41561-021-00768-3>>. 76

ETOURNEAU, J.; SGUBIN, G.; CROSTA, X.; SWINGEDOUW, D.; WILLMOTT, V.; BARBARA, L.; HOUSSAIS, M. N.; SCHOUTEN, S.; DAMSTé, J. S.; GOOSSE, H.; ESCUTIA, C.; CRESPIN, J.; MASSé, G.; KIM, J. H. Ocean temperature impact on ice shelf extent in the eastern antarctic peninsula. **Nature Communications**, v. 10, p. 544–548, 3 2019. ISSN 20411723. Disponível em: <<http://www.nature.com/articles/s41586-020-2120-4>>. 8, 41

FAHRBACH, E.; HARMS, S.; ROHARDT, G.; SCHRöDER, M.; WOODGATE, R. A. Flow of bottom water in the northwestern weddell sea. **Journal of Geophysical Research: Oceans**, v. 106, p. 2761–2778, 2 2001. ISSN 21699291. 45

FAHRBACH, E.; ROHARDT, G.; SCHEELE, N.; SCHRODER, M.; STRASS, V.; WISOTZKI, A. Formation and discharge of deep and bottom water in the northwestern weddell sea. **Oceanographic Literature Review**, v. 43, n. 5, p. 437, 1996. 45

FARINOTTI, D.; HUSS, M.; FüRST, J. J.; LANDMANN, J.; MACHGUTH, H.; MAUSSION, F.; PANDIT, A. A consensus estimate for the ice thickness distribution of all glaciers on earth. **Nature Geoscience**, v. 12, p. 168–173, 3 2019. ISSN 1752-0894. Disponível em: <<http://dx.doi.org/10.1038/s41561-019-0300-3http://www.nature.com/articles/s41561-019-0300-3>>. 31

FERON, S.; CORDERO, R. R.; DAMIANI, A.; MALHOTRA, A.; SECKMEYER, G.; LLANILLO, P. Warming events projected to become more frequent and last longer across antarctica. **Scientific Reports**, v. 11, 12 2021. ISSN 20452322. 1

FERREIRA, D.; MARSHALL, J.; BITZ, C. M.; SOLOMON, S.; PLUMB, A. Antarctic ocean and sea ice response to ozone depletion: a two-time-scale problem. **Journal of Climate**, v. 28, p. 1206–1226, 2 2015. ISSN 0894-8755. Disponível em: <<http://journals.ametsoc.org/doi/10.1175/JCLI-D-14-00313.1>>. 2, 30

FIGUEROLA, B.; HANCOCK, A. M.; BAX, N.; CUMMINGS, V. J.; DOWNEY, R.; GRIFFITHS, H. J.; SMITH, J.; STARK, J. S. A review and meta-analysis of potential impacts of ocean acidification on marine calcifiers from the southern ocean. **Frontiers in Marine Science**, v. 8, 2021. ISSN 22967745. 23

FOGT, R. L.; MARSHALL, G. J. The southern annular mode: variability, trends, and climate impacts across the southern hemisphere. **Wiley Interdisciplinary Reviews: Climate Change**, v. 11, p. 1–24, 2020. ISSN 17577799. 36, 68

FOGWILL, C. J.; TURNEY, C. S. M.; MENVIEL, L.; BAKER, A.; WEBER, M. E.; ELLIS, B.; THOMAS, Z. A.; GOLLEDGE, N. R.; ETHERIDGE, D.; RUBINO, M.; THORNTON, D. P.; OMMEN, T. D. van; MOY, A. D.; CURRAN, M. A. J.; DAVIES, S.; BIRD, M. I.; MUNKSGAARD, N. C.; ROOTES, C. M.; MILLMAN, H.; VOHRA, J.; RIVERA, A.; MACKINTOSH, A.; PIKE, J.; HALL, I. R.; BAGSHAW, E. A.; RAINSLEY, E.; BRONK-RAMSEY, C.; MONTENARI, M.; CAGE, A. G.; HARRIS, M. R. P.; JONES, R.; POWER, A.; LOVE, J.; YOUNG, J.; WEYRICH, L. S.; COOPER, A. Southern ocean carbon sink enhanced by sea-ice feedbacks at the antarctic cold reversal. **Nature Geoscience**, v. 13, p. 489–497, 7 2020. ISSN 1752-0894. Disponível em: <<https://www.nature.com/articles/s41561-020-0587-0>>. 41

FOLDVIK, A.; GAMMELSRøD, T.; ØTERHUS, S.; FAHRBACH, E.; ROHARDT, G.; SCHRöDER, M.; NICHOLLS, K. W.; PADMAN, L.; WOODGATE, R. A. Ice shelf water overflow and bottom water formation in the southern weddell sea. **Journal of Geophysical Research: Oceans**, v. 109, 2 2004. ISSN 21699291. 42, 45

FOSTER, T. D.; CARMACK, E. C. Frontal zone mixing and antarctic bottom water formation in the southern weddell sea. v. 23, p. 301–317, 1976. 45

FRANCO, B. C.; MATA, M. M.; PIOLA, A. R.; GARCIA, C. A. Northwestern weddell sea deep outflow into the scotia sea during the austral summers of 2000 and 2001 estimated by inverse methods. **Deep-Sea Research Part I: Oceanographic Research Papers**, v. 54, p. 1815–1840, 10 2007. ISSN 09670637. 45

FRIEDL, P.; SEEHAUS, T. C.; WENDT, A.; BRAUN, M. H.; HöPPNER, K. Recent dynamic changes on fleming glacier after the disintegration of wordie ice shelf, antarctic peninsula. **The Cryosphere**, v. 12, p. 1347–1365, 4 2018. ISSN 1994-0424. Disponível em: <<https://tc.copernicus.org/articles/12/1347/2018/>>. 60

FYKE, J.; LENAERTS, J. T.; WANG, H. Basin-scale heterogeneity in antarctic precipitation and its impact on surface mass variability. **Cryosphere**, v. 11, p. 2595–2609, 2017. ISSN 19940424. 37

GARABATO, A. C. N.; MCDONAGH, E. L.; STEVENS, D. P.; HEYWOOD, K. J.; SANDERS, R. J. On the export of antarctic bottom water from the weddell sea. **Deep Sea Research Part II: Topical Studies in Oceanography**, v. 49, p. 4715–4742, 1 2002. ISSN 09670645. Disponível em: <<https://linkinghub.elsevier.com/retrieve/pii/S096706450200156X>>. 45

GASSON, E.; KEISLING, B. The antarctic ice sheet: a paleoclimate modeling perspective. **Oceanography**, v. 33, 6 2020. ISSN 10428275. Disponível em: <<https://tos.org/oceanography/article/the-antarctic-ice-sheet-a-paleoclimate-modeling-perspective>>. 13

GIGLIO, D.; JOHNSON, G. C. Subantarctic and polar fronts of the antarctic circumpolar current and southern ocean heat and freshwater content variability: a view from argo. **Journal of Physical Oceanography**, v. 46, p. 749–768, 2016. ISSN 15200485. 33

GILLE, S.; MCKEE, D.; MARTINSON, D. Temporal changes in the antarctic circumpolar current: implications for the antarctic continental shelves. **Oceanography**, v. 29, p. 96–105, 12 2016. ISSN 10428275. Disponível em: <<https://tos.org/oceanography/article/temporal-changes-in-the-antarctic-circumpolar-current-implications-for-the>>. 15

GILLE, S. T. Warming of the southern ocean since the 1950s. **Science**, v. 295, p. 1275–1277, 2002. ISSN 00368075. 23, 33

_____. Decadal-scale temperature trends in the southern hemisphere ocean. **Journal of Climate**, v. 21, p. 4749–4765, 2008. ISSN 08948755. 23

GOLLEDGE, N. R. Selective erosion beneath the antarctic peninsula ice sheet during lgm retreat. **Antarctic Science**, v. 26, p. 698–707, 2014. ISSN 13652079. 35

GORDON, A. L. Seasonality of southern ocean sea ice. **Journal of Geophysical Research**, v. 86, p. 4193, 1981. ISSN 0148-0227. Disponível em: <<http://doi.wiley.com/10.1029/JC086iC05p04193>>. 34

GORDON, A. L.; HUBER, B.; MCKEE, D.; VISBECK, M. A seasonal cycle in the export of bottom water from the weddell sea. **Nature Geoscience**, v. 3, p. 551–556, 8 2010. ISSN 1752-0894. Disponível em: <<https://www.nature.com/articles/ngeo916>>. 69

GORDON, A. L.; VISBECK, M.; HUBER, B. Export of weddell sea deep and bottom water. **Journal of Geophysical Research: Oceans**, v. 106, p. 9005–9017, 5 2001. ISSN 21699291. 43, 45

GREENE, C. A.; THIRUMALAI, K.; KEARNEY, K. A.; DELGADO, J. M.; SCHWANGHART, W.; WOLFENBARGER, N. S.; THYNG, K. M.; GWYTHER, D. E.; GARDNER, A. S.; BLANKENSHIP, D. D. The climate data toolbox for matlab. **Geochemistry, Geophysics, Geosystems**, v. 20, p. 3774–3781, 2019. ISSN 15252027. 28, 29

GRINSTED, A.; MOORE, J. C.; JEVREJEVA, S. Application of the cross wavelet transform and wavelet coherence to geophysical time series. **Nonlinear Processes in Geophysics**, v. 11, p. 561–566, 11 2004. ISSN 1607-7946. Disponível em: <<https://npg.copernicus.org/articles/11/561/2004/>>. 74

GUDMUNDSSON, G. H.; PAOLO, F. S.; ADUSUMILLI, S.; FRICKER, H. A. Instantaneous antarctic ice sheet mass loss driven by thinning ice shelves. **Geophysical Research Letters**, v. 46, p. 13903–13909, 12 2019. ISSN 0094-8276. Disponível em: <<https://agupubs.onlinelibrary.wiley.com/doi/10.1029/2019GL085027>>. 39

GUTENSTEIN, M.; FENNIG, K.; SCHRöDER, M.; TRENT, T.; BAKAN, S.; ROBERTS, J. B.; ROBERTSON, F. R. Intercomparison of freshwater fluxes over ocean and investigations into water budget closure. **Hydrology and Earth System Sciences**, v. 25, p. 121–146, 2021. ISSN 16077938. 32

GWYTHER, D. E.; GALTON-FENZI, B. K.; DINNIMAN, M. S.; ROBERTS, J. L.; HUNTER, J. R. The effect of basal friction on melting and freezing in ice shelf-ocean models. **Ocean Modelling**, v. 95, p. 38–52, 11 2015. ISSN 14635003. 5, 39, 40

GWYTHER, D. E.; SPAIN, E. A.; KING, P.; GUIHEN, D.; WILLIAMS, G. D.; EVANS, E.; COOK, S.; RICHTER, O.; GALTON-FENZI, B. K.; COLEMAN, R. Cold ocean cavity and weak basal melting of the sørsdal ice shelf revealed by surveys using autonomous platforms. **Journal of Geophysical Research: Oceans**, v. 125, p. 1–17, 2020. ISSN 21699291. 5, 39

HAIDVOGEL, D. B.; ARANGO, H.; BUDGELL, W. P.; CORNUELLE, B. D.; CURCHITSER, E.; LORENZO, E. D.; FENNEL, K.; GEYER, W. R.; HERMANN, A. J.; LANEROLLE, L.; LEVIN, J.; MCWILLIAMS, J. C.; MILLER, A. J.; MOORE, A. M.; POWELL, T. M.; SHCHEPETKIN, A. F.; SHERWOOD, C. R.; SIGNELL, R. P.; WARNER, J. C.; WILKIN, J. Ocean forecasting in terrain-following coordinates: formulation and skill assessment of the regional ocean modeling system. **Journal of Computational Physics**, v. 227, p. 3595–3624, 2008. ISSN 00219991. 14, 16

HALL, A.; VISBECK, M. Synchronous variability in the southern hemisphere atmosphere, sea ice, and ocean resulting from the annular mode*. **Journal of Climate**, v. 15, p. 3043–3057, 11 2002. ISSN 0894-8755. Disponível em: <<http://journals.ametsoc.org/doi/10.1175/1520-0442(2002)015<3043:SVITSH>2.0.CO;2>>. 75, 76

HANNA, E.; NAVARRO, F. J.; PATTYN, F.; DOMINGUES, C. M.; FETTWEIS, X.; IVINS, E. R.; NICHOLLS, R. J.; RITZ, C.; SMITH, B.; TULACZYK, S.; WHITEHOUSE, P. L.; ZWALLY, H. J. Ice-sheet mass balance and climate change. **Nature**, v. 498, p. 51–59, 2013. ISSN 00280836. Disponível em: <<http://dx.doi.org/10.1038/nature12238>>. 25

HASKINS, R. K.; OLIVER, K. I.; JACKSON, L. C.; WOOD, R. A.; DRIJFHOUT, S. S. Temperature domination of amoc weakening due to freshwater hosing in two gcms. **Climate Dynamics**, v. 54, p. 273–286, 2020. ISSN 14320894. Disponível em: <<https://doi.org/10.1007/s00382-019-04998-5>>. 1, 41

HATTERMANN, T.; LEVERMANN, A. Response of southern ocean circulation to global warming may enhance basal ice shelf melting around antarctica. **Climate Dynamics**, v. 35, p. 741–756, 10 2010. ISSN 0930-7575. Disponível em: <<http://link.springer.com/10.1007/s00382-009-0643-3>>. 40

HATTERMANN, T.; SMEDSRUD, L.; NøST, O.; LILLY, J.; GALTON-FENZI, B. Eddy-resolving simulations of the fimbul ice shelf cavity circulation: basal melting and exchange with open ocean. **Ocean Modelling**, v. 82, p. 28–44, 10 2014. ISSN 14635003. Disponível em: <<http://dx.doi.org/10.1016/j.ocemod.2014.07.004https://linkinghub.elsevier.com/retrieve/pii/S1463500314000948>>. 40

HAUMANN, F. A.; GRUBER, N.; MüNNICH, M.; FRENGER, I.; KERN, S. Sea-ice transport driving southern ocean salinity and its recent trends. **Nature**, v. 537, p. 89–92, 9 2016. ISSN 0028-0836. Disponível em: <<https://www.nature.com/articles/nature19101>>. 4, 68

HAZIOT, S.; MARYNETS, K. Applying the stereographic projection to modeling of the flow of the antarctic circumpolar current. **Oceanography**, v. 31, p. 68–75, 9 2018. ISSN 10428275. Disponível em: <<https://tos.org/oceanography/article/applying-the-stereographic-projection-to-modeling-of-the-flow-of-the-antarc>>. 14

HEDSTRöM, K. S. Technical manual for a coupled sea-ice/ocean circulation model (version 5). In: **U.S. Department of the Interior - BOEM**. [S.l.: s.n.], 2018. v. 7, p. 182. 17, 20

HELLMER, H.; KAUKER, F.; TIMMERMANN, R.; DETERMANN, J.; RAE, J. Twenty-first-century warming of a large antarctic ice-shelf cavity by a redirected coastal current. **Nature**, v. 485, p. 225–228, 5 2012. ISSN 0028-0836. Disponível em: <<http://www.nature.com/articles/nature11064>>. 4, 33, 40

HELLMER, H. H. Impact of antarctic ice shelf basal melting on sea ice and deep ocean properties. **Geophysical Research Letters**, v. 31, 5 2004. ISSN 00948276. 15, 65, 76

HELLMER, H. H.; HUHN, O.; GOMIS, D.; TIMMERMANN, R. On the freshening of the northwestern weddell sea continental shelf. **Ocean Science**, v. 7,

p. 305–316, 5 2011. ISSN 1812-0792. Disponível em: <<https://os.copernicus.org/articles/7/305/2011/>>. 27

HENLEY, S. F.; CAVAN, E. L.; FAWCETT, S. E.; KERR, R.; MONTEIRO, T.; SHERRELL, R. M.; BOWIE, A. R.; BOYD, P. W.; BARNES, D. K.; SCHLOSS, I. R.; MARSHALL, T.; FLYNN, R.; SMITH, S. Changing biogeochemistry of the southern ocean and its ecosystem implications. **Frontiers in Marine Science**, v. 7, 7 2020. ISSN 22967745. 1, 23, 41

HENSCHKE, N.; ESPINASSE, B.; STOCK, C. A.; LIU, X.; BARRIER, N.; PAKHOMOV, E. A. The role of water mass advection in staging of the southern ocean salpa thompsoni populations. **Scientific Reports**, v. 13, 12 2023. ISSN 20452322. 13

HERSBACH, H.; BELL, B.; BERRISFORD, P.; HIRAHARA, S.; HORáNYI, A.; MUñOZ-SABATER, J.; NICOLAS, J.; PEUBEY, C.; RADU, R.; SCHEPERS, D.; SIMMONS, A.; SOCI, C.; ABDALLA, S.; ABELLAN, X.; BALSAMO, G.; BECHTOLD, P.; BIAVATI, G.; BIDLOT, J.; BONAVITA, M.; CHIARA, G.; DAHLGREN, P.; DEE, D.; DIAMANTAKIS, M.; DRAGANI, R.; FLEMMING, J.; FORBES, R.; FUENTES, M.; GEER, A.; HAIMBERGER, L.; HEALY, S.; HOGAN, R. J.; HóLM, E.; JANISKOVá, M.; KEELEY, S.; LALOYAUX, P.; LOPEZ, P.; LUPU, C.; RADNOTI, G.; ROSNAY, P.; ROZUM, I.; VAMBORG, F.; VILLAUME, S.; THéPAUT, J. The era5 global reanalysis. **Quarterly Journal of the Royal Meteorological Society**, v. 146, p. 1999–2049, 7 2020. ISSN 0035-9009. Disponível em: <<https://onlinelibrary.wiley.com/doi/abs/10.1002/qj.3803>>. 47

HO, M.; KIEM, A. S.; VERDON-KIDD, D. C. The southern annular mode: a comparison of indices. **Hydrology and Earth System Sciences**, v. 16, p. 967–982, 3 2012. ISSN 1607-7938. Disponível em: <<https://hess.copernicus.org/articles/16/967/2012/>>. 68

HOGG, A. E.; GUDMUNDSSON, G. H. Impacts of the larsen-c ice shelf calving event. **Nature Climate Change**, v. 7, p. 540–542, 8 2017. ISSN 1758-678X. Disponível em: <<https://www.nature.com/articles/nclimate3359>>. 36, 50

HOLLAND, D. M. The marine cryosphere. In: _____. [s.n.], 2013. v. 103, p. 413–442. Disponível em: <<https://linkinghub.elsevier.com/retrieve/pii/B9780123918512000167>>. 62

HOLLAND, D. M.; JENKINS, A. Modeling thermodynamic ice-ocean interactions at the base of an ice shelf. **Journal of Physical Oceanography**, v. 29, p. 1787–1800, 1999. ISSN 00223670. 46, 49

HOLLAND, D. M.; NICHOLLS, K. W.; BASINSKI, A. The southern ocean and its interaction with the antarctic ice sheet. **Science**, v. 367, p. 1326–1330, 2020. ISSN 10959203. Disponível em: <<https://www.sciencemag.org/lookup/doi/10.1126/science.aaz5491>>. 1, 34

HOLLAND, P. R.; BRISBOURNE, A.; CORR, H. F. J.; MCGRATH, D.; PURDON, K.; PADEN, J.; FRICKER, H. A.; PAOLO, F. S.; FLEMING, A. H. Oceanic and atmospheric forcing of larsen c ice-shelf thinning. **The Cryosphere**, v. 9, p. 1005–1024, 5 2015. ISSN 1994-0424. Disponível em: <<https://tc.copernicus.org/articles/9/1005/2015/>>. 33

HOLLAND, P. R.; JENKINS, A.; HOLLAND, D. M. Ice and ocean processes in the bellingshausen sea, antarctica. **Journal of Geophysical Research**, v. 115, p. C05020, 5 2010. ISSN 0148-0227. Disponível em: <<http://doi.wiley.com/10.1029/2008JC005219>>. 5, 6, 40

HOLLAND, P. R.; KWOK, R. Wind-driven trends in antarctic sea-ice drift. **Nature Geoscience**, v. 5, p. 872–875, 12 2012. ISSN 17520894. 37

HOLT, T.; GLASSER, N. Decadal changes in southwest antarctic peninsula ice shelves. **EGU General Assembly 2021**, p. 2617, 2021. Disponível em: <<https://meetingorganizer.copernicus.org/EGU21/EGU21-2617.html>>. 35

HOOKE, R. L. **Ice streams and ice shelves**. 12 2019. 350-386 p. Disponível em: <<https://www.cambridge.org/core/product/identifier/9781108698207%23CN-bp-13/type/book_part>>. 40

HOW, P.; BENN, D. I.; HULTON, N. R. J.; HUBBARD, B.; LUCKMAN, A.; SEVESTRE, H.; PELT, W. J. J. van; LINDBäCK, K.; KOHLER, J.; BOOT, W. Rapidly changing subglacial hydrological pathways at a tidewater glacier revealed through simultaneous observations of water pressure, supraglacial lakes, meltwater plumes and surface velocities. **The Cryosphere**, v. 11, p. 2691–2710, 11 2017. ISSN 1994-0424. Disponível em: <<https://tc.copernicus.org/articles/11/2691/2017/>>. 31

HOWAT, I. M.; PORTER, C.; SMITH, B. E.; NOH, M. J.; MORIN, P. The reference elevation model of antarctica. **Cryosphere**, v. 13, p. 665–674, 2019. ISSN 19940424. 24

HUGONNET, R.; MCNABB, R.; BERTHIER, E.; MENOUNOS, B.; NUTH, C.; GIROD, L.; FARINOTTI, D.; HUSS, M.; DUSSAILLANT, I.; BRUN, F.; KääB, A. Accelerated global glacier mass loss in the early twenty-first century. **Nature**, v. 592, p. 726–731, 4 2021. ISSN 0028-0836. Disponível em: <<http://dx.doi.org/10.1038/s41586-021-03436-zhttp://www.nature.com/articles/s41586-021-03436-z>>. 31

HUNKE, E. C. Viscous-plastic sea ice dynamics with the evp model: linearization issues. **Journal of Computational Physics**, v. 170, p. 18–38, 6 2001. ISSN 00219991. 18

HUNKE, E. C.; DUKOWICZ, J. K. An elastic–viscous–plastic model for sea ice dynamics. **Journal of Physical Oceanography**, v. 27, p. 1849–1867, 9 1997. ISSN 0022-3670. Disponível em: <<http://journals.ametsoc.org/doi/pdf/10.1175/1520-0485(1997)027%3C1849%

3AAEVPMF%3E2.0.CO%3B2http://journals.ametsoc.org/doi/abs/10.1175/1520-0485%281997%29027%3C1849%3AAEVPMF%3E2.0.CO%3B2>>. 18

HUOT, P. V.; FICHEFET, T.; JOURDAIN, N. C.; MATHIOT, P.; ROUSSET, C.; KITTEL, C.; FETTWEIS, X. Influence of ocean tides and ice shelves on ocean–ice interactions and dense shelf water formation in the d'urville sea, antarctica. **Ocean Modelling**, v. 162, 6 2021. ISSN 14635003. 46

HUTCHINSON, K.; DESHAYES, J.; SALLEE, J. B.; DOWDESWELL, J. A.; LAVERGNE, C. de; ANSORGE, I.; LUYT, H.; HENRY, T.; FAWCETT, S. E. Water mass characteristics and distribution adjacent to larsen c ice shelf, antarctica. **Journal of Geophysical Research: Oceans**, v. 125, 4 2020. ISSN 21699291. 45

Integorvernamental Panel on Climate Change (IPCC). **Climate Change 2007: impacts, adaptation, and vulnerability. Contribution of Working Group II to the Fourth Assessment Report of the Intergovernmental Panel on Climate Change**. 2007. 976 p. Disponível em: <<http://books.google.com/books?hl=en&lr=&id=TNo-SeGpn7wC&oi=fnd&pg=PA81&dq=Climate+Change+2007:+Impacts,+Adaptation+and+Vulnerability.+Contribution+of+Working+Group+II+to+the+Fourth+Assessment+Report+of+the+Intergovernmental+Panel+on+Climate+Change&ots=vP2>>. 3

_____. **The ocean and cryosphere in a changing climate. A special report of the Intergovernmental Panel on Climate Change**. 2019. 1-765 p. Disponível em: <<https://www.ipcc.ch/srocc/chapter/summary-for-policymakers/>>. 3, 37

_____. **Changing ocean, marine ecosystems, and dependent communities**. 5 2022. 447-588 p. Disponível em: <<https://www.cambridge.org/core/product/identifier/9781009157964%23c5/type/book_part>>. 1, 41

JACOBS, S.; HELMER, H.; DOAKE, C. S. M.; JENKINS, A.; FROLICH, R. M. Melting of ice shelves and the mass balance of antarctica. **Journal of Glaciology**, v. 38, p. 375–387, 1 1992. ISSN 0022-1430. Disponível em: <<https://www.cambridge.org/core/product/identifier/S0022143000002252/type/journal_article>>. 33, 40

JACOBS, S. S.; JENKINS, A.; GIULIVI, C. F.; DUTRIEUX, P. Stronger ocean circulation and increased melting under pine island glacier ice shelf. **Nature Geoscience**, v. 4, p. 519–523, 8 2011. ISSN 1752-0894. Disponível em: <<https://www.nature.com/articles/ngeo1188>>. 40

JANOUT, M. A.; HELLMER, H. H.; HATTERMANN, T.; HUHN, O.; SüLTENFUSS, J.; ØSTERHUS, S.; STULIC, L.; RYAN, S.; SCHRöDER, M.; KANZOW, T. Fris revisited in 2018: On the circulation and water masses at the filchner and ronne ice shelves in the southern weddell sea. **Journal of Geophysical Research: Oceans**, v. 126, 6 2021. ISSN 21699291. 43, 45

JEAN-MICHEL, L.; ERIC, G.; ROMAIN, B. B.; GILLES, G.; ANGéLIQUE, M.; MARIE, D.; CLéMENT, B.; MATHIEU, H.; OLIVIER, L. G.; CHARLY, R.; TONY, C.; CHARLES-EMMANUEL, T.; FLORENT, G.; GIOVANNI, R.; MOUNIR, B.; YANN, D.; PIERRE-YVES, L. T. The copernicus global 1/12° oceanic and sea ice glorys12 reanalysis. **Frontiers in Earth Science**, v. 9, 7 2021. ISSN 22966463. 47

JENKINS, A.; JACOBS, S. Circulation and melting beneath george vi ice shelf, antartica. **Journal of Geophysical Research: Oceans**, v. 113, 4 2008. ISSN 21699291. 45

JULLION, L.; GARABATO, A. C. N.; MEREDITH, M. P.; HOLLAND, P. R.; COURTOIS, P.; KING, B. A. Decadal freshening of the antarctic bottom water exported from the weddell sea. **Journal of Climate**, v. 26, p. 8111–8125, 10 2013. ISSN 0894-8755. Disponível em: <<http://journals.ametsoc.org/doi/10.1175/JCLI-D-12-00765.1>>. 33, 43

KEPPLER, L.; LANDSCHüTZER, P. Regional wind variability modulates the southern ocean carbon sink. **Scientific Reports**, v. 9, p. 1–10, 2019. ISSN 20452322. 36, 68

KERR, R.; DOTTO, T. S.; MATA, M. M.; HELLMER, H. H. Three decades of deep water mass investigation in the weddell sea (1984–2014): temporal variability and changes. **Deep Sea Research Part II: Topical Studies in Oceanography**, v. 149, p. 70–83, 3 2018. ISSN 09670645. Disponível em: <<https://doi.org/10.1016/j.dsr2.2017.12.002https://linkinghub.elsevier.com/retrieve/pii/S0967064517301261>>. 7, 33, 41

KERR, R.; HEYWOOD, K. J.; MATA, M. M.; GARCIA, C. A. On the outflow of dense water from the weddell and ross seas in occam model. **Ocean Science**, v. 8, p. 369–388, 2012. ISSN 18120784. 44, 45, 75, 82, 84

KERR, R.; MATA, M. M.; MENDES, C. R. B.; SECCHI, E. R. Northern antarctic peninsula: a marine climate hotspot of rapid changes on ecosystems and ocean dynamics. **Deep Sea Research Part II: Topical Studies in Oceanography**, v. 149, p. 4–9, 3 2018. ISSN 09670645. Disponível em: <<https://linkinghub.elsevier.com/retrieve/pii/S0967064518300912>>. 7, 25, 41

KHAZENDAR, A.; RIGNOT, E.; SCHROEDER, D. M.; SEROUSSI, H.; SCHODLOK, M. P.; SCHEUCHL, B.; MOUGINOT, J.; SUTTERLEY, T. C.; VELICOGNA, I. Rapid submarine ice melting in the grounding zones of ice shelves in west antarctica. **Nature Communications**, v. 7, p. 13243, 10 2016. ISSN 2041-1723. Disponível em: <<https://www.nature.com/articles/ncomms13243>>. 65

KIDSTON, J.; TASCHETTO, A. S.; THOMPSON, D. W.; ENGLAND, M. H. The influence of southern hemisphere sea-ice extent on the latitude of the mid-latitude jet stream. **Geophysical Research Letters**, v. 38, 8 2011. ISSN 00948276. 41

KIM, T. W.; HA, H. K.; WåHLIN, A. K.; LEE, S. H.; KIM, C. S.; LEE, J. H.; CHO, Y. K. Is ekman pumping responsible for the seasonal variation of warm circumpolar deep water in the amundsen sea? **Continental Shelf Research**, v. 132, p. 38–48, 2017. ISSN 18736955. 34

KIMMRITZ, M.; DANILOV, S.; LOSCH, M. On the convergence of the modified elastic–viscous–plastic method for solving the sea ice momentum equation. **Journal of Computational Physics**, Academic Press Inc., v. 296, p. 90–100, 9 2015. ISSN 00219991. Disponível em: <<https://linkinghub.elsevier.com/retrieve/pii/S0021999115003083>>. 19

KING, J. C.; TURNER, J.; MARSHALL, G. J.; CONNOLLEY, W. M.; LACHLAN-COPE, T. A. **Antarctic Peninsula climate variability and its causes as revealed by analysis of instrumental records**. [s.n.], 2003. 17-30 p. Disponível em: <<http://doi.wiley.com/10.1029/AR079p0017>>. 28

KLEMAN, J.; GLASSER, N. F. The subglacial thermal organisation (sto) of ice sheets. **Quaternary Science Reviews**, v. 26, p. 585–597, 2007. ISSN 02773791. 35

KLINCK, J. M.; HOFMANN, E. E.; BEARDSLEY, R. C.; SALIHOGLU, B.; HOWARD, S. Water-mass properties and circulation on the west antarctic peninsula continental shelf in austral fall and winter 2001. **Deep-Sea Research Part II: Topical Studies in Oceanography**, v. 51, p. 1925–1946, 2004. ISSN 09670645. 44, 45

KONRAD, H.; SHEPHERD, A.; GILBERT, L.; HOGG, A. E.; MCMILLAN, M.; MUIR, A.; SLATER, T. Net retreat of antarctic glacier grounding lines. **Nature Geoscience**, v. 11, p. 258–262, 4 2018. ISSN 1752-0894. Disponível em: <<https://www.nature.com/articles/s41561-018-0082-z>>. 5

KUMAR, A.; YADAV, J.; MOHAN, R. Seasonal sea-ice variability and its trend in the weddell sea sector of west antarctica. **Environmental Research Letters**, v. 16, 2021. ISSN 17489326. 27, 53

KUSAHARA, K. Summertime linkage between antarctic sea-ice extent and ice-shelf basal melting through antarctic coastal water masses' variability: A circumpolar southern ocean model study. **Environmental Research Letters**, v. 16, 7 2021. ISSN 17489326. 65, 69, 84

KUSAHARA, K.; HASUMI, H. Modeling antarctic ice shelf responses to future climate changes and impacts on the ocean. **Journal of Geophysical Research: Oceans**, v. 118, p. 2454–2475, 5 2013. ISSN 21699291. 15

_____. Pathways of basal meltwater from antarctic ice shelves: a model study. **Journal of Geophysical Research: Oceans**, v. 119, p. 5690–5704, 9 2014. ISSN 21699275. Disponível em: <<http://doi.wiley.com/10.1002/2014JC009915>>. 63

KUSAHARA, K.; REID, P.; WILLIAMS, G. D.; MASSOM, R.; HASUMI, H. An ocean-sea ice model study of the unprecedented antarctic sea ice minimum in 2016. **Environmental Research Letters**, v. 13, p. 084020, 8 2018. ISSN 1748-9326. Disponível em: <<https://iopscience.iop.org/article/10.1088/1748-9326/aad624>>. 13

KUSAHARA, K.; TATEBE, H.; HAJIMA, T.; SAITO, F.; KAWAMIYA, M. Antarctic sea ice holds the fate of antarctic ice-shelf basal melting in a warming climate. **Journal of Climate**, v. 36, p. 713–743, 2 2023. ISSN 15200442. 65

KUSTKA, A. B.; KOHUT, J. T.; WHITE, A. E.; LAM, P. J.; MILLIGAN, A. J.; DINNIMAN, M. S.; MACK, S.; HUNTER, E.; HISCOCK, M. R.; SMITH, W. O.; MEASURES, C. I. The roles of mcdw and deep water iron supply in sustaining a recurrent phytoplankton bloom on central pennell bank (ross sea). **Deep Sea Research Part I: Oceanographic Research Papers**, v. 105, p. 171–185, 11 2015. ISSN 09670637. Disponível em: <<https://linkinghub.elsevier.com/retrieve/pii/S0967063715001478>>. 13

LAGO, V.; ENGLAND, M. H. Projected slowdown of antarctic bottom water formation in response to amplified meltwater contributions. **Journal of Climate**, v. 32, p. 6319–6335, 2019. ISSN 08948755. 23, 39

LAROUR, E.; RIGNOT, E.; POINELLI, M.; SCHEUCHL, B. Physical processes controlling the rifting of larsen c ice shelf, antarctica, prior to the calving of iceberg a68. **Proceedings of the National Academy of Sciences of the United States of America**, v. 118, 2021. ISSN 10916490. 36

LECOMTE, O.; GOOSSE, H.; FICHEFET, T.; LAVERGNE, C. de; BARTHéLEMY, A.; ZUNZ, V. Vertical ocean heat redistribution sustaining sea-ice concentration trends in the ross sea. **Nature Communications**, v. 8, p. 258, 8 2017. ISSN 2041-1723. Disponível em: <<https://www.nature.com/articles/s41467-017-00347-4>>. 4

LEFEBVRE, W.; GOOSSE, H. Influence of the southern annular mode on the sea ice-ocean system: the role of the thermal and mechanical forcing. **Ocean Science**, v. 1, p. 145–157, 2005. ISSN 18120792. 30, 75, 76

LIGTENBERG, S. R. M.; HELSEN, M. M.; BROEKE, M. R. van den. An improved semi-empirical model for the densification of antarctic firn. **The Cryosphere**, v. 5, p. 809–819, 10 2011. ISSN 1994-0424. Disponível em: <<https://tc.copernicus.org/articles/5/809/2011/>>. 25

LIMA, L. S.; PEZZI, L. P.; MATA, M. M.; SANTINI, M. F.; CARVALHO, J. T.; SUTIL, U. A.; CABRERA, M. J.; ROSA, E. B.; RODRIGUES, C. C.; VEGA, X. A. Glacial meltwater input to the ocean around the antarctic peninsula: forcings and consequences. **Anais da Academia Brasileira de Ciencias**, v. 94, 2022. ISSN 16782690. 10, 24, 26, 28, 29

LIPSCOMB, W. H.; HUNKE, E. C.; LIPSCOMB, W. H. **CICE: the Los Alamos Sea Ice Model Documentation and Software User's Manual**. 2010. Disponível em: <<https://www.researchgate.net/publication/237249046>>. 16

LIU, J.; CURRY, J. A. Accelerated warming of the southern ocean and its impacts on the hydrological cycle and sea ice. **Proceedings of the National Academy of Sciences of the United States of America**, v. 107, p. 14987–14992, 2010. ISSN 00278424. 23

LIU, M.; TANHUA, T. Water masses in the atlantic ocean: characteristics and distributions. **Ocean Science**, v. 17, p. 463–486, 3 2021. ISSN 18120792. 42

LLANILLO, P. J.; KANZOW, T.; JANOUT, M. A.; ROHARDT, G. The deep-water plume in the northwestern weddell sea, antarctica: mean state, seasonal cycle and interannual variability influenced by climate modes. **Journal of Geophysical Research: Oceans**, v. 128, 2 2023. ISSN 21699291. 45

LOEWE, F. **The water budget in Antarctica**. [S.l.]: Dept. of Polar Research, National Science Museum apanese Antarctic Research Expedition. Scientific Reports, Special Issue No. 1., 1967. 101-110 p. 27

LOSCH, M. Modeling ice shelf cavities in a z coordinate ocean general circulation model. **Journal of Geophysical Research: Oceans**, v. 113, 8 2008. ISSN 0148-0227. Disponível em: <<https://agupubs.onlinelibrary.wiley.com/doi/10.1029/2007JC004368>>. 15

MA, H.; WU, L. Global teleconnections in response to freshening over the antarctic ocean. **Journal of Climate**, v. 24, p. 1071–1088, 2011. ISSN 08948755. 3

MACGREGOR, J. A.; BOISVERT, L. N.; MEDLEY, B.; PETTY, A. A.; HARBECK, J. P.; BELL, R. E.; BLAIR, J. B.; BLANCHARD-WRIGGLESWORTH, E.; BUCKLEY, E. M.; CHRISTOFFERSEN, M. S.; COCHRAN, J. R.; CSATHó, B. M.; MARCO, E. L. D.; DOMINGUEZ, R. T.; FAHNESTOCK, M. A.; FARRELL, S. L.; GOGINENI, S. P.; GREENBAUM, J. S.; HANSEN, C. M.; HOFTON, M. A.; HOLT, J. W.; JEZEK, K. C.; KOENIG, L. S.; KURTZ, N. T.; KWOK, R.; LARSEN, C. F.; LEUSCHEN, C. J.; LOCKE, C. D.; MANIZADE, S. S.; MARTIN, S.; NEUMANN, T. A.; NOWICKI, S. M.; PADEN, J. D.; RICHTER-MENGE, J. A.; RIGNOT, E. J.; RODRíGUEZ-MORALES, F.; SIEGFRIED, M. R.; SMITH, B. E.; SONNTAG, J. G.; STUDINGER, M.; TINTO, K. J.; TRUFFER, M.; WAGNER, T. P.; WOODS, J. E.; YOUNG, D. A.; YUNGEL, J. K. The scientific legacy of nasa's operation icebridge. **Reviews of Geophysics**, v. 59, 6 2021. ISSN 8755-1209. Disponível em: <<https://agupubs.onlinelibrary.wiley.com/doi/10.1029/2020RG000712>>. 52

MACK, S. L.; DINNIMAN, M. S.; KLINCK, J. M.; MCGILLICUDDY, D. J.; PADMAN, L. Modeling ocean eddies on antarctica's cold water continental shelves and their effects on ice shelf basal melting. **Journal of Geophysical Research: Oceans**, v. 124, p. 5067–5084, 7 2019. ISSN 2169-9275. Disponível em: <<https://onlinelibrary.wiley.com/doi/abs/10.1029/2018JC014688>>. 13, 15

MALYARENKO, A.; ROBINSON, N. J.; WILLIAMS, M. J.; LANGHORNE, P. J. A wedge mechanism for summer surface water inflow into the ross ice shelf cavity. **Journal of Geophysical Research: Oceans**, v. 124, p. 1196–1214, 2 2019. ISSN 21699291. 40

MARSHALL, G. J. Trends in the southern annular mode from observations and reanalyses. **Journal of Climate**, v. 16, p. 4134–4143, 2003. ISSN 08948755. 29, 36

MARSHALL, G. J.; THOMPSON, D. W. J.; BROEKE, M. R. The signature of southern hemisphere atmospheric circulation patterns in antarctic precipitation. **Geophysical Research Letters**, v. 44, p. 11,580–11,589, 11 2017. ISSN 0094-8276. Disponível em: <<https://onlinelibrary.wiley.com/doi/abs/10.1002/2017GL075998>>. 2

MARTINSEN, E. A.; ENGEDAHL, H. Implementation and testing of a lateral boundary scheme as an open boundary condition in a barotropic ocean model. **Coastal Engineering**, v. 11, p. 603–627, 12 1987. ISSN 03783839. Disponível em: <<https://linkinghub.elsevier.com/retrieve/pii/0378383987900287>>. 48

MARTINSON, D. G. Evolution of the southern ocean winter mixed layer and sea ice: open ocean deepwater formation and ventilation. **Journal of Geophysical Research**, v. 95, p. 11641, 1990. ISSN 0148-0227. Disponível em: <<http://doi.wiley.com/10.1029/JC095iC07p11641>>. 4

MARTINSON, D. G.; STAMMERJOHN, S. E.; IANNUZZI, R. A.; SMITH, R. C.; VERNET, M. Western antarctic peninsula physical oceanography and spatio–temporal variability. **Deep Sea Research Part II: Topical Studies in Oceanography**, v. 55, p. 1964–1987, 9 2008. ISSN 09670645. Disponível em: <<https://linkinghub.elsevier.com/retrieve/pii/S0967064508001525>>. 28

MASSOM, R. A.; STAMMERJOHN, S. E. Antarctic sea ice change and variability – physical and ecological implications. **Polar Science**, v. 4, p. 149–186, 8 2010. ISSN 18739652. Disponível em: <<http://www.nature.com/articles/s41586-020-2120-4https://linkinghub.elsevier.com/retrieve/pii/S1873965210000411>>. 40

MATHIOT, P.; JENKINS, A.; HARRIS, C.; MADEC, G. Explicit representation and parametrised impacts of under ice shelf seas in the lt;igt;zlt;/igt;lt;supgt;lt;/supgt; coordinate ocean model nemo 3.6. **Geoscientific Model Development**, v. 10, p. 2849–2874, 7 2017. ISSN 1991-9603. Disponível em: <<https://gmd.copernicus.org/articles/10/2849/2017/>>. 15

MCGUFFIE, K.; HENDERSON-SELLERS, A. Forty years of numerical climate modelling. **International Journal of Climatology**, v. 21, p. 1067–1109, 7 2001. ISSN 0899-8418. Disponível em: <<https://onlinelibrary.wiley.com/doi/10.1002/joc.632>>. 13

MCNEIL, B. I.; MATEAR, R. J. Southern ocean acidification: a tipping point at 450-ppm atmospheric co2. **Proceedings of the National Academy of**

Sciences of the United States of America, v. 105, p. 18860–18864, 2008. ISSN 00278424. 23

MELLOR, G. L.; KANTHA, L. An ice-ocean coupled model. **Journal of Geophysical Research**, v. 94, p. 10937, 1989. ISSN 0148-0227. Disponível em: <<http://doi.wiley.com/10.1029/JC094iC08p10937>>. 16, 19

MEREDITH, M.; SOMMERKORN, M.; CASSOTTA, S.; DERKSEN, C.; EKAYKIN, A.; HOLLOWED, A.; KOFINAS, G.; MACKINTOSH, A.; MELBOURNE-THOMAS, J.; MUELBERT, M.; OTTERSEN, G.; PRITCHARD, H.; SCHUUR, E. Polar regions. In: PöRTNER, H.-O.; ROBERTS, D.; MASSON-DELMOTTE, V.; ZHAI, P.; TIGNOR, M.; POLOCZANSKA, E.; MINTENBECK, K.; ALEGRíA, A.; NICOLAI, M.; OKEM, A.; PETZOLD, J.; RAMA, B.; WEYER, N. (Ed.). **IPCC Special Report on the Ocean and Cryosphere in a Changing Climate**. [S.l.: s.n.], 2019. p. 203–320. 4

MEREDITH, M. P.; FALK, U.; BERS, A. V.; MACKENSEN, A.; SCHLOSS, I. R.; BARLETT, E. R.; JEROSCH, K.; BUSSO, A. S.; ABELE, D. Anatomy of a glacial meltwater discharge event in an antarctic cove. **Philosophical Transactions of the Royal Society A: Mathematical, Physical and Engineering Sciences**, v. 376, p. 544–548, 3 2018. ISSN 1364503X. Disponível em: <<http://www.nature.com/articles/s41586-020-2120-4>>. 28, 39

MEREDITH, M. P.; KING, J. C. Rapid climate change in the ocean west of the antarctic peninsula during the second half of the 20th century. **Geophysical Research Letters**, v. 32, p. 1–5, 2005. ISSN 00948276. Disponível em: <<http://doi.wiley.com/10.1029/2005GL024042>>. 7, 25, 41, 44

MEREDITH, M. P.; SCHOFIELD, O.; NEWMAN, L.; URBAN, E.; SPARROW, M. The vision for a southern ocean observing system. **Current Opinion in Environmental Sustainability**, v. 5, p. 306–313, 9 2013. ISSN 18773435. 51

MERINO, N.; JOURDAIN, N. C.; SOMMER, J. L.; GOOSSE, H.; MATHIOT, P.; DURAND, G. Impact of increasing antarctic glacial freshwater release on regional sea-ice cover in the southern ocean. **Ocean Modelling**, v. 121, p. 76–89, 1 2018. ISSN 14635003. Disponível em: <<https://doi.org/10.1016/j.ocemod.2017.11.009https://linkinghub.elsevier.com/retrieve/pii/S1463500317301956>>. 36, 76

MERINO, N.; SOMMER, J. L.; DURAND, G.; JOURDAIN, N. C.; MADEC, G.; MATHIOT, P.; TOURNADRE, J. Antarctic icebergs melt over the southern ocean: climatology and impact on sea ice. **Ocean Modelling**, v. 104, p. 99–110, 8 2016. ISSN 14635003. Disponível em: <<http://dx.doi.org/10.1016/j.ocemod.2016.05.001https://linkinghub.elsevier.com/retrieve/pii/S1463500316300300>>. 32

MOFFAT, C.; MEREDITH, M. Shelf–ocean exchange and hydrography west of the antarctic peninsula: a review. **Philosophical Transactions of the Royal Society A: Mathematical, Physical and Engineering Sciences**, v. 376, p.

20170164, 6 2018. ISSN 1364-503X. Disponível em: <<https://royalsocietypublishing.org/doi/10.1098/rsta.2017.0164>>. 7

MORLIGHEM, M.; WILLIAMS, C. N.; RIGNOT, E.; AN, L.; ARNDT, J. E.; BAMBER, J. L.; CATANIA, G.; CHAUCHé, N.; DOWDESWELL, J. A.; DORSCHEL, B.; FENTY, I.; HOGAN, K.; HOWAT, I.; HUBBARD, A.; JAKOBSSON, M.; JORDAN, T. M.; KJELDSEN, K. K.; MILLAN, R.; MAYER, L.; MOUGINOT, J.; NOëL, B. P.; O'COFAIGH, C.; PALMER, S.; RYSGAARD, S.; SEROUSSI, H.; SIEGERT, M. J.; SLABON, P.; STRANEO, F.; VAN DEN BROEKE, M. R.; WEINREBE, W.; WOOD, M.; ZINGLERSEN, K. B. Bedmachine v3: complete bed topography and ocean bathymetry mapping of greenland from multibeam echo sounding combined with mass conservation. **Geophysical Research Letters**, v. 44, p. 11,051–11,061, 2017. ISSN 19448007. 31

MORRIS, E. M.; VAUGHAN, D. G. Spatial and temporal variation of surface temperature on the antarctic peninsula and the limit of viability of ice shelves. In: DOMACK, M. K. E.; LEVENTE, A.; BURNET, A.; BINDSCHADLER, R.; CONVEY, P. (Ed.). [s.n.], 2003. v. 79, p. 61–68. Disponível em: <<http://doi.wiley.com/10.1029/AR079p0061>>. 31, 34

MORRISON, A. K.; ENGLAND, M. H.; HOGG, A. M.; KISS, A. E. Weddell sea control of ocean temperature variability on the western antarctic peninsula. **Geophysical Research Letters**, v. 50, 8 2023. ISSN 0094-8276. Disponível em: <<https://agupubs.onlinelibrary.wiley.com/doi/10.1029/2023GL103018>>. 7

MOUGINOT, J.; SCHEUCHL, B.; RIGNOT, E. Mapping of ice motion in antarctica using synthetic-aperture radar data. **Remote Sensing**, v. 4, p. 2753–2767, 9 2012. ISSN 2072-4292. Disponível em: <<http://www.mdpi.com/2072-4292/4/9/2753>>. 27

MUNDAY, P. L.; WARNER, R. R.; MONRO, K.; PANDOLFI, J. M.; MARSHALL, D. J. Predicting evolutionary responses to climate change in the sea. **Ecology Letters**, v. 16, p. 1488–1500, 2013. ISSN 1461023X. 37

MUNNEKE, P. K.; MCGRATH, D.; MEDLEY, B.; LUCKMAN, A.; BEVAN, S.; KULESSA, B.; JANSEN, D.; BOOTH, A.; SMEETS, P.; HUBBARD, B.; ASHMORE, D.; BROEKE, M. V. den; SEVESTRE, H.; STEFFEN, K.; SHEPHERD, A.; GOURMELEN, N. Observationally constrained surface mass balance of larsen c ice shelf, antarctica. **The Cryosphere**, v. 11, p. 2411–2426, 11 2017. ISSN 1994-0424. Disponível em: <<https://tc.copernicus.org/articles/11/2411/2017/>>. 32

NAUGHTEN, K. A.; MEISSNER, K. J.; GALTON-FENZI, B. K.; ENGLAND, M. H.; TIMMERMANN, R.; HELLMER, H. H.; HATTERMANN, T.; DEBERNARD, J. B. Intercomparison of antarctic ice-shelf, ocean, and sea-ice interactions simulated by metroms-iceshelf and fesom 1.4. **Geoscientific Model Development**, v. 11, p. 1257–1292, 4 2018. ISSN 19919603. 15

NICHOLLS, K. W.; PUDSEY, C. J.; MORRIS, P. Summertime water masses off the northern larsen c ice shelf, antarctica. **Geophysical Research Letters**, v. 31, 5 2004. ISSN 00948276. 42, 45

ORSI, A. H.; JOHNSON, G. C.; BULLISTER, J. L. Circulation, mixing, and production of antarctic bottom water. **Progress in Oceanography**, v. 43, p. 55–109, 1999. 7, 42, 43

ORSI, A. H.; SMETHIE, W. M.; BULLISTER, J. L. On the total input of antarctic waters to the deep ocean: a preliminary estimate from chlorofluorocarbon measurements. **Journal of Geophysical Research: Oceans**, v. 107, 8 2002. ISSN 21699291. 45

OTOSAKA, I. N.; SHEPHERD, A.; IVINS, E. R.; SCHLEGEL, N. J.; AMORY, C.; BROEKE, M. R. V. D.; HORWATH, M.; JOUGHIN, I.; KING, M. D.; KRINNER, G.; NOWICKI, S.; PAYNE, A. J.; RIGNOT, E.; SCAMBOS, T.; SIMON, K. M.; SMITH, B. E.; SøRENSEN, L. S.; VELICOGNA, I.; WHITEHOUSE, P. L.; GERUO, A.; AGOSTA, C.; AHLSTRøM, A. P.; BLAZQUEZ, A.; COLGAN, W.; ENGDAHL, M. E.; FETTWEIS, X.; FORSBERG, R.; GALLéE, H.; GARDNER, A.; GILBERT, L.; GOURMELEN, N.; GROH, A.; GUNTER, B. C.; HARIG, C.; HELM, V.; KHAN, S. A.; KITTEL, C.; KONRAD, H.; LANGEN, P. L.; LECAVALIER, B. S.; LIANG, C. C.; LOOMIS, B. D.; MCMILLAN, M.; MELINI, D.; MERNILD, S. H.; MOTTRAM, R.; MOUGINOT, J.; NILSSON, J.; NOëL, B.; PATTLE, M. E.; PELTIER, W. R.; PIE, N.; ROCA, M.; SASGEN, I.; SAVE, H. V.; SEO, K. W.; SCHEUCHL, B.; SCHRAMA, E. J.; SCHRöDER, L.; SIMONSEN, S. B.; SLATER, T.; SPADA, G.; SUTTERLEY, T. C.; VISHWAKARMA, B. D.; WESSEM, J. M. V.; WIESE, D.; WAL, W. V. D.; WOUTERS, B. Mass balance of the greenland and antarctic ice sheets from 1992 to 2020. **Earth System Science Data**, v. 15, p. 1597–1616, 4 2023. ISSN 18663516. 5

PAOLO, F. S.; FRICKER, H. A.; PADMAN, L. Volume loss from antarctic ice shelves is accelerating. **Science**, v. 348, p. 327–331, 4 2015. ISSN 0036-8075. Disponível em: <<https://www.sciencemag.org/lookup/doi/10.1126/science.aaa0940>>. 4, 8, 32, 41

PAOLO, F. S.; GARDNER, A. S.; GREENE, C. A.; NILSSON, J.; SCHODLOK, M. P.; SCHLEGEL, N.-J.; FRICKER, H. A. Widespread slowdown in thinning rates of west antarctic ice shelves. **The Cryosphere**, v. 17, p. 3409–3433, 8 2023. ISSN 19940424. 52, 59, 60, 61, 62

PAOLO, F. S.; PADMAN, L.; FRICKER, H. A.; ADUSUMILLI, S.; HOWARD, S.; SIEGFRIED, M. R. Response of pacific-sector antarctic ice shelves to the el niño/southern oscillation. **Nature Geoscience**, v. 11, p. 121–126, 2 2018. ISSN 1752-0894. Disponível em: <<http://dx.doi.org/10.1038/s41561-017-0033-0http://www.nature.com/articles/s41561-017-0033-0>>. 34

PARDO, P. C.; PéREZ, F. F.; VELO, A.; GILCOTO, M. Water masses distribution in the southern ocean: Improvement of an extended omp (eomp) analysis. **Progress in Oceanography**, v. 103, p. 92–105, 9 2012. ISSN 00796611. 42

PARISE, C. K.; PEZZI, L. P.; HODGES, K. I.; JUSTINO, F. The influence of sea ice dynamics on the climate sensitivity and memory to increased antarctic sea ice. **Journal of Climate**, v. 28, p. 9642–9668, 2015. ISSN 08948755. 6, 29, 31, 34, 38, 41

PARK, W.; LATIF, M. Ensemble global warming simulations with idealized antarctic meltwater input. **Climate Dynamics**, v. 52, p. 3223–3239, 2019. ISSN 14320894. Disponível em: <<http://dx.doi.org/10.1007/s00382-018-4319-8>>. 23, 39

PARKINSON, C. L. A 40-y record reveals gradual antarctic sea ice increases followed by decreases at rates far exceeding the rates seen in the arctic. **Proceedings of the National Academy of Sciences of the United States of America**, v. 116, p. 14414–14423, 3 2019. ISSN 10916490. Disponível em: <<http://www.nature.com/articles/s41586-020-2120-4>>. 3, 6, 28, 36, 76

PARKINSON, C. L.; CAVALIERI, D. J. Antarctic sea ice variability and trends, 1979-2010. **Cryosphere**, v. 6, p. 871–880, 3 2012. ISSN 19940416. Disponível em: <<http://www.nature.com/articles/s41586-020-2120-4>>. 6

PAULING, A. G.; BITZ, C. M.; SMITH, I. J.; LANGHORNE, P. J. The response of the southern ocean and antarctic sea ice to freshwater from ice shelves in an earth system model. **Journal of Climate**, v. 29, p. 1655–1672, 3 2016. ISSN 0894-8755. Disponível em: <<http://www.nature.com/articles/s41586-020-2120-4http://journals.ametsoc.org/doi/10.1175/JCLI-D-15-0501.1>>. 4, 68

PAULING, A. G.; SMITH, I. J.; LANGHORNE, P. J.; BITZ, C. M. Time-dependent freshwater input from ice shelves: impacts on antarctic sea ice and the southern ocean in an earth system model. **Geophysical Research Letters**, v. 44, p. 10,454–10,461, 10 2017. ISSN 00948276. Disponível em: <<http://www.nature.com/articles/s41586-020-2120-4http://doi.wiley.com/10.1002/2017GL075017>>. 4, 36, 68

PELLICHERO, V.; SALLéE, J. B.; CHAPMAN, C. C.; DOWNES, S. M. The southern ocean meridional overturning in the sea-ice sector is driven by freshwater fluxes. **Nature Communications**, v. 9, 12 2018. ISSN 20411723. 23, 65

POWERS, J. G. Numerical prediction of an antarctic severe wind event with the weather research and forecasting (wrf) model. **Monthly Weather Review**, v. 135, p. 3134–3157, 9 2007. ISSN 00270644. 13

PRITCHARD, H. D.; LIGTENBERG, S. R.; FRICKER, H. A.; VAUGHAN, D. G.; BROEKE, M. R. V. D.; PADMAN, L. Antarctic ice-sheet loss driven by

basal melting of ice shelves. **Nature**, v. 484, p. 502–505, 2012. ISSN 00280836. Disponível em: <<http://dx.doi.org/10.1038/nature10968>>. 8, 34, 35, 39, 40, 41

PURICH, A.; CAI, W.; ENGLAND, M. H.; COWAN, T. Evidence for link between modelled trends in antarctic sea ice and underestimated westerly wind changes. **Nature Communications**, v. 7, p. 10409, 4 2016. ISSN 2041-1723. Disponível em: <<http://dx.doi.org/10.1038/ncomms10409http://www.nature.com/articles/ncomms10409>>. 2

PURICH, A.; DODDRIDGE, E. W. Record low antarctic sea ice coverage indicates a new sea ice state. **Communications Earth and Environment**, v. 4, 12 2023. ISSN 26624435. 3, 68

PURKEY, S. G.; JOHNSON, G. C. Antarctic bottom water warming and freshening: contributions to sea level rise, ocean freshwater budgets, and global heat gain. **Journal of Climate**, v. 26, p. 6105–6122, 2013. ISSN 08948755. 33, 37, 43

RACKOW, T.; WESCHE, C.; TIMMERMANN, R.; HELLMER, H. H.; JURICKE, S.; JUNG, T. A simulation of small to giant antarctic iceberg evolution: differential impact on climatology estimates. **Journal of Geophysical Research: Oceans**, v. 122, p. 3170–3190, 4 2017. ISSN 21699275. Disponível em: <<http://doi.wiley.com/10.1002/2016JC012513>>. 32

RAPHAEL, M. N.; HANDCOCK, M. S. A new record minimum for antarctic sea ice. **Nature Reviews Earth Environment**, v. 3, p. 215–216, 3 2022. ISSN 2662-138X. 3

RAPHAEL, M. N.; MARSHALL, G. J.; TURNER, J.; FOGT, R. L.; SCHNEIDER, D.; DIXON, D. A.; HOSKING, J. S.; JONES, J. M.; HOBBS, W. R. The amundsen sea low: variability, change, and impact on antarctic climate. **Bulletin of the American Meteorological Society**, v. 97, p. 111–121, 2016. ISSN 00030007. 29

REYNOLDS, R. W.; RAYNER, N. A.; SMITH, T. M.; STOKES, D. C.; WANG, W. An improved in situ and satellite sst analysis for climate. **Journal of Climate**, v. 15, p. 1609–1625, 7 2002. ISSN 0894-8755. Disponível em: <<http://journals.ametsoc.org/doi/10.1175/1520-0442(2002)015<1609:AIISAS>2.0.CO;2>>. 51

REYNOLDS, R. W.; SMITH, T. M.; LIU, C.; CHELTON, D. B.; CASEY, K. S.; SCHLAX, M. G. Daily high-resolution-blended analyses for sea surface temperature. **Journal of Climate**, v. 20, p. 5473–5496, 11 2007. ISSN 08948755. 52

RICHTER, O.; GWYTHER, D. E.; KING, M. A.; GALTON-FENZI, B. K. The impact of tides on antarctic ice shelf melting. **Cryosphere**, v. 16, p. 1409–1429, 4 2022. ISSN 19940424. 15, 46

RIGNOT, E. Accelerated ice discharge from the antarctic peninsula following the collapse of larsen b ice shelf. **Geophysical Research Letters**, v. 31, p. L18401, 2004. ISSN 0094-8276. Disponível em: <<http://doi.wiley.com/10.1029/2004GL020697>>. 7, 25, 27, 41

RIGNOT, E.; BAMBER, J. L.; BROEKE, M. R. van den; DAVIS, C.; LI, Y.; BERG, W. J. van de; MEIJGAARD, E. van. Recent antarctic ice mass loss from radar interferometry and regional climate modelling. **Nature Geoscience**, v. 1, p. 106–110, 2 2008. ISSN 1752-0894. Disponível em: <<http://www.nature.com/articles/ngeo102>>. 27

RIGNOT, E.; JACOBS, S.; MOUGINOT, J.; SCHEUCHL, B. Ice-shelf melting around antarctica. **Science**, v. 341, p. 266–270, 7 2013. ISSN 0036-8075. Disponível em: <<https://www.sciencemag.org/lookup/doi/10.1126/science.1235798>>. 31, 35, 52, 59, 60, 61

RIGNOT, E.; MOUGINOT, J.; SCHEUCHL, B.; BROEKE, M. van den; WESSEM, M. J. van; MORLIGHEM, M. Four decades of antarctic ice sheet mass balance from 1979–2017. **Proceedings of the National Academy of Sciences**, v. 116, p. 1095–1103, 1 2019. ISSN 0027-8424. Disponível em: <<http://www.pnas.org/lookup/doi/10.1073/pnas.1812883116>>. 27, 35

RIGNOT, E.; THOMAS, R. H. Mass balance of polar ice sheets. **Science**, v. 297, p. 1502–1506, 2002. ISSN 00368075. 31, 51

RINTOUL, S. R. The global influence of localized dynamics in the southern ocean. **Nature**, v. 558, p. 209–218, 2018. ISSN 14764687. 4, 39

RINTOUL, S. R.; GARABATO, A. C. N. 2. ed. [S.l.]: Elsevier. 471-492 p. ISSN 00746142. ISBN 9780123918512. 42

ROBIN, G. D. Q. Polar ice sheets: a review. **Polar Record**, v. 16, p. 5–22, 1 1972. ISSN 0032-2474. Disponível em: <<https://www.cambridge.org/core/product/identifier/S0032247400062380/type/journal_article>>. 25

ROBINSON, S. A.; KLEKOCIUK, A. R.; KING, D. H.; ROJAS, M. P.; ZúñIGA, G. E.; BERGSTROM, D. M. The 2019/2020 summer of antarctic heatwaves. **Global Change Biology**, v. 26, p. 3178–3180, 6 2020. ISSN 1354-1013. Disponível em: <<https://onlinelibrary.wiley.com/doi/10.1111/gcb.15083>>. 1

ROSEVEAR, M. G.; GAYEN, B.; GALTON-FENZI, B. K. The role of double-diffusive convection in basal melting of antarctic ice shelves. **Proceedings of the National Academy of Sciences of the United States of America**, v. 118, 2021. ISSN 10916490. 31

RYE, C. D.; MARSHALL, J.; KELLEY, M.; RUSSELL, G.; NAZARENKO, L. S.; KOSTOV, Y.; SCHMIDT, G. A.; HANSEN, J. Antarctic glacial melt as a driver of recent southern ocean climate trends. **Geophysical Research Letters**, v. 47, 6 2020. ISSN 0094-8276. Disponível em: <<https://onlinelibrary.wiley.com/doi/10.1029/2019GL086892>>. 1, 50

SANTINI, M. F.; SOUZA, R. B.; WAINER, I.; MUELBERT, M. M. Temporal analysis of water masses and sea ice formation rate west of the antarctic peninsula in 2008 estimated from southern elephant seals' srdl–ctd data. **Deep-Sea Research Part II: Topical Studies in Oceanography**, v. 149, p. 58–69, 3 2018. ISSN 09670645. 8, 45

SATHIYAMOORTHY, S.; MOORE, G. W. K. Buoyancy flux at ocean weather station bravo. **Journal of Physical Oceanography**, v. 32, p. 458–474, 2002. ISSN 0022-3670. Disponível em: <<http://journals.ametsoc.org/doi/10.1175/1520-0485(2002)032%3C0458:BFAOWS%3E2.0.CO;2>>. 27

SCAMBOS. Glacier acceleration and thinning after ice shelf collapse in the larsen b embayment, antarctica. **Geophysical Research Letters**, v. 31, p. L18402, 2004. ISSN 0094-8276. Disponível em: <<http://doi.wiley.com/10.1029/2004GL020670>>. 31, 39, 50

SCAMBOS, T.; FRICKER, H. A.; LIU, C. C.; BOHLANDER, J.; FASTOOK, J.; SARGENT, A.; MASSOM, R.; WU, A. M. Ice shelf disintegration by plate bending and hydro-fracture: satellite observations and model results of the 2008 wilkins ice shelf break-ups. **Earth and Planetary Science Letters**, v. 280, p. 51–60, 4 2009. ISSN 0012821X. 50

SCAMBOS, T.; HULBE, C.; FAHNESTOCK, M. **Climate-induced ice shelf disintegration in the Antarctic Peninsula**. [s.n.], 2013. 79-92 p. ISBN 9781118668450. Disponível em: <<https://doi.org/10.1029/AR079p0079http://doi.wiley.com/10.1029/AR079p0079>>. 31, 33

SCHAEFER, V. J. The formation of frazil and anchor ice in cold water. **Eos, Transactions American Geophysical Union**, v. 31, p. 885–893, 12 1950. ISSN 0002-8606. Disponível em: <<https://agupubs.onlinelibrary.wiley.com/doi/10.1029/TR031i006p00885>>. 19

SCHAFFER, J.; TIMMERMANN, R.; ARNDT, J. E.; KRISTENSEN, S. S.; MAYER, C.; MORLIGHEM, M.; STEINHAGE, D. A global, high-resolution data set of ice sheet topography, cavity geometry, and ocean bathymetry. **Earth System Science Data**, v. 8, p. 543–557, 10 2016. ISSN 18663516. 46, 61

SCHLOSSER, E.; HAUMANN, F. A.; RAPHAEL, M. N. Atmospheric influences on the anomalous 2016 antarctic sea ice decay. **Cryosphere**, v. 12, p. 1103–1119, 3 2018. ISSN 19940424. 41

SCHLÜSSEL, P. **Satellite remote sensing of evaporation over sea**. [s.n.], 1996. 431-461 p. ISBN 978-3-540-42377-5. Disponível em: <<http://download.springer.com/static/pdf/185/bfm%253A978-3-642-56668-4%252F1.pdf?auth66=1401995374_4d363c462609ae19e3de18b0ee51ef07&ext=.pdfhttp://link.springer.com/10.1007/978-3-642-56680-6http://link.springer.com/10.1007/978-3-662-03289-3_16>>. 30

SCHMIDTKO, S.; HEYWOOD, K. J.; THOMPSON, A. F.; AOKI, S. Multidecadal warming of antarctic waters. **Science**, v. 346, p. 1227–1231, 2014. ISSN 0036-8075. Disponível em: <<https://www.sciencemag.org/lookup/doi/10.1126/science.1256117>>. 4, 27, 44

SCHODLOK, M. P.; MENEMENLIS, D.; RIGNOT, E. J. Ice shelf basal melt rates around antarctica from simulations and observations. **Journal of Geophysical Research: Oceans**, v. 121, p. 1085–1109, 2016. ISSN 21699291. 5, 39, 43, 45

SCHULTZ, C.; DONEY, S. C.; ZHANG, W. G.; REGAN, H.; HOLLAND, P.; MEREDITH, M. P.; STAMMERJOHN, S. Modeling of the influence of sea ice cycle and langmuir circulation on the upper ocean mixed layer depth and freshwater distribution at the west antarctic peninsula. **Journal of Geophysical Research: Oceans**, p. 0–3, 8 2020. ISSN 2169-9275. Disponível em: <<https://onlinelibrary.wiley.com/doi/abs/10.1029/2020JC016109>>. 1, 34, 38, 40

SHARP, M.; TRANTER, M. Glacier biogeochemistry. **Geochemical Perspectives**, v. 6, p. 173–339, 10 2017. ISSN 22237755. Disponível em: <<http://www.geochemicalperspectives.org/online/v6n2>>. 30

SHCHEPETKIN, A. F.; MCWILLIAMS, J. C. The regional oceanic modeling system (roms): a split-explicit, free-surface, topography-following-coordinate oceanic model. **Ocean Modelling**, v. 9, p. 347–404, 2005. ISSN 14635003. 14, 16, 45

SHEPHERD, A.; FRICKER, H. A.; FARRELL, S. L. Trends and connections across the antarctic cryosphere. **Nature**, v. 558, p. 223–232, 6 2018. ISSN 0028-0836. Disponível em: <<http://www.nature.com/articles/s41586-018-0171-6>>. 3

SHEPHERD, A.; IVINS, E.; RIGNOT, E.; SMITH, B.; BROEKE, M. van den; VELICOGNA, I.; WHITEHOUSE, P.; BRIGGS, K.; JOUGHIN, I.; KRINNER, G.; NOWICKI, S.; PAYNE, T.; SCAMBOS, T.; SCHLEGEL, N.; A, G.; AGOSTA, C.; AHLSTRøM, A.; BABONIS, G.; BARLETTA, V.; BLAZQUEZ, A.; BONIN, J.; CSATHO, B.; CULLATHER, R.; FELIKSON, D.; FETTWEIS, X.; FORSBERG, R.; GALLEE, H.; GARDNER, A.; GILBERT, L.; GROH, A.; GUNTER, B.; HANNA, E.; HARIG, C.; HELM, V.; HORVAT, A.; HORWATH, M.; KHAN, S.; KJELDSEN, K. K.; KONRAD, H.; LANGEN, P.; LECAVALIER, B.; LOOMIS, B.; LUTHCKE, S.; MCMILLAN, M.; MELINI, D.; MERNILD, S.; MOHAJERANI, Y.; MOORE, P.; MOUGINOT, J.; MOYANO, G.; MUIR, A.; NAGLER, T.; NIELD, G.; NILSSON, J.; NOEL, B.; OTOSAKA, I.; PATTLE, M. E.; PELTIER, W. R.; PIE, N.; RIETBROEK, R.; ROTT, H.; SANDBERG-SøRENSEN, L.; SASGEN, I.; SAVE, H.; SCHEUCHL, B.; SCHRAMA, E.; SCHRöDER, L.; SEO, K.-W.; SIMONSEN, S.; SLATER, T.; SPADA, G.; SUTTERLEY, T.; TALPE, M.; TARASOV, L.; BERG, W. J. van de; WAL, W. van der; WESSEM, M. van; VISHWAKARMA, B. D.; WIESE, D.; WOUTERS, B. Mass balance of the antarctic ice sheet from 1992 to 2017.

Nature, v. 558, p. 219–222, 6 2018. ISSN 0028-0836. Disponível em: <<https://www.nature.com/articles/s41586-018-0179-y>>. 5

SHEPHERD, A.; WINGHAM, D.; PAYNE, T.; SKVARCA, P. Larsen ice shelf has progressively thinned. **Science**, v. 302, p. 856–859, 10 2003. ISSN 0036-8075. Disponível em: <<https://www.science.org/doi/10.1126/science.1089768>>. 8

SHEPHERD, A.; WINGHAM, D.; RIGNOT, E. Warm ocean is eroding west antarctic ice sheet. **Geophysical Research Letters**, v. 31, p. 1–4, 2004. ISSN 00948276. 39

SHEPHERD, J. G.; BREWER, P. G.; OSCHLIES, A.; WATSON, A. J. Ocean ventilation and deoxygenation in a warming world: introduction and overview. **Philosophical Transactions of the Royal Society A: Mathematical, Physical and Engineering Sciences**, v. 375, p. 20170240, 9 2017. ISSN 1364-503X. Disponível em: <<https://royalsocietypublishing.org/doi/10.1098/rsta.2017.0240>>. 23

SHI, J.-R.; TALLEY, L. D.; XIE, S.-P.; LIU, W.; GILLE, S. T. Effects of buoyancy and wind forcing on southern ocean climate change. **Journal of Climate**, v. 33, p. 10003–10020, 12 2020. ISSN 0894-8755. Disponível em: <<https://journals.ametsoc.org/doi/10.1175/JCLI-D-19-0877.1>>. 1

SHOKR, M.; YE, Y. Why does arctic sea ice respond more evidently than antarctic sea ice to climate change? **Ocean-Land-Atmosphere Research**, v. 2, 1 2023. ISSN 2771-0378. Disponível em: <<https://spj.science.org/doi/10.34133/olar.0006>>. 7

SIEGERT, M.; ATKINSON, A.; BANWELL, A.; BRANDON, M.; CONVEY, P.; DAVIES, B.; DOWNIE, R.; EDWARDS, T.; HUBBARD, B.; MARSHALL, G.; ROGELJ, J.; RUMBLE, J.; STROEVE, J.; VAUGHAN, D. The antarctic peninsula under a 1.5°c global warming scenario. **Frontiers in Environmental Science**, v. 7, 2019. ISSN 2296665X. 35

SIGMOND, M.; FYFE, J. C. Has the ozone hole contributed to increased antarctic sea ice extent? **Geophysical Research Letters**, v. 37, p. 2–6, 2010. ISSN 00948276. 3

SILER, N.; ROE, G. H.; ARMOUR, K. C.; FELDL, N. Revisiting the surface-energy-flux perspective on the sensitivity of global precipitation to climate change. **Climate Dynamics**, v. 52, p. 3983–3995, 4 2019. ISSN 14320894. 2

SILVANO, A.; RINTOUL, S. R.; PEñA-MOLINO, B.; HOBBS, W. R.; WIJK, E. van; AOKI, S.; TAMURA, T.; WILLIAMS, G. D. Freshening by glacial meltwater enhances melting of ice shelves and reduces formation of antarctic bottom water. **Science Advances**, v. 4, p. eaap9467, 4 2018. ISSN 2375-2548. Disponível em: <<https://advances.sciencemag.org/lookup/doi/10.1126/sciadv.aap9467>>. 2, 40

SIMPKINS, G. R.; CIASTO, L. M.; ENGLAND, M. H. Observed variations in multidecadal antarctic sea ice trends during 1979-2012. **Geophysical Research Letters**, v. 40, p. 3643–3648, 2013. ISSN 00948276. 36

SMITH, B.; FRICKER, H. A.; GARDNER, A. S.; MEDLEY, B.; NILSSON, J.; PAOLO, F. S.; HOLSCHUH, N.; ADUSUMILLI, S.; BRUNT, K.; CSATHO, B.; HARBECK, K.; MARKUS, T.; NEUMANN, T.; SIEGFRIED, M. R.; ZWALLY, H. J. Pervasive ice sheet mass loss reflects competing ocean and atmosphere processes. **Science**, v. 368, p. 1239–1242, 6 2020. ISSN 0036-8075. Disponível em: <<https://www.science.org/doi/10.1126/science.aaz5845>>. 5, 6, 8

SMITH, R.; BAKER, K.; FRASER, W.; HOFMANN, E.; KARL, D.; KLINK, J.; QUENTIN, L.; PREZELIN, B.; ROSS, R.; TRIVELPIECE, W.; VERNET, M. The palmer lter: A long-term ecological research program at palmer station, antarctica. **Oceanography**, v. 8, p. 77–86, 1995. ISSN 10428275. Disponível em: <<https://tos.org/oceanography/article/the-palmer-lter-a-long-term-ecological-research-program-atpalmerstation-ant>>. 52

SNOW, K.; HOGG, A. M.; SLOYAN, B. M.; DOWNES, S. M. Sensitivity of antarctic bottom water to changes in surface buoyancy fluxes. **Journal of Climate**, v. 29, p. 313–330, 1 2016. ISSN 0894-8755. Disponível em: <<http://journals.ametsoc.org/doi/10.1175/JCLI-D-15-0467.1>>. 33

ST-LAURENT, P.; KLINCK, J. M.; DINNIMAN, M. S. On the role of coastal troughs in the circulation of warm circumpolar deep water on antarctic shelves. **Journal of Physical Oceanography**, v. 43, p. 51–64, 1 2013. ISSN 0022-3670. Disponível em: <<http://journals.ametsoc.org/doi/10.1175/JPO-D-11-0237.1>>. 15

STAMMERJOHN, S. E.; MARTINSON, D. G.; SMITH, R. C.; YUAN, X.; RIND, D. Trends in antarctic annual sea ice retreat and advance and their relation to el niño-southern oscillation and southern annular mode variability. **Journal of Geophysical Research: Oceans**, v. 113, 3 2008. ISSN 21699291. 2, 36

STARK, J. S.; RAYMOND, T.; DEPPELER, S. L.; MORRISON, A. K. **Antarctic Seas**. 2.. ed. [s.n.], 2019. 1-44 p. ISBN 9780128050682. Disponível em: <<https://doi.org/10.1016/B978-0-12-805068-2.00002-4https://linkinghub.elsevier.com/retrieve/pii/B9780128050682000024>>. 31

STEIG, E.; DING, Q.; BATTISTI, D.; JENKINS, A. Tropical forcing of circumpolar deep water inflow and outlet glacier thinning in the amundsen sea embayment, west antarctica. **Annals of Glaciology**, v. 53, p. 19–28, 9 2012. ISSN 0260-3055. Disponível em: <<https://www.cambridge.org/core/product/identifier/S0260305500251690/type/journal_article>>. 76

STEIN, K.; TIMMERMANN, A.; KWON, E. Y.; FRIEDRICH, T. Timing and magnitude of southern ocean sea ice/carbon cycle feedbacks. **Proceedings of the National Academy of Sciences**, v. 117, p. 4498–4504, 3 2020. ISSN 0027-8424.

Disponível em: <<http://www.nature.com/articles/s41586-020-2120-4http://www.pnas.org/lookup/doi/10.1073/pnas.1908670117>>. 4, 68

STERN, A. A.; ADCROFT, A.; SERGIENKO, O. Modeling ice shelf cavities and tabular icebergs using lagrangian elements. **Journal of Geophysical Research: Oceans**, v. 124, p. 3378–3392, 5 2019. ISSN 21699291. 15

SUN, S.; PATTYN, F.; SIMON, E. G.; ALBRECHT, T.; CORNFORD, S.; CALOV, R.; DUMAS, C.; GILLET-CHAULET, F.; GOELZER, H.; GOLLEDGE, N. R.; GREVE, R.; HOFFMAN, M. J.; HUMBERT, A.; KAZMIERCZAK, E.; KLEINER, T.; LEGUY, G. R.; LIPSCOMB, W. H.; MARTIN, D.; MORLIGHEM, M.; NOWICKI, S.; POLLARD, D.; PRICE, S.; QUIQUET, A.; SEROUSSI, H.; SCHLEMM, T.; SUTTER, J.; WAL, R. S. W. van de; WINKELMANN, R.; ZHANG, T. Antarctic ice sheet response to sudden and sustained ice-shelf collapse (abumip). **Journal of Glaciology**, v. 66, p. 891–904, 12 2020. ISSN 0022-1430. Disponível em: <<https://www.cambridge.org/core/product/identifier/S0022143020000672/type/journal_article>>. 31

SWART, N. C.; GILLE, S. T.; FYFE, J. C.; GILLETT, N. P. Recent southern ocean warming and freshening driven by greenhouse gas emissions and ozone depletion. **Nature Geoscience**, v. 11, p. 836–841, 2018. ISSN 17520908. Disponível em: <<http://dx.doi.org/10.1038/s41561-018-0226-1>>. 1, 3, 23, 33, 36, 41

SWART, S.; GILLE, S. T.; DELILLE, B.; JOSEY, S.; MAZLOFF, M.; NEWMAN, L.; THOMPSON, A. F.; THOMSON, J.; WARD, B.; PLESSIS, M. D. D.; KENT, E. C.; GIRTON, J.; GREGOR, L.; PETRA, H.; HYDER, P.; PEZZI, L. P.; SOUZA, R. B. D.; TAMSITT, V.; WELLER, R. A.; ZAPPA, C. J. Constraining southern ocean air-sea-ice fluxes through enhanced observations. **Frontiers in Marine Science**, v. 6, p. 1–10, 2019. ISSN 22967745. 37

TAMSITT, V.; ENGLAND, M. H.; RINTOUL, S. R.; MORRISON, A. K. Residence time and transformation of warm circumpolar deep water on the antarctic continental shelf. **Geophysical Research Letters**, v. 48, 10 2021. ISSN 19448007. 40, 78

TEDESCO, M. **Remote sensing and the cryosphere**. 1 2015. 1-16 p. Disponível em: <<https://onlinelibrary.wiley.com/doi/10.1002/9781118368909.ch1>>. 51

TEWARI, K.; MISHRA, S. K.; SALUNKE, P.; DEWAN, A. Future projections of temperature and precipitation for antarctica. **Environmental Research Letters**, v. 17, 1 2022. ISSN 17489326. 13

THOMPSON, A. F.; STEWART, A. L.; SPENCE, P.; HEYWOOD, K. J. The antarctic slope current in a changing climate. In: . [S.l.]: Blackwell Publishing, 2018. v. 56, p. 741–770. 47, 63, 64, 78

TIMMERMANN, R.; WANG, Q.; HELLMER, H. Ice-shelf basal melting in a global finite-element sea-ice/ice-shelf/ocean model. **Annals of Glaciology**, v. 53, p. 303–314, 9 2012. ISSN 0260-3055. Disponível em: <<https://www.cambridge.org/core/product/identifier/S0260305500252026/type/journal_article>>. 15

TORRENCE, C.; COMPO, G. P. A practical guide to wavelet analysis. **Bulletin of the American Meteorological Society**, v. 79, p. 61–78, 1 1998. ISSN 0003-0007. Disponível em: <<http://journals.ametsoc.org/doi/10.1175/1520-0477(1998)079<0061:APGTWA>2.0.CO;2>>. 70, 71

TOURNADRE, J.; BOUHIER, N.; GIRARD-ARDHUIN, F.; RéMY, F. Antarctic icebergs distributions 1992–2014. **Journal of Geophysical Research: Oceans**, v. 121, p. 327–349, 1 2016. ISSN 2169-9275. Disponível em: <<https://onlinelibrary.wiley.com/doi/abs/10.1002/2015JC011178>>. 33

TREASURE, A. M.; ROQUET, F.; ANSORGE, I. J.; BESTER, M. N.; BOEHME, L.; BORNEMANN, H.; CHARRASSIN, J. B.; CHEVALLIER, D.; COSTA, D. P.; FEDAK, M. A.; GUINET, C.; HAMMILL, M. O.; HARCOURT, R. G.; HINDELL, M. A.; KOVACS, K. M.; LEA, M. A.; LOVELL, P.; LOWTHER, A. D.; LYDERSEN, C.; MCINTYRE, T.; MCMAHON, C. R.; MUELBERT, M. M.; NICHOLLS, K.; PICARD, B.; REVERDIN, G.; TRITES, A. W.; WILLIAMS, G. D.; BRUYN, P. J. N. D. **Marine mammals exploring the oceans pole to pole: A review of the meop consortium**. 6 2017. 132-138 p. 51

TURNER, J.; COLWELL, S. R.; MARSHALL, G. J.; LACHLAN-COPE, T. A.; CARLETON, A. M.; JONES, P. D.; LAGUN, V.; REID, P. A.; IAGOVKINA, S. Antarctic climate change during the last 50 years. **International Journal of Climatology**, v. 25, p. 279–294, 3 2005. ISSN 0899-8418. Disponível em: <<http://doi.wiley.com/10.1002/joc.1130>>. 27, 28

TURNER, J.; COMISO, J. Solve antarctica's sea-ice puzzle. **Nature**, v. 547, p. 275–277, 7 2017. ISSN 0028-0836. Disponível em: <<https://www.nature.com/articles/547275a>>. 3

TURNER, J.; LU, H.; WHITE, I.; KING, J. C.; PHILLIPS, T.; HOSKING, J. S.; BRACEGIRDLE, T. J.; MARSHALL, G. J.; MULVANEY, R.; DEB, P. Absence of 21st century warming on antarctic peninsula consistent with natural variability. **Nature**, v. 535, p. 411–415, 7 2016. ISSN 0028-0836. Disponível em: <<http://dx.doi.org/10.1038/nature18645http://www.nature.com/articles/nature18645>>. 32

TURNER, J.; MARSHALL, G. J.; CLEM, K.; COLWELL, S.; PHILLIPS, T.; LU, H. Antarctic temperature variability and change from station data. **International Journal of Climatology**, v. 579, p. 544–548, 3 2019. ISSN 10970088. Disponível em: <<http://www.nature.com/articles/s41586-020-2120-4>>. 32

VAUGHAN, D.; COMISO, J.; ALLISON, I.; CARRASCO, J.; KASER, G.; KWOK, R.; MOTE, P.; MURRAY, T.; PAUL, F.; REN, J.; RIGNOT, E.;

SOLOMINA, O.; STEFFEN, K.; ZHANG, T. Observations: cryosphere coordinating. In: . [S.l.: s.n.], 2013. p. 317–382. 31

VAUGHAN, D. G.; MARSHALL, G. J.; CONNOLLEY, W. M.; PARKINSON, C.; MULVANEY, R.; HODGSON, D. A.; KING, J. C.; PUDSEY, C. J.; TURNER, J. Recent rapid regional climate warming on the antarctic peninsula. **Climatic Change**, v. 60, p. 243–274, 2003. ISSN 01650009. 28

VENEGAS, S. A.; DRINKWATER, M. R. Sea ice, atmosphere and upper ocean variability in the weddell sea, antarctica. **Journal of Geophysical Research: Oceans**, v. 106, p. 16747–16765, 8 2001. ISSN 0148-0227. Disponível em: <<https://agupubs.onlinelibrary.wiley.com/doi/10.1029/2000JC000594>>. 75, 84

VERFAILLIE, D.; PELLETIER, C.; GOOSSE, H.; JOURDAIN, N. C.; BULL, C. Y. S.; DALAIDEN, Q.; FAVIER, V.; FICHEFET, T.; WILLE, J. D. The circum-antarctic ice-shelves respond to a more positive southern annular mode with regionally varied melting. **Communications Earth Environment**, v. 3, p. 139, 6 2022. ISSN 2662-4435. Disponível em: <<https://www.nature.com/articles/s43247-022-00458-x>>. 61, 68, 75, 76

VERNET, M.; GEIBERT, W.; HOPPEMA, M.; BROWN, P. J.; HAAS, C.; HELLMER, H. H.; JOKAT, W.; JULLION, L.; MAZLOFF, M.; BAKKER, D. C. E.; BREARLEY, J. A.; CROOT, P.; HATTERMANN, T.; HAUCK, J.; HILLENBRAND, C.; HOPPE, C. J. M.; HUHN, O.; KOCH, B. P.; LECHTENFELD, O. J.; MEREDITH, M. P.; GARABATO, A. C. N.; NöTHIG, E.; PEEKEN, I.; LOEFF, M. M. R. van der; SCHMIDTKO, S.; SCHRöDER, M.; STRASS, V. H.; TORRES-VALDéS, S.; VERDY, A. The weddell gyre, southern ocean: present knowledge and future challenges. **Reviews of Geophysics**, v. 57, p. 623–708, 9 2019. ISSN 8755-1209. Disponível em: <<https://onlinelibrary.wiley.com/doi/abs/10.1029/2018RG000604>>. 33, 60

VIZCAíNO, M.; MIKOLAJEWICZ, U.; JUNGCLAUS, J.; SCHURGERS, G. Climate modification by future ice sheet changes and consequences for ice sheet mass balance. **Climate Dynamics**, v. 34, p. 301–324, 2 2010. ISSN 0930-7575. Disponível em: <<https://link.springer.com/10.1007/s00382-009-0591-y>>. 23

WACHTER, P.; BECK, C.; PHILIPP, A.; HöPPNER, K.; JACOBEIT, J. Spatiotemporal variability of the southern annular mode and its influence on antarctic surface temperatures. **Journal of Geophysical Research: Atmospheres**, v. 125, 2020. ISSN 21698996. 23

WALKER, C. C.; GARDNER, A. S. Rapid drawdown of antarctica's wordie ice shelf glaciers in response to enso/southern annular mode-driven warming in the southern ocean. **Earth and Planetary Science Letters**, v. 476, p. 100–110, 10 2017. ISSN 0012821X. 69

WANG, X.; ZHANG, Z.; WANG, X.; VIHMA, T.; ZHOU, M.; YU, L.; UOTILA, P.; SEIN, D. V. Impacts of strong wind events on sea ice and water mass properties in antarctic coastal polynyas. **Climate Dynamics**, v. 57, p. 3505–3528,

12 2021. ISSN 0930-7575. Disponível em: <<https://link.springer.com/10.1007/s00382-021-05878-7>>. 5, 43

WILSON, E. A.; RISER, S. C.; CAMPBELL, E. C.; WONG, A. P. Winter upper-ocean stability and ice-ocean feedbacks in the sea ice-covered southern ocean. **Journal of Physical Oceanography**, v. 49, p. 1099–1117, 4 2019. ISSN 15200485. 51

WONG, A. P.; WIJFFELS, S. E.; RISER, S. C.; POULIQUEN, S.; HOSODA, S.; ROEMMICH, D.; GILSON, J.; JOHNSON, G. C.; MARTINI, K.; MURPHY, D. J.; SCANDERBEG, M.; BHASKAR, T. V.; BUCK, J. J.; MERCEUR, F.; CARVAL, T.; MAZE, G.; CABANES, C.; ANDRé, X.; POFFA, N.; YASHAYAEV, I.; BARKER, P. M.; GUINEHUT, S.; BELBéOCH, M.; IGNASZEWSKI, M.; BARINGER, M. O.; SCHMID, C.; LYMAN, J. M.; MCTAGGART, K. E.; PURKEY, S. G.; ZILBERMAN, N.; ALKIRE, M. B.; SWIFT, D.; OWENS, W. B.; JAYNE, S. R.; HERSH, C.; ROBBINS, P.; WEST-MACK, D.; BAHR, F.; YOSHIDA, S.; SUTTON, P. J.; CANCOUëT, R.; COATANOAN, C.; DOBBLER, D.; JUAN, A. G.; GOURRION, J.; KOLODZIEJCZYK, N.; BERNARD, V.; BOURLèS, B.; CLAUSTRE, H.; D'ORTENZIO, F.; RESTE, S. L.; TRAON, P. Y. L.; RANNOU, J. P.; SAOUT-GRIT, C.; SPEICH, S.; THIERRY, V.; VERBRUGGE, N.; ANGEL-BENAVIDES, I. M.; KLEIN, B.; NOTARSTEFANO, G.; POULAIN, P. M.; VéLEZ-BELCHí, P.; SUGA, T.; ANDO, K.; IWASASKA, N.; KOBAYASHI, T.; MASUDA, S.; OKA, E.; SATO, K.; NAKAMURA, T.; SATO, K.; TAKATSUKI, Y.; YOSHIDA, T.; COWLEY, R.; LOVELL, J. L.; OKE, P. R.; WIJK, E. M. van; CARSE, F.; DONNELLY, M.; GOULD, W. J.; GOWERS, K.; KING, B. A.; LOCH, S. G.; MOWAT, M.; TURTON, J.; RAO, E. P. R.; RAVICHANDRAN, M.; FREELAND, H. J.; GABOURY, I.; GILBERT, D.; GREENAN, B. J.; OUELLET, M.; ROSS, T.; TRAN, A.; DONG, M.; LIU, Z.; XU, J.; KANG, K. R.; JO, H. J.; KIM, S. D.; PARK, H. M. **Argo data 1999–2019: two million temperature-salinity profiles and subsurface velocity observations from a global array of profiling floats**. 9 2020. 51

WOUTERS, B.; MARTIN-ESPANOL, A.; HELM, V.; FLAMENT, T.; WESSEM, J. M. van; LIGTENBERG, S. R. M.; BROEKE, M. R. van den; BAMBER, J. L. Dynamic thinning of glaciers on the southern antarctic peninsula. **Science**, v. 348, p. 899–903, 5 2015. ISSN 0036-8075. Disponível em: <<https://www.sciencemag.org/lookup/doi/10.1126/science.aaa5727>>. 5, 6

ZHANG, J. Increasing antarctic sea ice under warming atmospheric and oceanic conditions. **Journal of Climate**, v. 20, p. 2515–2529, 3 2007. ISSN 08948755. Disponível em: <<http://www.nature.com/articles/s41586-020-2120-4>>. 24

ZHANG, L.; DELWORTH, T. L.; COOKE, W.; YANG, X. Natural variability of southern ocean convection as a driver of observed climate trends. **Nature Climate Change**, v. 9, p. 59–65, 2019. ISSN 17586798. Disponível em: <<http://dx.doi.org/10.1038/s41558-018-0350-3>>. 36

ZHOU, Q.; HATTERMANN, T. Modeling ice shelf cavities in the unstructured-grid, finite volume community ocean model: implementation and

effects of resolving small-scale topography. **Ocean Modelling**, v. 146, p. 101536, 2 2020. ISSN 14635003. Disponível em: <<https://linkinghub.elsevier.com/retrieve/pii/S1463500319301738>>. 15

ZHOU, S.; MEIJERS, A. J.; MEREDITH, M. P.; ABRAHAMSEN, E. P.; HOLLAND, P. R.; SILVANO, A.; SALLéE, J. B.; ØSTERHUS, S. Slowdown of antarctic bottom water export driven by climatic wind and sea-ice changes. **Nature Climate Change**, v. 13, p. 701–709, 7 2023. ISSN 17586798. 43, 78

APPENDIX A - SUPPLEMENTARY MATERIALS CHAPTER 4 - THE ROLE OF ICE SHELF BASAL MELTING ON WATER MASS STRUCTURE AND OCEAN DYNAMICS AROUND THE ANTARCTIC PENINSULA

A.1 Model assessment

A.1 and A.2 - Supplementary figures of vertical assessment of the CTRL Experiment, related to *in situ* observations.

Figure A.1 - Western Antarctic Peninsula validation.

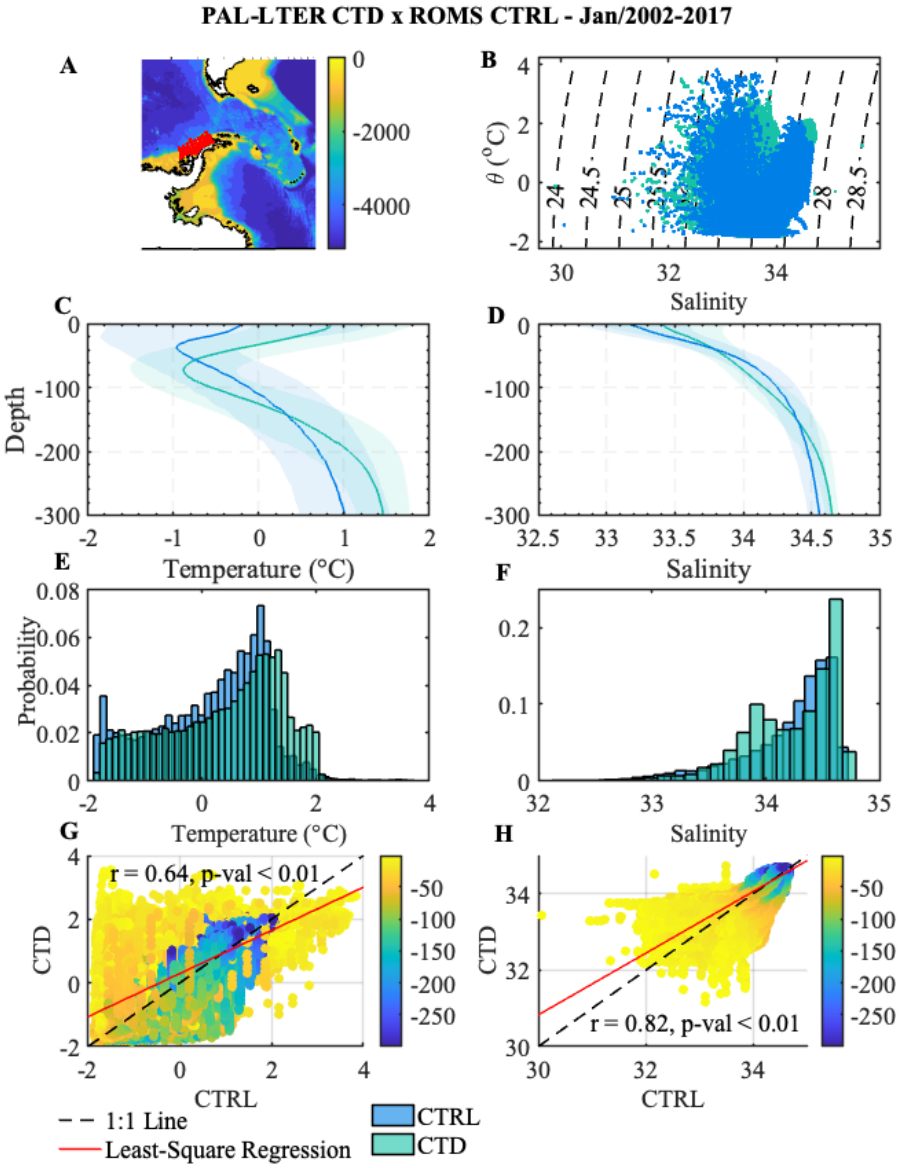

Comparison of observed and modeled features. The observations are from January 2002 to 2017 Palmer Long-Term Ecological Research Project cruises, and the model output is averaged over the same month and data points. (A) Location of data points evaluated; (B) TS-diagrams of observed (CTD) and modeled (CTRL-ROMS) simulation; Mean vertical profiles with standard deviation, and histograms are represented in (C) and (D) Temperature (°C), and (E) and (F) Salinity, respectively. The last rows (G) and (H) are the scatter plots for observed and modeled potential temperature and salinity, color-coded for depth. The dashed line indicates the 1:1 relationship, and the red solid line is the least-square regression.

SOURCE: Author.

Figure A.2 - Eastern Antarctic Penninsula validation.

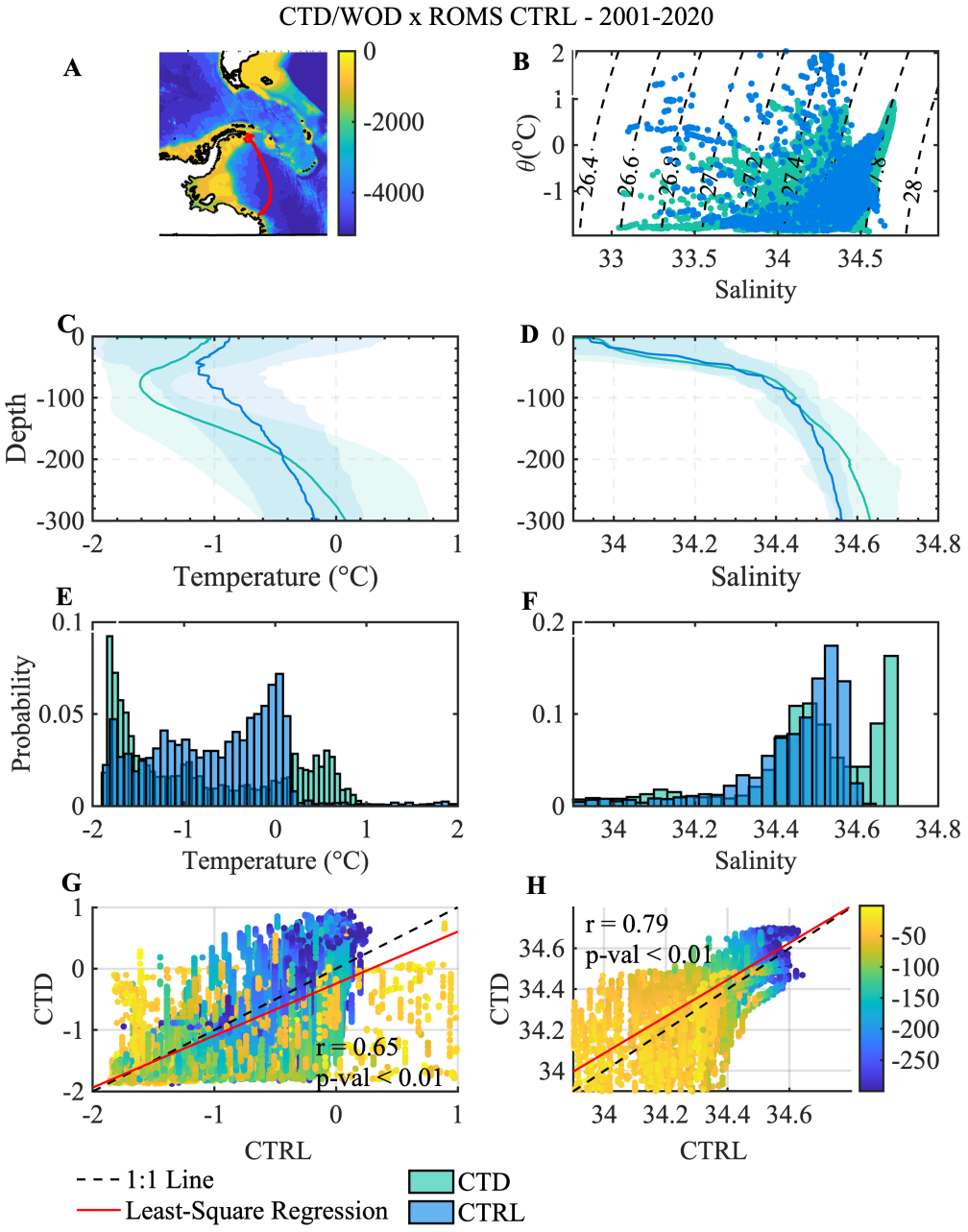

Comparison of observed and modeled features. The observations are from January 2002 to 2020 from World Ocean Databases (WOD), from autonomous pinniped bathythermograph (APB), and the model output is averaged over the same month and data points. (A) Location of data points evaluated; (B) TS-diagrams of observed (CTD) and modeled (CTRL-ROMS) simulation; Mean vertical profiles with standard deviation, and histograms are represented in (C) and (D) Temperature (°C), and (E) and (F) Salinity, respectively. The last rows (G) and (H) are the scatter plots for observed and modeled potential temperature and salinity, color-coded for depth. The dashed line indicates the 1:1 relationship, and the red solid line is the least-square regression.

SOURCE: Author.

A.2 Basal melting

A.3 - Supplementary figure representing the tracers of meltwater along the water column from each ice shelf separately.

Figure A.3 - Horizontal distribution of the basal meltwater tracer from each ice shelf along the water column.

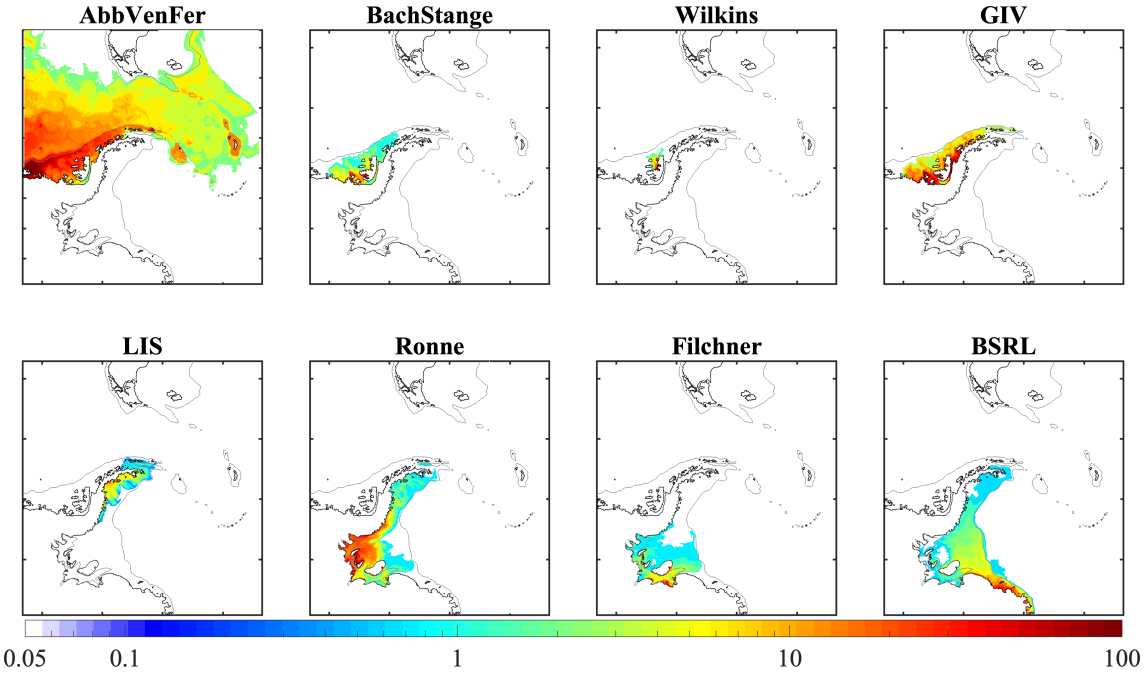

Horizontal distribution of the basal meltwater tracers along the water column from each ice shelf. The one dye unit of the dye concentration represents the freshwater concentration of 10^{-4}. Here is the concentration five years from the start of the initial dye spread.

SOURCE: Author.

A.3 Vertical profiles

A.4, A.5, A.6 - Bellingshausen Sea cross-slope sections.

A.7, A.8, A.9,A.10 - Weddell Sea cross-slope sections.

A.11, A.12 - Drake and SR4 subsections

A.13, A.14 - LIS and Ronne Filchner along-shelf break subsections (isobath 1000m).

A.3.1 Bellingshausen Sea

Figure A.4 - Section CS 1.

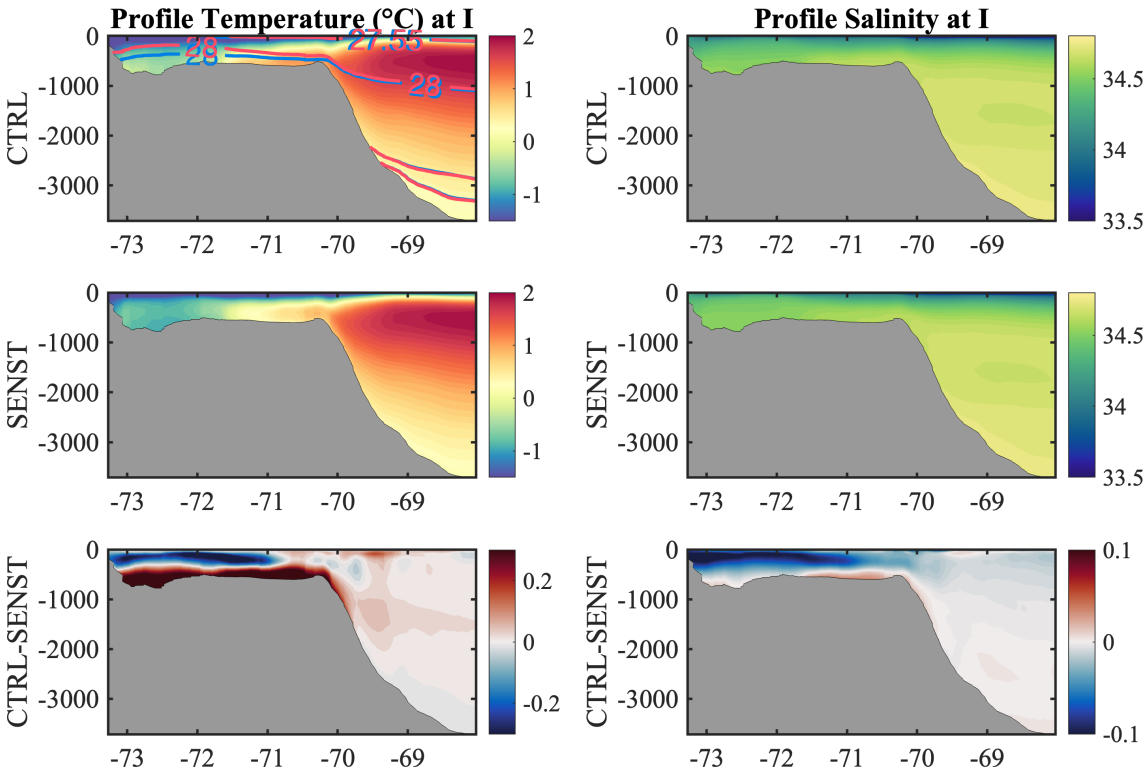

Temperature and Salinity profiles. The blue and red lines represent the neutral density, for CTRL and SENST, respectively. The x-axis indicates the latitudes (°S).

SOURCE: Author.

Figure A.5 - Section CS 2.

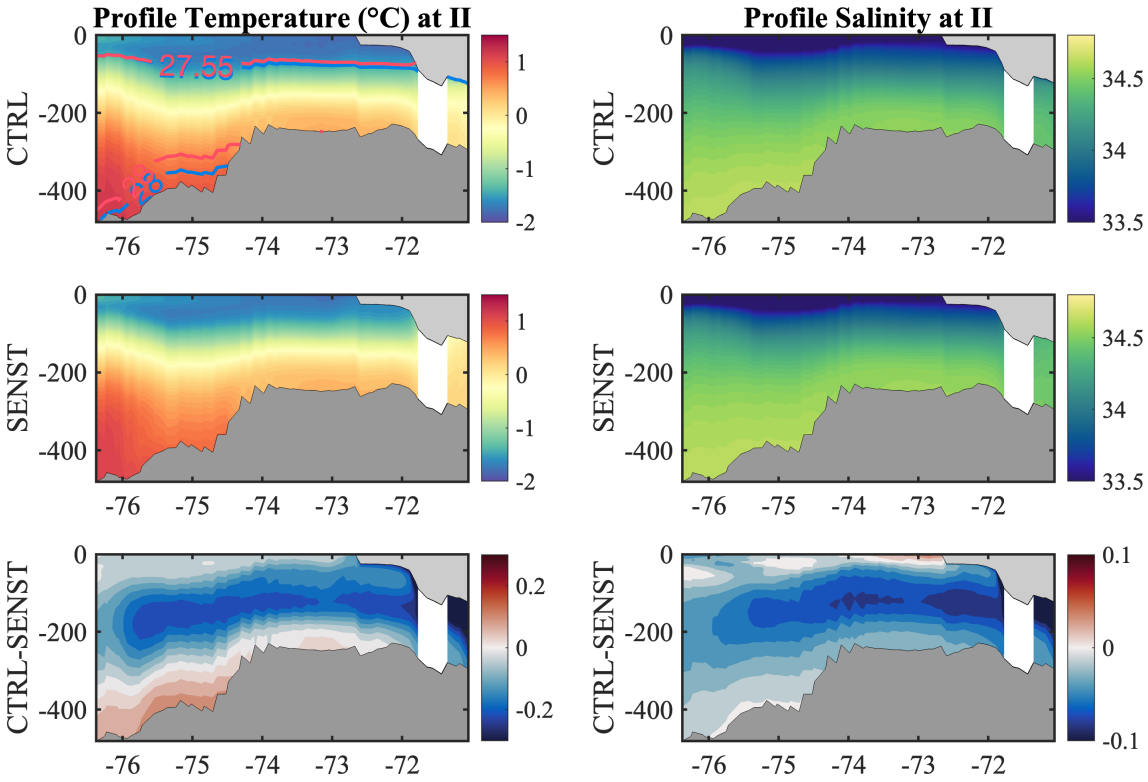

Temperature and Salinity profiles. The blue and red lines represent the neutral density, for CTRL and SENST, respectively. The x-axis indicates the longitudes (°W).

SOURCE: Author.

Figure A.6 - Section CS 3.

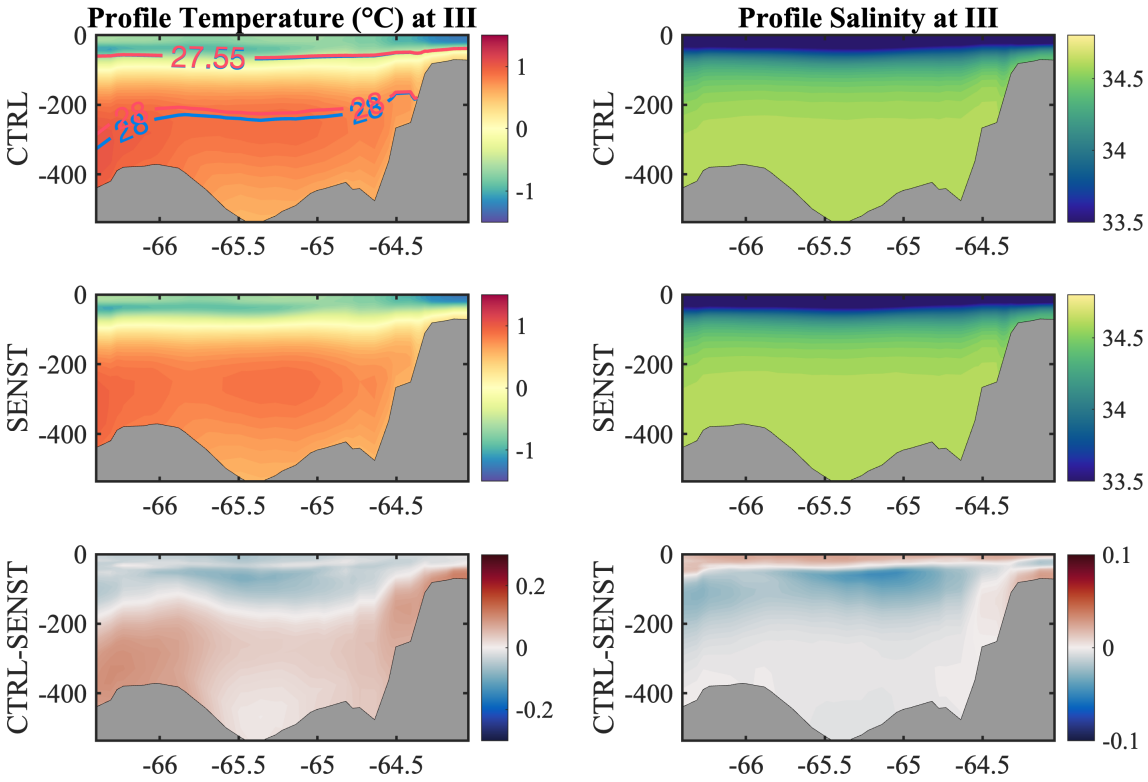

Temperature and Salinity profiles. The blue and red lines represent the neutral density, for CTRL and SENST, respectively. The x-axis indicates the longitudes (°W).

SOURCE: Author.

A.3.2 Weddell Sea

Figure A.7 - Section CS 4.

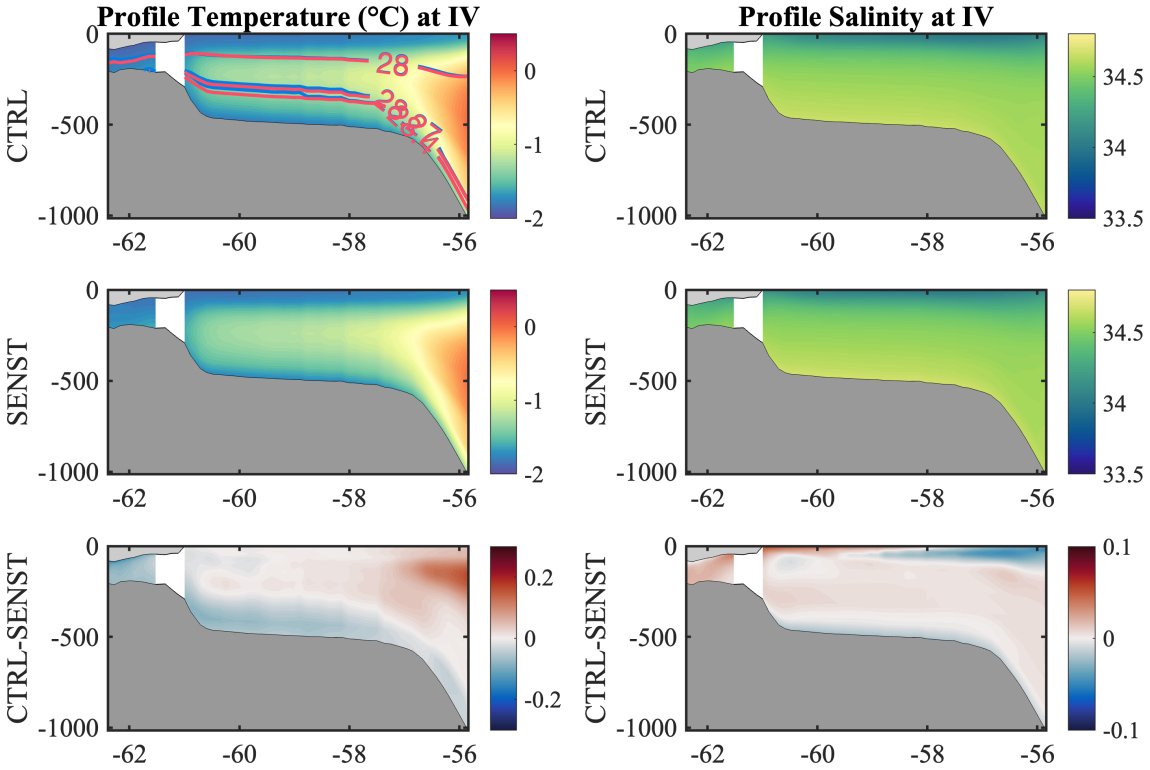

Temperature and Salinity profiles. The blue and red lines represent the neutral density, for CTRL and SENST, respectively. The x-axis indicates the longitudes (°W).

SOURCE: Author.

Figure A.8 - Section CS 5.

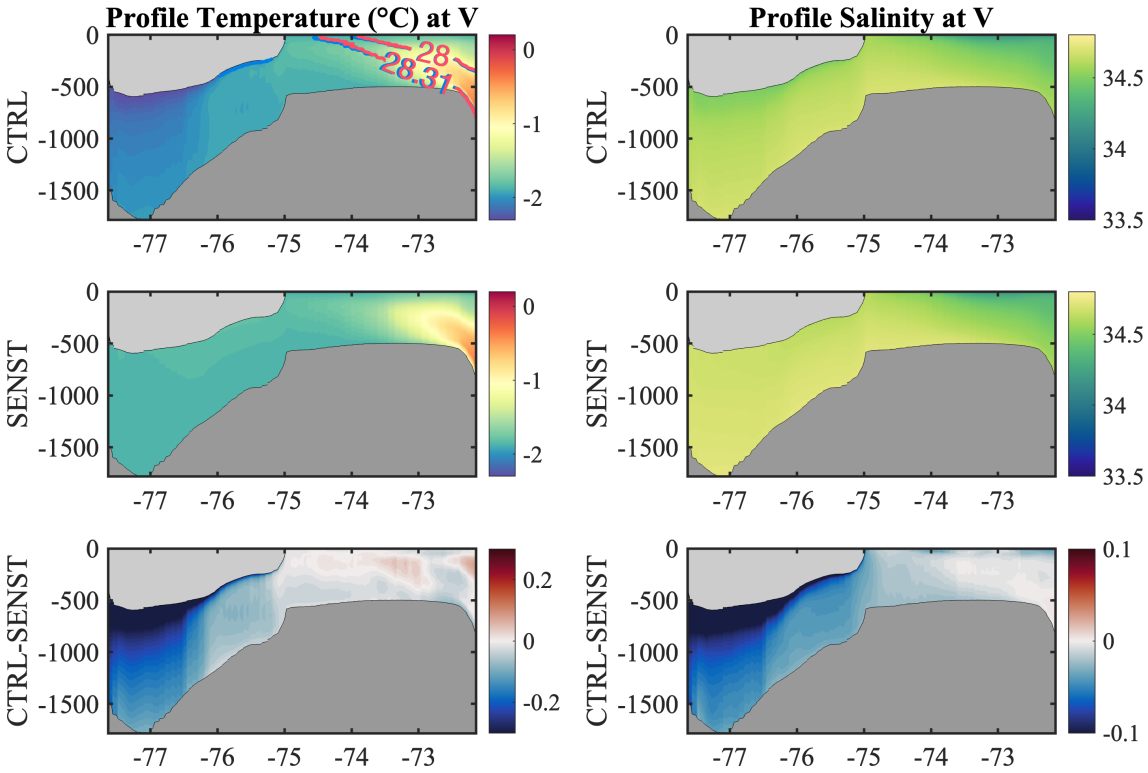

Temperature and Salinity profiles. The blue and red lines represent the neutral density, for CTRL and SENST, respectively. The x-axis indicates the latitudes (°S).

SOURCE: Author.

Figure A.9 - Section CS 6.

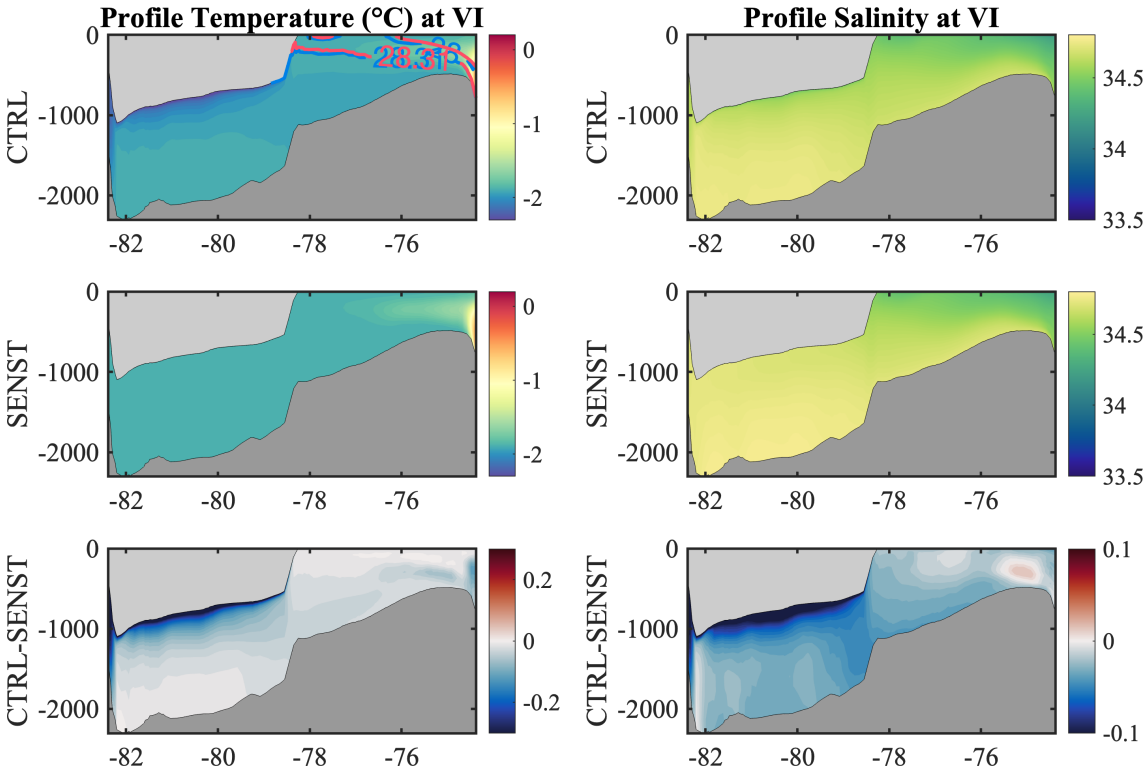

Temperature and Salinity profiles. The blue and red lines represent the neutral density, for CTRL and SENST, respectively. The x-axis indicates the latitudes (°S).

SOURCE: Author.

Figure A.10 - Section CS 7.

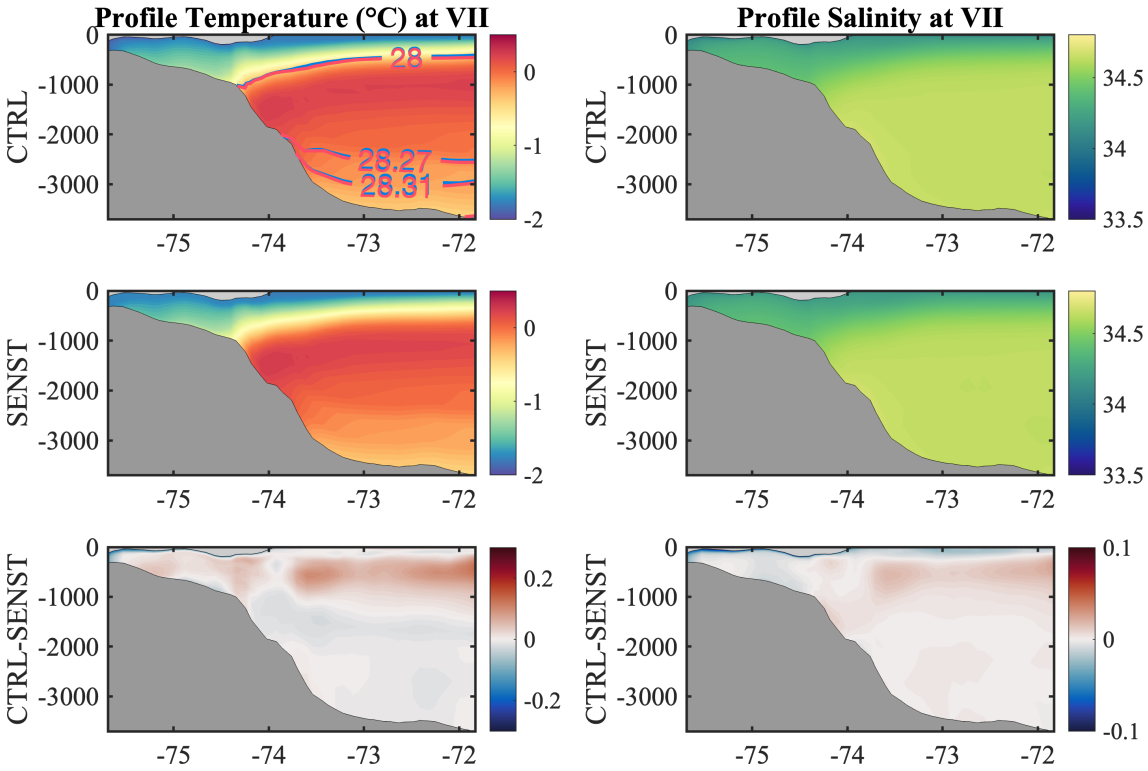

Temperature and Salinity profiles. The blue and red lines represent the neutral density, for CTRL and SENST, respectively. The x-axis indicates the latitudes (°S).

SOURCE: Author.

A.3.3 Drake and SR4 sub-sections

Figure A.11 - Section A - Drake.

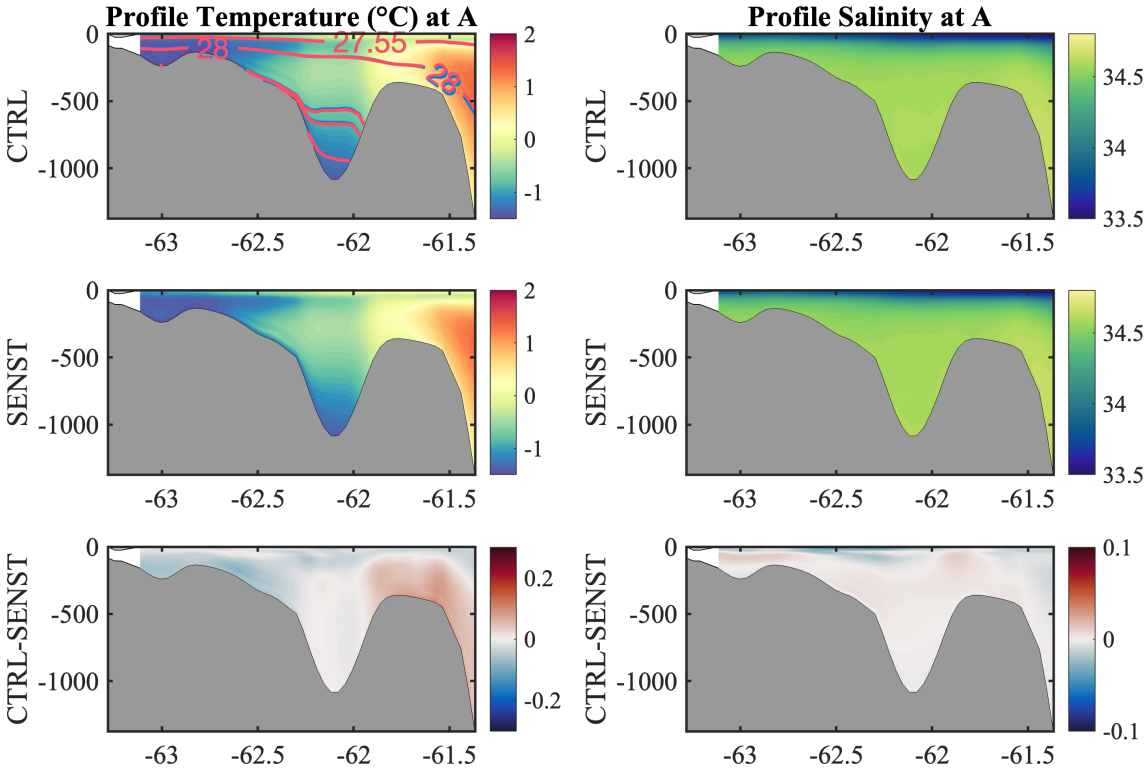

Temperature and Salinity profiles. The blue and red lines represent the neutral density, for CTRL and SENST, respectively. The x-axis indicates the latitudes (°S).

SOURCE: Author.

Figure A.12 - Section B - SR4.

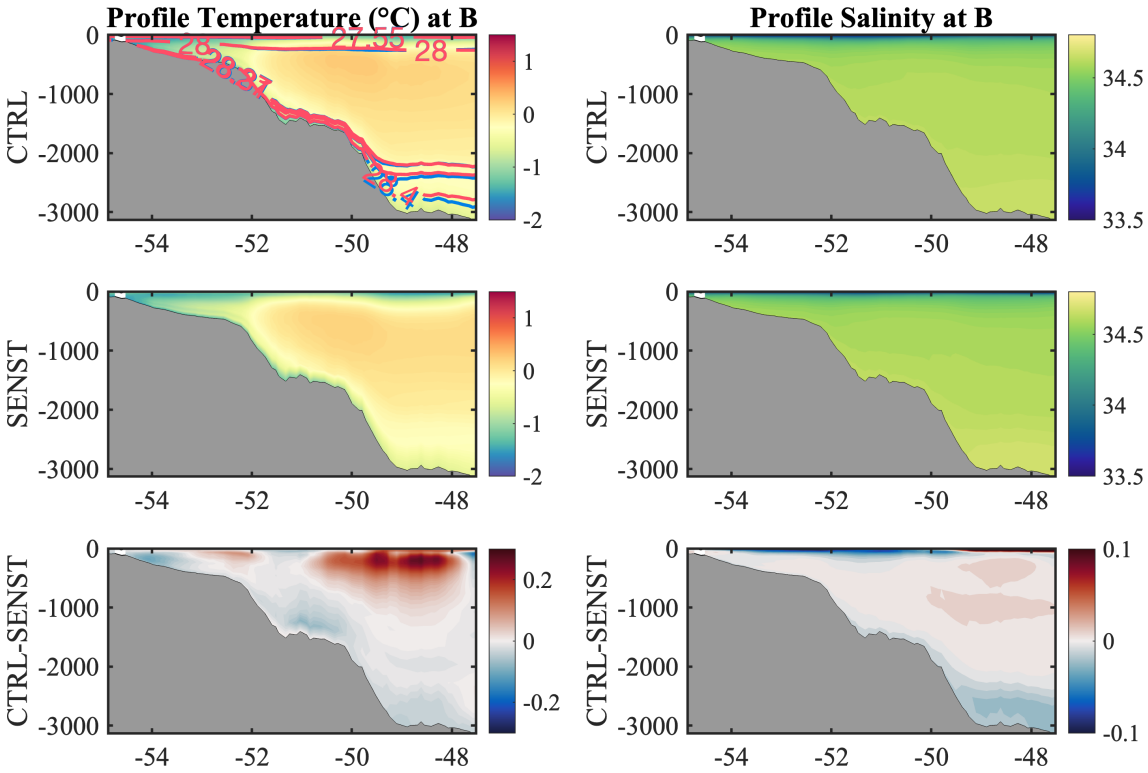

Temperature and Salinity profiles. The blue and red lines represent the neutral density, for CTRL and SENST, respectively. The x-axis indicates the longitudes (°W).

SOURCE: Author.

A.3.4 Along-Shelf Break sections

Figure A.13 - Section AS I - LIS region.

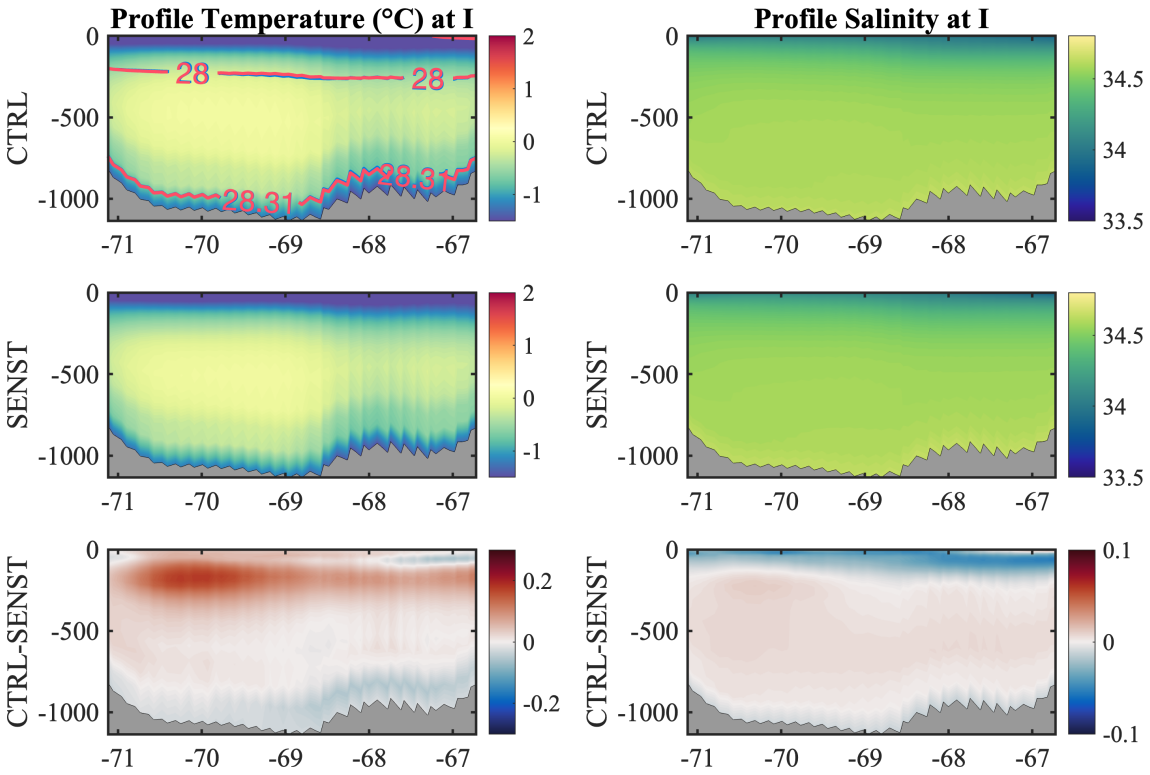

Temperature and Salinity profiles. The blue and red lines represent the neutral density, for CTRL and SENST, respectively. The x-axis indicates the latitudes (°S).

SOURCE: Author.

Figure A.14 - Section AS II - Ronne Filchner region.

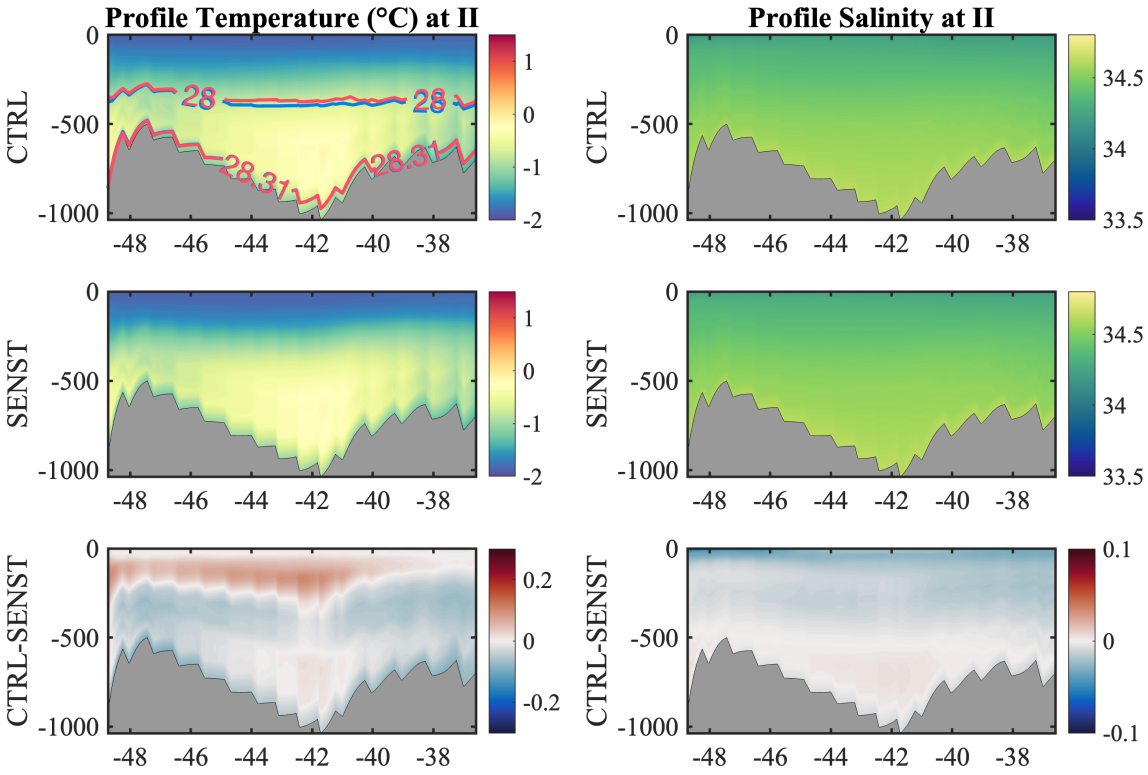

Temperature and Salinity profiles. The blue and red lines represent the neutral density, for CTRL and SENST, respectively. The x-axis indicates the longitudes (°W).

SOURCE: Author.

A.4 Water masses time series

A.15, A.16, A.17 - Bellingshausen Sea cross-slope sections.

A.18, A.19, A.20,A.21 - Weddell Sea cross-slope sections.

A.22, A.23 - Drake and SR4 subsections

A.24, A.25 - LIS and Ronne Filchner along-shelf break subsections (isobath 1000m).

A.4.1 Bellingshausen Sea

Figure A.15 - Water masses (%) in CS 1 along time.

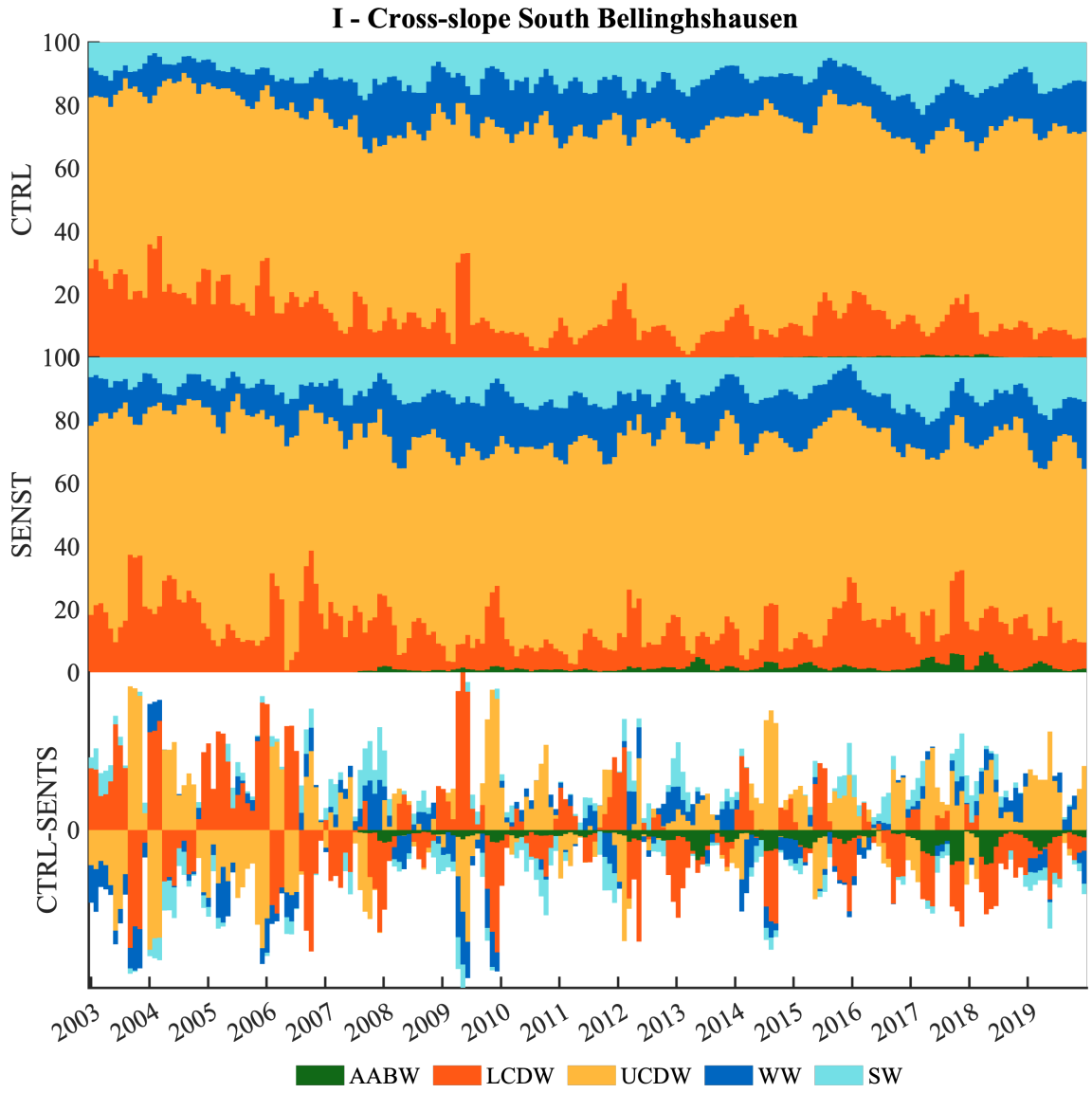

Time serie of the water masses proportions (%) in the total water column through the time.

SOURCE: Author.

Figure A.16 - Water masses (%) in CS 2 along time.

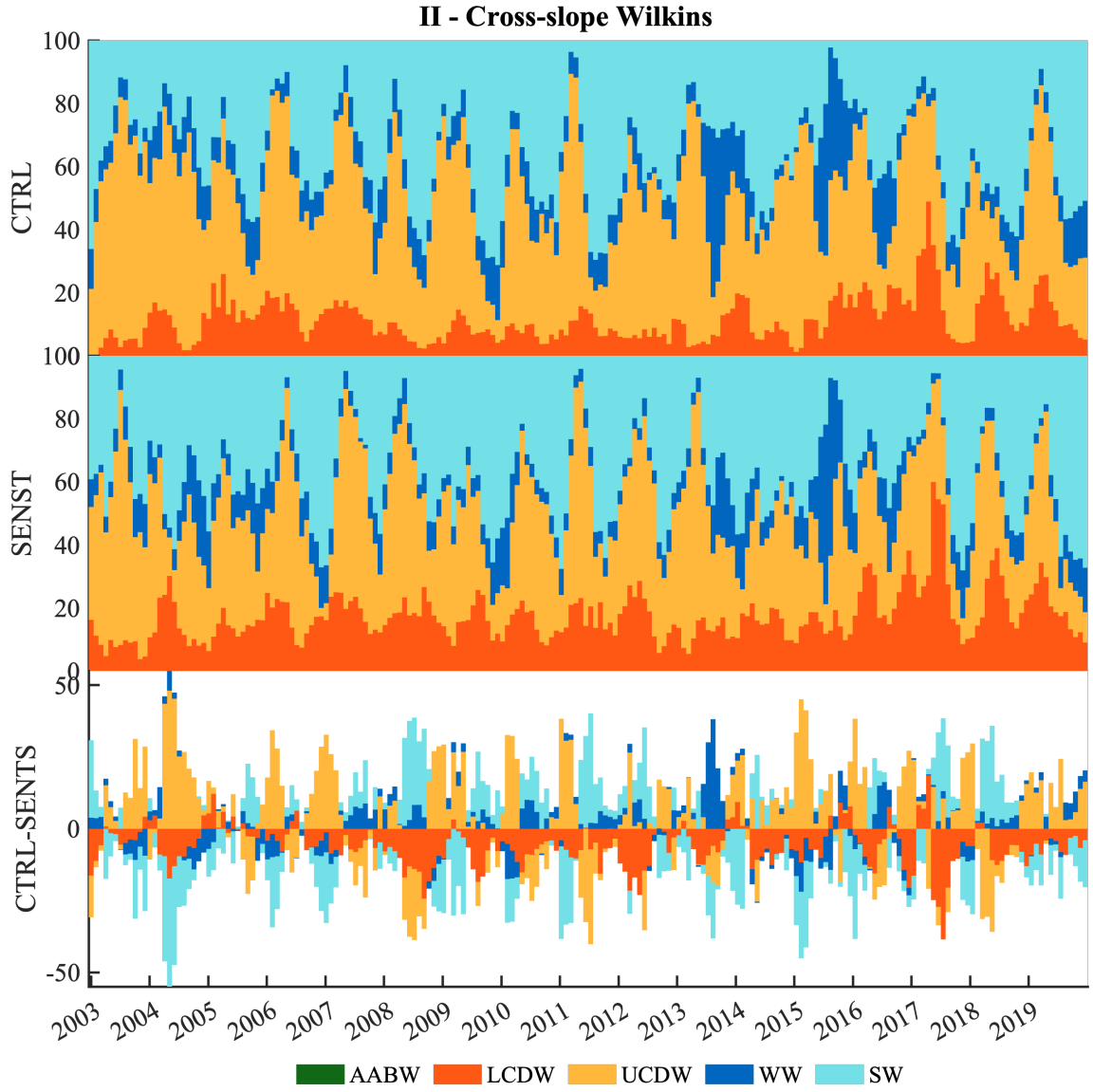

Time serie of the water masses proportions (%) in the total water column through the time.

SOURCE: Author.

Figure A.17 - Water masses (%) in CS 3 along time.

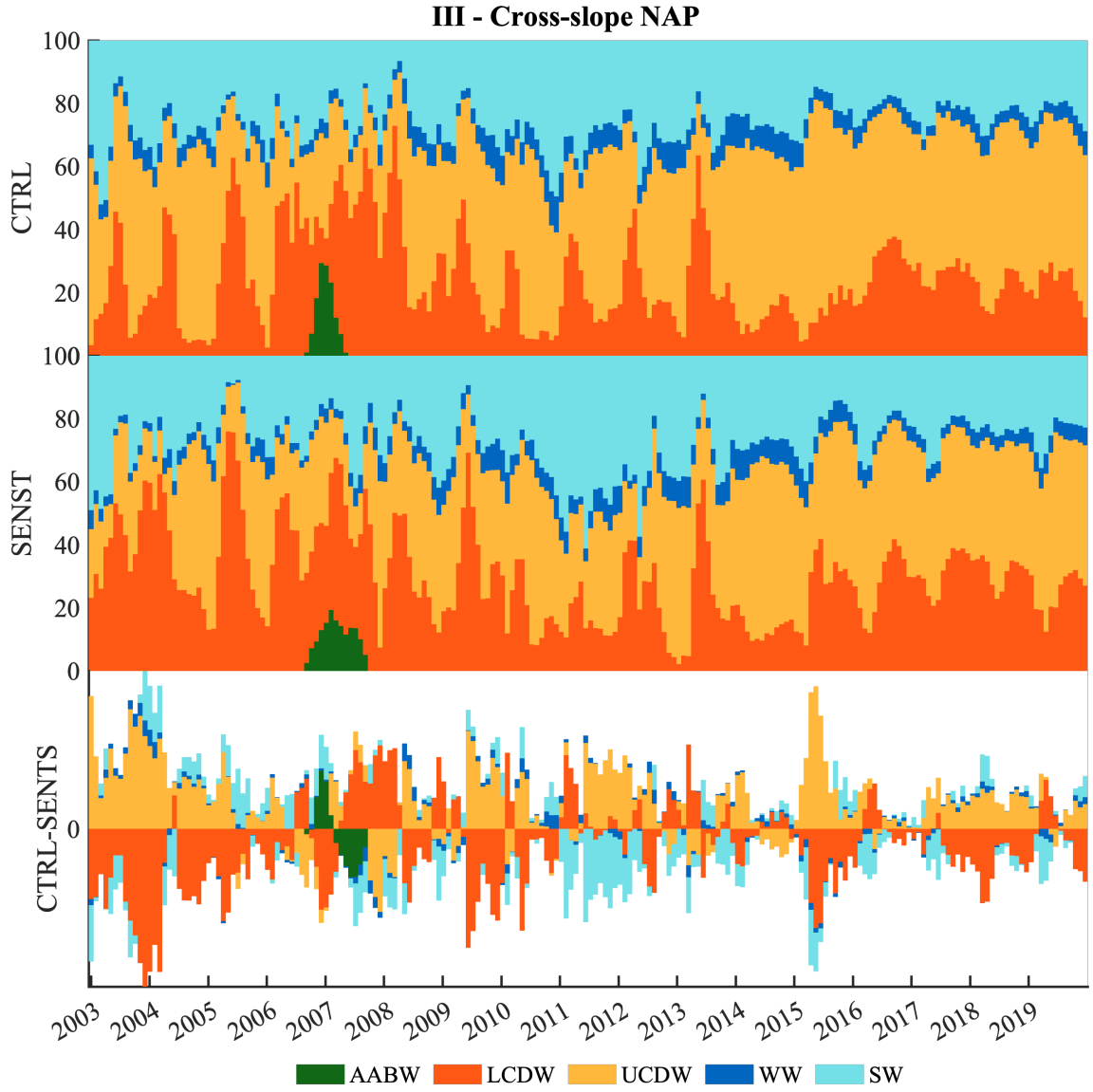

Time serie of the water masses proportions (%) in the total water column through the time.

SOURCE: Author.

A.4.2 Weddell Sea

Figure A.18 - Water masses (%) in CS 4 along time.

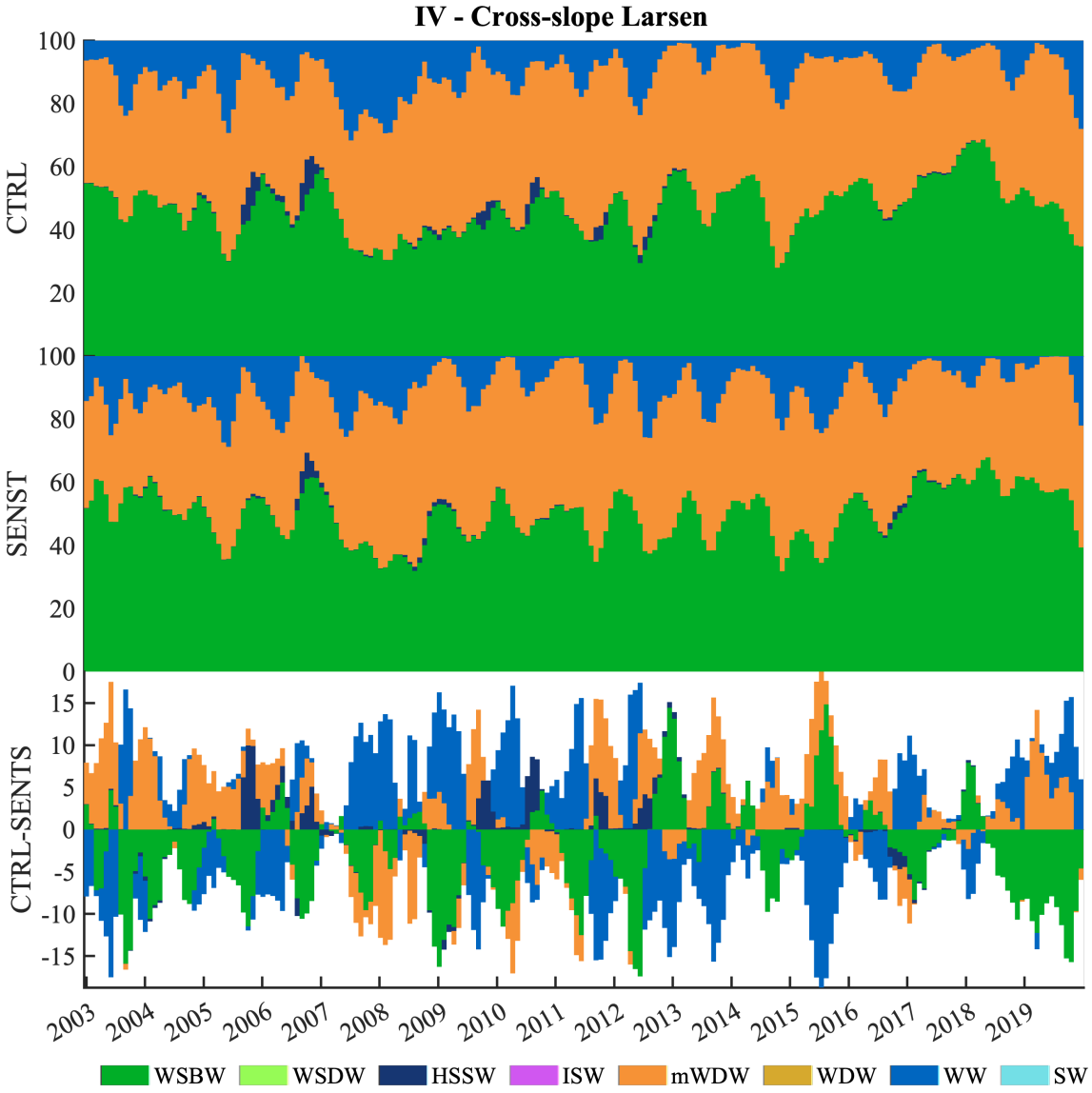

Time serie of the water masses proportions (%) in the total water column through the time.

SOURCE: Author.

Figure A.19 - Water masses (%) in CS 5 along time.

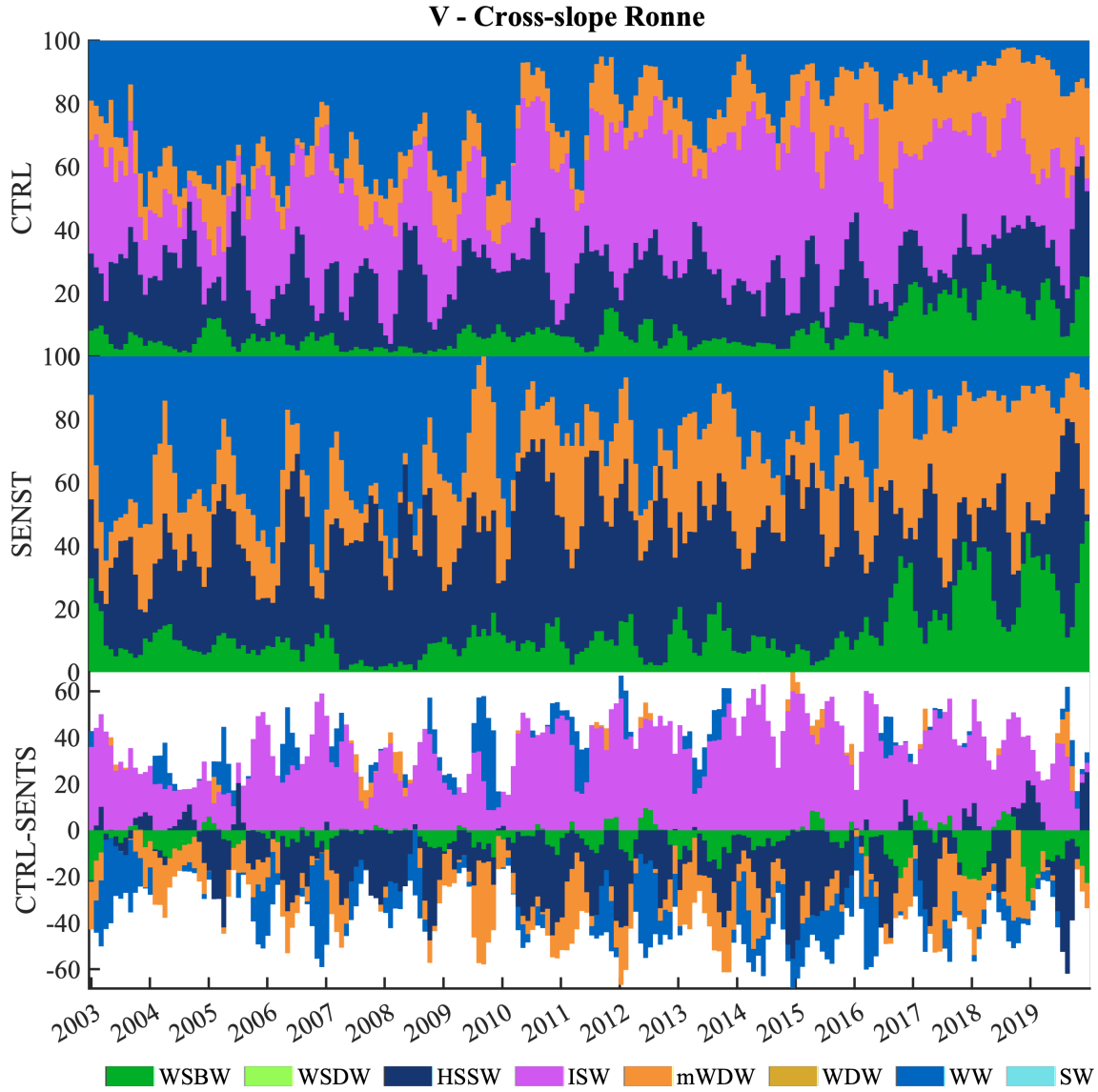

Time serie of the water masses proportions (%) in the total water column through the time.

SOURCE: Author.

Figure A.20 - Water masses (%) in CS 6 along time.

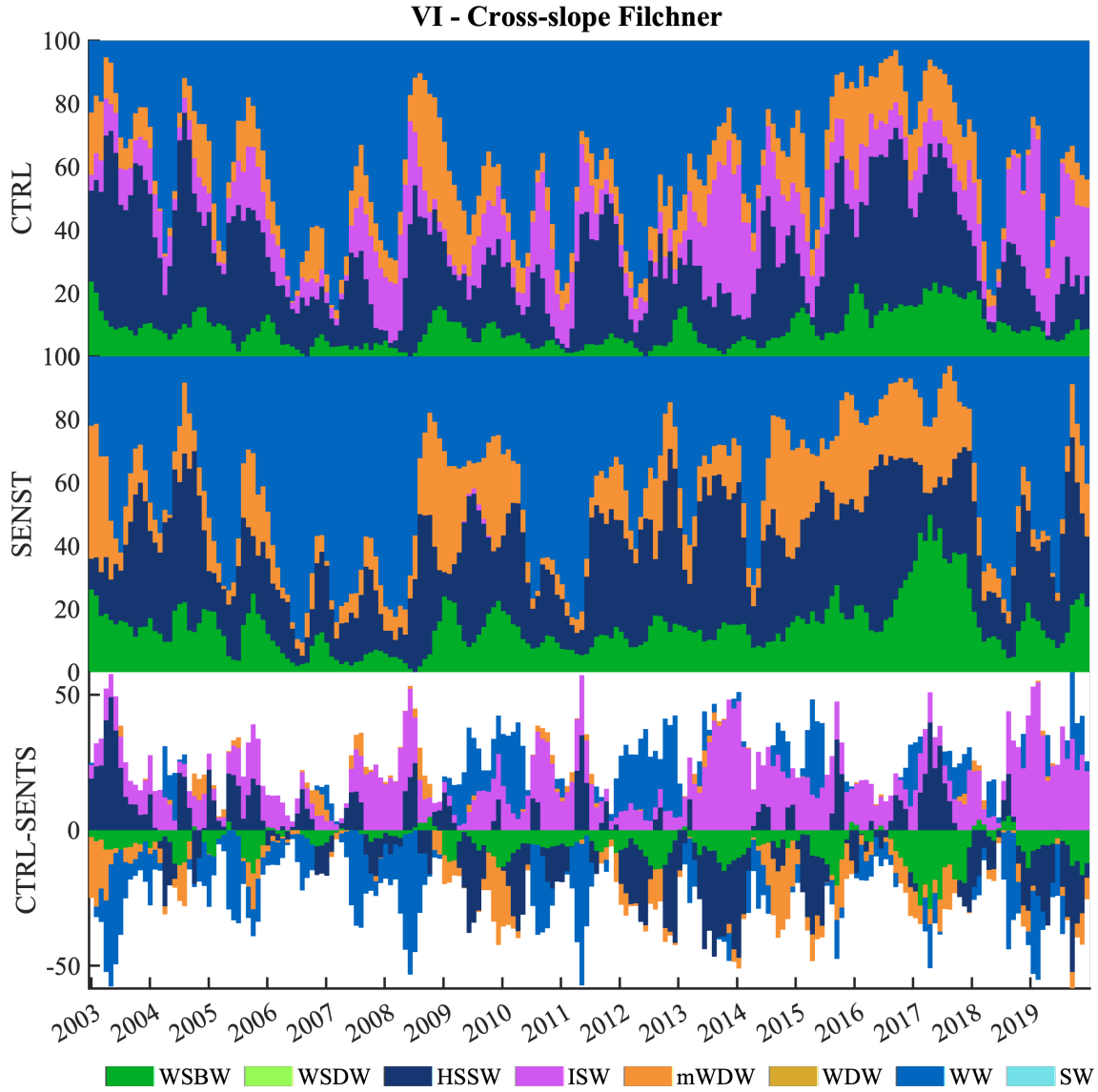

Time serie of the water masses proportions (%) in the total water column through the time.

SOURCE: Author.

Figure A.21 - Water masses (%) in CS 7 along time.

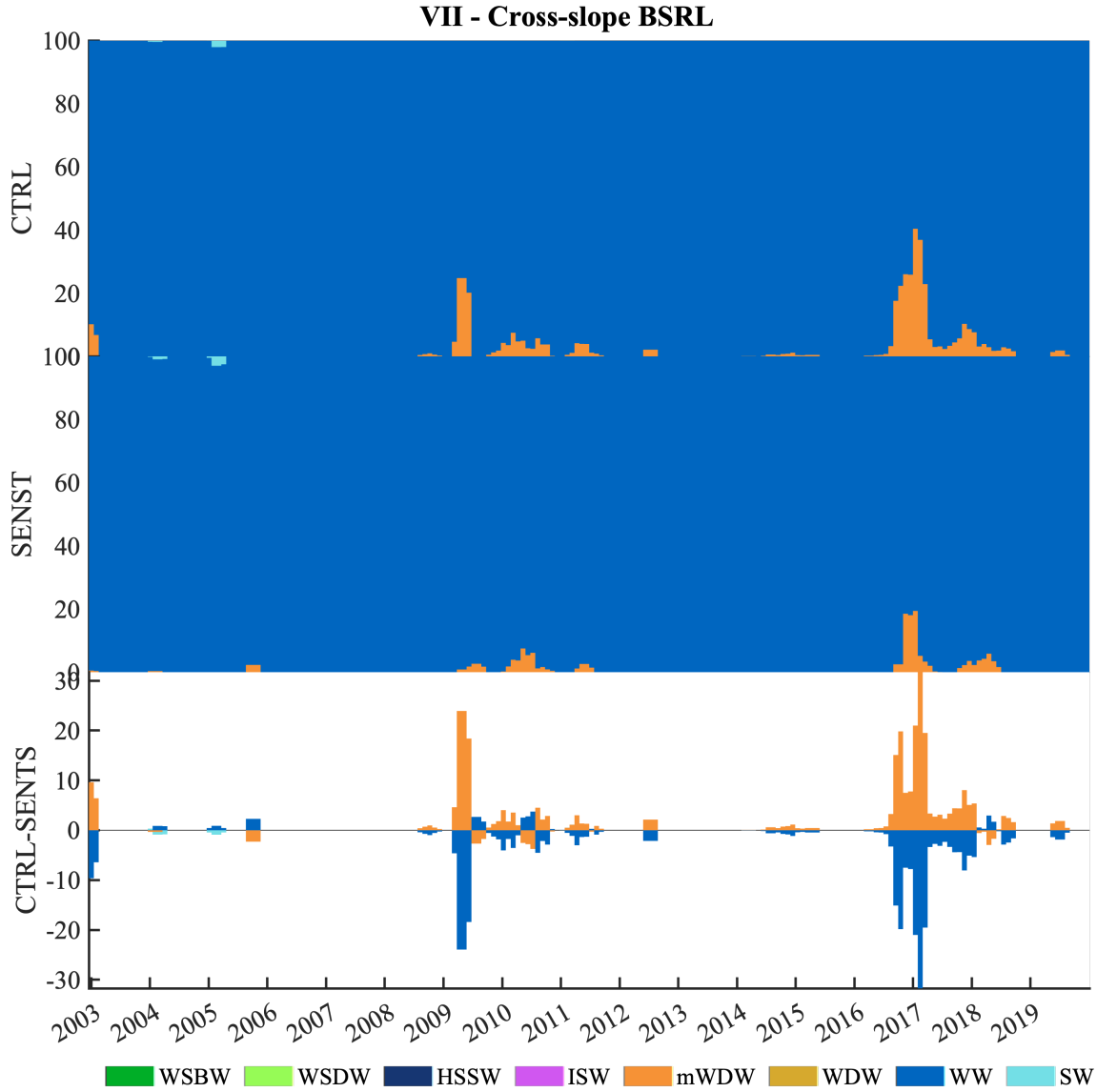

Time serie of the water masses proportions (%) in the total water column through the time.

SOURCE: Author.

A.4.3 Drake and SR4 sub-sections

Figure A.22 - Water masses (%) in Drake sub-section along time.

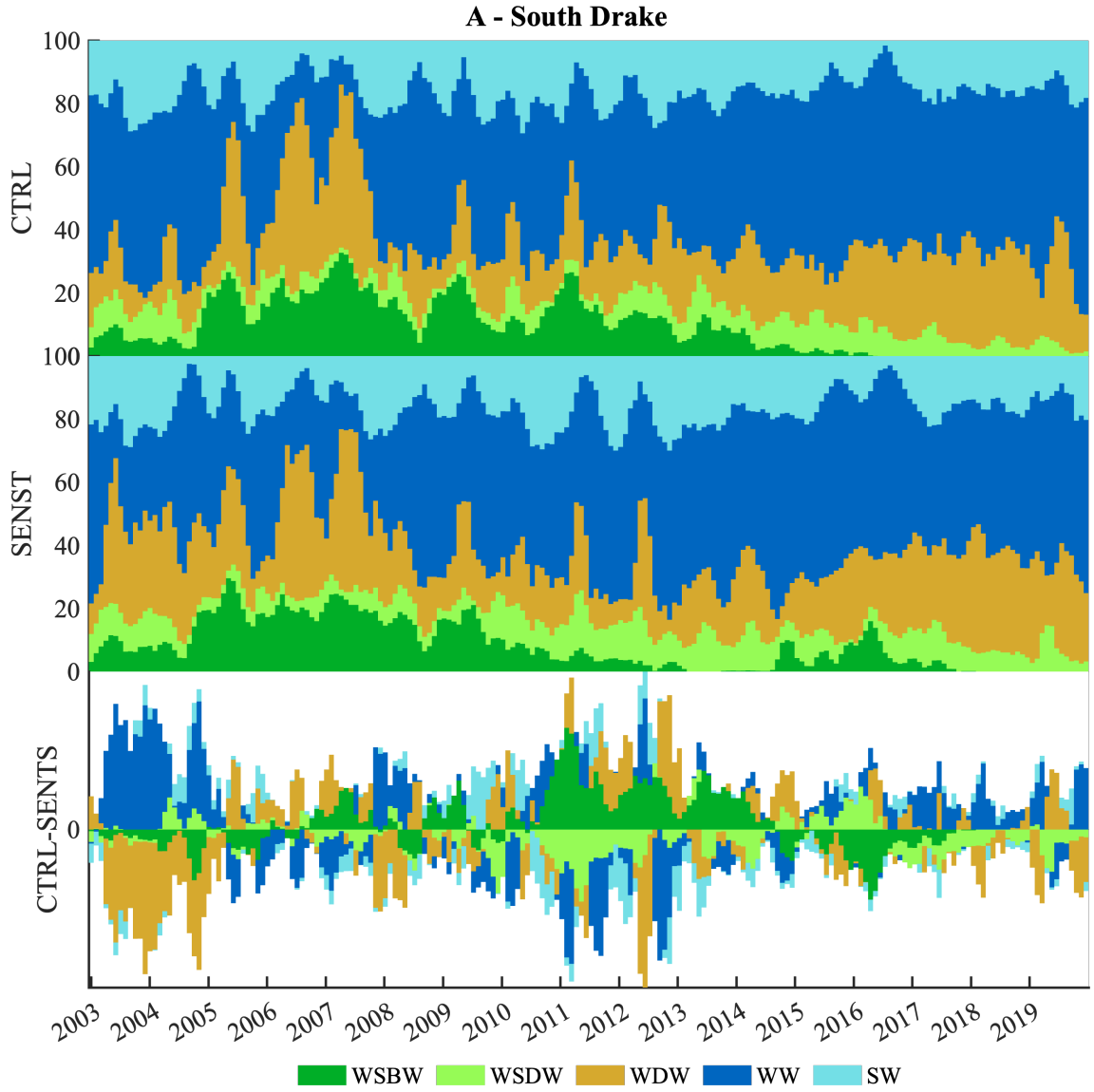

Time serie of the water masses proportions (%) in the total water column through the time.

SOURCE: Author.

Figure A.23 - Water masses (%) in SR4 sub-section along time.

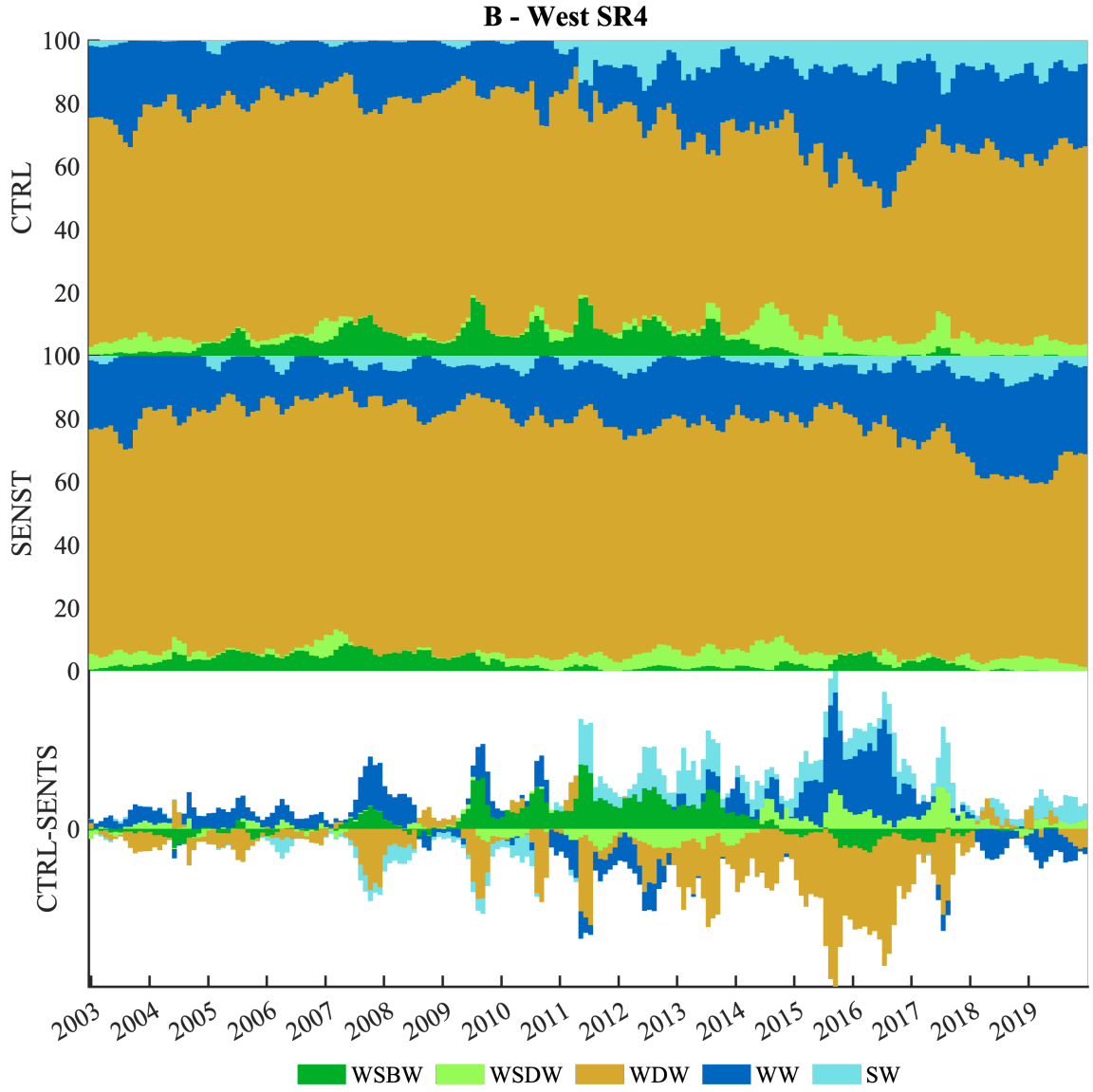

Time serie of the water masses proportions (%) in the total water column through the time.

SOURCE: Author.

A.4.4 Along-Shelf Break sections

Figure A.24 - Water masses (%) in AS I.

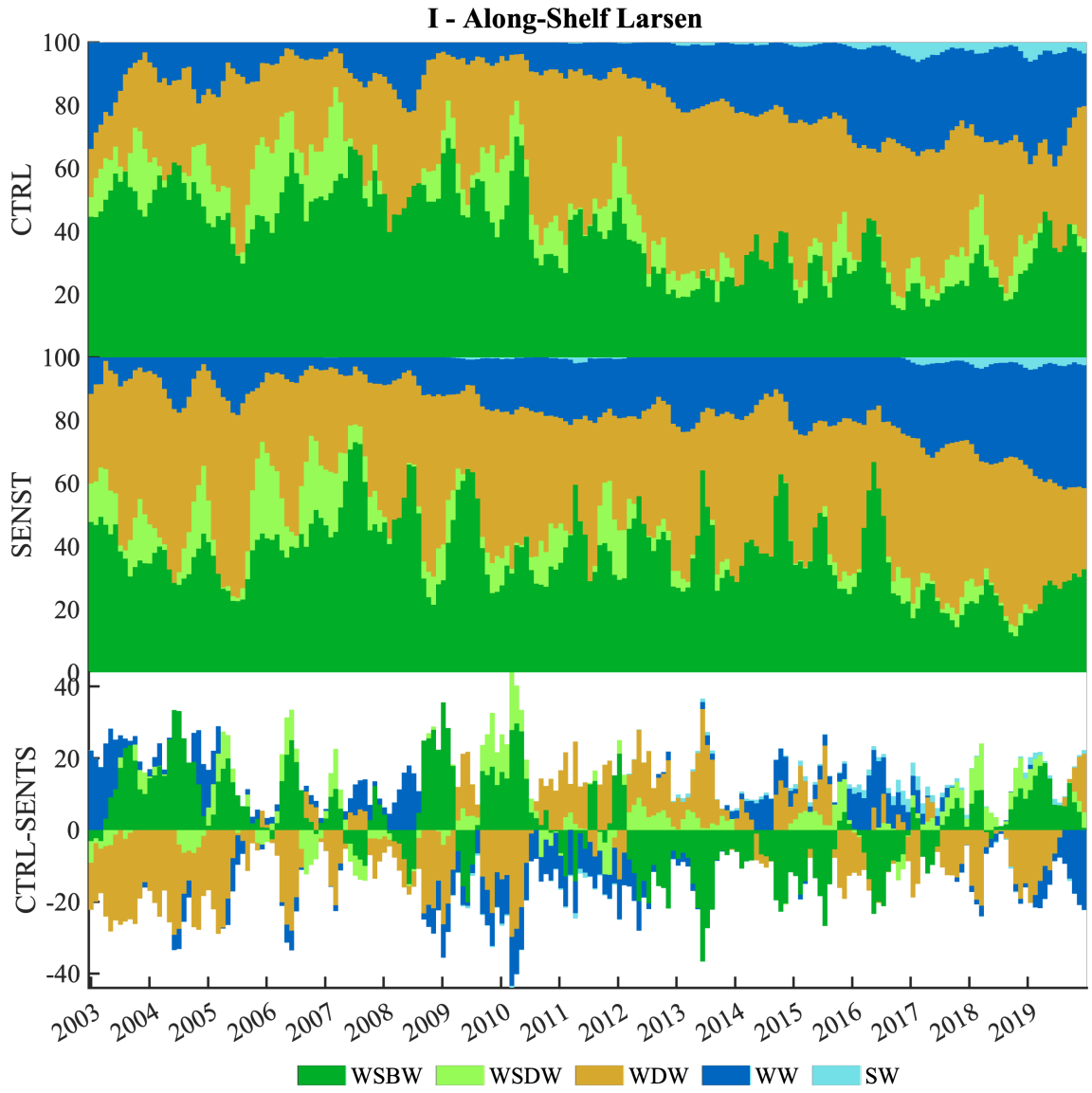

Time-series of the water masses proportions (%) in the total water column through the time.

SOURCE: Author.

Figure A.25 - Water masses (%) in AS II.

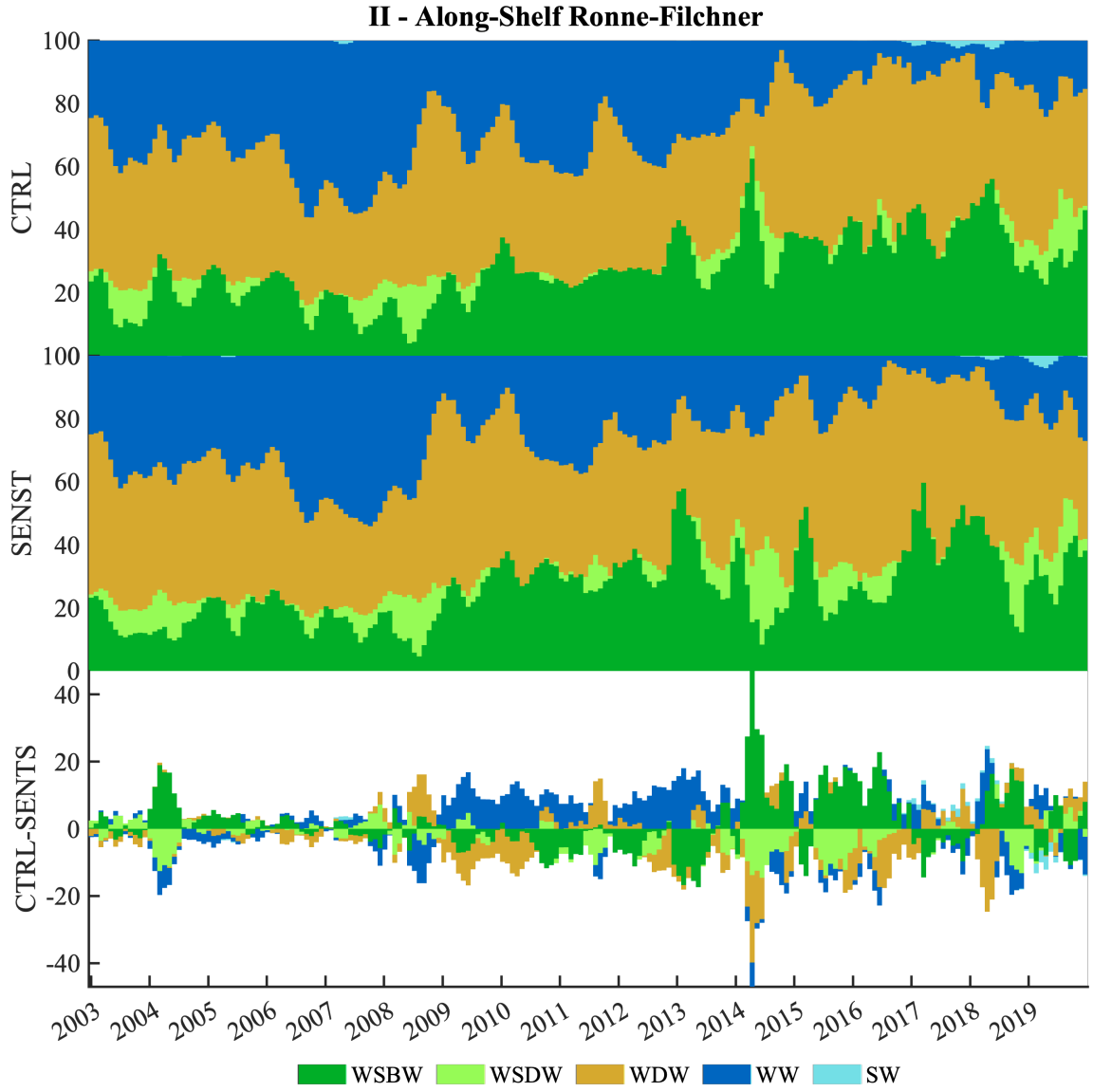

Time serie of the water masses proportions (%) in the total water column through the time.

SOURCE: Author.